8-14-2014

Investigation of the Assembly, Activity, and Lipid Dependence of Mitochondrial Respiratory Complex II via Model Membrane Systems

Christine T. Schwall
University of Connecticut - Storrs, christine.schwall@uconn.edu

Investigation of the Assembly, Activity, and Lipid Dependence of Mitochondrial Respiratory Complex II via Model Membrane Systems

Christine Therese Schwall

University of Connecticut, 2014

Mitochondrial respiratory Complex II, also referred to as succinate dehydrogenase (SDH) and succinate: ubiquinone oxidoreductase (SQR), is a critical control point central to cellular energy metabolism as it links the Tricarboxylic Acid (TCA) Cycle and the electron transport chain (ETC). Complex II oxidizes succinate to fumarate as part of the TCA Cycle and passes these electrons through a series of redox centers to a membrane-bound ubiquinone molecule as part of the OXPHOS system to generate cellular energy. It is composed of four subunits, two of which form a soluble catalytic dimer (SdhA/SdhB) and two of which compose a membrane-anchoring dimer (SdhC/SdhD). As the smallest complex of the OXPHOS system, Complex II is often overlooked, but dysfunction of the complex has been implicated in various neurodegenerative diseases, tumorigenic states, and the aging process. As Complex II is a membrane-bound enzyme, model membrane systems such as liposomes and discoidal bilayer nanoparticles (termed nanodiscs) are necessary to study the enzyme in solution. The first part of this thesis investigates the relationship between Complex II and the characteristic mitochondrial membrane phospholipid, cardiolipin (CL) by substituting the lipids present in the nanodisc system. The studies presented here support that CL is necessary for efficient Complex II activity and inter-dimer stability, also decreasing the reactive oxygen species formation by the complex. In addition, the presence of various types of CL in the membrane enhance to differing levels the

dehydration and packing in the interfacial region of the bilayer. The second part of this thesis focuses on the assembly of holoenzyme Complex II. First, Complex II membrane subunits can form dynamic interactions with each other as well as with homologs found in the mitochondrial inner membrane, possibly revealing a novel regulatory mechanism within the organelle. Second, soluble Helix I of the SdhC membrane subunit is largely involved in modulating and recognizing the correct interaction between the membrane and catalytic dimers. Overall, Complex II assembly and activity prove to be dynamic processes that require regulation by the surrounding lipid, namely cardiolipin, and protein environments.

Investigation of the Assembly, Activity, and Lipid Dependence of Mitochondrial Respiratory Complex II via Model Membrane Systems

Christine Therese Schwall

B.S. Fordham University, 2009

A Dissertation

Submitted in Partial Fulfillment of the

Requirements for the Degree of Doctor of Philosophy

at the

University of Connecticut

2014

APPROVAL PAGE

Doctor of Philosophy Dissertation

Investigation of the Assembly, Activity, and Lipid Dependence of Mitochondrial Respiratory Complex II via Model Membrane Systems

Presented by

Christine Therese Schwall, B.S.

Major Advisor _____

Nathan N. Alder

Associate Advisor _____

Debra A. Kendall

Associate Advisor _____

Carolyn M. Teschke

University of Connecticut

2014

Acknowledgements

~ In Memory of my Father, Alan J. Schwall ~

I feel incredibly blessed to have made it this far in my career and my life and I would not have been able to do so without the guidance and encouragement of so many. For all of those who have touched me along the way and enlightened my scientific journey, I thank you. I would like to thank the following people in a special way:

Thank you to my mother, Therese Schwall, for your guidance throughout my life. I have always aspired to be half the woman you are; you are so selfless and giving and I am truly blessed to call you my mother and my best friend. Without your support I would be lost. Thanks also to my brother, David, for without your antics and ridiculous nature I would not have enjoyed the journey nearly as much, even if you drive me crazy most of the time.

Thank you especially to my father, Alan Schwall, for everything that you gave me. If it were not for you, I never would have chosen Fordham University and started this path towards a career in science. You always supported and pushed me to my furthest limits and made me believe I could do anything. I know that you are watching over me every day, but I wish that you were here today to join me in celebrating this great accomplishment, because if it were not for you, I would not have made it here. This thesis is in memory of, and dedicated to, you.

Thank you to my fiancé, Robert Pecci, for your unending support through it all. I have more than my fair share of ups and downs and you are incredibly supportive, understanding, and patient. Without you and your love, I would be lost.

Thank you to Gran for believing in me and also seeing something special and intelligent beneath the surface; I also wish you were here to see me now. Thank you to my best friend, Sara

Quinn; your love and support through everything I (and we) have been through is astounding and you have pushed me to find myself when no one else could. For that, I will be forever grateful.

Thank you, Dr. Nathan Alder for everything over the past few years. From the moment I stepped into your laboratory you have done nothing but encourage me to accomplish the seemingly impossible. You have taught me not only how to be a better researcher, but also a better writer, presenter, and person. My graduate career certainly would not have been the same without you and I would not have it any other way.

Thank you to all past and present members of the Alder Lab who helped me so much along the way: Sally Chamberland, Christopher Filler, Matthew Greenwood, Victoria Greenwood, Brian Holder, Dr. Judith Landin, Ashley Long, Ketan Malhotra, Margaret Mayer, Kasturi Mitra, John Moffitt, Cate O'Brien, Amee Patel, Stephanie Sass, Murugappan Sathappa, and Melissa Skoryk.

I would also like to thank my associate advisors and examiners for their unending support and guidance: Dr. Debra Kendall, Dr. Carolyn Teschke, Dr. Arlene Albert, and Dr. Victoria Robinson. In addition, thank you to the second floor of the Biology Physics Building for all of the fun times that broke up the science. Others at the University of Connecticut who have helped me so much from designing experiments to utilizing the Electron Microscopy facilities and obtaining zeta potential data to understanding the ins-and-outs of fellowship payments: Stephen Daniels, The Kumar Laboratory (Chemistry Department; in particular Ajith Pattammattel), Dr. Linda McCollam-Guilani, and Anne St. Onge. I would also like to thank the various collaborators who have influenced the development of my project while at the University of Connecticut, including: Dr. Robert Birge and Dr. Matthew Ranaghan (University of

Connecticut), Dr. Anthony Watts (University of Oxford), Dr. Urs Boelsterli (University of Connecticut), and Dr. Stefan Grimm (Imperial College London).

Thank you to all those who touched my life while at Fordham University, including Dr. Donna Heald, Maria Noonan, and Father John Denniston. Special thanks to Dr. James Ciaccio for seeing something special in me and nominating me for a Clare Boothe Luce Fellowship and to my undergraduate mentor Dr. Ipsita Banerjee for pushing me harder than I thought possible and allowing me to fail and learn from my mistakes. Thank you to everyone at the Universität Duisberg-Essen for teaching me about life in Germany, exposing me to German culture, and teaching me so much about Surface Plasmon Resonance and nanoparticle technology.

Lastly, thank you to the organizations and departments that have supported my research efforts from my time at Fordham University through the University of Connecticut. These include: the Clare Boothe Luce Undergraduate Scholarship Program, the DAAD Research in Science and Engineering (RISE) Summer Program, the National Science Foundation Graduate Research Fellowship Program, and the University of Connecticut Graduate School (for the Doctoral Dissertation Fellowship) and Molecular and Cell Biology Department (for the Outstanding Scholar Fellowship and the Jean Lucas-Lenard Special Summer Fellowship in Biochemistry).

Table of Contents

List of Figures and Tables

Page

Chapter 1

Appendix C

Abbreviations

$\Delta\mu_{H+}$ electrochemical proton potential

3-NP 3-nitropropionic acid

BMH bis(maleimido)hexane

BODIPY-FL 4,4-difluoro-5,7-dimethyl-4-bora-3a,4a-diaza-*s*-indacene-3-propionic acid

Ca^{2+} calcium

CL cardiolipin

CMC critical micelle concentration

Crd1 cardiolipin synthase

DB decylubiquinone

DCPIP dichlorophenolindophenol

DDM dodecyl-β-D-maltoside

DMPC 1,2-dimyristoyl-*sn*-glycero-3-phosphocholine

DMSOdimethylsulfoxide

DPH 1,6-diphenyl-1,3,5-hexatriene

DSS disuccinimidyl suberate

dTOCL deoxy-tetraoleoylcardiolipin

DTT dithiothreitol

EDTA ethylenediamine tetraacetic acid

EGS energy-generating system (amino acids)

ETC electron transport chain

FRET Förster resonance energy transfer

GP generalized polarization

H_{II} hexagonal phase

HDL high density lipoprotein

IANBD *N*-((2-(iodoacetoxy)ethyl)-*N*-methyl)amino-7-nitrobenz-2-oxa-1,3-diazole

IASD 4-acetamido-4'-((iodoacetyl)amino)stilbene-2-2'-disulfonic acid

IM inner membrane

ISC iron-sulfur cluster

Laurdan 6-dodecanoyl-2-dimethylaminonaphthalene

LUV large unilamellar vesicle (liposome)

Mg^{2+} magnesium

MLCLmonolysocardiolipin

MSP membrane scaffolding protein

NBD 7-nitrobenz-2-oxa-1,3-diazolyl

ND nanodisc

OM outer membrane

OXPHOS oxidative phosphorylation

PA phosphatidic acid

PC phosphatidylcholine

PE phosphatidylethanolamine

PG phosphatidylglycerol

PHD prolyl hydroxylase

PI phosphatidylinositol

PIN protease inhibitors

PMS phenazine methosulfate

POPC 1-palmitoyl-2-oleoyl-*sn*-glycero-3-phosphocholine

POPE 1-palmitoyl-2-oleoyl-*sn*-glycero-3-phosphoethanolamine

POPG 1-palmitoyl-2-oleoyl-*sn*-glycero-3-phosphoglycerol

PS phosphatidylserine

Q ubiquinone (oxidized, Ub)

QFR quinol: fumarate reductase

QH_2 ubiquinol (reduced)

Q_D distal ubiquinone

Q_P proximal ubiquinone

RNasin RNase inhibitor

ROS reactive oxygen species

SDH succinate dehydrogenase

SMA **s**tyrene maleic acid

SMPB succinimidyl 4-(*p*-maleimidophenyl)butyrate

SQR succinate: quinone oxidoreductase

SUV small unilamellar vesicle (liposome)

Taz1 taffazin (CL deacylase)

TCA tricarboxylic acid

TMCLtetramyristoylcardiolipin

TOCL tetraoleoylcardiolipin

TTFA thenoyltrifluoroacetone

Ub ubiquinone (Q)

Chapter 1

Introduction

1.1. Mitochondria and mitochondrial membrane biology

Mitochondria are the sites of many important metabolic processes within the eukaryotic cell, including oxidative phosphorylation (OXPHOS), the Tricarboxylic Acid (TCA) cycle, metal metabolism (synthesizing heme and Fe-S clusters), and calcium (Ca^{2+}) regulation [1]. Given these essential roles, mitochondrial dysfunction underpins many characterized human diseases including myopathies, neurodegenerative disorders such as Huntington's disease, cancers, and the aging process. Based on the Endosymbiosis Theory, mitochondria are evolutionarily derived from an α-proteobacterium having been taken up, or engulfed, by a host cell [2]. This is supported by multiple lines of evidence, including, but not limited to, the lipid and protein composition of the mitochondrial double membrane and the existence of mitochondrial DNA that encodes various core subunits of some respiratory chain complexes [2].

1.1.1. Mitochondrial membrane composition

Mitochondria have two distinct membranes, the outer membrane (OM) and the inner membrane (IM) that are separated by an aqueous intermembrane space and that enclose the innermost aqueous compartment, the matrix (**Figure 1.1**). The lipid composition of both membranes is dominated by glycerophospholipids, including phosphatidylcholine (PC; ~40% of the total phospholipid in the membrane) and phosphatidylethanolamine (PE; ~30% of the total phospholipid) as the most abundant, with the remaining lipid composition including phosphatidylinositol (PI), phosphatidylserine (PS), phosphatidic acid (PA), and cardiolipin (CL, **Figure 1.2**, [2]). The OM, as compared to the IM, has a relatively low protein to lipid ratio (1:1, by weight, respectively, which accounts for only ~4% of the total mitochondrial protein) and contains both α-helical and β-barrel transmembrane proteins [3]. The OM also contains multiple pore-forming proteins and complexes, including porins, that permit the free passage of small (< 3

kDa) molecules and equilibration with the cytosol. In addition, the OM tends to have higher levels of PI and sterols as compared to the IM, with the exception of the yeast OM [4]. By contrast, the IM is an energy-conserving membrane that maintains an electrochemical proton potential ($\Delta\mu_{H+}$) to drive many vital processes such as OXPHOS. In addition, the IM is much more protein rich as compared to the OM (3-4:1, by weight, protein-to-phospholipid ratio that accounts for approximately 21% of the total mitochondrial protein [3]) and contains only α-helical membrane proteins. The IM is also divided into two continuous, but morphologically distinct parts: the inner boundary membrane, which is in closer proximity to the OM, and the cristae membrane, which forms invaginations into the matrix, thereby providing a larger IM surface area that accommodates the complexes of the OXPHOS system [2]. In addition, the IM contains much higher amounts (between 10-30% of the total lipid content) of the signature mitochondrial phospholipid, CL, which will be explained further in Section 1.3. Lipids [4].

The IM cristae are enriched in many mitochondrial membrane proteins, including the components of the respiratory chain that generate a majority of the cellular energy as ATP (**Figure 1.3**, [5]). In total, the complexes of the respiratory chain transport ten protons across the IM for every two electrons that are passed through the entire chain from NADH to oxygen [6]. The OXPHOS system is composed of four major complexes that make up the respiratory chain: Complex I (NADH: ubiquinone oxidoreductase, which is replaced by multiple NADH dehydrogenases in yeast), Complex II (succinate: ubiquinone oxidoreductase), Complex III (ubiquinol: cytochrome *c* reductase or cytochrome bc_1 complex), and Complex IV (cytochrome *c* oxidase) along with the F_1F_O-ATP Synthase (Complex V) as well as the ADP/ATP and phosphate carriers [7]. These complexes have historically been viewed as randomly distributed entities within the IM cristae that are functionally connected by freely-diffusing electron carriers

(ubiquinone and cytochrome *c*). However, emerging evidence strongly suggests that some of the respiratory chain complexes assemble together into supercomplexes or respirasomes that support an overall higher stability of each individual complex as well as allow more efficient electron tunneling to occur between complexes (i.e. as a solid state electron transport mechanism) [2]. In addition, these supercomplexes are able to sequester the ubiquinone and cytochrome electron carriers, preventing them from leaking electrons that could cause ROS formation [6, 8]. The composition of these supercomplexes is dynamic, seemingly dependent on the physiological conditions of the cell, and various complex stoichiometries have been observed, including: supercomplex trimers III_2IV_1 and tetramers III_2IV_2 in yeast and trimers I-III_2 and higher order oligomers of Complex IV in mammals [6, 9, 10]. Further, it has been shown that the ADP/ATP Carrier and the TIM23 translocon, both residing in the IM, may also interact with the respiratory complexes; in the case of TIM23 the interaction occurs through the Tim21 subunit to facilitate insertion of proteins into the IM [11, 12]. The existence of Complex II within supercomplex structures has been questioned [7, 9]. However, some groups have found evidence to support that a small population of Complex II may loosely interact with the other respiratory chain complexes to form fully functional respirasomes and also may form higher molecular weight species involving interactions with other Complex II enzymes as well as Complex V [13, 14].

The electron tunneling capacity of these respiratory chain supercomplexes and respirasomes is modulated by a mobile pool of ubiquinone (or coenzyme Q) molecules in the IM that act as electron carriers between Complexes I and II and Complex III [15]. The pool behavior is established when the rate of diffusion of both the oxidized ubiquinone and reduced ubiquinol molecules is faster than the oxidation-reduction reactions occurring at the respiratory chain enzymes within the IM [16, 17]. This pool comprises most of the ubiquinone found in the

IM with only a minority (between 10% and 32%) bound to mammalian proteins, but both of these ubiquinone species, pool and bound, exist in equilibrium [16]. It is thought that mainly Complex II pulls directly from the mobile pool as ubiquinone may primarily be directly shuttled between Complexes I and III as a result of supercomplex formation. However, the pool also contributes to ubiquinone shuttling within supercomplexes in that it drives binding of ubiquinone molecules into the site between Complexes I and III and therefore acts as a reservoir for this bound ubiquinone [18]. In evidence of this phenomenon, when phospholipids are fused to mitochondrial membranes, diluting the ubiquinone pool, there is a decrease in respiratory chain activity most likely due to the decreased ability of the diluted pool to drive the binding of ubiquinone to Complexes I and III [17, 18].

1.1.2. *Mitochondria and Reactive Oxygen Species*

The production and balance of reactive oxygen species (ROS) within the mitochondria are intimately linked to intracellular signaling and regulation as well as to apoptosis and cell death. The typical type of ROS generated in mitochondria is the superoxide anion, O_2^-, which is a precursor to the majority of other ROS and is mostly formed during electron transport and cellular respiration in the IM [19]. Recently, it has been shown that not only are Complexes I and III of the respiratory chain major producers of ROS, but Complex II can contribute to the superoxide pool as well. An estimated 1-2% of the electrons that enter the OXPHOS complexes are diverted to superoxide anion formation [20]. Being at the site of ROS production, mitochondrial proteins and lipids are especially subject to oxidative damage. For example, the respiratory chain, among other protein complexes, as well as polyunsaturated fatty acids found within phospholipids and mitochondrial DNA are all major targets of ROS because of the highly oxidizable iron-sulfur centers, heme groups, and copper centers that many of the molecules

contain [19, 21]. In particular, it has been shown that the stability of Complex I and respiratory chain supercomplexes that contain Complex I are especially sensitive to ROS-induced oxidative damage [22]. Additionally, ROS sensitivity of the respiratory chain, especially at Complexes III and IV, is heightened when lipoperoxidative damage is incurred upon the unsaturated fatty acids of phospholipids, predominantly CL [21]. However, physiological or moderate levels of ROS are involved in intracellular signaling and can induce limited autophagy and mitophagy, the degradation of damaged proteins and mitochondria, respectively, which in turn can promote overall cell survival especially under conditions of cellular nutrient depletion. On the other hand, if levels of ROS increase too far, full cell death can be triggered *via* autophagic or apoptotic processes [19].

1.2. Complex II structure, function, and biogenesis

Complex II, also referred to as succinate dehydrogenase (SDH) and succinate: ubiquinone oxidoreductase (SQR), is located in the IM of the mitochondria bridging the TCA cycle and the ETC. Complex II oxidizes succinate to fumarate as part of the TCA Cycle and then passes the resulting electrons and protons from succinate through multiple redox centers to the lipophilic electron carrier ubiquinone as part of the ETC. As the linkage point between these two bioenergetic processes, Complex II has the potential to be a central control point critical to regulating basic metabolic processes within the cell.

Complex II falls into the larger family of oxidoreductases that includes both succinate: quinone oxidoreductases (SQRs) and quinol: fumarate oxidoreductases (QFRs) that catalyze the opposite reaction and participate primarily in anaerobic respiration [23, 24]. In particular, Complex II is a Class I SQR, which is considered the most typical and catalyzes the energetically

favorable oxidation of succinate, passing the resulting electrons to the ubiquinone molecule in the membrane [25]. As a Class I SQR, mitochondrial Complex II contains a Type C membrane anchor, which is comprised of two subunits with three transmembrane helices each that coordinate a single heme molecule at the interface between them [26]. It is important to note that as a Type C enzyme, Complex II does not directly contribute to the generation of a membrane potential across the IM, as the other respiratory chain complexes do, because calculations from standard reduction potentials have revealed that the overall oxidation-reduction reaction catalyzed by Complex II is not sufficiently exergonic to support proton translocation (or generation of a membrane potential) across the IM [16]. In addition, the protons resulting from succinate oxidation are released to the same side of the membrane from which they are taken up for ubiquinone reduction, which does not allow them to contribute to gradient formation [26].

1.2.1. Complex II Structure and Function

Complex II is a heterotetrameric enzyme that can be separated into two heterodimers: the soluble catalytic dimer that oxidizes succinate to fumarate and the integral membrane dimer that anchors the catalytic dimer and passes electrons to ubiquinone as part of the ETC (**Figure 1.4**). Crystal structures of Complex II and the related QFRs have been solved for various prokaryotic species including *Escherichia coli* and *Wolinella succinogenes* [27-31] as well as for the eukaryotic nematode, avian, and porcine species [32-36]. A homology model for the yeast Complex II has also been constructed that is based on the *E. coli* and *W. succinogenes* SQR and QFR structures [37, Figure 1.4]. These structures support an overall model of the enzyme in which the smaller of the two catalytic subunits (Fe-S protein Sdh2, **Figure 1.4**, blue) acts as the linkage point between the larger catalytic subunit (flavoprotein Sdh1, **Figure 1.4**, red) and the membrane dimer (Sdh3/4, **Figure 1.4**, yellow/green). Within the complex, the membrane dimer

forms an antiparallel helix bundle within the membrane that stabilizes part of the binding pocket for ubiquinone [37]. Notably, whereas the catalytic subunits share a high degree of sequence conservation between prokaryotic and eukaryotic species (approximately 50% homology), there is higher variability among the sequences of each of the membrane subunits (approximately 20% homology). However, the membrane subunits are similar in conformation among all known structures, which is especially pronounced in the high structural conservation of the heme-binding pocket and the ubiquinone-binding site [36, 38, 39]. Further, as with other respiratory complexes [40, 41], many of the Complex II structures support tight binding interactions between lipid molecules and the membrane dimer. The *E. coli* SQR structure was shown to contain one each of tightly bound CL and PE molecules, while the porcine structure contained two PE molecules, which were interpreted to mediate interactions between the membrane subunits [6, 31, 36].

In eukaryotes, the catalytic dimer is often referred to as succinate dehydrogenase (SDH) and the two proteins are referred to as SdhA and SdhB in mammals or as Sdh1p and Sdh2p in yeast. SdhA is an approximately 70 kDa flavoprotein that contains the FAD moiety covalently bound through a histidine linkage near the catalytic site of succinate oxidation. The covalent linkage between FAD and SdhA increases the redox potential of FAD, which allows the oxidation of succinate by Complex II; when FAD is bound non-covalently, the enzyme is unable to complete SDH activity (i.e. succinate oxidation) [42, 43]. SdhB is approximately 27 kDa and contains three Fe-S centers, [2Fe-2S], [4Fe-4S], and [3Fe-4S] that constitute a linear path for electron flux from FAD to the ubiquinone in the membrane. SdhB also confers overall structural stability to the holoenzyme as 40% of the total surface area of SdhB contributes to interactions with SdhA and the membrane dimer [36]. When the catalytic dimer is separated from the

membrane dimer, which can occur at low pH or in the presence of chaotropic reagents, it is considerably more unstable as compared to when it is securely interacting with the membrane dimer [44].

The holoenzyme is referred to as succinate: ubiquinone oxidoreductase (SQR) and includes both SdhA and SdhB as well as the membrane-bound SdhC and SdhD (in mammals, or Sdh3p and Sdh4p in yeast) [23, 37, 45]. SdhC and SdhD are each approximately 16 kDa with three transmembrane-spanning helices (six total transmembrane segments in the assembled enzyme), four of which form an antiparallel helix bundle and two of which act to stabilize the dimer within the membrane [46]. The membrane subunits also coordinate a low-spin, hexa-coordinated *b*-type heme between them *via* a histidine residue in each subunit [47-54]. In yeast, the heme is bound by the traditional histidine residue in Sdh3p, but is thought to interact with a non-canonical cysteine residue in Sdh4p because there is no conserved histidine at this site; such atypical coordination has led some groups to question the presence or role of the heme moiety within Complex II [47, 50, 51]. The membrane subunits also contain a proximal ubiquinone-binding site (Q_P) located close to the interface with SdhB and a putative distal site (Q_D) located on the opposite side of the heme molecule whose relevance is also disputed [29, 30, 35, 37, 38, 55-58]. It has been postulated that both ubiquinone binding sites help in facilitating exchange of bound ubiquinone with the quinone pool within the membrane. Dual sites may also be needed to balance efficient catalysis and decrease production of free radicals from the unstable ubisemiquinone intermediate that could damage the mitochondrial membrane and oxidative machinery [15, 37, 57].

Overall, electrons are passed a total distance of approximately 40 Å between succinate and ubiquinone within Complex II (**Figure 1.5**, [30]). Electrons from succinate enter Complex

II at SdhA and are immediately passed to FAD, the first redox center in the linear electron chain within the complex. Direct electron transfer is favored between redox centers of Complex II because there is less than 14 Å between each of the electron carriers, which enables electron tunneling [59]. These short distances are thought to overcome the unfavorable decrease in reduction potential of the [4Fe-4S] redox center as compared to the [2Fe-2S] center immediately preceding it (a drop of 260 mV in porcine Complex II). Further, not only is the presence of heme in the yeast Complex II disputed, but the function of the heme in all species is inconclusive as its low reduction potential (-185 mV in porcine Complex II) poses a thermodynamic barrier to electron transfer from the [3Fe-4S] center. The low reduction potential may not completely inhibit electron transfer, as it has been shown that even unfavorable free energy pathways can allow electron transfer if the centers are located in close proximity [59]. However, the heme is located farther away from the [3Fe-4S] center as compared to ubiquinone and this distance is at the edge of the 14 Å acceptable distance for such direct electron transfer (7.1 Å for ubiquinone compared to 13.3 Å for the heme in porcine) [26, 59].

Given that the role of the heme in Complex II electron transfer is disputed, other roles for this redox center have been proposed. First, it is postulated that heme may play more of a structural role rather than taking part in electron transport through the complex. When heme is not present, the holoenzyme is less stable and the ubiquinone binding site is disrupted, leading to loss of SQR activity [60, 61]. It has also been hypothesized that the heme can act as an excess electron acceptor that would prevent electrons that cannot be passed to a fully reduced ubiquinol from instead being passed to the surrounding environment and causing free radical damage to the mitochondria [62]. This hypothesis is further supported by the evidence that *E. coli* QFR that lacks a heme molecule but is otherwise structurally similar to Complex II and that catalyzes the

opposite reaction of SQR, is a higher producer of ROS as compared to Complex II. This is thought to arise in QFR because without a high potential heme moiety electrons are kept at the flavin molecule where they are then passed or leaked to oxygen, forming ROS [15]. However, other studies by the Cecchini group did not find evidence to support that a loss of heme contributes to an increase in ROS formed by Complex II in *E. coli* [63, 64]. Further, the redox potential of the heme in eukaryotic Complex II (-185 mV in porcine) as compared to that of *E. coli* (+36 mV) is much lower, which would discourage even excess electrons from being passed to this moiety [31, 36, 65]. Hence, the role of the Complex II heme remains poorly understood and more work needs to be completed in order to determine its true function within Complex II.

The overall enzymatic activity of Complex II can be split into two separately observable activities *in vitro*: succinate dehydrogenase (SDH) activity that reflects the presence of an active catalytic dimer only and succinate: quinone oxidoreductase (SQR) activity that detects the presence of an active holoenzyme (**Figure 1.6**). SDH activity requires that only the catalytic dimer be present so that electrons from succinate can be passed through FAD and all three [Fe-S] centers. On the other hand, SQR activity requires that the catalytic dimer be docked to the membrane dimer so that electrons from the [3Fe-4S] center of SdhB can be passed to the ubiquinone located within the membrane between SdhC and SdhD. *In vitro*, both of the assays utilize an artificial colorimetric electron acceptor, dichlorophenolindophenol (DCPIP), that undergoes an extinction in absorbance at 600 nm upon reduction [66].

Complex II activity is regulated *in vivo* primarily by phosphorylation and acetylation of SdhA [67]. Specific chemical inhibitors have also been identified that bind to the catalytic site (**Figure 1.7A**) and the ubiquinone-binding site (**Figure 1.7B**). Inhibitors that act at the succinate (or dicarboxylate) binding site tend to be competitive inhibitors that are also TCA Cycle

intermediates. Examples include oxaloacetate and malate, which is oxidized by Complex II to enol-oxaloacetate that then is able to inhibit the enzyme [25, 67, 68]. Additionally, a toxin produced by certain plants and fungi that is similar structurally to succinate, known as 3-nitropropionic acid (3-NP), has been found to act as a suicide inhibitor of the complex through the succinate-binding site [34]. Inhibitors of the quinone binding site include the metal chelator thenoyltrifluoroacetone (TTFA), atpenin A5 (a competitive ubiquinone analog that prevents electron transfer from the [3Fe-4S] cluster to ubiquinone), and carboxins, which are able to specifically inhibit SQR activity [25, 69, 70]. It has been shown that of these, the antifungal compound atpenin A5 is very specific and is also more effective than other Complex II inhibitors at hindering activity [71]. In addition, a molecule called HQNO is able to inhibit Complex II activity by binding at the quinone-binding site; however, HQNO is also able to bind and inhibit Complex III, making it a non-specific Complex II inhibitor. Some inhibitors of Complex II are more recently being considered for, and developed into, anti-cancer therapeutics, such as MitoVES, which is a mitochondrially targeted vitamin E succinate molecule [72, 73].

Recently, our laboratory engaged in a collaborative effort with the Boelsterli laboratory in the Department of Pharmaceutical Sciences at the University of Connecticut aimed at understanding the mechanism of isoniazid-induced cell death and mitochondrial Complex I dysfunction [74]. Isoniazid is an antituberculosis drug that has been associated with drug-induced liver injury in susceptible patients, but the lack of understanding regarding the mechanism by which this occurs has delayed development of screens to identify susceptibility. However, it had been known that a metabolite of isoniazid, called hydrazine, is able to interfere with mitochondrial energy production and function. While we are still unclear of the mechanism by which this occurs, as increased succinate concentrations were unable to compete away the

inhibitory effects, hydrazine proved to be not only an inhibitor of Complex I, but also a potent Complex II inhibitor. These results may shed light on the overall pathway by which hydrazine interferes with normal mitochondrial function and assist in developing assays to determine susceptibility to liver injury by isoniazid-based drugs.

1.2.2. Complex II Biogenesis and Assembly

Although the structure of Complex II is fairly well established, the process by which the holoenzyme is assembled is still uncertain. Unlike the other respiratory chain complexes, all of the Complex II subunits are encoded by nuclear genes; therefore, all four subunits must first be targeted to the mitochondria with a cleavable amino-terminal presequence. Such presequences, although lacking a consensus sequence, usually contain a 15-50 amino acid peptide sequence that forms an amphipathic α-helix with a hydrophobic face and a basic (positively charged, usually +3 to +6) hydrophilic face [12, 54]. Proteins targeted to the mitochondrion by presequences are transported across the OM *via* the TOM (Translocase of the Outer Mitochondrial Membrane) complex and across the IM *via* the TIM23 (Translocase of the Inner Mitochondrial Membrane) complex, which transports matrix-located proteins as well as single-spanning integral membrane proteins [2]. Upon entering the mitochondrial matrix, the presequences of both soluble, matrix-directed proteins (for example, SdhA and SdhB) and membrane proteins (such as SdhC and SdhD) are cleaved by the mitochondrial-processing peptidase [75].

Once in the matrix, cofactors are inserted into Complex II protein subunits. FAD is covalently attached to SdhA through what is thought to be a self-catalytic process assisted and enhanced by chaperones, such as the eukaryotic Sdh5 (bacterial homolog SdhE), which are thought to deliver FAD to SdhA [76, 77]. This process is further stimulated by the presence of SdhB as well as succinate, malate, and fumarate. In addition, the covalent attachment of FAD to

SdhA increases the redox potential of FAD and therefore the "oxidative power" of Complex II as a whole [78-80]. The assembly of the [Fe-S] centers into SdhB, where cysteine residues act as ligands, is now known to occur through a complex biosynthetic machinery, not simply spontaneously [25, 81]. Once the centers are formed through the help of molecular scaffolds (iron-sulfur clusters or ISCs) and chaperones, they are transferred to SdhB [81-83]. It has very recently been shown that the transfer process itself is modulated by two separate LYR motifs within SdhB that are able to interact with these chaperones, such as HSC20, Sdh6/SDHAF1, and Sdh7/SDHAF3 [84, 85]. It is postulated that FAD attachment to SdhA is promoted by the presence of SdhB, but also that both FAD and Fe-S cofactor attachment precede catalytic dimer assembly; therefore, SdhA and SdhB are likely to interact closely with each other once inside the matrix [15]. Further, a new SdhA assembly factor has recently been identified, Sdh8/SDHAF4, that binds preferably to flavinylated SdhA and facilitates the interaction of SdhA with SdhB to form the catalytic dimer while also preventing spurious ROS formation by SdhA [86].

Once the complementary membrane subunits have been inserted into the IM and assembled together, possibly through the addition of the heme moiety, the catalytic dimer will then attach to the membrane dimer *via* SdhB, forming the holoenzyme [87, 88]. This interaction between the catalytic and membrane dimers is mainly hydrophobic in nature and can be disrupted by the presence of chaotropic reagents, but is also mediated by a number of conserved polar contacts [89, 90]. It has also been observed in past studies that the catalytic dimer will not assemble with the membrane dimer if heme is not present, that the [3Fe-4S] cluster of SdhB must be protected from reduction and oxidation for catalytic dimer re-attachment, and that both membrane subunits in *E. coli* are required for heme to ligate the complex [25, 91]. These results

also provide several independent lines of evidence supporting the assertion that heme plays more of a structural, rather than catalytic, role within Complex II [91, 92].

The general chaperones that facilitate the overall subunit assembly of Complex II are poorly understood as well, but various studies have provided evidence supporting important roles for the following proteins. One group identified Tcm62p, a member of the hsp60 protein family that is found in yeast and which is thought to form a complex with at least three Sdh subunits, as a potential stabilizer of Sdh2p until it is able to bind Sdh1p [93]. In addition, Abc1p, previously thought to be involved solely in Complex III biogenesis, is believed to be involved in modifications to the final structures of Complexes II and IV as well [46]. Further, the Flx1 mitochondrial transporter, likely to transport flavin into the mitochondria, has been implicated in Complex II assembly as well [67].

This complex assembly process became even more complicated recently when multiple homologs to Sdh4p were identified in yeast (**Figure 1.8**). These include Tim18p (39.5% identical to Sdh4p), which is a subunit of the TIM22 Complex, another translocase of the IM, that transports integral IM proteins with multiple membrane-spanning helices that do not contain cleavable presequences, and an open reading frame of unknown function in yeast, YLR164w (52.6% identity with Sdh4p) [94, 95]. Tim18p has previously been shown to be critical for the assembly of the Tim54p subunit into the TIM22 Complex [96]. It has further been found that Sdh3p interacts with Tim18p and is necessary for the assembly of the TIM22 Complex; in addition, when Sdh3p is knocked out in yeast, the levels of Tim18p, along with Sdh4p, are significantly decreased [96]. Moreover, YLR164w (Shh4p) and a paralog of Sdh3p, YMR118c (Shh3p), are able to complement Sdh4p and Sdh3p knockouts, respectively, and are thought to change Complex II catalytic activity under non-optimal growth conditions [97]. These

observations suggest that Complex II membrane subunits are part of a complex interactive network, or interactome, with other membrane proteins and complexes [94, 96] and that the assembly of Complex II may be more intricate and more highly regulated than previously thought.

Complex II subunits have also been implicated in the operation of other membrane complexes. For example, it has been demonstrated that fumarate reductase, which catalyzes the reverse reaction of reducing fumarate to succinate, is involved in the assembly and function of the bacterial flagellar switch complex [98]. Further, it has been proposed that succinate dehydrogenase, namely SdhA, is a component of the mitochondrial ATP-sensitive potassium channel as some of the functions and inhibitor-sensitivities of these complexes overlap [99, 100]. Overall, Complex II and its homologous counterparts are influential in more processes than simply respiration and energy production within the cell.

1.2.3. *Complex II and Disease*

As the linkage point between the TCA Cycle and the ETC and as a potential critical control point for cellular energy metabolism, it is no surprise that Complex II dysfunction is associated with a multitude of different disease types. Mutations in Complex II have been implicated in various tumorigenic diseases [67, 101], most notably paraganglioma and a derivative of this phenotype, pheochromocytoma [45, 101-106]. Abnormal activity of Complex II has also been linked to general mitochondrial dysfunction that involves the loss of membrane potential, increased calcium concentrations and the production of reactive oxygen species (ROS), which not only affect the mitochondria but can also be exported to the cytoplasm causing further damage [107, 108].

Complex II mutation has also been linked to the potential development of Huntington's Disease and other neurological disorders, including Leigh Syndrome [15, 109, 110]. Mutations in the *SDHA* gene of Complex II are predominantly associated with the development of Leigh Syndrome and are linked with compromised SDH activity and lowered energy production [103]. Leigh Syndrome is a very rare early onset degenerative neurological condition that affects the central nervous system [67, 111]. It is associated with disorders in movement such as seizures as well as general weakness.

Mutations in *SDHB, SDHC,* and *SDHD*, on the other hand, have been extensively linked to autosomal dominant hereditary paraganglioma and its subtype pheochromocytoma. Paraganglioma is characterized by benign, highly vascularized tumors in the head and neck regions of the body that derive from the neural crest paraganglial system, which includes the adrenal medulla [42, 112-117]. The most common site for this type of tumor formation is the carotid body, which acts as an important oxygen sensor. Pheochromocytoma is a hormonally active form of paraganglioma and is characterized by catechol-secreting tumors that tend to develop in the non-head and neck regions of the body [105, 118]. More recently, mutations in *SDHA* have also even been linked to the development of paraganglioma [119] and mutations in the cofactor required for SdhA flavinylation, Sdh5, have also been linked to paraganglioma and pheochromocytoma development [104, 118, 120].

Of note, mutations in *SDHC* are more rare compared to mutations in *SDHB* and *SDHD* [121]. Further, mutations of *SDHB* tend to be associated with non-head and neck paragangliomas and have a higher frequency of being malignant (as high as 50%) and of leading to a poorer prognosis, as compared to mutations of *SDHD*; however, twenty percent of the amino acids in SdhD have been implicated in tumor formation [91, 102, 105, 118]. In addition, the

largest number of diseases associated with Complex II have been linked to mutations in *SDHD* and other diseases stemming from complications with Complex II include renal cell carcinoma [115, 122], certain types of colon and gastric cancers [45, 111, 123], and childhood T cell leukemias [124, 125]. *SDHB, SDHC* and *SDHD* are classified as tumor suppressor genes because loss of heterozygosity results in loss of protein function [42, 105, 126-129]. The best characterized heritable pathogenic missense mutations include L130P in SdhC and R35G, P46L, D57Y, L60P, H67L, Y79C, and L104P in SdhD (**Figure 1.9**).

Complex II has also been implicated in the aging process because of its ability to produce free radicals in the form of ROS [45, 68, 73, 130, 131]. Mutations in the counterpart to yeast *SDHC* in *C. elegans*, known as *mev-1*, lead to a decreased lifespan and rapid aging [42, 132, 133]. This is relevant in light of accumulating evidence that Complex II with key SdhC or SdhB mutations, particularly those within or near the [3Fe-4S] center and the proximal quinone binding site, generates ROS that may lead to oxidative stress resulting in a shortened lifespan [45, 132, 134].

Complex II-associated tumorigenesis has been suggested to occur by multiple different mechanisms. First, a pseudo-hypoxic cellular response can be caused by increased succinate levels, which result from certain mutations in Complex II. Within the cell there is a heterodimeric hypoxia-inducible transcription factor (HIF1α, β) that is induced under conditions of low oxygen (hypoxia) in order to promote glycolysis when the oxidative phosphorylation system is less efficient. HIF1α also induces the growth of blood vessels to help transport oxygen to cells suffering from hypoxia [106]. Under normoxic (normal oxygen levels) conditions, HIF1α is hydroxylated by a prolyl hydroxylase (PHD) enzyme and inactivated or degraded. When Complex II is mutated, succinate may build up in the cell and inhibit PHD as succinate is

also a natural product of the hydroxylase, preventing PHD from hydroxylating HIF1α and effectively preventing HIF1α from undergoing the degradative processes [135]. Under these so-called pseudo-hypoxic conditions, with the cell unable to degrade HIF1α, the transcription factor is able to activate genes that are involved with angiogenesis, cell proliferation and survival, and glycolysis, likely promoting tumorigenesis and paraganglioma formation [45, 105, 135]. It has also been suggested that higher levels of ROS can inhibit PHD as well, leading to this pseudo-hypoxic response [106]. In addition, it has more recently been hypothesized that the production of ROS by Complex II may also have implications in the tumorigenic disease states linked directly with the complex [45, 105, 106, 127, 136].

Current work indicates that Complex II may also be a key mediator of apoptosis. The Grimm group has recently shown that decreased pH (intracellular acidification), which is generally an early apoptotic signal, triggers a separation between the catalytic and membrane dimers of Complex II [131, 137]. The separation of the heterodimers introduces a disconnect in the electron transfer pathway within the enzyme, separating the SDH and SQR activities and preventing electrons from succinate from completely passing to the final intracomplex acceptor, ubiquinone (**Figure 1.10**). Electrons are instead passed from the FAD molecule or the [Fe-S] centers to surrounding oxygen molecules, leading to the formation of ROS, which can then contribute to the induction of cellular apoptosis. This overall process, triggered by the sensitivity of Complex II to its surrounding pH, identifies the enzyme as an important apoptotic sensor and is consistent with previous findings that *SDHB*, *SDHC*, and *SDHD* act as tumor suppressor genes [131]. It is important to note, however, that if both enzymatic activities are blocked (SDH and SQR activities) increased levels of succinate would result due to lack of overall Complex II activity. Succinate can then be transported to the cytosol where it can influence the development

of a pseudo-hypoxic state that promotes glycolysis, which would allow total dysfunction of Complex II to contribute to tumor formation rather than apoptosis [138].

Even more recently, it has been proposed that ROS formation by Complex II is not only a major contributor to the overall ROS creation within mitochondria, but also "antithetically" depends on the concentration of succinate present in the cell [69]. First, succinate is necessary to begin the reduction of redox centers within Complex II that can then pass electrons to oxygen, forming ROS. In this way, an increase in succinate concentration would favor higher ROS production. On the other hand, succinate bound to the active site of Complex II prevents oxygen from accessing the FAD moiety that is thought to be the primary center of ROS formation, although the [Fe-S] centers and ubiquinone molecule are not excluded from contributing to ROS as well. In this respect, increasing succinate concentration would decrease the formation of ROS. Therefore, there exists an optimal succinate concentration for maximal ROS production by Complex II that would lead to apoptosis.

1.3. Lipids

As an integral component of biological membranes, phospholipids are intricately linked to the proper structure and function of membrane protein complexes and as such can be divided into categories based on location and function in relation to these complexes. The complement of lipids within the bilayer that are not in immediate contact with a particular membrane protein or complex are referred to as bulk lipids. Annular lipids are found at the surface of a membrane protein and provide a layer between the protein and the bulk bilayer lipids. They are thought to be important for inserting the protein within the bilayer and keeping it positioned correctly. Non-annular lipids, on the other hand, mediate the interaction and interfaces between subunits or

proteins making up a larger complex and can also act as cofactors to activate enzymes. They are able to seal spaces and gaps that could be caused by such interactions, maintaining electrical and other gradients across a particular bilayer [139].

In addition, lipids serve specific roles in the proper functioning of the mitochondria as a whole as well as its individual membrane proteins and complexes. As some examples, lipids influence respiratory chain complex activity, transport processes across the mitochondrial membranes including import and assembly of newly synthesized proteins, and osmotic and phase behaviors of mitochondrial membranes [4, 140]. It has even been found that PE is critical to the correct later-stage folding of the *E. coli* membrane protein lactose permease [141], as well as to the correct functioning of the translocase complex of the mitochondrial OM, the TOM complex [142]. Further, anionic phospholipids can act as organization sites for both soluble and integral membrane proteins and complexes [143]. In particular, the signature phospholipid of energy conserving membranes, CL, supports many, if not all, of the above listed mitochondrial protein complex functions. These include supporting OXPHOS, supporting the formation of cristae as well as allowing mitochondrial fission and fusion to occur, and acting as a mitochondrial membrane identifier, which is important for integrating various mitochondrial and cellular extra-mitochondrial processes [144, 145].

1.3.1. Cardiolipin Structure

CL is unique to energy-conserving membranes, including the IM of the mitochondria and bacterial plasma membranes. This lipid has a distinctive structure that includes two phosphatidylglycerol backbone fragments esterified to a central glycerol moiety, thus giving it four acyl chains and a double headgroup, in comparison with typical glycerophospholipids, which have two acyl chains and a single headgroup (**Figure 1.11**). Despite the fact that each

phosphate of CL has a titratable group, it has been supported that CL in fact has two p*K*a values, with pKa_1 < 4.0 and pKa_2 > 8.0, the second of which is a conformational p*K*a and is able to shift when titrated [146]. The shifting pKa_2 results from the intramolecular hydrogen bonding between the hydroxyl group of the central glycerol moiety and the phosphates from the surrounding headgroups, forming a bicyclic structure with both headgroup phosphates and the glycerol [147, 148]. This causes the headgroup to contain a single anionic charge at physiological pH due to a resonance effect that allows the anionic charge to be shared between both headgroups (**Figure 1.12**, left). CL is therefore referred to as an acid-anion at physiological pH because of this tight bicyclic headgroup structure. The resonance acid-anion structure is thought to allow CL to act as a proton buffer or proton sink that can then facilitate proton transfer from the bulk matrix to respiratory chain complexes, namely Complex III [40, 149]. Under certain conditions, it is even thought that acid-anion structures can occur between adjacent CL molecules as well, further facilitating the capacity of CL to act as a proton buffer [146]. In contrast, if the central glycerol hydroxyl group is removed, as in deoxyCL, or if the CL molecule contains asymmetrical acyl chains or is lacking one acyl chain, as in lysoCL, the resonance-stabilized headgroup is unable to form and CL displays two p*K*a values that are much closer together, pKa_1 = 1.8 and pKa_2 = 4.0 [148, 150], and more typical of phosphates within a glycerophospholipid. This view has been recently questioned, however, and it has been postulated that the acid-anion structure and divergent p*K*as of CL are an artifact of experimental design and CL does in fact contain two anionic charges at neutral pH, reopening the question of how CL truly exists at physiological pH [151].

It has also been demonstrated that CL is essential to the structure and function of various proteins and complexes within mammalian IMs [152, 153]. It is implicated in stabilizing the

structure of various respiratory chain complexes, has been crystallized with Complexes III and IV, and recent molecular dynamics simulations support the location of CL binding sites within Complex III and Complex IV as well [41, 139, 154, 155]. While it has traditionally never been shown to be important for eukaryotic Complex II, it has been crystallized with the *E. coli* SQR where it occupies space at the interface of the membrane subunits and is stabilized by hydrogen bonds with the enzyme [6]; it is common for CL to be located at such an interface between monomer subunits of a protein complex [156]. In addition, I have shown that reconstituted Complex II requires CL for stability and functionality (Chapter 3, [157]); therefore, CL may be more important for Complex II structural stability and activity than previously thought. Even more, CL has been implicated in the stability of respiratory chain supercomplexes, where it is again thought to stabilize the interaction between Complexes III and IV [10, 158-160]. These supercomplexes (respirasomes) constitute multiple respiratory chain complexes organized into a single larger complex to enhance efficiency of electron transport *via* substrate channeling [9, 18, 161, 162]. Further, CL is critical to the proper functionality of the ADP/ATP carrier as well as recruiting this protein carrier to regions of the IM where OXPHOS complexes are located in order to increase the efficiency of energy metabolism [163-165].

Due to its four acyl chains forming a bulky hydrophobic region, CL is referred to as an inverted conical lipid whose acyl chain cross-sectional area is larger than that of its headgroup region. This causes CL to be classified as an inverted-micellar or non-bilayer preferring lipid and to adapt a hexagonal (H_{II}) phase in the presence of divalent cations and low pH [166]. The preference for a H_{II} phase is in contrast to a major component of the IM, PC, which is a cylindrical phospholipid that favors a bilayer or lamellar conformation. The proportions of bilayer and non-bilayer lipids within a membrane are tightly controlled and it has even been

shown that non-bilayer lipids can alter the lateral pressure of the membrane and induce packing defects that may enable the insertion of membrane proteins [167]. CL tends to be found in areas of the mitochondrial membrane that are highly curved, such as the cristae membrane of the IM or membrane regions susceptible to fusion events [168, 169]. When there are mutations in any of the enzymes involved in the CL synthesis pathway, either eliminating CL or causing changes in the acyl-chain composition of the lipid, there are large changes in the ultrastructure of the IM, underscoring the importance of the non-bilayer propensity of CL in relation to overall mitochondrial structure. These results are further supported by findings that the acyl chain composition of CL affects H_{II} structure formation; longer acyl chains that are unsaturated are more likely to favor formation of the H_{II} phase [170, 171].

1.3.2. Cardiolipin and Divalent Cations

The propensity of CL to form a H_{II} phase is especially apparent in the presence of divalent cations, which are able to reduce the charge repulsion between negatively charged CL headgroups and further reduce the headgroup cross-sectional area [172]. Additionally, because the headgroup of CL is so small, it is unable to use conformational or orientation-based changes in this region to compensate for the added charge of the divalent cations [173]. In particular, CL is known to have a higher affinity for calcium (Ca^{2+}) ions as compared to magnesium (Mg^{2+}) and other divalent cations, making the presence of Ca^{2+} particularly effective at inducing the H_{II} phase of CL and therefore membrane structural alterations, which can allow membrane fusion [143, 172]. It has been shown that Ca^{2+} is able to induce these changes by effectively dehydrating and neutralizing CL headgroups, allowing them to pack more closely together, resulting in formation of a H_{II} structure. In contrast, Mg^{2+} and even barium (Ba^{2+}) are less able

to dehydrate CL structures and are more likely to form mixed lamellar and H_{II} structures of CL when present in solution [174].

1.3.3. Cardiolipin Biosynthesis

Due to its highly specialized structure, CL is synthesized by a unique biosynthetic pathway in the IM (**Figure 1.13**) [175]. First of all, CL is synthesized within the mitochondria, similar to phosphatidylethanolamine (PE) and phosphatidylglycerol (PG), other phospholipids found within both the OM and IM. Briefly, PG, an immediate precursor of CL, is synthesized from PA, cytidine-triphosphate (CTP), and glycerol-3-phosphate through a number of enzymatically catalyzed steps. Cardiolipin synthase (Crd1) then catalyzes a condensation reaction with PG and CDP-diacylglycerol to produce an immature form of CL. This form of CL is considered immature because it does not contain the canonical acyl chains that would be found within a typical CL molecule located in the IM. Instead, this immature version of CL typically contains four shorter (14 carbon), saturated acyl chains.

Immature CL then enters a remodeling cycle that begins with the removal, by a deacylase, of one of its acyl chains to produce monolysocardiolipin (MLCL). MLCL is then re-acylated by taffazin (Taz1) to produce a CL species with four acyl chains [176]. After multiple rounds through this remodeling cycle, mature CL with four longer (typically 16 or 18 carbons), unsaturated acyl chains that are symmetric about its chiral centers is produced and ready for full incorporation into the membrane. Of note, the final mature type of CL that is produced is both species and tissue specific, but is always symmetrical and structurally uniform [177]. The symmetrical nature fosters the ability of CL to exist as an acid-anion at physiological pH; it has been hypothesized that MLCL, which is asymmetrical due to having only three acyl chains, is

unable to produce the usual resonance-stabilized mature CL structure found at near neutral pH [150].

In addition, CL synthesis is linked with the synthesis of other phospholipids, such as its precursor PG, and when CL is not present OXPHOS function under stress conditions, such as high temperature, is greatly reduced [178-180]. In this way, CL behaves as a "stabilizer" of mitochondrial function [181]. While the essential activities of CL can be compensated by PG or PE (another non-bilayer favoring lipid) in some circumstances, they cannot entirely replace the function of CL, and if any combination of these lipids is not synthesized, more dire effects are seen, such as reduced mitochondrial membrane potential, which affects a number of mitochondrial processes including protein import [182-186]. It has also been shown that lack of either PE or CL has different effects on the respiratory chain, supporting the limited complementarity of these H_{II}-favoring phospholipids [187]. Further, when the *Taz1* gene is mutated leading to alterations in the biosynthesis and metabolism of CL, the X-linked disease Barth syndrome often results, which is characterized by defects in OXPHOS assembly and function, among others [188, 189].

1.4. Model membrane systems

Membrane proteins constitute roughly one third of any given proteome and are involved in a number of processes including transport, signal transduction, adhesion, and cell-to-cell communication, and are therefore popular candidates for therapeutic drug targets [190, 191]. Despite the importance of membrane proteins, they are poorly understood as compared to soluble membrane proteins. This is due to the fact that the use of traditional biochemical and biophysical experimental methods to study them is hindered because of their low expression

yields, insolubility (they tend to aggregate in aqueous solution), and formation of non-native structures after purification [190]. The development of model membrane systems has been instrumental in such experimentation by providing a near-native environment in which to study membrane proteins.

1.4.1. Detergents

Traditionally, detergents have been utilized to maintain membrane protein solubility in aqueous solutions or dispersions as they are similar in amphipathicity to phospholipids: both have polar and nonpolar regions. However, detergents generally have a more hydrophilic character than phospholipids, which allows them to be more soluble within aqueous solutions as compared to phospholipids alone [192]. In order for a detergent to shield a membrane protein from the aqueous phase and remove the protein from its native membrane bilayer, the concentration of detergent molecules in solution generally needs to be greater than the critical micelle concentration (CMC) of that particular detergent. The CMC is the concentration at which a detergent will spontaneously form micelles, or monolayer vesicles, in which the detergent hydrophobic tails are shielded within the core of the micelle and the more hydrophilic heads face the aqueous environment. The CMCs of ionic detergents can be up to 100 times greater than those for nonionic detergents because of the electrostatic repulsion between ionized headgroups that disfavors micellar formation [192]. In addition, ionic detergents tend to be more effective in breaking protein-protein or intra-protein interactions, whereas nonionic detergents tend to be used for disrupting lipid-protein interactions and solubilizing intact membrane proteins from their native bilayer [193]. At concentrations of detergent higher than the CMC, the detergent molecules are able to bind and incorporate into the bilayer and induce a lamellar-to-micellar phase transition as well as saturate and replace the lipid binding sites of the membrane

proteins so that they are solubilized by the detergent as opposed to being bound by the lipid membrane [192].

Detergent molecules are likely to form micelles, as opposed to the inverted hexagonal phase favored by many inverted cone-shaped lipids, due to the larger cross-sectional area of the detergent headgroup as opposed to the hydrophobic tail region. Detergents generally have one hydrophobic chain per headgroup in contrast to the two or four chains per headgroup that phospholipids generally contain. The increased number of tails per headgroup for phospholipids causes them to prefer a bilayer (if they are cylindrical in shape) or inverted hexagonal phase (if they are cone shaped), rather than a micellar phase (preferred by inverted cone-shaped detergents or lysophospholipids). In addition to forming structures dissimilar from phospholipid bilayers, monolayer detergent micelles tend to be irregular in shape as they are disorganized and can be compacted [194]; for these reasons, systems that more closely mimic native biological membranes as compared to detergents were developed to solubilize membrane proteins.

1.4.2. *Bicelles*

Bicelles, which are lipid bilayer discs that are "belted" by detergents or short-chain lipids, are one way in which membrane proteins can be studied in solution [195]. Bicelles are advantageous because they are amenable to spectroscopic approaches and are monodisperse, similar to detergent micelles, but they contain a much smaller amount of detergent and are bilayer-like in nature, providing them with characteristics more similar to bilayer vesicles [196]. Because short-chain lipids are required for bicelle structure, there is a limit on the type and variety of lipids that can be incorporated. In addition, even though it is presumed that limited short-chain lipids are incorporated into the planar bilayer of the bicelle, they may in fact partially localize there and affect activity or stability of incorporated proteins [196]. While suitable for

certain NMR studies, other model membrane systems may be more appropriate for different biochemical and biophysical studies.

1.4.3. Amphipols

Another way in which to solubilize membrane proteins is to use amphipathic polymers, known as amphipols, that have a variable number of hydrophobic and hydrophilic pendant groups that are able to wrap around membrane proteins and keep them soluble within solution by protecting their hydrophobic transmembrane regions [197]. Some groups believe that the polymers, such as styrene maleic acid (SMA), are able to destabilize membranes and form discs that encapsulate a membrane protein as well as surrounding lipids (**Figure 1.14**, [198-200]). They have comparable stability to liposomes and are favorable because they solubilize membrane proteins away from their native membranes without the use of detergents [199, 201]. In addition, amphipols are thought to stabilize and support native protein-protein folds and protein-lipid interactions to a better extent as compared to detergents [197].

Our group in collaboration with the Albert Laboratory at the University of Connecticut and the Watts Laboratory at the University of Oxford has used the SMA copolymer to show that it is capable not only of solubilizing membrane proteins, but of removing fully functional protein complexes directly from intact mitochondrial membranes [202]. We demonstrated that SMA is able to disrupt the membrane potential across the IM and remove not only membrane proteins and entire complexes, but also select lipids that are presumably tightly bound to the membrane proteins and required for function. A downside of using amphipathic polymers is that the lipid composition is restricted to that of the originating membrane used for membrane protein extraction and they are therefore not optimal systems in which to study protein-lipid interactions through direct experimental alteration of the lipid environment. In addition, the size of the discs

cannot be adjusted to regulate the formation of oligomeric states of the membrane protein of interest.

1.4.4. Liposomes

A predominant model membrane system used extensively by our laboratory and others is the liposome, which allows usually challenging membrane proteins to be studied in a more native and functional state [203]. Liposomes, vesicles of phospholipid bilayers that are formed through hydration of lipid mixtures and subsequent agitation or addition of energy (e.g. through sonication followed by an extrusion process), have been successfully used to study a wide range of membrane proteins including bacteriorhodopsin, respiratory cytochromes, and various ATPases [190, 204-207]. Liposomes have also been added to cell-free translation systems in order to provide a lipid bilayer environment in which translated membrane proteins, such as human stearoyl-CoA desaturase complex, connexin-43, and the ADP/ATP Carrier, can fold correctly [203, 208-213]. One benefit of using liposomes as a model membrane is their versatility in regards to lipid composition and size [214]. Liposomes are also advantageous because they contain distinct inner and outer compartments that can maintain ion gradients and encapsulate certain molecules on a single side to mimic the native state of a membrane protein [214]. However, in some cases, technical problems such as sample heterogeneity and light-scattering can plague spectroscopic-based approaches when working with liposomes, which led our laboratory to utilize a second model-membrane system in our studies as well.

1.4.5. Nanodiscs

More recently, a novel model membrane system, the nanodisc, has been developed that allows membrane proteins to be reconstituted in a native-like environment as homogeneous and monodisperse samples. Nanodiscs are discoidal phospholipid bilayers bound by a belt of

membrane scaffold proteins (MSPs) that self-assemble upon the removal of detergent from a solution of phospholipid and MSP [215-218]. They are beneficial not only because of their monodispersity as compared to liposomes, micelles, and polymer-stabilized bilayers, but also due to their stability over a wide range of temperatures, decreased light scattering, and better representation of lipid phase transitions within native membranes as compared to liposomes [190, 219]. In addition, they allow experimental access to both sides of the membrane bilayer, which can be beneficial in ligand-binding studies [215].

The membrane scaffolding protein (MSP) used to belt the nanodiscs was developed by the Sligar Laboratory through specific engineering of the human apolipoprotein, apoA-I, which is a high density lipoprotein (HDL) found in humans [220]. HDLs naturally bind free lipids and cholesterol throughout the body and transport them to the liver, a process known as reverse cholesterol transport [221]. It has been shown that lipid-bound apoA-I assumes not only a higher α-helical content, but also allows (or samples) only a limited number of conformations [190]. A pair of apoA-I proteins binds around the outside of the HDL particles in an antiparallel arrangement stabilized by salt bridges and proline stacking interactions [221]. When the lipid-to-apoA-I ratio is approximately 100-to-1, discoidal HDL particles tend to form, whereas when the ratio is higher, the particles tend to be more spheroidal in shape [190]. During nanodisc assembly it has been observed that altering the lipid-to-MSP ratio in the final assembly reactions influences the final size and shape of nanodisc particles as well [222]. When the amino-terminal globular domain comprised of 43 amino acids is removed from apoA-I it tends to have a higher α-helical content and adapt a more discoidal structure in solution, similar to how it would behave in the presence of lipids [215]. For this reason, the simplest MSP is structurally equivalent to the

remaining 200 carboxy-terminal amino acids of apoA-I once the 43 amino-terminal residues have been removed [190].

By engineering the MSP in this way, it is likely to form an amphipathic α-helical discoidal belt around phospholipids in solution, protecting the hydrophobic acyl chains from the surrounding aqueous solution. The 11- or 22-mer helices are broken up by proline and glycine residues in order to allow more flexibility and enable the MSP to form the belt-like discoidal shape [220]. Further, additional α-helices can be inserted into the MSP sequence to form scaffolding proteins of a particular length, which alter the diameter of the nanodiscs that are formed (**Figure 1.15**). For example, MSP1 is the smallest MSP construct, forming nanodiscs of approximately 9.5 nm in diameter, whereas MSP1E3 has three additional 22-amino acid α-helices inserted, forming a nanodisc of approximately 12.1 nm in diameter [223]. In addition, removing the most amino-terminal 11 residues on the MSP construct does not change the size of the nanodisc formed and they have been removed in many constructs; this is denoted as –D1; for example, as in MSP1D1 or MSP1E3D1 in the case of a construct with additional helices [217]. Based on extensive characterization (chemical crosslinking analyses, mass spectrometry, scintillation counting), it is postulated that two MSPs wrap around the circumference of each nanodisc, one above the other, protecting the hydrophobic chains of each monolayer within the bilayer, in what is termed the "belt" model (**Figure 1.15**, [216-218]). The MSPs are thought to be flexible both in solution and within the nanodisc structure causing the discs to be more dynamic, rather than static, structures [224].

A variety of membrane proteins and complexes of varying size have been reconstituted into nanodiscs, including bacteriorhodopsin, proteorhodopsin (a study on which our laboratory collaborated with the Birge group in the University of Connecticut Department of Chemistry),

cytochrome P450s, G-protein-coupled receptors, bacterial chemoreceptors, the mitochondrial voltage-dependent anion channel (VDAC-1), and the SecYEG complex [190, 223, 225-234]. While certain cytochrome *c* oxidases have also been incorporated into nanodiscs, our group was the first to incorporate a respiratory chain complex, Complex II, into nanodiscs directly from solubilized mitochondrial membranes ([235], Chapter 3). Our study, as well as a few other studies, including one focusing on phosphoinositide and another on bacterial chemoreceptor-PE dependence, have utilized the nanodisc platform to study protein-lipid interactions in more detail as the exact lipid content of the discs can be easily manipulated [236, 237]. Recently, nanodiscs have also been physisorbed to silicon surfaces and used in arrays to screen the interaction of soluble proteins or ligands with membrane proteins and are even being developed as drug delivery systems and in immune-protective responses [238-240].

1.5. Figures and Tables

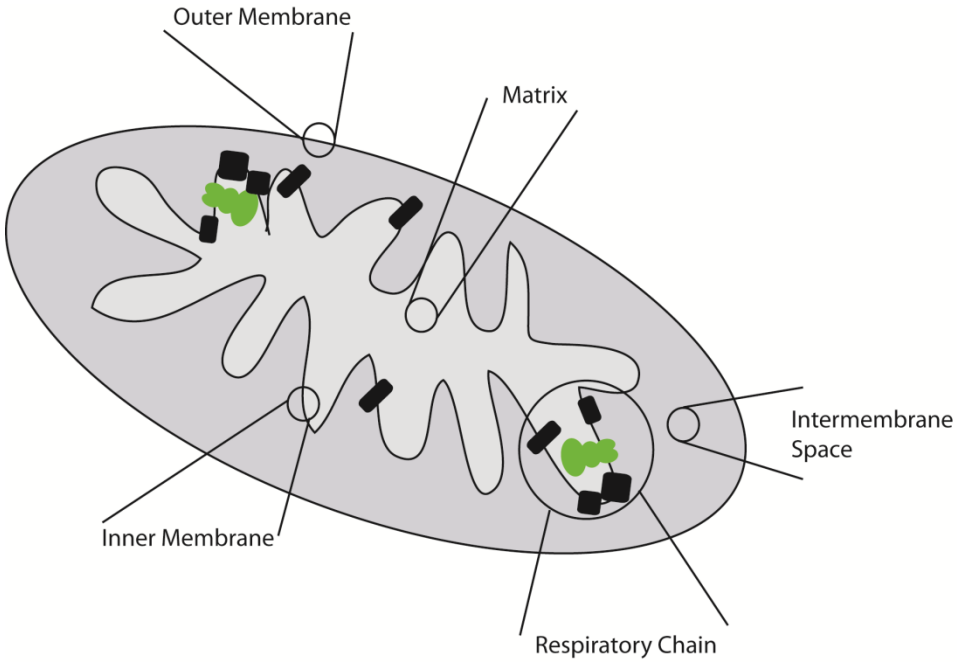

Figure 1.1. Schematic of mitochondrial compartments and membranes. Mitochondria are surrounded by two membranes, the outer and inner membranes (OM and IM, respectively), that enclose an aqueous matrix and are separated by an aqueous intermembrane space. The IM is the location of the respiratory chain complexes, including Complex II (green), which oxidizes succinate to fumarate within the matrix and passes the resulting electrons to the lipophilic electron carrier molecule, ubiquinone, located within the IM.

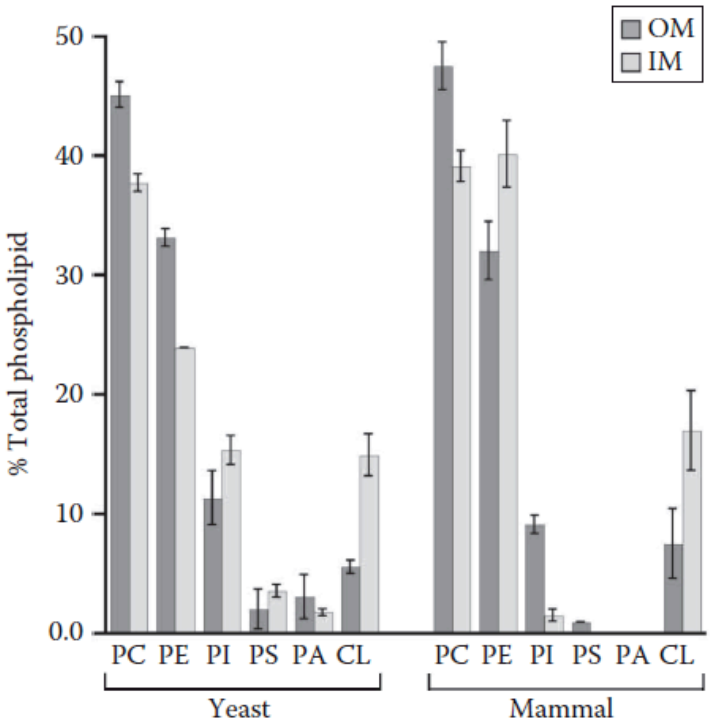

Figure 1.2. Comparison of yeast and mammalian mitochondrial OM and IM phospholipid compositions. PC and PE are the most prominent lipids in both the OM and IM bilayers of yeast and mammals, whereas CL is significantly more abundant in the IM of mitochondria from all eukaryotes [2].

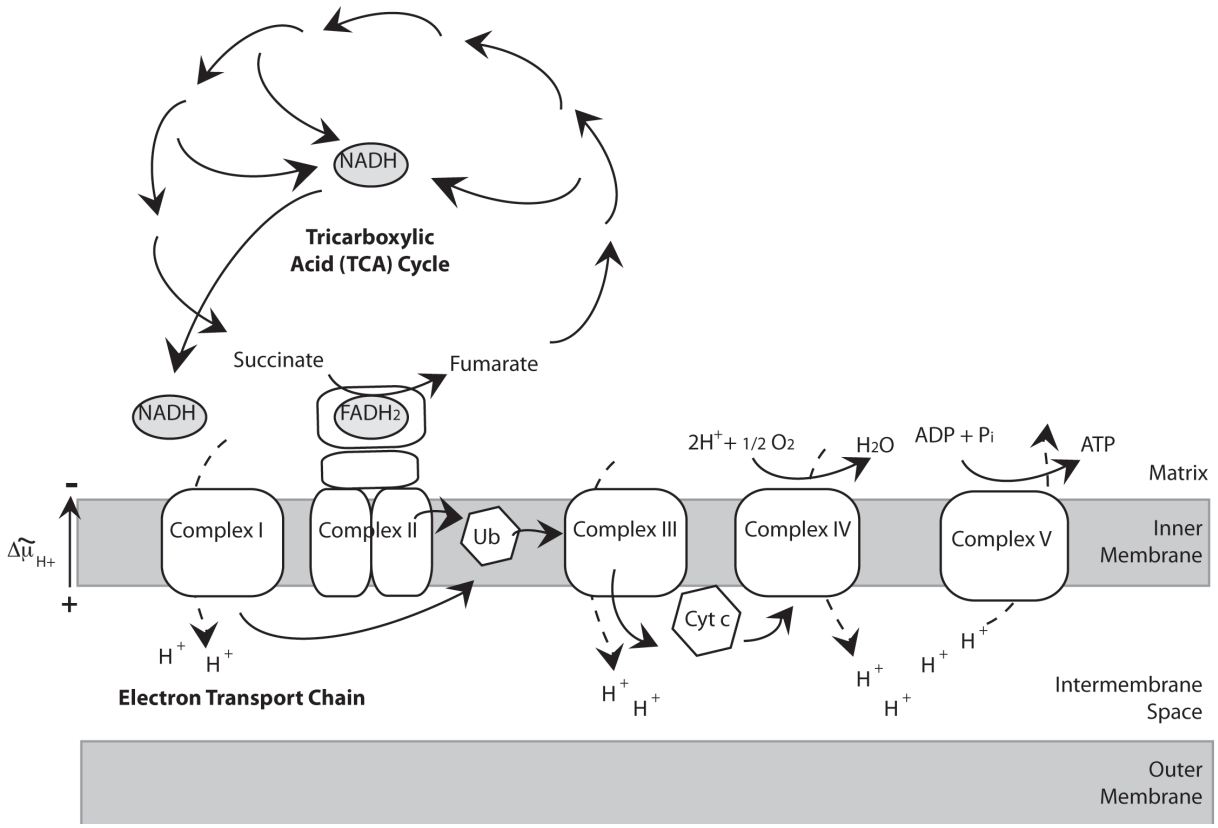

Figure 1.3. Schematic of the Tricarboxylic Acid Cycle and Electron Transport Chain within the Mitochondria. The Tricarboxylic Acid (TCA) Cycle within the matrix and the electron transport chain (ETC) within the IM are connected through Complex II activity, which couples succinate oxidation with the reduction of membrane-bound ubiquinone (Ub). In addition, NADH from the TCA Cycle is shuttled to Complex I (or NADH dehydrogenases in yeast) and these electrons are passed to Ub as well. Electrons from Ub are passed through Complex III to the intermembrane space-located cytochrome c (Cyt c), which then transports electrons to Complex IV, where oxygen is reduced to water. The energy generated from electron transport allows Complexes I, III, and IV to pump protons into the intermembrane space from the matrix, building up a proton gradient. The energy stored within this gradient is utilized by Complex V (ATP Synthase) in order to synthesize ATP from ADP and P_i in the matrix.

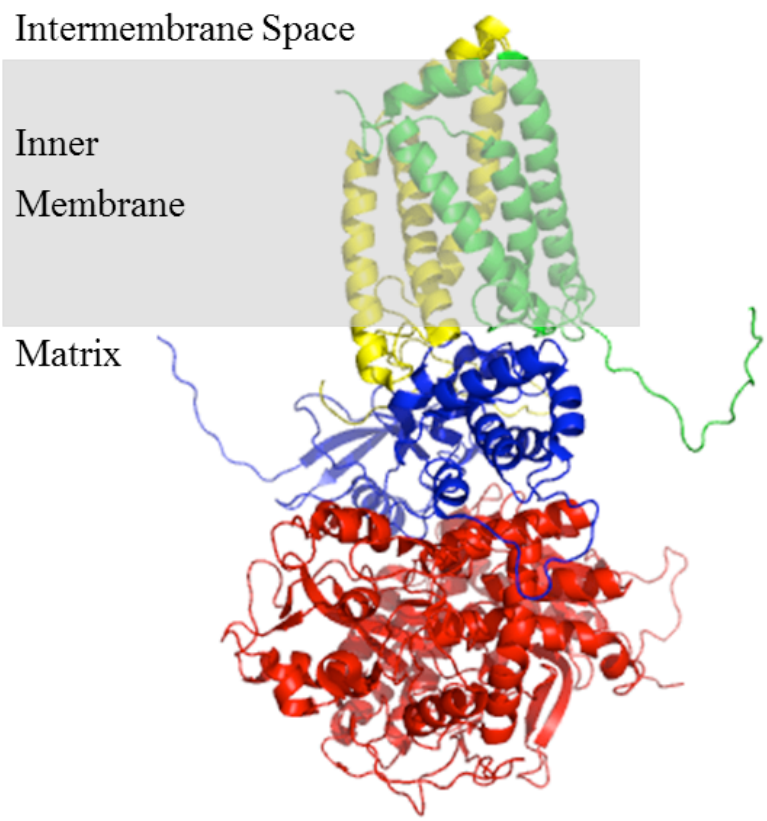

Figure 1.4. Homology model of yeast Complex II. The soluble catalytic dimer (succinate dehydrogenase subunit) consists of Sdh1p (red) and Sdh2p (blue). The membrane-embedded dimer is composed of Sdh3p (yellow) and Sdh4p (green). The model was developed using the Modeler6v2 program with templates from *E. coli* succinate dehydrogenase (PDB Structure 1NEK), *E. coli* fumarate reductase (PDB Structure 1LOV), and *W. succinogenes* fumarate reductase (PDB Structure 1QLA). Figure derived from PDB Structure 1PB4 in Swiss-PdbViewer 4.0.1 and [37].

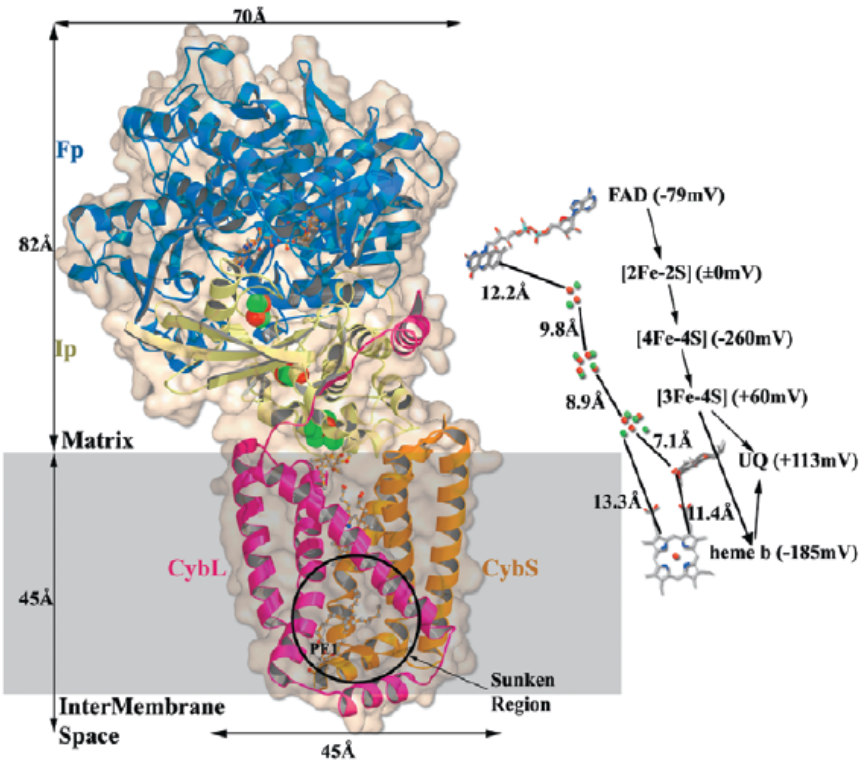

Figure 1.5. Crystal structure of porcine Complex II. The soluble catalytic dimer is represented by SdhA (Fp, blue) and SdhB (Ip, pale yellow) and the membrane-embedded dimer is composed of SdhC (CybL, magenta) and SdhD (CybS, orange), which are shown here within the IM (gray box). Redox centers are represented within the structure and are also aligned at the right side of the figure in order to more accurately portray the edge-to-edge distances (no more than 14 Å) between each of the redox centers within the linear chain. Figure adapted from [36].

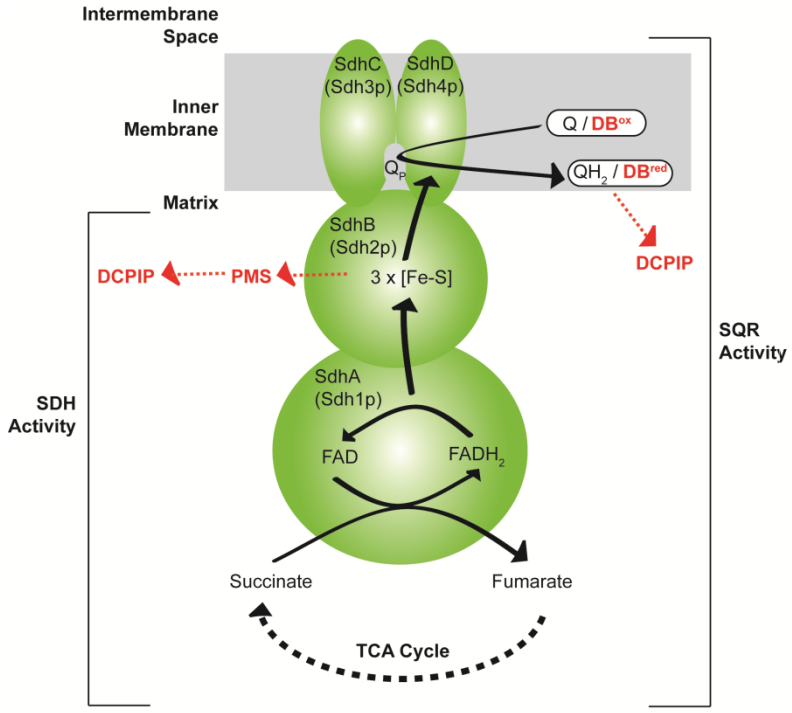

Figure 1.6. Schematic of separable *in vitro* Complex II activities. Succinate dehydrogenase (SDH) activity reflects the presence of an active catalytic dimer only. The electron pathway begins with succinate passing electrons to FAD as it is oxidized, which then passes these electrons through three [Fe-S] centers. Instead of making their way to the ubiquinone (Q) within the membrane, the *in vitro* assay includes the redox mediator phenazine methosulfate (PMS), which takes electrons from the [Fe-S] clusters and then passes them to the artificial electron acceptor, DCPIP. Succinate: ubiquinone oxidoreductase (SQR) activity reflects the presence of a functional holoenzyme. Electrons from succinate are passed through FAD, the three [Fe-S] centers, then to a ubiquinone analog (decylubiquinone, DB), and finally to the artificial electron acceptor, DCPIP. DCPIP reduction in both assays is monitored spectroscopically as an extinction in absorbance at 600 nm. Figure adapted from [157].

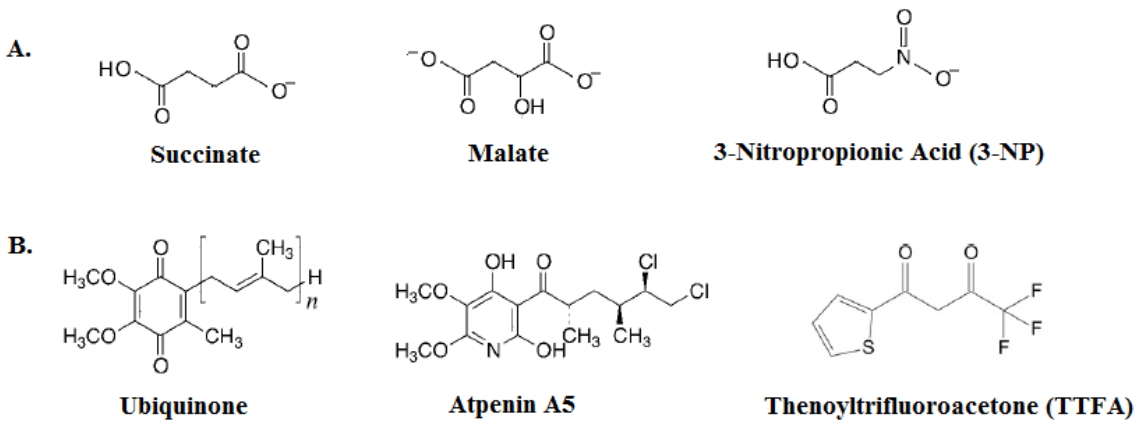

Figure 1.7. Chemical structures of Complex II inhibitors and native substrates. A selection of examples of Complex II inhibitors and structural comparison to those of native Complex II substrates. (**A**) Substrates and inhibitors of the SdhA catalytic site. From left to right, succinate, its substrate, malate, a TCA Cycle intermediate that also acts as an inhibitor, and 3-nitropropionic acid (3-NP), another inhibitor. (B) Substrates and inhibitors of the membrane subunit ubiquinone binding site. From left to right, ubiquinone, its natural substrate, and two inhibitors, atpenin A5 and thenoyltrifluoroacetone (TTFA). Figure adapted from [68, 71].

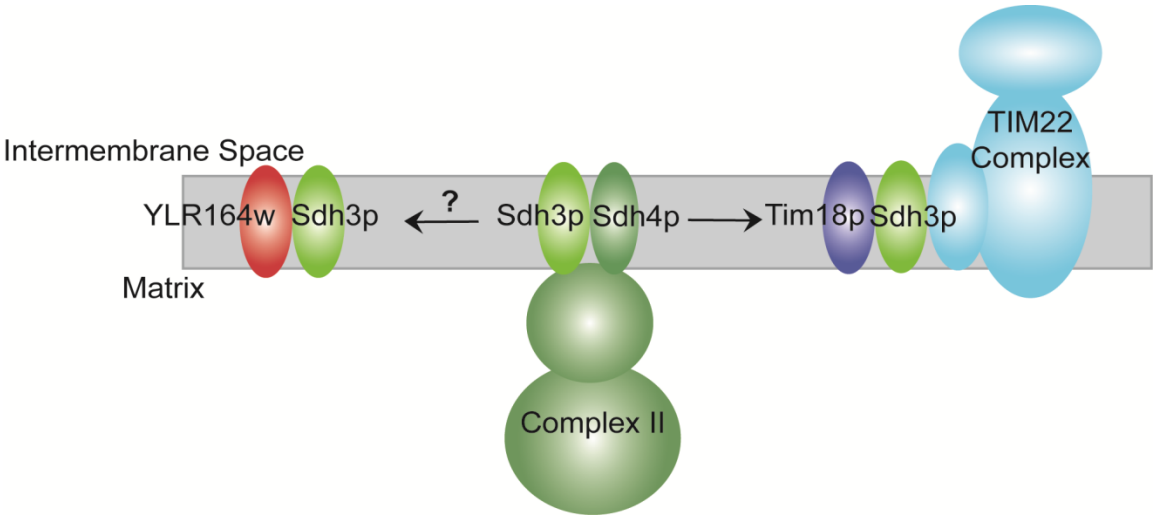

1.8. Experimentally determined and hypothesized interactions of Complex II membrane subunits and their homologs. It has been found in yeast that the Sdh4p membrane subunit of Complex II has multiple homologs, including Tim18p, part of the TIM22 (Translocase of the Inner Mitochondrial Membrane) Complex, and YLR164w, an open reading frame of unknown function. Recent experimental evidence supports that Sdh3p is able to interact with Tim18p and is necessary for the proper integration of Tim18p into the TIM22 Complex. Figure adapted from [96].

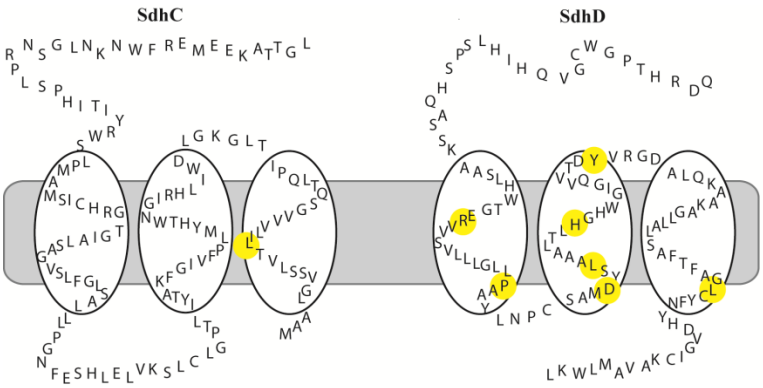

	Porcine	Human	Yeast
SdhC	L130P	L158P	F187
SdhD	R35G	R70G	K73
	P46L	P81L	T84
	D57Y	D92Y	D98
	L60P	L95P	F101
	H67L	H102L	Y108
	Y79C	Y114C	Y120
	L104P	L139P	I148

Figure 1.9. Clinically identified mutations within the membrane subunits of Complex II.

On the left, a schematic of the porcine membrane subunits, SdhC and SdhD, with homologous residues to the clinically identified mutations in humans noted by the yellow highlighted circles. On the right, a comparison table of these mutations and the homologous residues among human, porcine, and yeast membrane subunits.

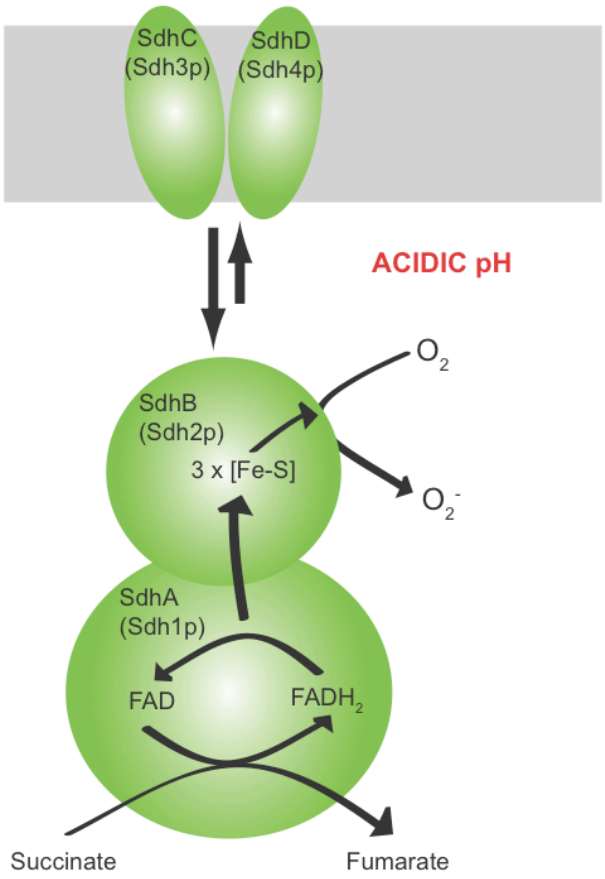

Figure 1.10. Schematic of the detachment of the catalytic dimer from the membrane dimer and the resulting potential for ROS production. When a decrease in the pH of the surrounding environment occurs, the soluble catalytic dimer (SDH) can detach from the membrane dimer of Complex II, causing a dissociation of the SDH and SQR activities. Electrons from the oxidation of succinate can no longer be passed through the entire redox chain within Complex II to membrane-bound ubiquinone and instead are passed to matrix oxygen species, forming ROS. Figure adapted from [131, 157].

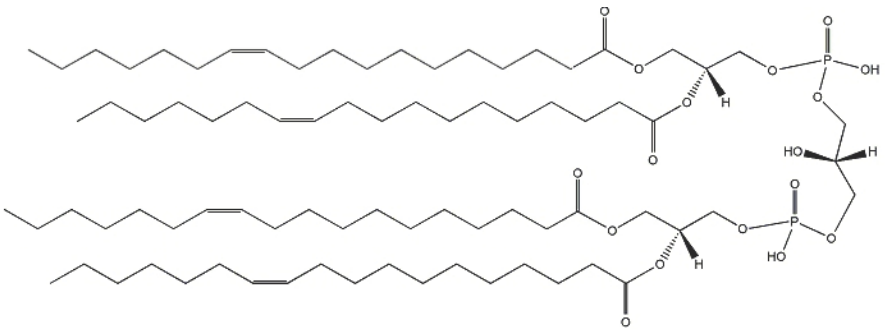

Figure 1.11. Chemical structure of 1',3'-bis[1,2-dioleoyl-*sn*-glycero-3-phospho]-*sn*-glycerol or tetraoleoylcardiolipin (TOCL). This particular form of CL is termed tetraoleoyl-CL, which has four acyl chains that are each 18:1(9*Z*). Figure adapted from [157].

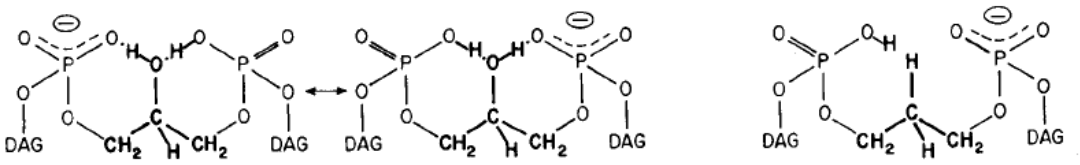

Cardiolipin **deoxy-Cardiolipin**

Figure 1.12. Resonance effect of CL compared to its deoxy-analog. When the hydroxyl group is removed from the central glycerol moiety of CL, the ability to form an acid anion structure due to resonance is abolished. In this way, deoxyCL has two similar p*K*as, while CL has two disparate ones, the second of which is a shifting p*K*a that causes CL to hold a single anionic charge at physiological pH. Figure adapted from [148].

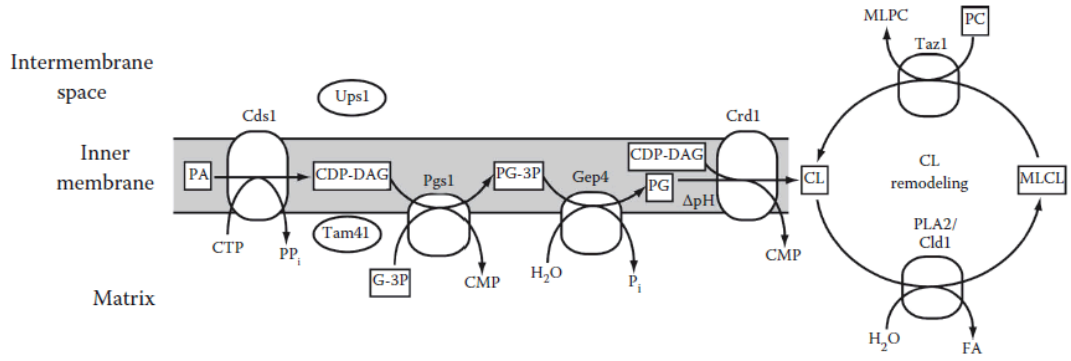

Figure 1.13. CL biosynthesis pathway. CL is synthesized from phosphatidic acid (PA) through multiple enzymatically-catalyzed steps within the IM of the mitochondria. After synthesis from its immediate precursor, phosphatidylglycerol (PG), CL undergoes a cyclic remodeling process consisting of multiple deacylation and reacylation reactions, finally resulting in a mature CL with four symmetrical, unsaturated acyl chains. Figure adapted from [2].

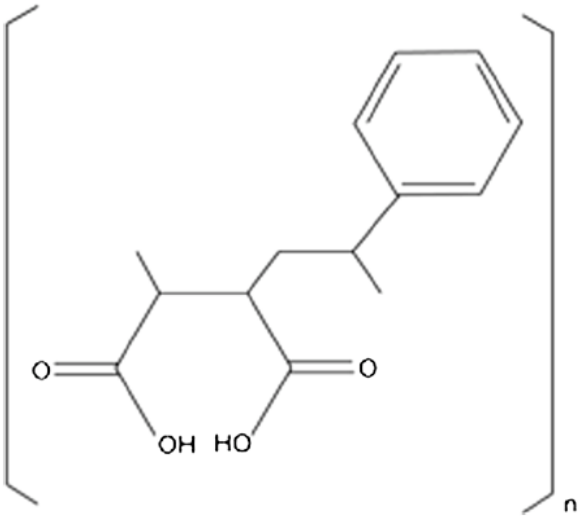

Figure 1.14. SMA copolymer structure. The SMA copolymer is composed of styrene (hydrophobic) and maleic acid (hydrophilic) groups, which lends it an amphipathic nature allowing it to shield lipid bilayers from aqueous environments. Figure adapted from [202].

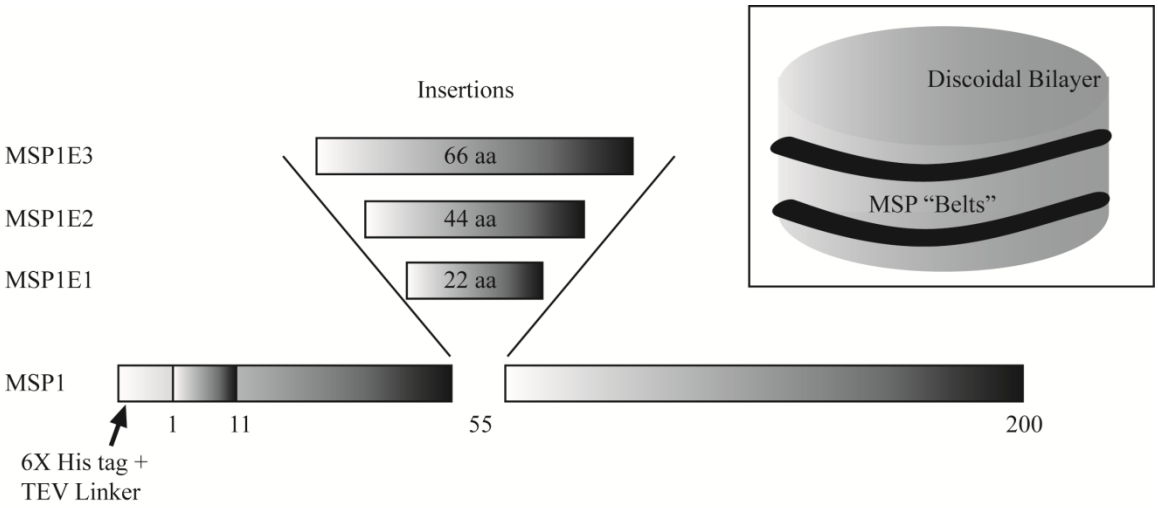

Figure 1.15. Membrane scaffolding protein (MSP) design and structure within nanodiscs. MSP1 is the simplest design for MSP, with a hexa-histidine tag separated by a TEV cleavage site linker from the N-terminus of MSP. If an increasing number of 22-amino acid amphipathic α-helical segments are added into the MSP1 sequence to increase its length (MSP1E1-E3), the diameter of the nanodiscs formed is increased. Two copies of the MSP act as belts, one above the other, encircling the circumference of the discoidal lipid bilayer to form a nanodisc particle (inset).

Chapter 2

Materials and Methods

2.1. Materials

Chemicals were obtained from Sigma Aldrich (St. Louis, MO) or Thermo Fisher Scientific, Inc. (Pittsburg, PA). All lipids were purchased from Avanti Polar Lipids (Alabaster, AL) as stocks in chloroform. Fluorescent probes, 4,4-difluoro-5,7-dimethyl-4-bora-3a,4a-diaza-*s*-indacene-3-propionic acid (BODIPY-FL); 6-((4,4-difluoro-1,3-dimethyl-5-(4-methoxyphenyl)-4-bora-3a,4a-diaza-*s*-indacene-2-propionyl)amino)hexanoic acid (BODIPY-TMR); 1,6-diphenyl-1,3,5-hexatriene (DPH); 6-dodecanoyl-2-dimethylaminonaphthalene (Laurdan); and 7-nitrobenz-2-oxa-1,3-diazole (NBD) were obtained from Molecular Probes, Inc. (Eugene, OR).

2.2 Methods

2.2.1. Mitochondria Solubilization

Mitochondria isolated from *Saccharomyces cerevisiae* (strain D273-10B) as previously described [241] were solubilized in buffer (50 mM potassium phosphate [pH 7.4], 50 mM KCl) with DDM at a final detergent : mitochondrial protein ratio of 1.5g : 1.0g (~3% [w/v] DDM). Mitochondria were incubated at RT for 25 min and then subjected to a clarifying centrifugation step to remove non-solubilized membranes. Supernatant containing solubilized mitochondrial IM proteins was taken for use in Nanodisc (ND) assemblies.

2.2.2. Lipid Preparation

Lipid stocks (DMPC or POPC), POPC/POPE lipid mix (50:50 mol%; 70:30 mol%), POPC/POPE/DMPC (40:40:20 mol%), POPC/POPE/POPG lipid mix (40:40:20 mol%), biomimetic lipid mix (POPC, POPE, and CL in 40:40:20 mol%), or CL-derivative lipid mix (POPC, POPE, and dTOCL or MLCL in 40:40:20 mol%) in chloroform were dried under a N_2 stream and desiccated under vacuum overnight to remove all traces of organic solvent, as

described [230]. For use in liposome preparation, lipid was reconstituted in Hydration Buffer (10 mM Tris-HCl [pH 7.5], 100 mM NaCl) at RT (above T_m) and allowed to sit with intermittent vortexing for approximately 15 min at RT. For pH-alteration experiments Glycine Hydration Buffer (50 mM Glycine [pH 3.0 or pH 9.0], 100 mM NaCl) was used in place of Hydration Buffer; for membrane subunit assembly experiments, Hydration Buffer with 2 mM $MgCl_2$ was used. Lipids were then extruded through either 0.1 μm or 0.4 μm membranes 17 times to form small or large unilamellar vesicles (SUVs or LUVs), respectively. For use in nanodisc preparations, lipid was reconstituted in MSP buffer (20 mM Tris-HCl [pH 7.4], 100 mM NaCl, 0.5 mM EDTA) with 59 mM sodium cholate and bath sonicated until all lipid was completely in solution.

2.2.3. In vitro Translation System

Wheat germ system master mixes utilized for *in vitro* translations of Complex II membrane subunits were assembled as in [242]. Co-translational incorporation of the membrane subunits into liposomes (100 nm, SUVs) was completed by adding 0.25 mg SUVs with and without CL to the wheat germ translation mixes. Briefly, translation buffer (20 mM HEPES [pH 7.5], 100 mM potassium acetate, 3 mM magnesium acetate), 1 mM DTT, 200 mM spermidine, 8 mM S-adenosyl-methionine, protease inhibitor cocktail, RNase inhibitor, amino acid mixtures, wheat germ, and appropriate mRNA were incubated at RT for 40 min. To radioactively label the membrane subunits, ^{35}S-Methionine (0.0788 μCi) was added to the master mix and an amino acid mixture lacking methionine was used.

2.2.4. Nanodisc Assembly

Membrane Scaffolding Protein (MSP1E3D1) was synthesized and purified as described [223]. Lipid, MSP1E3D1 (in lipid: MSP1E3D1 ratios of 122:1 [DMPC], 108:1 [POPC], 140:1

[POPC/POPE], 143:1 [POPC/POPE/POPG], and 143:1 [biomimetic]), DDM-solubilized mitochondria, and MSP buffer ([cholate]=14.8 mM) were incubated at RT for 30 min. Pre-hydrated Bio-Beads SM Hydrophobic Interaction Adsorbent (Bio-Rad Laboratories, Inc., Hercules, CA) were added and rotated for 2 hrs at RT to remove detergent and allow ND self-assembly to proceed. Following bead removal and incubation with Ni-NTA agarose, samples were subjected to step gradients of MSP buffer and imidazole (up to 400 mM) to isolate NDs with His-tagged MSP. The first two elution samples were combined (E*), dialyzed into MSP buffer to remove imidazole and concentrated in Centricon 3000 MWCO tubes in an Eppendorf Centrifuge 5804R.

2.2.5. SDS-PAGE and Immunoblot Analysis

12.5% or 15% SDS-PAGE gels in a Bio-Rad Mini-PROTEAN® system were run at 150 V for approximately 1 hour. To detect the presence of FAD, NBD, or BODIPY, gels were scanned on a Bio-Rad Pharos FX Plus Molecular Imager with External Lasers using Quantity One software (version 4.6.9) under the FITC fluorescent setting (488 nm laser, 530 nm emission filter). For these gels, the high MW band represents Sdh1p-FAD and the lower-migrating bands represent unrelated mitochondrial flavoproteins [104]. The presence of FAD was considered an indicator for the presence of the catalytic dimer [157]. The same gel was subsequently stained with Coomassie blue.

Immunoblots were conducted with primary antibodies against Sdh1p (αSdh1p, a generous gift of Dr. Bernard Lemire) and Sdh3p (αSdh3p, custom made, Pacific Immunology) with Amersham ECL Plex Cy5-conjugated secondary antibody. Blots were scanned on the Bio-Rad Imager under the Cy5 fluorescent setting (635 nm laser, 695 nm emission filter). To detect radioactively-labeled Complex II membrane subunits, the gels were first incubated in destain

(50% (v/v) methanol and 10% (v/v) acetic acid) twice for 5 min each, incubated once in dH_2O for 10 min, and dried onto filter paper in a Bio-Rad Model 583 Gel Dryer for 40 min. The dried gel was placed in a Bio-Rad Exposure Cassette-K under a General Purpose Kodak Storage Phosphor Screen overnight and scanned on the Bio-Rad Imager under the Radioisotopes- K-screen setting (532 nm laser, 390 nm emission filter, low sample intensity).

2.2.6. Fluorescence Specifications

Steady-state fluorescence measurements were completed in a Spex Fluorolog 3-22 photon counting spectrofluorometer (HORIBA Jobin Yvon) equipped with photon-counting electronics, double-grating excitation and emission monochromators, and a 450-W xenon lamp using the FluorEssence software program. All measurements were completed at RT in quartz microcuvettes. In all cases, fluorescent samples were measured in parallel with blank samples (lacking the dye but otherwise identical to the fluorescent sample) used to obtain the emission originating from the probe by subtraction.

Chapter 3

The Stability and Activity of Respiratory Complex II is Cardiolipin-Dependent

Derived from: Schwall C.T., Greenwood V.L., and Alder N.N., The stability and activity of respiratory Complex II is cardiolipin-dependent, *Biochimica et Biophysica Acta: Bioenergetics*, 1817 (2012), 1588-1596.

3.1. Abstract

Respiratory Complex II of the mitochondrial inner membrane serves as a link between the tricarboxylic acid (TCA) cycle and the electron transport chain (ETC). Complex II dysfunction has been implicated in a wide range of heritable mitochondrial diseases, including cancer, by a mechanism that likely involves the production of reactive oxygen species (ROS). Many studies have focused on the effects of individual SDH mutations; however, the potential role that lipids may play in Complex II activity is unknown. To address this issue, we have reconstituted Complex II into nanoscale model membrane particles, termed nanodiscs (NDs), with defined lipid compositions. In the present report, we demonstrate for the first time that a native-like IM lipid composition, specifically the presence of cardiolipin, is critical for the optimal stability and enzymatic activity of the complex, as well as in the curtailment of ROS production.

3.2. Materials and Methods

For Materials, Mitochondria Solubilization, Lipid Preparation, Nanodisc Assembly, and SDS-PAGE and Immunoblot Analysis details, please see Chapter 2.

3.2.1. Size Exclusion Chromatography

A GE Healthcare ÄKTApurifier system with a Superdex 200 10/300 GL column was used for gel filtration chromatography, monitoring absorbance at 280 nm. The following standards with previously reported Stokes diameters [243] were used to calibrate the column: blue dextran (8.3 mL), β-amylase (12.2 mL, 7.4 nm), alcohol dehydrogenase (13.5 mL), BSA (14.3 mL, 6.58 nm), carbonic anhydrase (16.7 mL, 4.0 nm) and cytochrome c (18.1 mL, 3.76 nm).

3.2.2. Electron Microscopy

ND samples containing a biomimetic blend of lipids only (empty) and those containing mitochondrial membrane proteins (loaded) were imaged by negative staining (uranyl acetate) transmission electron microscopy after 100X dilution in ddH2O. Images were collected at 180,000X magnification on a Tecnai Biotwin G2 Spirit transmission electron microscope.

*3.2.3. Complex II Activity Assays (**Figure 3.1**)*

Assays were conducted as previously described [66] on an Amersham Biosciences Ultrospec 2100 pro UV/Vis Spectrophotometer in 1 cm quartz cuvettes following the extinction of DCPIP absorbance (ε_{600} = 20.7 $mM^{-1}cm^{-1}$). Intact mitochondria were isolated as described [241] from *S. cerevisiae* wild type strain (D273-10B) or from *S. cerevisiae* deletion mutant YKO strain *Δcrd1* (Open Biosystems), which lacks the cardiolipin synthase gene *CRD1*.

3.2.3.1. Succinate Dehydrogenase (SDH) Activity (PMS-mediated)

Master mix (50 mM Tris [pH 7.5], 5 mM Succinate [pH 7.5], 0.5 mM dichlorophenolindophenol [DCPIP], 0.1 mM phenazine methosulfate [PMS]) was added to the sample and incubated for 10 min prior to measurements.

3.2.3.2. Succinate: Quinone Oxidoreductase (SQR) Activity (DB-mediated)

Samples were pre-incubated with 10 μM decylubiquinone (DB) before adding master mix (50 mM KPO4 [pH 7.5], 1 mM EDTA, 62 μM DCPIP) and 0 to 20 mM K-Succinate [pH 7.5] prior to measurements. Where indicated, samples were pre-incubated with 2.5 mM thenoyltrifluoroacetone (TTFA) inhibitor for 5 min prior to DB incubation. DCPIP reduction was monitored over the linear range (30 s for all ND and **Table 3.1** values; 20 s for temperature-sensitivity experiments with intact mitochondria).

3.2.4. FAD Quantification

Analyses were performed with commercially available kits (BioVision, Inc.) following manufacturer's instructions. Briefly, isolated mitochondria and ND samples from each lipid type were resuspended in Assay Buffer containing NP-40 detergent (BioVision FAD Assay Kit) and centrifuged to remove insoluble material. Samples were then deproteinized by perchloric acid precipitation (BioVision Deproteinizing Sample Prep Kit) and the resulting sample was used to determine the quantity of FAD. A colorimetric assay was used to determine amount of FAD by adding FAD standards or the sample to a mixture of Assay Buffer, the OxiRed Probe, and Enzyme Mix from the FAD Assay Kit. Absorbance was read at 570 nm and the reaction was linear with time to an absorbance of 1.8. These values were used to determine the FAD content of samples utilized for SQR activity assay analysis (represented as μmol DCPIP reduced min^{-1} μmol FAD^{-1}). Specific SQR activities for intact mitochondria (**Table 3.1**) were consistent with published values [e.g. 244].

3.2.5. ROS Production Assay

Analyses were performed using the MitoSOX assay kit (Invitrogen Molecular Probes) following manufacturer's instructions. Briefly, ND samples from each lipid type were pre-incubated with 10 μM DB, mixed with 16 mM K-Succinate and 10 μM MitoSOX reagent and incubated for 10 min at RT and added to 10 μg salmon testes DNA. Where indicated, samples were pre-incubated with 2.5 mM TTFA for 5 min. Fluorescence emission spectra were measured for each sample pre- and post-DNA addition (λ_{ex} = 510 nm, λ_{em} = 530-630 nm, 1 sec integration time, 4 nm slit widths).

3.2.6. Data Representation and Statistical Analysis

SDS-PAGE gels, immunoblot gels, SEC elution profiles, and kinetic analyses are representative of at least three independent experiments. SQR activity is represented as % change (compared to Biomimetic ND elution (E*) fractions) in DCPIP absorbance over the initial 30 sec time period divided by the initial absorbance. SDH activity is represented as total % change in DCPIP absorbance compared to Biomimetic ND elution (E*) fractions, as with SQR activity. Fluorescence values for ROS production are represented as background corrected (empty ND samples) intensities that are normalized according to the highest emission intensity for that data set and summed to determine the total area under each curve, which were then relativized according to the lipid-type of maximum value, POPC. The results presented for the cytochrome spectra, kinetic analysis, activity assays, and ROS production assay are shown as means ± standard errors of the means (s.e.m.) of at least three independent experiments. A two-tailed student T-test (equal variance) was used to determine statistical significance ($p \leq 0.1$ or $p \leq 0.01$) for activity assay and ROS production assay measurements.

3.3. Results and Discussion

3.3.1. Reconstitution of Complex II from Isolated Mitochondria into NDs

Traditional means of ND reconstitution originate with a single overexpressed membrane protein or biomembrane whose protein content consists mostly of a single protein or complex. In this report, we have optimized the procedure for reconstituting the entire complement of membrane proteins solubilized from mitochondria into NDs, showing that: (i) a single complex (Complex II in this case) could be reconstituted in an active state with sufficient yield to accurately measure enzymatic activity among the population of reconstituted proteins, and (ii)

the effect of lipids on the assembly and activity of Complex II could be assayed by synthesizing NDs with different lipid combinations.

By this process, detergent-solubilized membrane proteins from mitochondria isolated from yeast (*S. cerevisiae*) were reconstituted into NDs of a defined lipid composition and the preparations were isolated by affinity chromatography and exchanged into a buffer compatible with our analyses (**Figure 3.2A**). To recapitulate the native IM, we assembled NDs with a biomimetic blend of lipids that included POPC (16:0/18:1), POPE (16:0/18:1) and 18:1 CL in molar ratios of 40:40:20, respectively. Based on size exclusion chromatography, empty NDs prepared without mitochondrial proteins (**Figure 3.2B**, black trace) had a Stokes diameter consistent with the published value of ~12nm for this MSP [217]. By comparison, NDs assembled with mitochondrial membrane proteins were larger and had a broader hydrodynamic size distribution (**Figure 3.2B**, red trace). The reconstitution of membrane proteins into affinity column-purified NDs was further confirmed by gel analysis of total protein content (**Figure 3.3A**) and characteristic cytochrome absorbance spectra (**Figure 3.3B**). Transmission electron micrographs showed that both empty NDs and those containing membrane proteins yielded particles with homogeneous MSP-limited diameters (**Figure 3.2C**), confirming proper ND assembly.

To assay for the successful reconstitution of intact Complex II within NDs specifically, we conducted gel analysis of all affinity chromatography fractions and found that Complex II subunits co-eluted with the scaffolding protein at high imidazole concentrations (**Figure 3.2D**). To confirm that Complex II retention on the column was indeed ND-dependent, we performed mock assembly reactions in the absence of MSP and found that Complex II subunits eluted in the flow through (**Figure 3.4**). To confirm that Complex II reconstituted into NDs retained SQR

enzymatic activity, we measured the succinate-dependent, decylubiquinone (DB)-mediated reduction of dichlorophenolindophenol (DCPIP) for both detergent-solubilized mitochondrial membranes and ND preparations (**Figure 3.2E**). While both preparations showed saturation kinetics with comparable K_m values, we found that Complex II in NDs had a maximal reaction velocity that was ~30 times that of complexes in detergent. We conclude that we have reconstituted fully-assembled and catalytically competent Complex II holoenzymes directly from mitochondrial membranes into NDs.

3.3.2. CL Promotes Complex II Stability

Having optimized the procedures for reconstituting mitochondrial complexes into NDs, we had an excellent experimental platform for testing the influence of lipid composition on the stability and activity of Complex II. Hence, we performed ND assembly reactions with the following phospholipid compositions (**Figure 3.5**): (i) DMPC (14:0/14:0) only, (ii) POPC (16:0/18:1) only, (iii) POPC (16:0/18:1) and POPE (16:0/18:1) in a 50:50 molar ratio and (iv) POPC, POPE and CL in a 40:40:20 molar ratio ("biomimetic," described above).

To assay the effects of these lipid compositions on Complex II stability, we adapted our affinity column purification strategy to test for the association of the Sdh1p/Sdh2p soluble catalytic dimer with the Sdh3p/Sdh4p membrane-bound subunits (**Figure 3.6**). With each of the four different lipid compositions, most of the Complex II membrane subunits (based on αSdh3p immunoblots) were stably incorporated into NDs (*i.e.* appearing in the elution fractions, **Figure 3.6**, lanes 9-10), and very little appeared free in earlier fractions. In contrast, whereas the soluble dimer (based on FAD fluorescence) was stably associated with NDs containing a biomimetic lipid composition (**Figure 3.6**, lanes 9-10), a large percentage of the flavoprotein remained

unbound (*i.e.* appeared in wash steps, **Figure 3.6**, lanes 3-7) for all other preparations. We therefore conclude that the biomimetic lipid composition stabilized the interaction between the membrane and soluble subunits. The destabilizing effect was observed when NDs were prepared with short chain lipids (DMPC only), with longer chain, monounsaturated lipids (POPC only) and with lipid combinations that included non-bilayer (H_{II} phase) preferring lipids in amounts consistent with the mitochondrial IM (POPC and POPE). Among our four lipid combinations, the ternary biomimetic composition uniquely contained CL; we thus conclude that the presence of CL in the bilayer stabilized the interaction between membrane bound subunits and the catalytic dimer.

3.3.3. CL is Essential for Optimal Complex II Enzymatic Activity

We then measured the catalytic activity of Complex II reconstituted into NDs with the same four lipid compositions as above (**Figure 3.7**). As described, SQR activity, assayed by electron transfer from succinate to DCPIP *via* the ubiquinone (Q) analog DB, requires an intact holocomplex; SDH activity, assayed by electron transfer from succinate to DCPIP *via* the redox mediator PMS, requires only a stable catalytic dimer (**Figure 3.1**). SQR activity time course measurements revealed that complexes reconstituted with biomimetic lipids had robust electron transport rates from succinate to the membrane-bound electron carrier, whereas the transport rates of complexes reconstituted with all other lipid compositions were extremely low (**Figure 3.7A**, compare solid blue trace with all other traces). As expected, the negative control sample (mock assembly in the absence of MSP) showed no SQR activity (**Figure 3.7A**, blue dashed line). Notably, the potent inhibitor TTFA, which blocks electron flow by binding at the Q site,

reduced our measured rates of catalysis by ~83% (**Figure 3.7A**, blue dotted line), confirming that we were monitoring genuine Complex II SQR activity.

In addition, we performed a comprehensive analysis of SDH and SQR activities of all fractions from the affinity chromatography steps. The relative SQR activities were clearly highest in the elution fractions of NDs with the biomimetic lipid composition (**Figure 3.7B**), consistent with our observed requirement of CL to form a stable holocomplex (**Figure 3.6**). The relative SDH activities were highest in the elution fraction for biomimetic samples, but relatively higher in earlier fractions for other lipid combinations (**Figure 3.7C**), consistent with the observed dissociation of the catalytic dimer from membrane subunits when CL is lacking (**Figure 3.6**).

Taken together, the results from **Figure 3.6** and **Figure 3.7** demonstrate that CL is required to stabilize the interaction between the membrane-bound heterodimer and catalytic heterodimer of Complex II. It has been previously shown that the soluble SdhA/B dimer, fully active in SDH activity, dissociates from the membrane in the presence of chaotropes and organic solvents and more recently that it dissociates during matrix acidification, as would occur during apoptosis [131 & references therein]. Our results strongly suggest that CL is required for the proper folding and/or interactions of the membrane subunits, which, in turn, may be required to form an interactive surface with the Fe-S protein and hence stabilize the complex. These results also indicate that the loss of SQR activity that likely occurs with Complex II delipidation during mitochondrial solubilization is reversible upon reconstitution with biomimetic lipids. Notably, a CL molecule was shown to co-crystallize with the membrane subunits of the homologous complex in *E. coli* [30]. CL was not observed in a homologous structure from porcine [36];

however, the structure did contain two PE molecules, which share non-bilayer propensity with CL.

To further confirm that CL is required to maintain SQR activity, we measured the specific activities of ND preparations made with different lipids and isolated by our affinity purification procedure (normalized with respect to the concentration of catalytic dimer FAD, **Table 3.1**). Complex II reconstituted into NDs with CL had an approximately 9-fold higher specific activity than complexes reconstituted with lipids containing similar acyl chain lengths (POPC and POPC/POPE), and an approximately 85-fold higher activity than those in the presence of short chain phospholipids (DMPC). Hence, even when measured on a catalytic dimer-specific basis, CL enhances the catalytic efficiency of Complex II. CL may therefore not only stabilize the complex, as described above (Section 3.3.2), but also promote catalysis by other mechanisms (see Section 3.4 and Chapter 7).

We further tested the effects of CL on Complex II activity in organello. It has been reported that although CL is not absolutely required for OXPHOS activity, this lipid does enhance OXPHOS efficiency, particularly under unfavorable conditions [164, 177, 245]. For example, *S. cerevisiae Δcrd1* mutants (lacking the gene encoding cardiolipin synthase, *CRD1*), which have no CL in their mitochondrial membranes, can grow in non-fermentable medium [178, 186]. Yet mitochondria from *S. cerevisiae Δcrd1* strains show lower OXPHOS activity at elevated temperatures [179] and have significant uncoupling (lower ADP/O ratio and higher state 4 respiration) at high respiration rates [181]. To test for possible effects of CL on Complex II catalysis within intact mitochondria, we compared SQR activity for mitochondria isolated from wild type and *Δcrd1 S. cerevisiae* strains at 26°C and at 40°C. At the lower temperature, wild type and *Δcrd1* strains had similar rates (0.098 ± 0.0062 and 0.079 ± 0.0069 μmol DCPIP

reduced min^{-1} mg mitochondrial $protein^{-1}$, respectively). But at higher temperature, whereas SQR activity from the wild type strain did not change appreciably (~2% increase), that of the *Δcrd1* strain was reduced (~17% decrease). While these results support a role for CL in the maintenance of Complex II stability and/or activity, they also suggest that the absence of CL in intact mitochondria has less of an effect on Complex II activity than it does in our reconstituted system. This is likely due to a compensatory increase in the synthesis of other phospholipids (phosphatidylglycerol and PE) in *Δcrd1* strains, which may partially replace the function of CL [158, 159, 180, 186 and see Section 3.3.4].

3.3.4. Phosphatidylglycerol Partially Assumes the Role of CL in Complex II Activity

CL has several properties that may contribute to its role in energy conserving membranes: its unique dimeric structure with four acyl chains, its propensity to form non-bilayer structures in the presence of divalent cations, and its anionic phosphodiester headgroup. Phosphatidylglycerol (PG), like CL, is an anionic phospholipid. As an immediate biosynthetic precursor to CL, PG does not accumulate to a significant extent in the mitochondrial IM. However, in *S. cerevisiae Δcrd1* null strains, the amount of PG increases to levels similar to that of CL in wild type strains [159, 180, 186]. The notion that PG may partially compensate for the lack of CL is underscored by inability of strains lacking both PG and CL (with a null mutation in *PGS1* which encodes PG phosphate synthase) to grow on nonfermentable carbon sources [186, 246].

Our experimental system allowed us to directly test whether PG could functionally replace the role of CL in Complex II structure and function; more specifically, whether the anionic headgroup was responsible for maintaining holocomplex stability and/or redox activity.

Hence, we prepared samples with lipid mixtures of POPC, POPE, and POPG in molar ratios of 40:40:20, respectively. When POPG-containing NDs were subjected to our complex stability assay, a large fraction of the Sdh1p was released early in the affinity purification (**Figure 3.8A**, lanes 3-7). We therefore conclude that, like the other CL-lacking DMPC, POPC, and POPC/POPE preparations (**Figure 3.6**), POPG-containing NDs had a weak interaction between the membrane-bound and catalytic subunits. On the other hand, POPG-containing NDs with holocomplexes that remained after purification displayed SQR activity that approached that of CL-containing preparations, assayed by time course measurements (**Figure 3.8B**) and by FAD-normalized specific activity (**Table 3.1**). Hence, while PG does not promote stability of Complex II, it does appear to enhance catalysis. By extension, these results suggest that that hydrophobic domain of CL is important for mediating complex subunit interactions, whereas the anionic headgroup plays a role in promoting redox activity.

3.3.5. The Phospholipid-Dependence of Complex II ROS Production Rates

The production of ROS (primarily O_2^-) by Complex II can result from a block in the redox chain from succinate to Q [131]. Our observation that Complex II reconstituted with particular lipid combinations in the absence of CL had negligible SQR activity (**Figure 3.7B**, E* fraction) but robust SDH activity (**Figure 3.7C**, E* fraction) suggested that in these cases, electrons from succinate oxidation may not be efficiently transferred to the Q-binding site and may therefore react with O_2 to produce O_2^-. To test this, we measured the succinate-dependent production of O_2^- by Complex II with all lipid combinations in the presence of DB using the superoxide-specific reporter MitoSOX Red (**Figure 3.9**). In the presence of DMPC or POPC alone (**Figure 3.9**, red and yellow bars), Complex II had significantly higher O_2^- production rates

than when reconstituted with biomimetic lipids (**Figure 3.9**, blue bar), consistent with the predicted block of electron flux to the Q-binding site in the former samples. As a control, Complex II in biomimetic NDs that were pre-treated with TTFA had 44% higher O_2^- production rates than mock-treated (ethanol only) samples, demonstrating that our monitored ROS production was in fact from Complex II. Interestingly, Complex II in the presence of POPG, having measured SQR activities intermediate between biomimetic samples and those lacking CL (**Figure 3.8B**, **Table 3.1**), appeared to also have intermediate rates of ROS production (**Figure 3.9**, orange bar). Taken together, these results are consistent with the prediction that a reduced efficiency of electron transfer from the catalytic dimer to the Q-site may result in excess electron leakage. Notably, however, this inverse relationship between SQR catalytic efficiency and ROS production does not hold for Complex II reconstituted with POPC/POPE. Whereas PE does not markedly stabilize the holocomplex (**Figure 3.6**) or promote SQR activity (**Figure 3.7**), it does appear to lower ROS production rates to levels comparable to CL-containing samples (**Figure 3.9**, green bar). We speculate that this may be related to the non-bilayer (H_{II}) propensity of PE, which could be a contributing factor in curtailing Complex II ROS production.

3.4. Brief Conclusions

We have presented evidence that CL is essential for the structure and function of mitochondrial Complex II by: (i) maintaining the interaction between the catalytic dimer and membrane subunits (**Figure 3.6**), (ii) promoting electron flux from succinate to the Q reduction site in the bilayer (**Figure 3.7**), and (iii) reducing ROS production (**Figure 3.9**). Our results and working model are summarized in **Figure 3.10**. We propose that CL may stabilize the holocomplex by promoting the proper folding and/or helical packing interactions of the

membrane subunits, which may in turn present an interactive site for the Fe-S subunit (Sdh2p/SdhB). Our observation that CL also enhances Complex II catalysis *per se* (FAD-normalized SQR activity, **Table 3.1**) indicates that it may assume a more direct catalytic function as it does for other respiratory complexes. The catalytic Q site of Complex II is formed at the interface of the Fe-S subunit and the two membrane subunits, wherein amino acids from each subunit contribute to an extensive hydrogen bonding network with the bound ubiquinone [30, 35, 36, 38, 247]. The results from our analysis suggest that CL may be involved in stabilizing these interactions, allowing conformational dynamics required for movement of the ubiquinone into the catalytic site, and/or facilitating the proton transfer pathway to the Q-site. CL forms a resonance-stabilized bicyclic structure that is protonated at physiological pH, and may therefore act as a proton sink that recruits protons to specific sites within enzymes of energy-transducing membranes [40, 146]. In the yeast cytochrome bc_1 complex, for example, a single peripheral CL molecule is bound between monomers in proximity to the quinone binding site, and this lipid has been implicated in the conduction of protons from the bulk solvent to the ubiquinone [149, 160]. A similar proton antenna function may also concentrate protons at the interfacial region near the quinone binding pocket of Complex II, thereby promoting Q protonation. In this regard, it is noteworthy that our POPG-containing preparations showed enhanced SQR activity (**Figure 3.8**, **Table 3.1**), consistent with the notion that this acidic phospholipid may also serve as an anionic proton antenna as it might in the cytochrome b_6f complex of thylakoid membranes [139]. More recently, the activity of the respiratory complex NarGHI in *E. coli* was shown to be enhanced by a CL molecule that binds in the vicinity of the Q site, likely promoting the correct interaction with the menaquinol substrate [145].

3.5. Figures and Tables

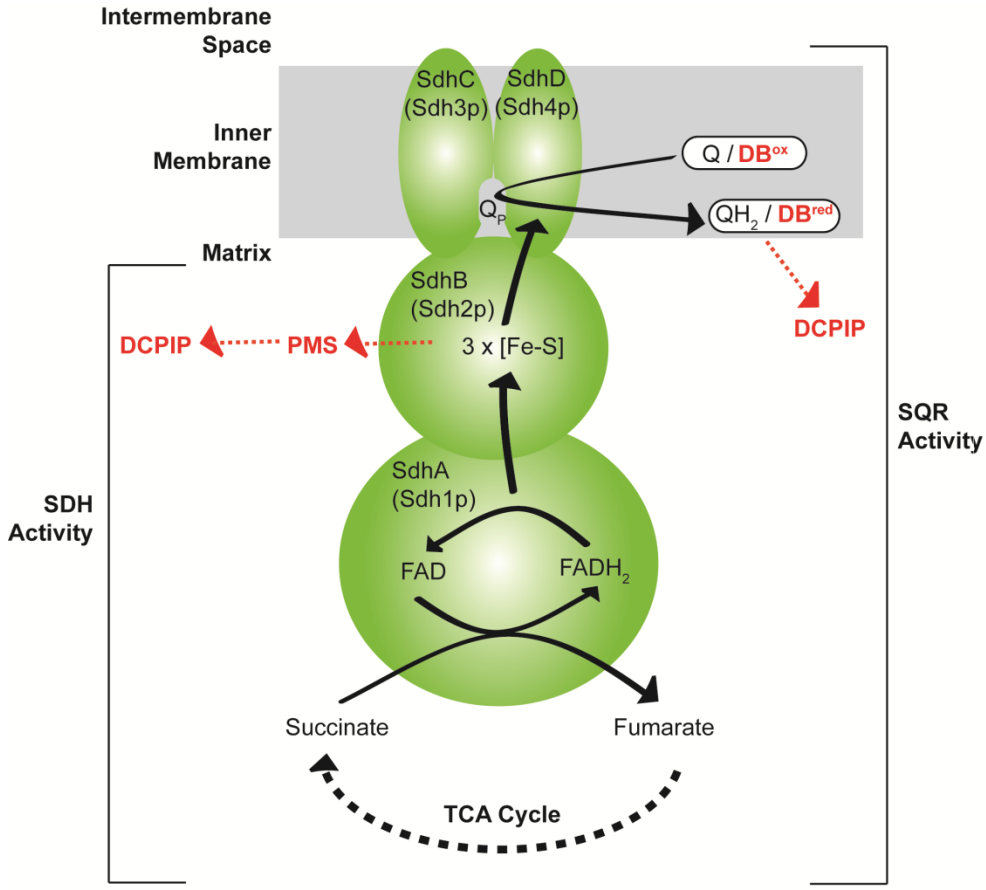

Figure 3.1. Schematic of Complex II illustrating SDH and SQR activities. In the Complex II catalytic cycle *in vivo*, the metabolite succinate is oxidized to fumarate by the SdhA (Sdh1p) flavoprotein. Electrons are then transferred singly through the Fe-S redox centers of SdhB (Sdh2p) to the coenzyme Q binding cavity (Q_P) at the interface of the SdhC/D (Sdh3p/4p) membrane subunits and the Fe-S subunit. At this site, the reduction of ubiquinone (Q) to ubiquinol (QH_2) *via* the ubisemiquinone intermediate requires two protons and two electrons from the oxidation of succinate. A second distal ubiquinone binding site (Q_D) may exist on the opposing side of the bilayer toward the intermembrane space (not shown). Note that the heme-*b*

coordinated by the membrane subunits is not depicted in this figure. Complex II therefore links the TCA cycle and the ETC. The catalytic cycle of Complex II can be conceptually divided into two experimentally separable stages. The first, succinate dehydrogenase (SDH) activity, occurs as the SdhA/B catalytic dimer oxidizes succinate to fumarate and under experimental conditions, electrons are transferred to the final acceptor dichlorophenolindophenol (DCPIP) *via* the redox mediator phenazine methosulfate (PMS). Hence, this assay measures succinate oxidase activity independently of electron transfer to Q. The second, succinate: ubiquinone oxidoreductase (SQR) activity, involves the transfer of electrons that result from succinate oxidation along a linear path of redox centers to the Q binding pocket where electrons are transferred to DCPIP *via* the supplied Q analog decylubiquinone (DB). Electron flow of the physiological cycle is depicted in black text and arrows. Electron flow under experimental conditions using added redox mediators is depicted in red text and dotted arrows.

	Preparation	Specific activity[a] (μmol DCPIP min^{-1} μmol FAD^{-1})
Complex II in Nanodiscs	DMPC	17.4 ± 45.4
	POPC	166.9 ± 83.6
	POPC / POPE	162.8 ± 58.6
	POPC / POPE / POPG	883.1 ±120.4
	Biomimetic	1482.7 ± 173.8
	DDM-solubilized mitochondria	72.8 ± 39.7
	Intact mitochondria	499.4 ± 37.7

[a]Errors shown represent standard errors.

Table 3.1. Specific SQR activity of Complex II.

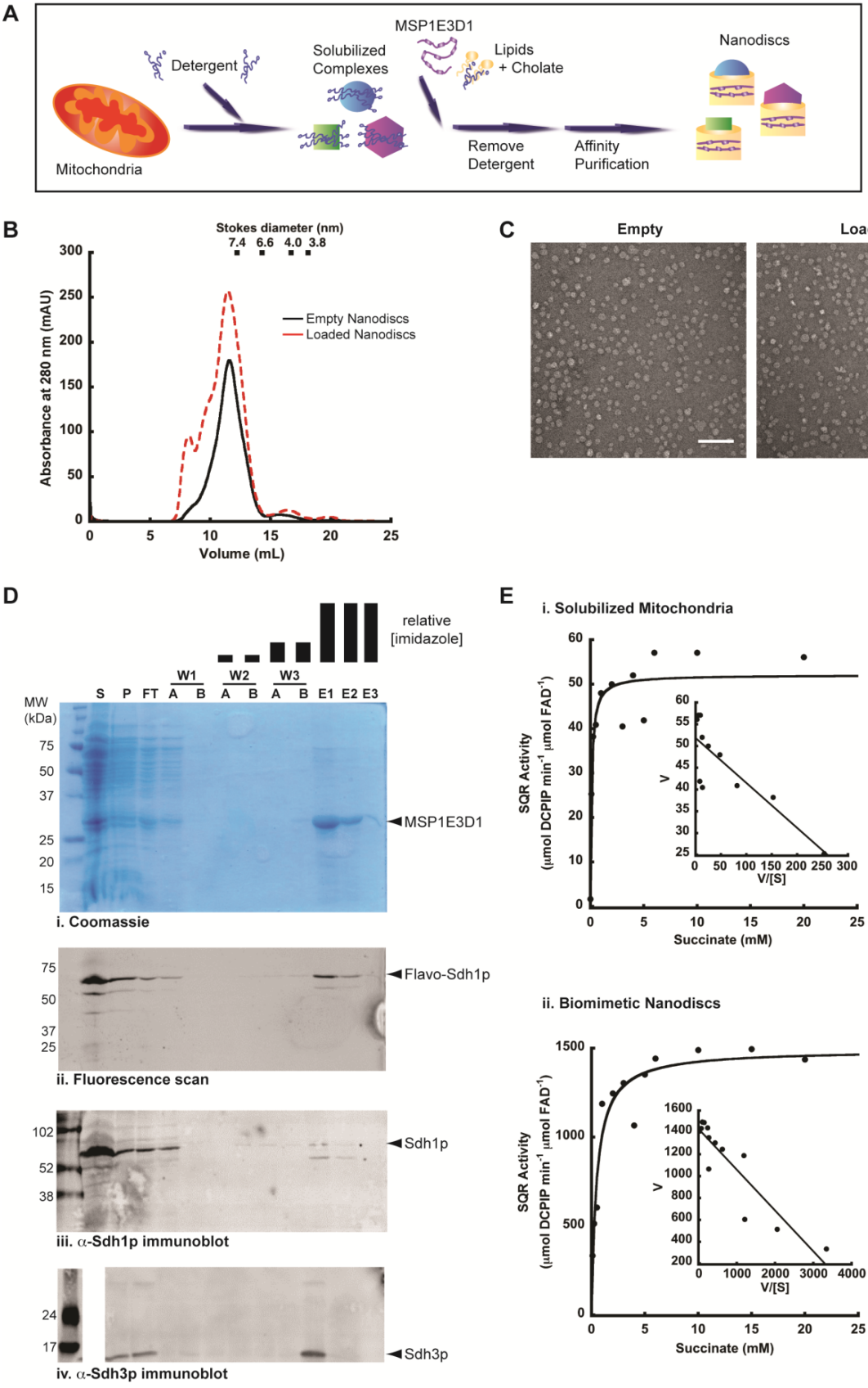
A
MSP1E3D1
Detergent
Solubilized Complexes
Lipids + Cholate
Nanodiscs
Mitochondria
Remove Detergent
Affinity Purification
B
Stokes diameter (nm)
7.4 6.6 4.0 3.8
Absorbance at 280 nm (mAU)
Empty Nanodiscs
Loaded Nanodiscs
Volume (mL)
C
Empty
Loaded
D
relative [imidazole]
W1 W2 W3
S P FT A B A B A B E1 E2 E3
MW (kDa)
MSP1E3D1
i. Coomassie
Flavo-Sdh1p
ii. Fluorescence scan
Sdh1p
iii. α-Sdh1p immunoblot
Sdh3p
iv. α-Sdh3p immunoblot
E
i. Solubilized Mitochondria
SQR Activity (μmol DCPIP min⁻¹ μmol FAD⁻¹)
V
V/[S]
Succinate (mM)
ii. Biomimetic Nanodiscs

Figure 3.2. Reconstitution of active Complex II into NDs. (**A**) Schematic of assembly process to produce NDs containing mitochondrial membrane complexes. Following detergent solubilization of mitochondria, membrane complexes are added to a reaction containing scaffolding protein (MSP1E3D1) and cholate-solubilized lipids. ND self-assembly occurs following the selective removal of detergent with hydrophobic adsorbents, and elution of the reaction over a nickel affinity column allows for purification of assembled NDs (which possess an N-terminal His tag on MSP1E3D1). (**B**) Size exclusion fractionation of NDs containing lipid only (empty, black trace) and NDs assembled with mitochondrial membrane complexes (loaded, dashed red trace). Chromatograms display absorbance at 280 nm (total protein content), and were calibrated by molecular mass standards (above). (**C**) Electron micrographs of empty NDs (left panel) and NDs assembled with mitochondrial membrane proteins (right panel) at 180,000X magnification. (scale bar = 100 nm). (**D**) Fractions from Ni-NTA column purification of NDs resolved by SDS-PAGE and analyzed as indicated by: (i) Coomassie stain, (ii) in-gel fluorometry (to visualize the FAD moiety covalently bound to Sdh1p), and immunoblots with antibodies against (iii) Sdh1p (αSdh1p) and (iv) Sdh3p (αSdh3p). Abbreviations are S: supernatant and P: pellet from mitochondrial solubilization; FT: column flow through; W1A-W3B: column wash steps; E1-E3: column elution steps. Note relative imidazole concentrations depicted above. (**E**) Michaelis-Menten plots and Eadie-Hofstee diagrams (inset) of SQR activity for (i) DDM-solubilized mitochondria (K_m = 0.10 mM and V_{max} = 51.9 μmol DCPIP min^{-1} μmol FAD^{-1}) and (ii) ND-bound Complex II (K_m = 0.37 mM and V_{max} = 1432.3 μmol DCPIP min^{-1} μmol FAD^{-1}).

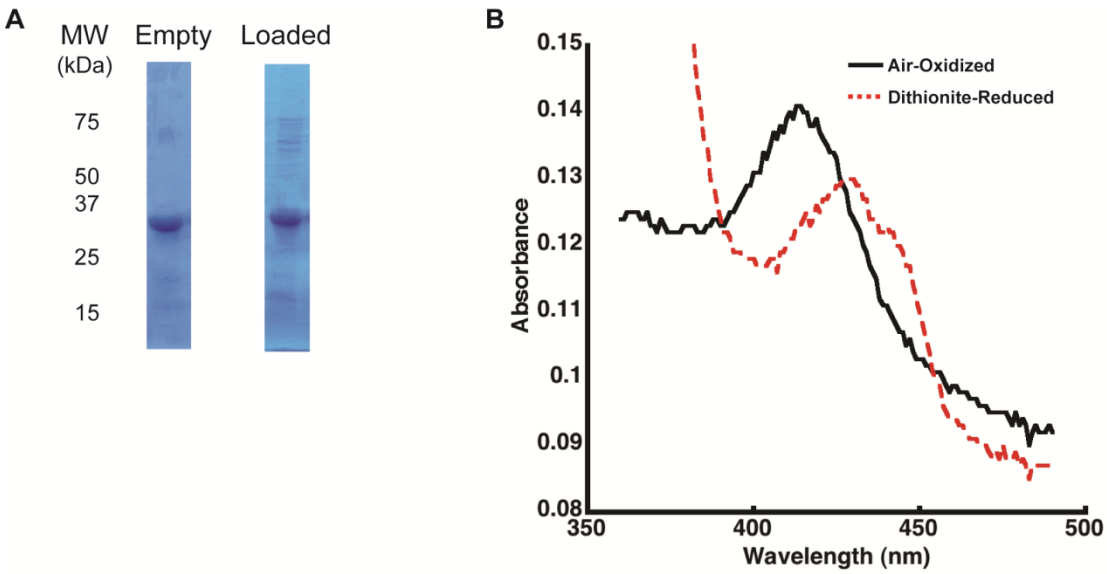

Figure 3.3. Reconstitution of mitochondrial membrane proteins into affinity-purified NDs. (**A**) Coomassie-stained SDS-PAGE gels of purified NDs assembled in the absence ("Empty") and in the presence ("Loaded") of solubilized mitochondrial membrane proteins. Both samples contained MSP1E3D1 (dominant band at ~32 kDa). The successful encapsulation of mitochondrial membrane proteins and complexes is shown by the appearance of many additional proteins in the "loaded" samples that are not present in the empty NDs. (**B**) Visible absorbance spectra of loaded NDs to support assembly with heme-rich mitochondrial proteins in the air-oxidized (black line) and dithionite-reduced (dashed red line) states. Upon reduction, there is a characteristic red shift in the absorbance maximum of the Soret region (γ band) from ~412 nm to ~430 nm. The dithionite-dependent appearances of β and α bands were not easily resolvable in these ND preparations.

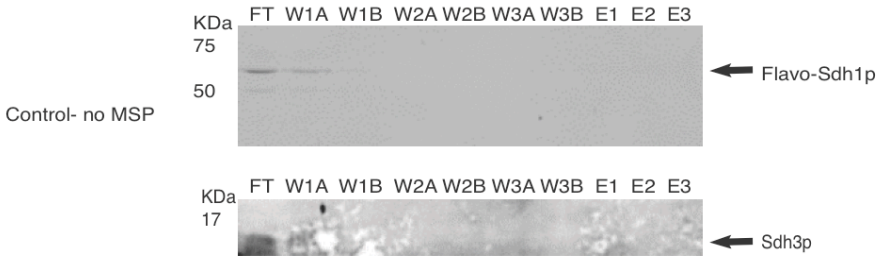

Figure 3.4. Negative control assembly reaction performed in the absence of scaffolding protein MSP1E3D1. Samples were prepared with solubilized mitochondrial complexes but in the absence of scaffolding protein and nickel affinity column fractions were analyzed exactly as described (see **Figure 3.2D**) by FAD fluorescence and immunoblot against Sdh3p (αSdh3p).

DMPC

PC (14:0/14:0)

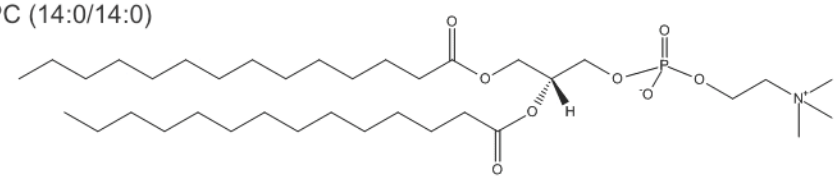

1,2-dimyristoyl-*sn*-glycero-3-phosphocholine

POPC

PC (16:0/18:1(9Z))

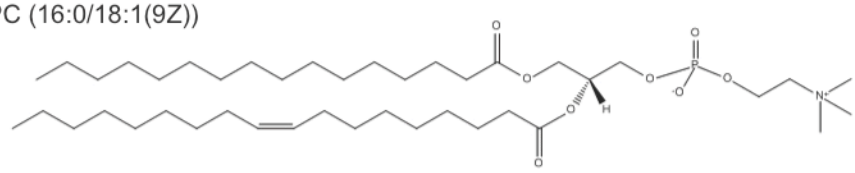

1-palmitoyl-2-oleoyl-*sn*-glycero-3-phosphocholine

POPE

PE (16:0/18:1(9Z))

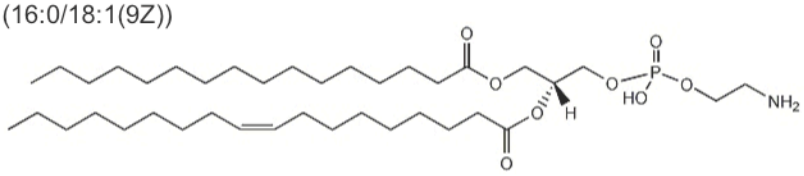

1-palmitoyl-2-oleoyl-*sn*-glycero-3-phosphoethanolamine

POPG

PG (16:0/18:1(9Z))

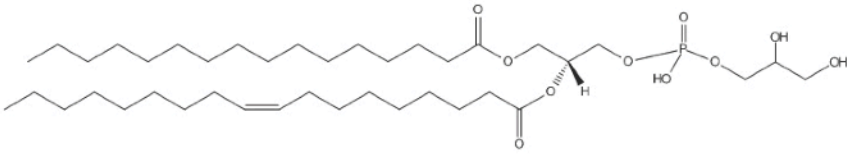

1-palmitoyl-2-oleoyl-*sn*-glycero-3-phosphoglycerol

Tetraoleoyl CL

CL(1'-[18:1(9Z)/18:1(9Z)],3'-[18:1(9Z)/18:1(9Z)]

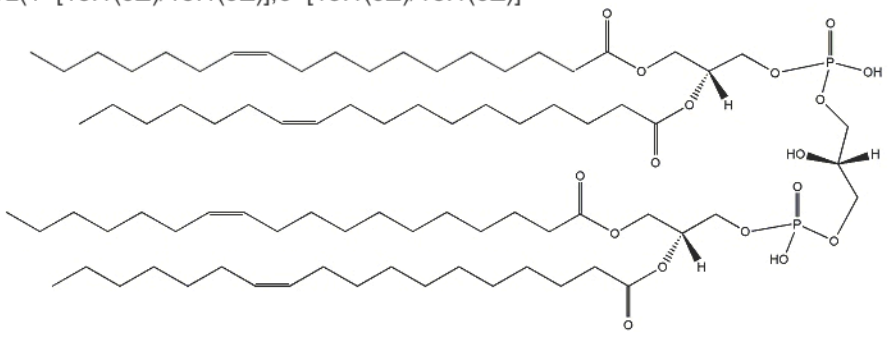

1',3'-bis[1,2-dioleoyl-*sn*-glycero-3-phospho]-*sn*-glycerol

Figure 3.5. Different phospholipids used for ND assembly in this study to test the dependence of Complex II stability and activity on lipid composition. Images were derived from the structure database from the LIPID MAPS Consortium website (http://www.lipidmaps.org).

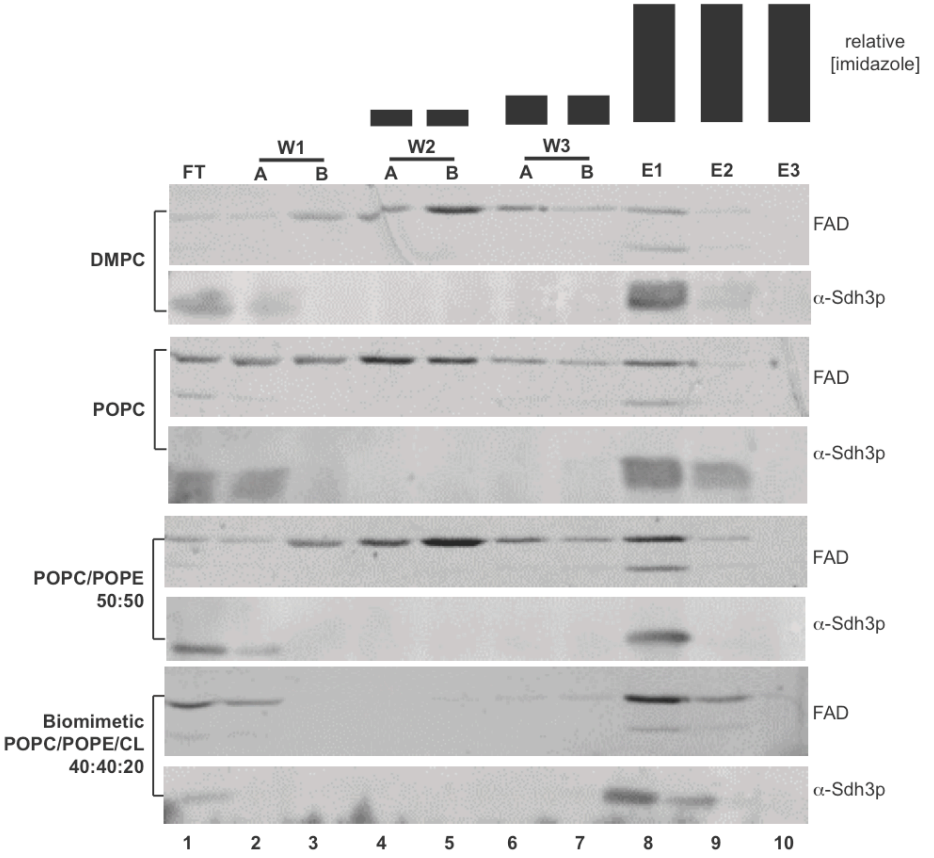

Figure 3.6. The stability of Complex II is dependent on lipid composition. Membrane proteins from DDM-solubilized mitochondria were reconstituted into NDs with the indicated lipid compositions and subjected to affinity chromatography to isolate the NDs. Subunits co-eluting with MSP1E3D1 (fractions E1 and E2) were considered to be stably associated with the NDs; those eluting at the earlier fractions were not stably associated. The fluorescent FAD signal was used as the marker for the soluble dimer and immunodetection with antiserum against Sdh3p (αSdh3p) was used as the marker for the membrane dimer. Column fraction designations are identical to those in **Figure 3.2D**, except supernatant and pellet lanes are not present.

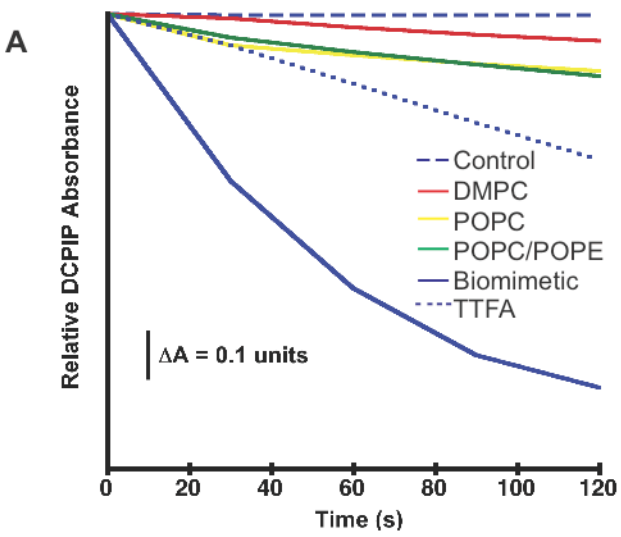
A
Relative DCPIP Absorbance
Control
DMPC
POPC
POPC/POPE
Biomimetic
TTFA
ΔA = 0.1 units
0
20
40
60
80
100
120
Time (s)

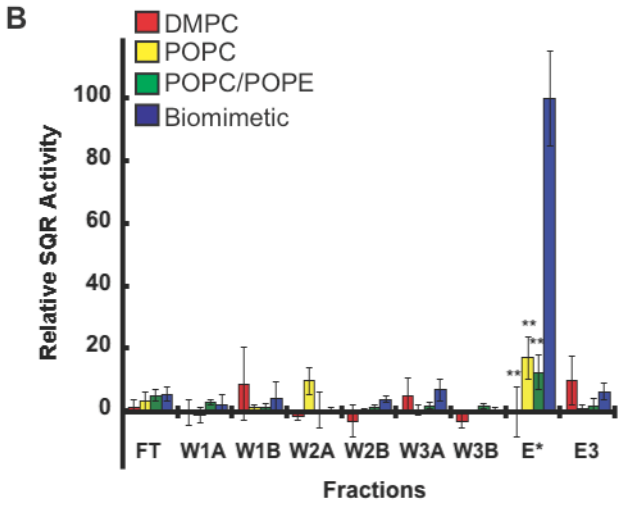
B
DMPC
POPC
POPC/POPE
Biomimetic
Relative SQR Activity
100
80
60
40
20
0
FT
W1A
W1B
W2A
W2B
W3A
W3B
E*
E3
Fractions

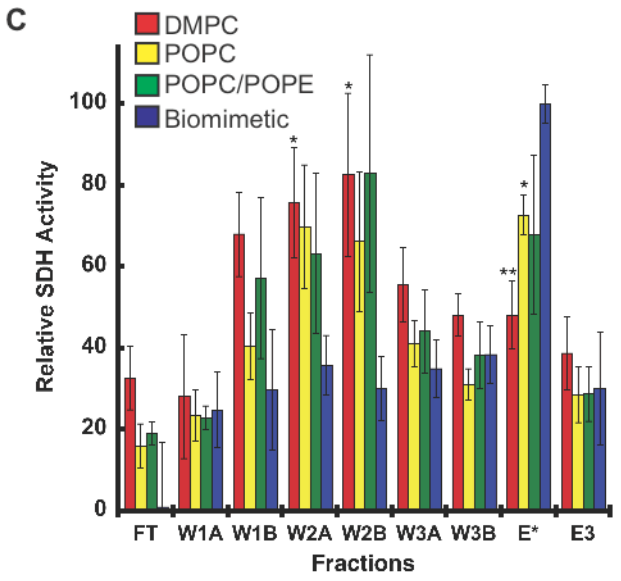
C
DMPC
POPC
POPC/POPE
Biomimetic
Relative SDH Activity
100
80
60
40
20
0
FT
W1A
W1B
W2A
W2B
W3A
W3B
E*
E3
Fractions

Figure 3.7. Enzymatic activity of Complex II reconstituted into NDs of different lipid composition. Assays were designed to monitor SQR activity (mediated by DB) or SDH activity (mediated by PMS), in both cases quantified colorimetrically as the extinction of DCPIP absorbance. (**A**) Signal-averaged time course traces of SQR activity for Complex II reconstituted in NDs containing DMPC only (red), POPC only (yellow), POPC with POPE (green), biomimetic lipids (blue), biomimetic lipids treated with TTFA (blue dotted), and prepared with biomimetic lipids but without MSP1E3D1 (blue dashed). (**B**) Relative SQR activity of column fractions for ND samples with the indicated lipid composition, determined from the initial reaction velocity (30 s following succinate addition). (**C**) Relative SDH activity of column fractions for ND samples with the indicated lipid compositions. For both panels B and C, E* represents fractions E1 and E2, which were pooled, and statistical differences are represented in relation to biomimetic NDs (* = $p \leq 0.1$; ** = $p \leq 0.01$).

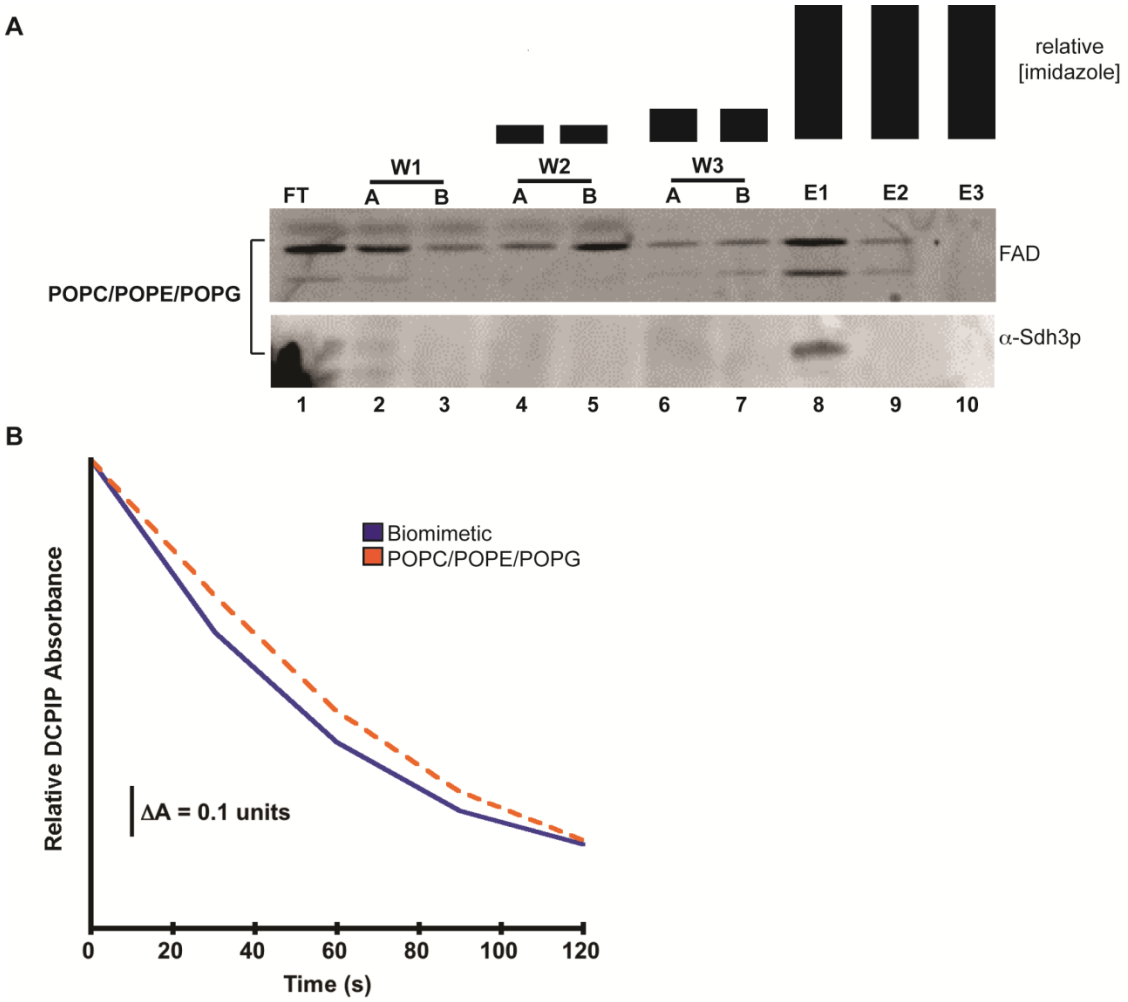

Figure 3.8. Stability and enzymatic activity of Complex II reconstituted into NDs with POPG. (**A**) Elution profiles of NDs assembled with POPG replacing the CL present in biomimetic samples. Preparation of samples and column fraction designations are identical to those in **Figure 3.6**. (**B**) Signal-averaged time course traces of SQR activity for Complex II reconstituted in NDs containing either biomimetic lipids with CL (blue) or biomimetic-like lipids with POPG replacing the CL (dashed orange).

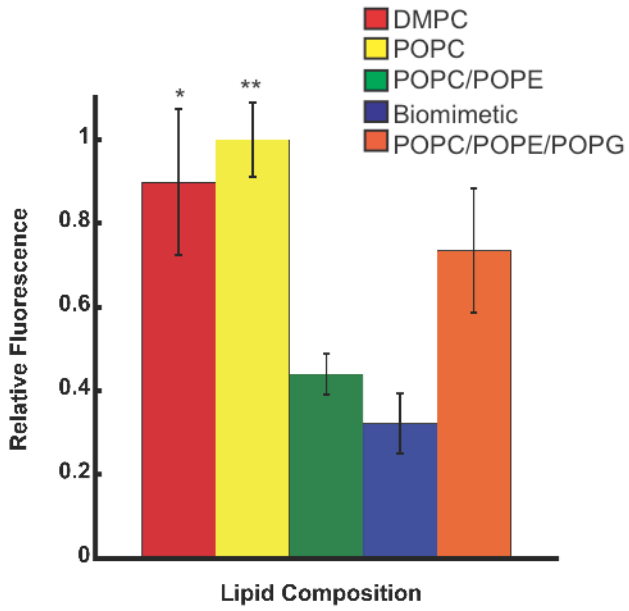

Figure 3.9. ROS formation as determined by MitoSOX fluorescence analysis. Statistical significance identical to **Figure 3.7C**, but statistics are represented in relation to biomimetic and POPC/POPE NDs.

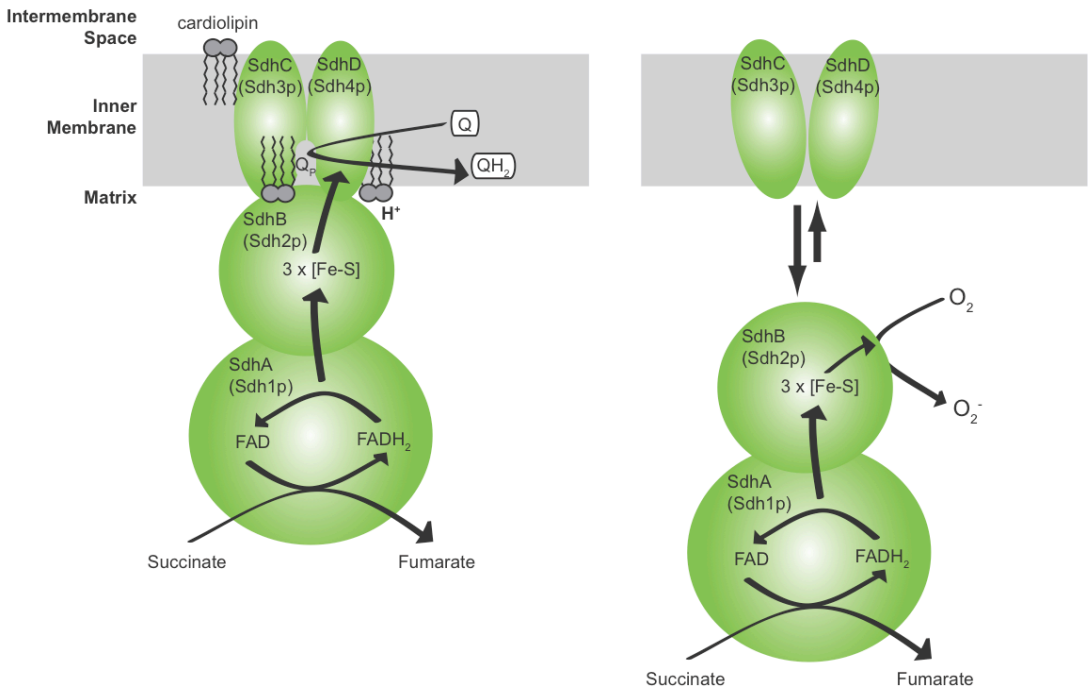

Figure 3.10. Working model for the role of CL in the stability and catalytic activity of Complex II. In the presence of CL (left panel), the holocomplex is fully assembled and efficient in SQR activity. In the absence of CL (right panel), the soluble catalytic heterodimer is not as stably associated with the membrane heterodimer, promoting the transfer of succinate-derived electrons to O_2 to form O_2^-.

Chapter 4

Divalent Cation-Dependent Structural Alterations in Cardiolipin-Containing Biomembranes

Derived from Schwall C.T. and Alder N.N., Divalent cation-dependent structural alterations in cardiolipin-containing biomembranes, *Manuscript in preparation*.

4.1. Abstract

Cardiolipin (CL), a unique phospholipid of the mitochondrial inner membrane (IM), will preferentially form curved hexagonal (H_{II}) structures, rather than a linear bilayer, when in aqueous dispersions in the presence of divalent cations. It is important to understand the implications that this behavior of CL in solution has on that of CL within native membranes in order to determine if induction of localized highly curved structures has implications in the disease states to which CL deletion and dysfunction have been linked. The goal of the present work is to study the behavior of CL-containing membranes at the levels of both headgroup and acyl chains in the presence of the divalent cations magnesium (Mg^{2+}) and calcium (Ca^{2+}). Here, we use fluorescent probes, Laurdan and DPH, which localize to different bilayer regions in order to gain a better understanding of the interaction between CL and divalent cations within IM-mimicking liposomes (large unilamellar vesicles, LUVs). We show that divalent cations induce more ordered packing in the interfacial region when interacting with CL, whereas headgroup variants of this lipid show no such interaction.

4.2. Materials and Methods

For Materials, Lipid Preparation, and Fluorescence Specifications, please see Chapter 2.

4.2.1. Large Unilamellar Vesicle (LUV) Preparation

LUVs were synthesized as described in Chapter 2. For fluorescence measurements, the fluorescent probes were added to the initial lipid mixes at a ratio of 200:1 (lipid: fluorophore). LUVs were subjected to size-exclusion chromatography on a Sephadex G-50 column to separate LUVs from excess unincorporated fluorescent probe. Fractions with assembled LUVs were identified by detecting a peak absorbance due to light scattering of the LUVs at approximately

260 nm [248, 249] on an Amersham Bioscience Ultrospec 2100 pro UV/Vis Spectrophotometer and subsequently pooled and stored at 4°C until utilized in further analyses.

4.2.2. Fluorescence Measurements

Measurements were completed as described in Chapter 2 with a final lipid concentration of approximately 500 μM. Divalent cations were titrated from stock solutions of either $MgCl_2$ or $CaCl_2$ (in ddH_2O) to the final concentrations specified (between 0 and 20 mM; 0:1 and 10:1 cation: lipid ratio).

4.2.2.1. Laurdan Generalized Polarization

Laurdan, 6-dodecanoyl-2-dimethylaminonaphthalene, is an environment-sensitive probe whose fluorescent naphthalene moiety embeds within the interfacial region of the membrane near the glycerol base of the phospholipid headgroups; it has been shown to incorporate into the membrane without perturbing the native lipid packing [250-253]. It has previously been used to study thermotropic phase transitions and the impacts of cholesterol and membrane-interacting proteins on phospholipid bilayers [254-256].

Excitation wavelength was set at 340 nm and emission was monitored from 410 to 510 nm (2 nm slit widths). As Laurdan is an environment sensitive probe whose fluorescent moiety localizes to the interfacial region of the bilayer, shifts in the emission spectrum of Laurdan are indicative of polarity (or hydration) changes in the bilayer near the headgroup. The generalized polarization (GP) of Laurdan, $GP = (I_{440}-I_{490})/(I_{440}+I_{490})$, quantifies these shifts wherein a GP value closer to 1.0 (or closer to 0.2, the highest value determined during the current experiments) indicates a lower polarity and less hydration of the probe (I_{440} and I_{490} are the emission intensities at 440 and 490 nm, respectively). In these experiments, GP measurements reflect at minimum two separate liposome preparations of at least four sets of measurements each.

4.2.2.2. DPH Anisotropy

DPH, 1,6-diphenyl-1,3,5-hexatriene, is a rod-shaped molecule that inserts into the bilayer parallel to the phospholipid acyl chains [257, 258]. By monitoring its anisotropy or polarization, it is possible to gain an understanding of membrane packing at the level of acyl chains within the bilayer [259, 260].

Excitation wavelength was set at 360 nm and emission wavelength was set at 430 nm (2 nm excitation and emission slit widths). DPH localizes to the hydrophobic core region of the bilayer and changes in its rotational movement (measured as fluorescence anisotropy) within the bilayer are indicative of the packing or lateral diffusion of the phospholipid acyl chains. The anisotropy (r) of DPH was determined as $r = (I_{VV}-GI_{VH})/(I_{VV}+2GI_{VH})$, where subscripts denote orientation of the polarizers (i.e. $_{VV}$ indicates that both the excitation and emission polarizers are oriented vertically to the incident light), I is the intensity of emission, and G is the correction factor for the fluorometer determined as $G = I_{HV}/I_{HH}$. In these experiments, anisotropy measurements reflect at minimum two separate liposome preparations of at least six sets of measurements each with individual sample data collected three sequential times to account for minor variation in anisotropy readings due to instrument variability.

4.2.3. Zeta Potential

Measurements of zeta potential represent the surface charge density slightly above the membrane interface [169]. Here, zeta potential values were calculated from electrophoretic mobilities based on the Smoluchowski relationship using a ZetaPlus Zeta Potential Analyzer (Brookhaven Instruments Corp., Holtsville, NY). LUVs at 1 mg/ mL (approximately 1 mM) and pH 7.5 were titrated with $MgCl_2$ or $CaCl_2$ (Hydration Buffer [pH 7.5]) at 25°C to obtain identical cation: lipid molar ratios identical to the fluorescence-based experiments, which ranged from 0:1

to 10:1 cation: lipid. Each value is an average of six runs of at least three cycles each from two separate liposome preparations.

4.2.4. Turbidity Measurements

Solution turbidity measurements were completed on an Amersham Biosciences Ultrospec 2100 pro UV/Vis Spectrophotometer in 1 cm quartz cuvettes. Wavelength scans were conducted to determine wavelength at which the maximum absorbance of LUVs occurred. Absorbance measurements were then made at a near-maximal wavelength to confirm that addition of calcium up to 5 mM did not induce a shift from lamellar to hexagonal phase for LUVs containing CL, which was monitored by an increase in absorbance (i.e. turbidity) at 300 nm [172, 261]. Note that parallel measurements with the addition of water were completed to account for dilution effects.

4.2.5. Transmission Electron Microscopy

Samples of each LUV type were imaged by negative staining (uranyl acetate) transmission electron microscopy after 20x or 40x dilution in Hydration Buffer. Images were collected at 23,000x magnification on a Tecnai Biotwin G2 Spirit electron microscope at the University of Connecticut Electron Microscopy Facility.

4.2.6. Data Representation and Statistical Analysis

All generalized polarizations and anisotropy measurements are representative of at least two independent samples, each measured at least four separate times. Zeta potential values and absorbance measurements are representative of two independent samples, each measured at least three separate times. Values displayed for Mg^{2+} and Ca^{2+} additions are corrected for effects due to buffer addition/dilution. All values are displayed as means ± standard errors of the means

(s.e.m.). A two-tailed student T-test (equal variance) was used to determine statistical significance ($p \leq 0.05$).

4.3. Results and Discussion

4.3.1. Ordering of LUVs in the Absence of Divalent Cations

As CL is uniquely found in energy-conserving membranes, we modeled our bilayer LUVs on the mitochondrial IM; any changes to the lipid mixtures were made as substitutions for TOCL (CL with four 18:1 acyl chains). For example, our IM mimetic LUVs consisted of phosphatidylcholine (POPC), phosphatidylethanolamine (POPE), and tetraoleoylcardiolipin (TOCL) in a 40:40:20 mol% ratio and the addition of deoxy-CL (dTOCL), monolyso-CL (MLCL), or phosphatidylglycerol (POPG) to the membrane occurred as a replacement of TOCL (note that dTOCL and MLCL also contain only 18:1 acyl chains). Deoxy-TOCL, MLCL, and POPG were used to investigate the effects of the cations on different physiochemical features of CL. Deoxy-TOCL lacks the hydroxyl group on the central glycerol moiety of the headgroup, breaking the proposed resonance between headgroups within a CL molecule, which would effectively cause the molecule to have two separate negative charges at physiological pH, as compared to TOCL, which is hypothesized to contain a single negative charge at neutral pH due to the resonance-stabilized headgroup structure (**Figure 4.1**, [146]). MLCL lacks a single acyl chain, leaving only three acyl chains attached to the CL double headgroup. It has been theorized that the missing acyl chain causes a shift in the headgroup structure of CL, breaking the resonance between the two phosphates as well (**Figure 4.1**, [150]). POPG is the native biosynthetic precursor of CL that also contains a mono-anionic headgroup, but only two acyl chains. In addition, we confirmed that these lipid combinations formed LUVs (as compared to

micelles or other non-bilayer structures) by conducting transmission electron microscopy imaging of all LUV samples (**Figure 4.2**).

While previous studies concerning the large-scale effect of cations on CL have revealed that cations can induce CL to take on a highly curved reverse-micellar structure that can induce membrane fusion [172, 173], we were interested in dissecting the effect of increasing concentrations of different divalent cations within the headgroup and hydrophobic core regions of stable CL-containing membranes. In order to do this we utilized the fluorescent probes Laurdan and DPH, which have been used extensively to study membrane packing and interfacial hydration in various membrane types and under different environmental conditions [252, 254, 257, 259]. When used in parallel, the probes yield a comprehensive readout of the physical state of a bilayer because Laurdan is sensitive to the presence of water in the interfacial region of the bilayer and reports on lipid headgroup hydration, whereas DPH is used to monitor the rigidity of the hydrophobic acyl chain region at the core of the membrane [169]. As an example, a previous study utilized both probes to look at the influence of pH on the ordering of CL-containing membranes, finding that low pH decreased membrane surface charge and that addition of CL to the membrane was necessary to form IM cristae-like morphology [169].

Upon beginning our studies, we observed that among all of the LUV types, those containing the anionic phospholipids TOCL, dTOCL, MLCL, or POPG had lower GP values than the LUVs containing the zwitterionic POPC and POPE only (**Table 4.1**). The results may be interpreted as the charge repulsion between the anionic phospholipids forcing more space between headgroups of the membrane, allowing more water molecules into the interfacial region. As explained earlier, this was reflected in the observed lowering of GP values of Laurdan for these LUVs as compared to the POPC/POPE LUVs without anionic phospholipids present.

These results are further supported by measurements of the zeta potential for each LUV sample in the absence of cations (**Table 4.1**): all LUVs containing anionic phospholipids have a more negative zeta potential value as compared to POPC/POPE only LUVs. The larger negative values support that liposomes containing anionic phospholipids are more stable particles and less likely to aggregate as compared to those containing only the zwitterionic POPC/POPE lipids. These results are also in line with previous molecular dynamics work that showed that as the amount of CL within a membrane increased, there was an increase in the hydration level of the interfacial region, probably due to the larger spaces maintained between the smaller, repulsive anionic CL headgroups [262].

In addition, MLCL-containing LUVs have significantly lower DPH anisotropy values as compared to all other LUVs when divalent cations are not present (**Table 4.2**). This supports that when MLCL is the only anionic lipid in the membrane, there is a higher rotational mobility of DPH due to an increase in the lateral mobility of the bilayer hydrophobic core. This makes sense because with only three acyl chains, instead of the typical four, there may be a higher degree of thermal disorder within the nonpolar core, allowing DPH more rotational mobility. On the other hand, POPG- and dTOCL-containing LUVs displayed higher anisotropy values comparable to POPC/POPE only LUVs, whereas TOCL-containing LUVs displayed anisotropy values midway between these two extremes. The higher DPH anisotropy values of POPG-containing LUVs may be explained by the fact that POPG has only two acyl chains per headgroup that may be able to pack closely with the identical acyl chains of POPC and POPE, as compared to the four unsaturated acyl chains of TOCL. The higher anisotropy values for dTOCL-containing LUVs may be explained when one considers that dTOCL theoretically cannot form the resonance-stabilized bicyclic headgroup structure that TOCL maintains at

physiological pH and contains two anionic charges (one on each phosphate of the headgroup). Without this rigidifying structure, which could otherwise hold the CL acyl chains in register, the acyl chains of dTOCL may be "off-balance," thereby shifting the placement of the unsaturation point of the acyl chains in the depth of the bilayer allowing closer packing of the acyl chains of dTOCL with those of POPC and POPE [150]. Alternatively, electrostatic repulsion between the two anionic phosphates may widen the diameter of the headgroup causing dTOCL to adapt a cylindrical, rather than wedge-shaped (as for TOCL), molecular geometry. In this way, its acyl chains may be more aligned with the cylindrical POPC within the lamellar bilayer.

4.3.2. Effect of Divalent Cations on LUVs- Interfacial Region

After considering native (in the absence of divalent cations) hydration and packing levels of the IM-mimicking LUVs, we treated these LUVs with increasing concentrations of Mg^{2+} or Ca^{2+} to determine the effect of divalent cations on Laurdan GP values. Note that turbidity measurements (Absorbance at 300 nm) were made to confirm that titration of cations was not inducing lamellar to hexagonal-like phase shifts (**Figure 4.3**). Titration of Mg^{2+} or Ca^{2+} into POPC/POPE LUVs did not cause any noticeable or significant change in GP values, which is not unexpected as there are no anionic phospholipids with which the cations could interact (**Figures 4.4** and **4.5**, red line).

On the other hand, addition of either cation to TOCL-, dTOCL-, MLCL-, or POPG-containing LUVs caused an increase in the GP of Laurdan (**Figures 4.4** and **4.5**, yellow line, blue line, purple line, or green line, respectively). Interestingly, the decrease in headgroup hydration, which was reflected in the increase in GP, occurred at the 1.0 mM addition of Mg^{2+} or Ca^{2+} (2:1 cation: lipid molar ratio) for TOCL-containing LUVs, but occurred later in the titration at higher

cation: lipid ratios for dTOCL- and MLCL-containing LUVs. Also, the seeming increase in POPG-containing LUVs was not statistically significant, indicating that the slight divalent cation-induced increase in packing at the interfacial region was not as pronounced as compared to the CL-containing LUVs. Further, a previous study using submicrosecond molecular dynamics simulations of POPG bilayers supported that increases in ordering and tightening of these bilayers can occur only when an excess of Ca^{2+} ions were added to the bilayers and not when a 1:1 ratio, which they term "counterions," of lipid-to-cation was present [263]. This may give an indication as to why POPG-containing LUVs did not display larger changes in response to divalent cations even though a phospholipid with an anionic headgroup that can interact with cations was present.

The zeta potential analysis of divalent cation titrations is consistent with the Laurdan-based approach. POPC/POPE LUVs did not display any detectable change in the zeta potential values as either Mg^{2+} or Ca^{2+} was titrated into the solution (**Figures 4.6** and **4.7**). In addition, any bilayer containing anionic phospholipids showed a cation-dependent increase in the zeta potential values from strongly negative to almost neutral. Titrations with both cations induced very strong increases in zeta potential values at the 1:1 cation: lipid ratio, but as the titration continued this effect seemed to decrease. This was especially true for titrations with Mg^{2+}, as it seemed that there was still a slight increase as Ca^{2+} was titrated in at higher cation: lipid ratios. While there was no distinct effect of cations on individual LUV types containing various anionic phospholipids, the lack of distinct differences could indicate that the packing changes occurring in the interfacial region of the bilayers were not due to localized changes in charge surrounding the anionic LUVs. There may be a more specific interaction occurring, such as the displacement of water ions for cations or differences in the number of cations binding per anionic headgroup

(1 Ca2+ per 2 TOCL as compared to 1 Ca2+ per 1 dTOCL), that varies according to the charge localization across the headgroup.

In order to probe the mechanism behind the specific packing differences among anionic LUVs, TOCL-containing LUVs were formed and purified in Glycine Hydration Buffer (pH 9.0). As explained previously, it is theorized that CL has two p*K*as due to the resonance effect across the hydroxyl moiety in the glycerol headgroup, one below pH 4.0 and one above pH 8.0. When the pH is raised to 9.0, there should be two negative charges on the TOCL headgroup, mimicking the hypothesized state of the headgroup of dTOCL. When the cations were titrated into TOCL-containing LUVs at pH 9.0, the trend effectively matched that seen with the dTOCL-containing LUVs (**Figure 4.8**, compare light green and blue lines, respectively), supporting that the higher cation concentrations needed to induce changes within the dTOCL-containing membranes may be linked with having two formal charges on each phosphate of the CL headgroup, rather than one resonating charge. This can be explained by the idea that a single Ca^{2+} ion can interact with two TOCL molecules at physiological pH because each has a single negative charge; however, dTOCL and TOCL at pH 9.0 have two negative charges that would only allow a single Ca^{2+} ion to interact with one TOCL molecule. At the same concentration of Ca^{2+}, TOCL lipids would become more closely packed than dTOCL or TOCL lipids at pH 9.0. In addition, even though the titration of TOCL-containing LUVs at pH 9.0 closely mimics that of dTOCL-containing LUVs, it is not identical, leading us to propose that some TOCL headgroups at pH 9.0 may be singly charged (rather than both phosphates being deprotonated), which is possible when considering the shifting pKa_2 of the TOCL headgroup can extend upwards of pH 9.5 [151].

In addition, TOCL-containing LUVs were also assembled and purified in Glycine Hydration Buffer (pH 3.0), at a pH below the first p*K*a of TOCL. At low pH, the headgroup of

TOCL should be neutral and we would expect the TOCL-containing LUVs to behave as those containing POPC and POPE only. The results supported this hypothesis in that TOCL at pH 3.0 not only had a higher GP as compared to TOCL at pH 7.4 when cations were not present (indicating closer packing of the headgroups), but also did not display a change in GP as divalent cations were titrated into the sample (**Figure 4.8**, pink line).

To investigate the effects of divalent cations on TOCL further, as LUVs containing this lipid displayed the most extreme packing alterations as they were added, we titrated divalent cations up to 20 mM (40:1 cation: lipid ratio). Surprisingly, it appeared that there were two phase changes of TOCL-containing LUVs when Ca^{2+} (not Mg^{2+}) was added to the samples: one that occurred at lower Ca^{2+} concentrations that were close to a 2:1 ratio of lipid-to-cation, and one of which occurred at higher concentrations, where a large excess of cation as compared to lipid was present (**Figure 4.9**). The first phase change most likely represents an initial dehydration of the interfacial region of the bilayer, as addition of cations to phospholipid bilayers has previously been seen to mimic a dehydration event [174]. The lipid headgroups would then be able to pack more closely due to the removal of water coupled with a decrease in the charge repulsion between TOCL anionic headgroups, which would be shielded by the divalent cations. The second phase change is more extreme and could be attributed to a strain within the LUVs as TOCL attempts to induce negative curvature into the bilayer. This would push the headgroups of all phospholipids within the membrane closer together, effectively dehydrating the interfacial region and greatly increasing the GP of the Laurdan probe.

In addition, note that this large change in GP of the TOCL-containing LUVs occurred when Ca^{2+} was titrated, but not Mg^{2+}, which runs counter to what we saw at the lower concentrations of cations in that both cations had similar effects on GP values. Using molecular

dynamics simulations it has previously been shown that Ca^{2+} holds onto the water molecules in its first solvation shell for only a few picoseconds, as compared to hundreds of picoseconds for Mg^{2+} [264]. It may be that as the Mg^{2+} ions were more tightly shielded by waters, they were unable to induce as strong a change in the ordering of the TOCL bilayer as Ca^{2+}, whose charges were not shielded as tightly by its solvation shell. Once a higher concentration of the less shielded Ca^{2+} cations was introduced into the system, Ca^{2+} was able to disrupt the bilayer of TOCL-containing LUVs and induce H_{II} formation. In addition, it has previously been shown in solutions of pure CL that while both Mg^{2+} and Ca^{2+} can induce H_{II} CL structures, at lower concentrations of Mg^{2+} (3 mM) it is more likely that there will be a mix of lamellar and hexagonal phases as compared to the induction of a purely hexagonal phase in the presence of Ca^{2+} [174]. All of these results are consistent with previous work supporting that CL has a higher affinity for Ca^{2+} than for Mg^{2+} [143].

Taken together, at the interfacial region of a bilayer, divalent cations are able to induce ordering or structural changes in TOCL-, dTOCL-, MLCL-, and POPG-containing LUVs, but not in POPC/POPE-containing bilayers. The increase in GP values, indicative of a more dehydrated headgroup region of the bilayer, when Ca^{2+} was titrated into TOCL-containing LUVs most likely reflect induction of large levels of strain into the bilayer, with the lipid headgroups becoming much more closely packed.

4.3.3. Effect of Divalent Cations on LUVs- Acyl Chains

In addition to looking at the effects of divalent cations at the interfacial region of the membrane, which is in direct contact with the cations, we were also interested in any effects on packing among the acyl chains composing the hydrophobic core of the membrane. Unlike our

observations in the interfacial region, titration of Mg^{2+} or Ca^{2+} to LUVs containing DPH did not induce significant effects on any of the bilayers (**Table 4.2**). When POPC/POPE LUVs were studied, there was no effect of adding in Mg^{2+} or Ca^{2+} on the anisotropy of DPH within the hydrophobic core of the membrane, which is not unexpected as the headgroup region of these LUVs was unaffected as well (**Table 4.2**). On the other hand, TOCL-, dTOCL- MLCL-, and POPG-containing LUVs also did not display a significant change in anisotropy values as either cation was titrated, which was in contrast to what was observed in the interfacial region with both the Laurdan and zeta potential measurements (**Table 4.2**).

4.4. Brief Conclusions

Overall, these studies have utilized fluorescent probes complemented by other techniques to investigate the packing interactions of bilayer lipids, namely those containing CL, in the presence of divalent cations, which has implications for the mitochondrial IM and its role in apoptosis as Ca^{2+} is an important signaling molecule in this process. Monitoring the behavior of these probes allowed us to propose that divalent cations were able to induce a stronger structural change in ordering and lipid packing in the interfacial region of the membrane as compared to the acyl-chain region. This was due to the cations alleviating charge repulsion between adjacent anionic CL headgroups and also forming crosslinks between separate CL molecules, which allowed them to move closer together; however, these spatial alterations did not appear to be translated further to the acyl chain region of the bilayer. A previous study focusing on the effects of acyl chain unsaturation and lipid type on bilayer ordering also found that changes in packing at the headgroup and acyl chain regions of the bilayer may not be consistent and may in fact be "structurally uncoupled" [259]. In addition, it has been shown that Ca^{2+} tends to interact with the

bilayer in the interfacial region, the same region that the fluorescent moiety of Laurdan intercalates and the region in which we saw the most significant changes in bilayer hydration and ordering [265]. Further, the variation in behavior between TOCL and dTOCL, as well as the investigation of TOCL-containing LUVs at various pH, supports the hypothesis that at neutral pH the TOCL headgroup exists as a singly-charged resonance-stabilized acid anion [148].

Further, the variation in behavior of TOCL-, MLCL-, and dTOCL-containing bilayers in the presence of divalent cations has implications for the pathogenic mechanisms underlying Barth Syndrome (**Figure 4.10**). Until very recently, it was believed that the CL remodeling pathway, which produces mature CL with symmetric, unsaturated acyl chains from asymmetric immature CL with fully saturated acyl chains, was necessary for the proper functioning of mitochondria because CL acyl chain specificity was integral to function. However, it has newly been shown that it may in fact be the decreased levels of CL and increased levels of MLCL that are contributing to mitochondrial dysfunction, rather than the particular acyl chain composition of the CL molecules [266]. The results here support that the pathogenesis of Barth Syndrome, which is linked to malfunction in CL remodeling, may be related to the decrease in packing between phospholipid headgroups and the decrease in lateral mobility of the acyl chains for MLCL-containing, as compared to TOCL-containing, bilayers. This lower packing and increased hydration of the bilayer may have detrimental implications for various processes occurring at, or within, the mitochondrial IM, leading to the development of the Barth Syndrome phenotype.

4.5. Figures and Tables

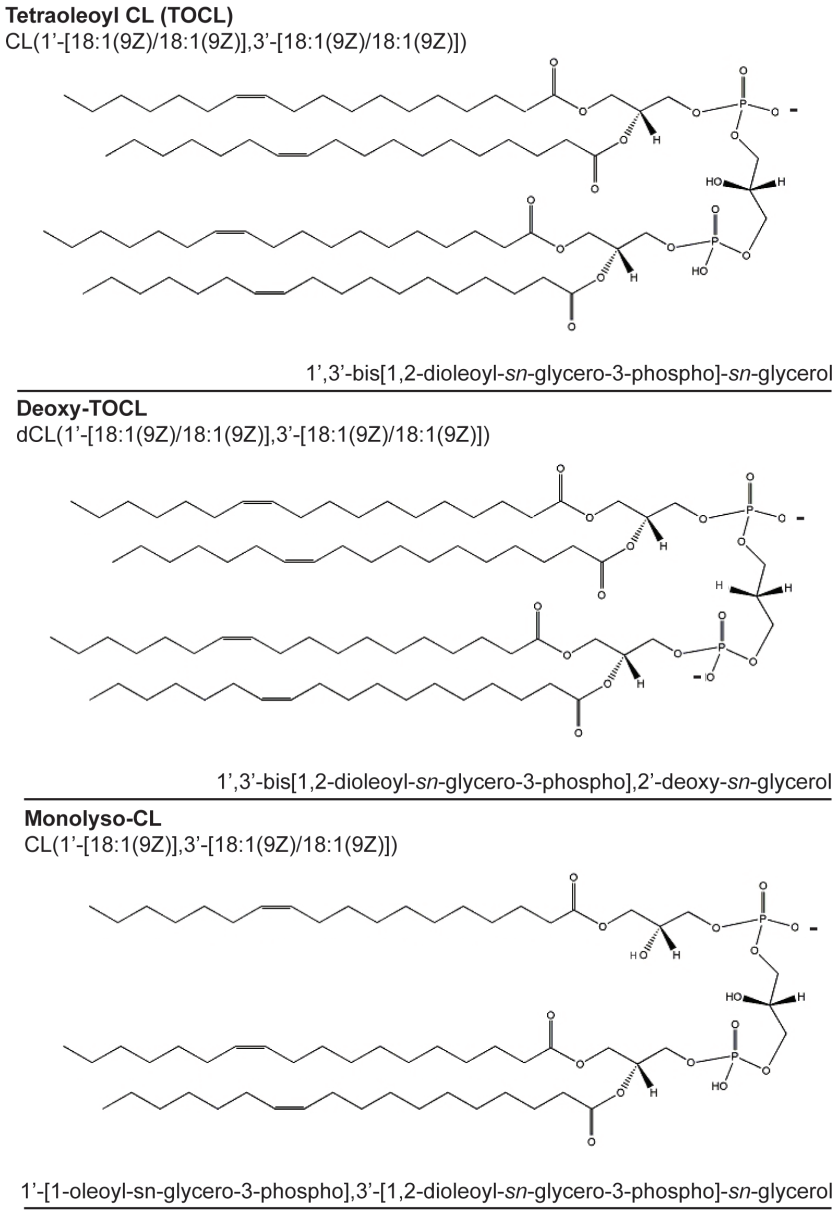

Figure 4.1. Different CL variants used for LUV assembly in this study. Images were derived from the structure database from the LIPID MAPS Consortium website (http://www.lipidmaps.org).

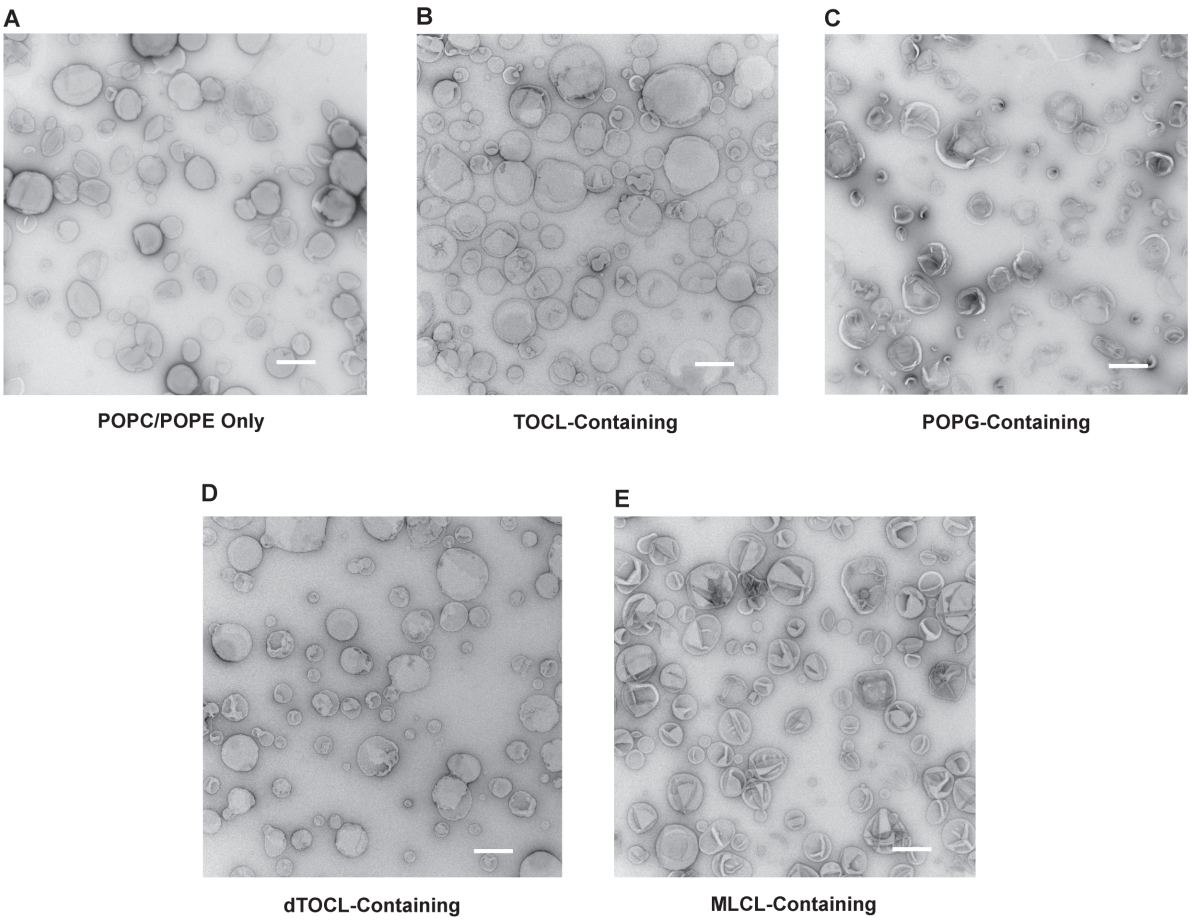

Figure 4.2. TEM Images of LUVs. Negative staining transmission electron microscopy images were taken of all LUV samples at 23,000X magnification (scale bars = 500 nm). (**A**) POPC/POPE only; (**B**) TOCL-Containing; (**C**) POPG-Containing; (**D**) dTOCL-Containing; (**E**) MLCL-Containing.

Table 4.1.

Preparation	Laurd Generalized P
POPC/POPE Only	0.189 ±
TOCL-Containing	0.142 ±
POPG-Containing	0.115 ±
dTOCL-Containing	0.163 ±
MLCL-Containing	0.084 ±

Errors shown represent standard errors.
Statistical significance ($p < 0.05$) is repre
POPC/POPE Only LUVs.

	DPH Anisotropy Values		
Preparation	Molar Ratio 0:1 Calcium:Phospholipid	Molar Ratio 10:1 Calcium:Phospholipid	Difference
POPC/POPE Only	0.120 ± 0.0031	0.119 ± 0.0030	- 0.001
TOCL-Containing	0.111 ± 0.0016*	0.112 ± 0.0019*	0.001
POPG-Containing	0.120 ± 0.0019	0.121 ± 0.0020	0.001
dTOCL-Containing	0.119 ± 0.0008	0.121 ± 0.0010	0.002
MLCL-Containing	0.098 ± 0.0060*	0.099 ± 0.0050*	0.001

Errors shown represent standard errors.
Statistical significance ($p < 0.05$) is represented by * in relation to POPC/POPE Only LUVs.

Table 4.2. Divalent Cations are Unable to Induce Ordering in LUV Acyl Chain Region.

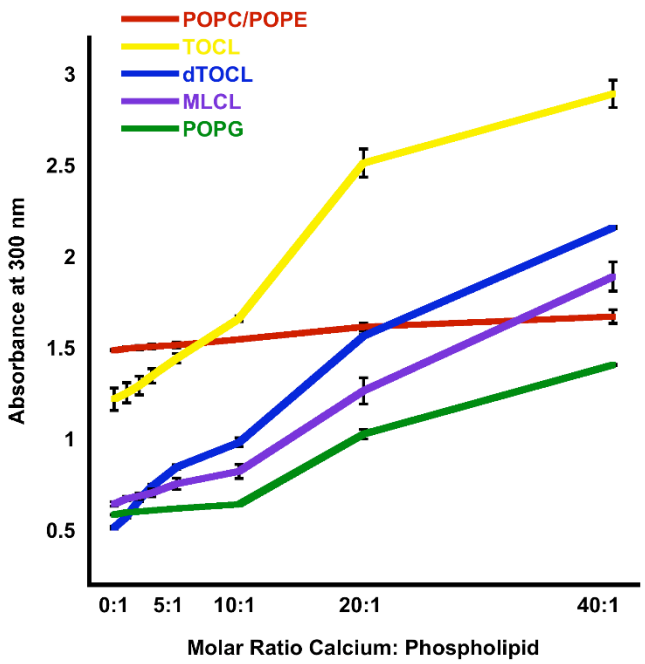

Figure 4.3. Turbidity measurements to confirm lamellar LUVs. Calcium chloride solution was added to LUVs of varying lipid composition in order to confirm that addition of the cation did not induce a lamellar-to-hexagonal phase transition within our titrations. Note that a large, rapid increase in absorbance at 300 nm (turbidity) indicates a phase transition and this does not occur prior to 10:1 calcium: phospholipid molar ratios. POPC/POPE (red line), TOCL-containing (yellow line), POPG-containing (green line), dTOCL-containing (blue line), or MLCL-containing (purple line). Turbidity measurements were completed as in Section 4.2.4. Traces are represented as averages of at minimum two independent experiments of at least three measurements each with standard errors of the mean (s.e.m.).

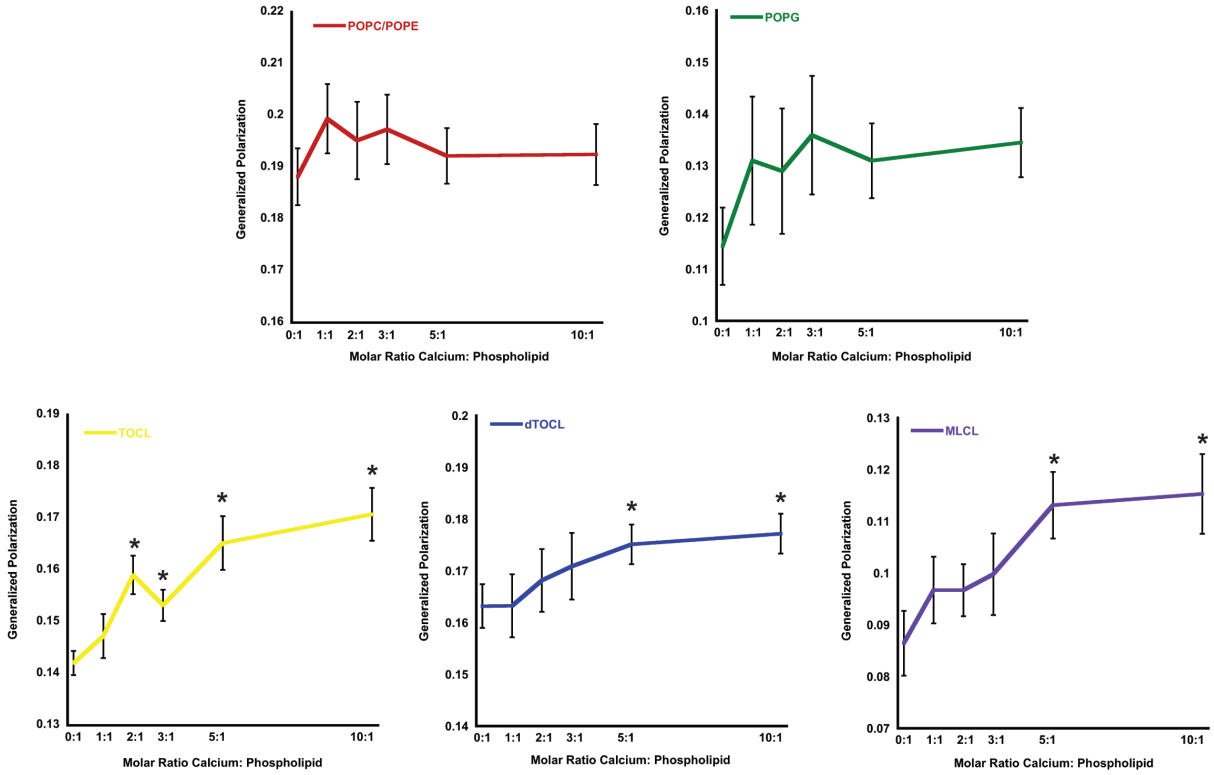

Figure 4.4. Calcium induces order of the interfacial region of the bilayer in TOCL-containing LUVs. Calcium chloride solution was added to LUVs of varying lipid composition. POPC/POPE (red line), TOCL-containing (yellow line), POPG-containing (green line), dTOCL-containing (blue line), or MLCL-containing (purple line). Generalized polarization values were determined as in Section 4.2.2.1. Traces are represented as averages of at minimum two independent experiments of at least four measurements each with standard errors of the mean (s.e.m.). Statistical differences are represented in relation to 0 mM calcium addition (* = $p \leq 0.05$).

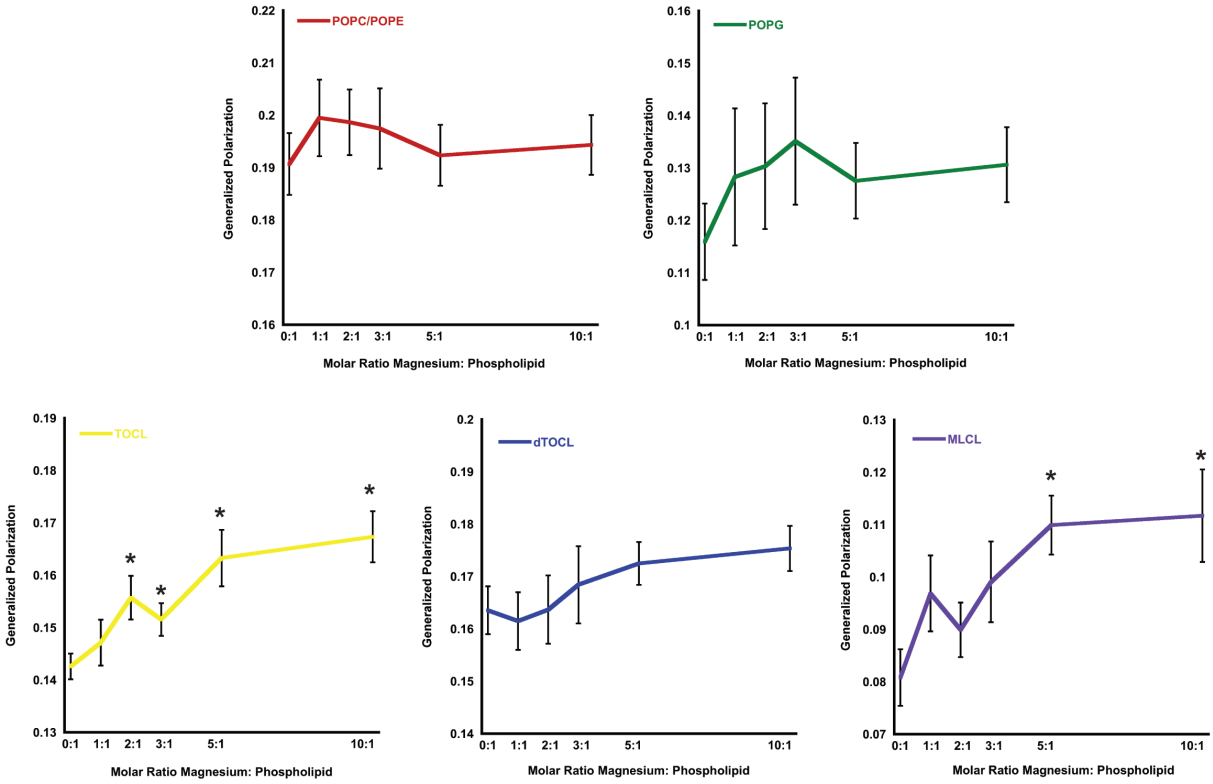

Figure 4.5. Magnesium induces order of the interfacial region of the bilayer in TOCL-containing LUVs. Magnesium chloride solution was added to LUVs of varying lipid composition. POPC/POPE (red line), TOCL-containing (yellow line), POPG-containing (green line), dTOCL-containing (blue line), and MLCL-containing (purple line). Generalized polarization values were determined as in Section 4.2.2.1. Traces are represented as averages of at minimum two independent experiments of at least four measurements each with s.e.m. Statistical differences are represented in relation to 0 mM magnesium addition (* = $p \leq 0.05$).

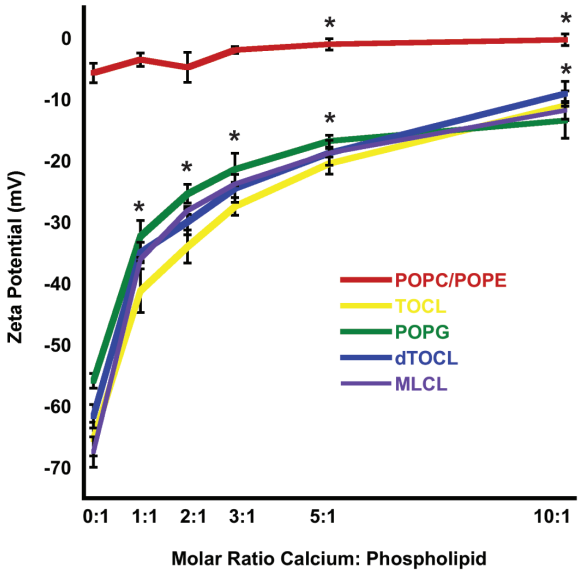

Figure 4.6. Calcium neutralizes the surface charge of anionic phospholipid-containing LUVs. Calcium chloride solution was added to LUVs of varying lipid composition. POPC/POPE (red line), TOCL-containing (yellow line), POPG-containing (green line), dTOCL-containing (blue line), or MLCL-containing (purple line). Zeta potential was measured as described in Section 4.2.3. Traces are represented as averages of at minimum two independent experiments of at least three measurements each with s.e.m. Statistical differences are represented in relation to 0 mM calcium addition (* = $p \leq 0.05$).

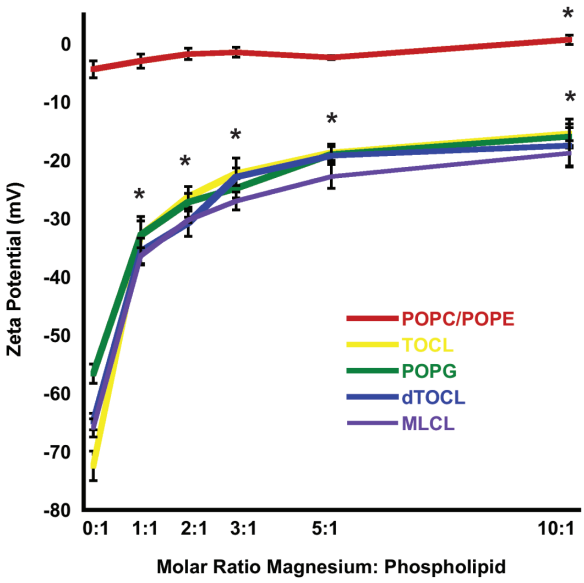

Figure 4.7. Magnesium neutralizes the surface charge of anionic phospholipid-containing LUVs. Magnesium chloride solution was added to LUVs of varying lipid composition. POPC/POPE (red line), TOCL-containing (yellow line), POPG-containing (green line), dTOCL-containing (blue line), or MLCL-containing (purple line). Zeta potential was measured as described in Section 4.2.3. Traces are represented as averages of at minimum two independent experiments of at least three measurements each with s.e.m. Statistical differences are represented in relation to 0 mM magnesium addition (* = $p \leq 0.05$).

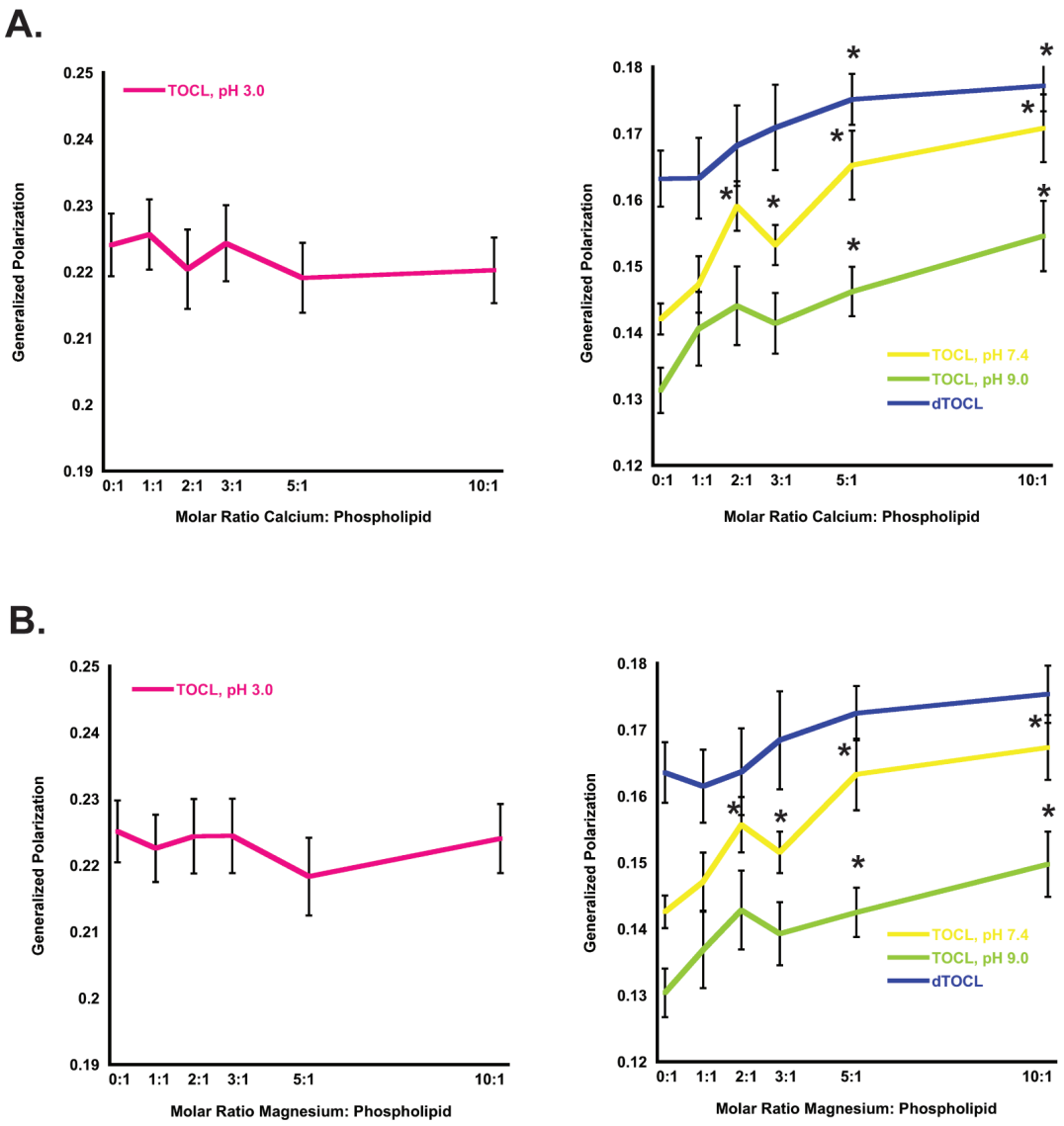

Figure 4.8. Analysis of effect of divalent cations on TOCL-containing LUVs at various pH. Calcium (**A**) and magnesium (**B**) were titrated into the following LUVs: TOCL (pH 3.0) (pink line), TOCL (pH 7.4) (yellow line), TOCL (pH 9.0) (light green line), and dTOCL (blue line) for comparison. Generalized polarization values were determined as in Section 4.2.2.1. Traces are represented as averages of at minimum two independent experiments of at least four measurements each with s.e.m. Statistical differences are represented in relation to 0 mM cation addition (* = $p \leq 0.05$).

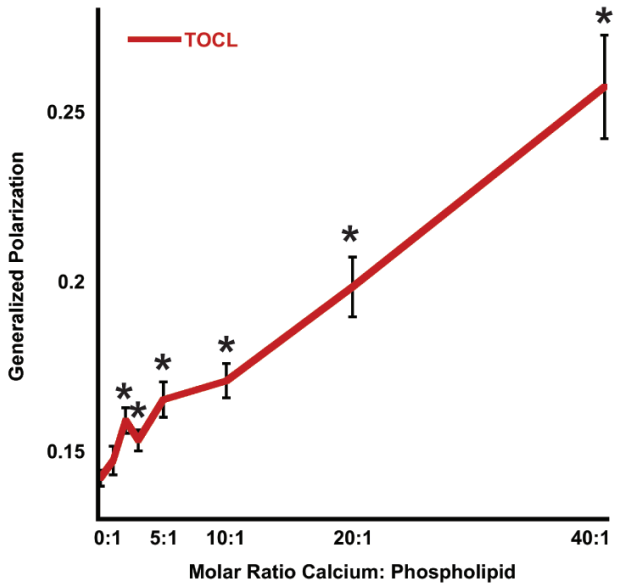

Figure 4.9. Titration of calcium up to 20 mM (40:1 calcium to lipid ratio). There is evidence for a biphasic effect that may indicate that Ca^{2+} is able to enhance ordering of membranes containing TOCL until there is too much strain on the bilayer and the LUVs burst (as supported by turbidity measurements, data not shown), allowing TOCL in solution to enter H_{II} (hexagonal, inverted micellar) phase. Generalized polarization values were determined as in Section 4.2.2.1. Traces are represented as averages of at minimum two independent experiments of at least four measurements each with s.e.m. Statistical differences are represented in relation to 0 mM cation addition (* = $p \leq 0.05$).

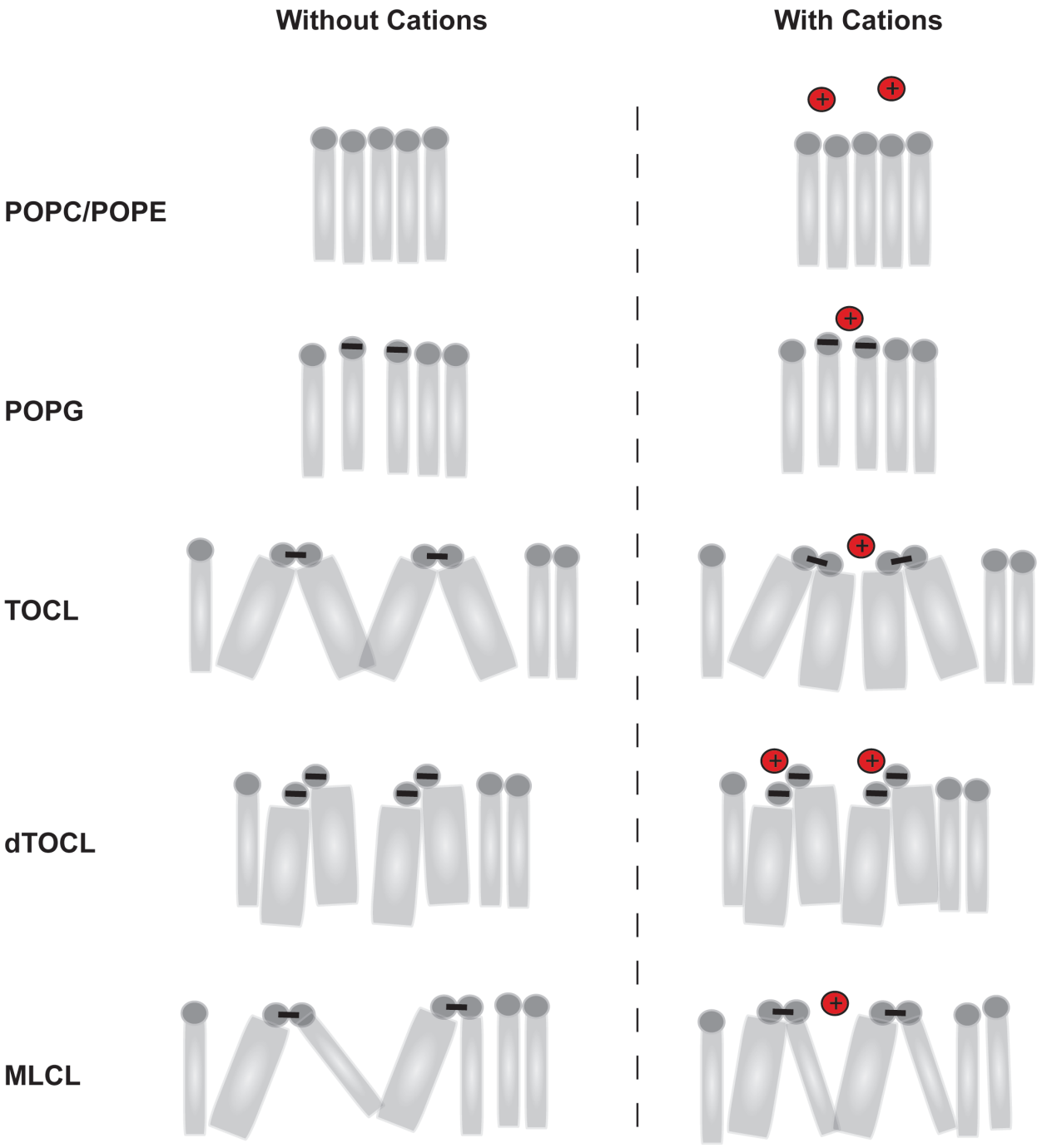

Figure 4.10. Hypothesized effects of divalent cations on various CL-containing bilayers based on present results. While there is no effect of titrating cations into solutions of zwitterionic lipid-containing LUVs (POPC/POPE only), titrating the cations into solutions of

LUVs with anionic phospholipids (POPG, TOCL, dTOCL, MLCL) results in dehydration of the interfacial region of the bilayers and phospholipids packing more closely together. In addition, LUVs containing different forms of CL (TOCL, dTOCL, MLCL) do not behave identically: bilayers containing TOCL- and MLCL-containing LUVs display a more marked effect of cations as compared to dTOCL-containing LUVs.

Chapter 5

Complex II Membrane Subunit Assembly:

A Crosslinking-Based Analysis

Other authors who have contributed to the studies presented in this chapter are Victoria L. Greenwood and Nathan N. Alder. All coauthors are from the University of Connecticut (Storrs, CT 06269, USA).

5.1. Abstract

The assembly process of holoenzyme Complex II within the mitochondrial inner membrane (IM) is largely unknown and made more complicated by the numerous homologs of the Complex II membrane subunits that exist within the membrane. In bacteria, the flagellar switch complex needs to associate with Complex II (SDH) and fumarate reductase (FRD) in order for the correct assembly and switching function of the flagella to occur [98]. There are also two homologs to Sdh4p found in yeast, Tim18p, an integral IM protein that is part of the TIM22 import complex, and YLR164w, a protein with a currently unknown function. It has recently been shown that Sdh3p is able to interact with Tim18p in a way that regulates the assembly of the TIM22 complex, supporting the possibility that these proteins may have a larger regulatory role within the mitochondrial IM than previously believed [96]. The functions of heme and cardiolipin (CL), the signature phospholipid of the IM, in the context of Complex II assembly have also been relatively elusive [46, 47, 51, 157, 267]. Further, while mutants of Complex II that lead to disease states have been identified, the mechanism underlying their pathogenicity is poorly understood.

Therefore, it is necessary to investigate the assembly process of Complex II membrane subunits and the factors that influence dimer formation. In order to evaluate the assembly of the membrane subunits in isolation, we investigated the interaction among Sdh3p, Sdh4p, Tim18p, and YLR164w from *S. cerevisiae* and SdhC and SdhD from the mammalian *Sus scrofa* using a novel cell-free translation system in the presence of IM-mimicking liposomes (large unilamellar vesicles, LUVs). We explored the influence of homologous partner proteins on the unexpected homodimerization of Sdh3p and SdhC and we showed that CL was necessary for membrane protein incorporation into liposomes and homodimer formation. In addition, we found that the

presence of heme enhanced the ability of Sdh3p to form a homodimer and that the presence of partner proteins Sdh4p and SdhD, as well as their homologs, interrupted homodimer formation, likely due to formation of a dynamic heterodimer species. Lastly, we found evidence that the possible mechanism of pathogenicity in a mutant construct of SdhD, Asp 57 Tyr, which has previously been identified as leading to dysfunction of Complex II, may be through inhibition of native Complex II membrane dimer formation.

5.2. Materials and Methods

For Materials, Lipid Preparation, *In vitro* Translation System, and SDS-PAGE and Immunoblot Analysis please see Chapter 2.

5.2.1. Mutagenesis of SDH3, SDHC, SDHD

Site-directed mutagenesis by PCR of mature (lacking a pre-sequence) wild type constructs of *SDH3*, *SDHC*, and *SDHD* was performed as previously described [51]. For the mutagenesis of the heme coordination site in *SDH3*, complimentary mutagenic primers that flank amino acid 106 were designed to change the His residue at this position to an Ala residue, in order to remove the heme coordination site (**Table 5.1**). Pathogenic mutants of *SDHC* and *SDHD* were generated by designing complimentary mutagenic primers that flank the following amino acid residues (with mutations in parentheses): *SDHC* Leu 130 (Pro), *SDHD* Arg 35 (Gly), *SDHD* Pro 46 (Leu), *SDHD* Asp 57 (Tyr), *SDHD* Leu 60 (Pro), *SDHD* His 67 (Leu), *SDHD* Tyr 79 (Cys), and *SDHD* Leu 104 (Pro) (**Table 5.1**, [36]).

5.2.2. Sucrose-Floatation Purification

Translation reactions were brought to 150 μL with hydration buffer, layered on top of a 15% sucrose cushion (15% w/w sucrose in hydration buffer), and subjected to centrifugation at

55K RPM in a Beckman Coulter Optima™ TLX Ultracentrifuge in a TLS-55 swinging bucket rotor for 2 hrs at 15°C. The top ("floated") 150 μL fractions were removed and used for cofactor and crosslinker incubations as the top fraction contains proteins incorporated within floated LUVs [203].

5.2.3. Heme Reconstitution and Incubation

It has previously been shown that heme can be added to proteins externally and the *b*-type cytochrome will be able to form through incorporation and coordination of the heme [268, 269]. Heme was dissolved in 50% EtOH and 100 μL aliquots of 1 M NaOH were added until heme was fully solubilized. This was diluted 4 times in Dilution Buffer (50 mM Tris-HCl, 50 mM NaCl, 5 mM TX-100) and absorbance readings were taken at 385 nm on an Amersham Biosciences Ultrospec 2100 pro UV/Vis Spectrophotometer in 1 cm quartz cuvettes ($\varepsilon = 56\ mM^{-1}cm^{-1}$ at 385 nm for heme). Proteoliposome samples were split in half and incubated with 3 μM heme or a mock heme solution (that consisted of the same chemical and buffer components as heme without the heme cytochrome) at RT for 20 min after sucrose gradient purification.

5.2.4. Crosslinker Incubation

Heme- and mock-treated proteoliposomes were split in half and diluted to 200 μL in crosslinking buffer (20 mM HEPES pH 7.5, 80 mM KCl, 3 mM $MgCl_2$, 250 mM Sucrose, 2 mM KPO_4, 3 mM Malate, 3 mM Pyruvate). Appropriate crosslinker (disuccinimidyl suberate (DSS) for primary amino group conjugation or bis(maleimido)hexane (BMH) for sulfhydryl group conjugation reconstituted in dimethylsulfoxide (DMSO)) was added to 50 μM or an equivalent volume of DMSO was added for control samples and incubated at RT for 30 min. Samples were treated with quencher (40 mM Tris-HCl and 40 mM DTT final concentrations) for 15 min at RT to stop the reaction.

5.2.5. Data Representation and Statistical Analysis

SDS-PAGE gels are representative of at least three independent experiments and crosslinking efficiencies are averages of at least three separate SDS-PAGE gels. Band quantification for crosslinking efficiency analysis was completed using Quantity One software. Crosslinking efficiency data is represented as a percentage of the band intensity (calculated as a relative quantity compared to the intensities of all bands on the gel) of the crosslinked (dimer) species (background corrected) compared to the total band intensity of the crosslinked species and the non-crosslinked (monomer) translation combined, unless otherwise noted. A two-tailed student T-test (unequal variance) was used to determine statistical significance ($p \leq 0.05$).

5.3. Results and Discussion

The holoenzyme of Complex II is assembled *in vivo* as a heterodimer of Sdh3p/SdhC and Sdh4p/SdhD within the membrane that forms a base with which the soluble catalytic dimer Sdh1p/SdhA and Sdh2p/SdhB can then interact (numerals and letters correspond to yeast and mammalian nomenclature, respectively). By utilizing our developed *in vitro* translation system, various constructs of the membrane-bound Complex II subunits were produced and incorporated into proteoliposomes in order to study this first stage of holoenzyme formation: membrane heterodimer assembly. In our crosslinking-based approach, proteoliposomes were purified *via* floatation on a sucrose cushion and then treated with appropriate crosslinker. Two types of homobifunctional crosslinkers were applied in this study, disuccinimidyl suberate (DSS), which reacts with primary amino groups to link Lys residues, and bis(maleimido)hexane (BMH) that crosslinks the sulfhydryl groups of Cys residues. The reason for using two crosslinkers was that Sdh3p does not natively contain Cys residues, therefore DSS was used for studies involving

Sdh3p while BMH proved to be more potent crosslinker for SdhC, which does contain multiple Cys residues, as do Sdh4p and SdhD.

5.3.1. Sdh3p and SdhC Homodimerize; Sdh4p and SdhD are Unable to Homodimerize

Unexpectedly, we first found that in the presence of IM-mimicking lipid environments, Sdh3p and SdhC favor homodimerization (**Figure 5.1A**). The darker bands (open arrows) near the bottom of the gel represent the monomeric species of each protein (Sdh3p is 16.7 kDa; SdhC is 15 kDa) [36, 46]. It was clear that with crosslinker present, a homodimer species of Sdh3p or SdhC was assembled and sustained within the nonpolar environment provided by the liposomes, but SdhC seemed to crosslink to a greater extent than Sdh3p (filled arrows). While at first these results were surprising, the homodimerization of Sdh3p and SdhC may act as a regulatory system within the mitochondria. A regulatory role for Sdh3p and SdhC homodimerization is further supported by evidence that Sdh4p and SdhD do not form detectable crosslink-stabilized homodimers (**Figure 5.1B**). However, it is important to note that Sdh4p and SdhD may form more dynamic, transient homodimers allowing them to sample the surrounding membrane for a heterodimer binding partner. Unless Sdh3p encounters an Sdh4p native partner protein, potentially also requiring the presence of the catalytic dimer subunits Sdh1p and Sdh2p, it will homodimerize until the appropriate signals or proteins for holoenzyme Complex II assembly are present within the local environment as well.

5.3.2. Sdh3p and SdhC homodimerization is dependent on the presence of lipid

The homodimerization of Sdh3p and SdhC was a novel and intriguing finding that we investigated further to determine the external factors that may influence such dimerization. First,

we wanted to determine the necessity of the lipid environment for this newfound homodimerization. After completing a cell-free translation in the presence of LUVs, which provide a mitochondrial IM-mimicking (CL-containing) environment, the reaction was floated on a sucrose cushion for purification and the floated fraction was removed and treated with appropriate crosslinker (**Figure 5.2**, "Float."). In parallel, an *in vitro* translation was also completed in the absence of LUVs and was then treated with crosslinker (**Figure 5.2**, "Trans."). It was found that only protein that was incorporated into the liposomes, which is represented by the "Floated" lanes, and treated with crosslinker could form homodimers.

There was evidence of higher molecular weight species in the lanes representing translations in the absence of LUVs that were similar in molecular weight to the dimer formed by Sdh3p. It has previously been shown that SDS can have stabilizing effects on the assembly of heme-binding transmembrane *b*-type cytochromes [270], even without the presence of crosslinker, and we briefly speculated that these species may represent SDS-stabilized Sdh3p or SdhC homodimers that survived electrophoresis. This hypothesis could be discounted because identical higher molecular weight species were present in both Sdh3p and SdhC translations and Sdh3p and SdhC are of different molecular weights (16.7 and 15 kDa, respectively). In addition, these species were not of exactly the same mobility as the crosslinked species seen in the floated lanes. Instead, it is likely that the species we observed in the translation-only (in the absence of LUVs; **Figure 5.2**, "Trans.") lanes are wheat germ proteins from the cell-free translation system that were common between the two constructs and were not actually dimers of Sdh3p or SdhC. These proteins would not be present in the samples translated in the presence of LUVs and then floated on sucrose because excess unincorporated protein aggregates and pellets to the bottom of the sucrose gradients (i.e. is removed from the floated fractions). These results provide evidence

that a native-like lipid environment is necessary in order for the membrane subunits of Complex II to interact and form crosslink-stabilized homodimers.

5.3.3. Cardiolipin-dependent homodimerization of Sdh3p and SdhC

Next, we wanted to determine if dimerization was dependent on lipid type or if a general lipid environment (as represented by the LUVs) was the only requirement. To study this, we made two preparations of liposomes mimicking the IM of the mitochondrion: one containing cardiolipin (CL), the signature phospholipid of the energy conserving mitochondrial IM, and the other devoid of CL, containing only POPC and POPE, the predominant phospholipids of the IM. As shown by us and several other groups, CL is necessary for the correct assembly, activity, and stability of mitochondrial IM complexes, such as the ADP/ATP Carrier and Complex II itself [163, 189, 271, 272]. Interestingly we found a stark contrast between translations completed in the presence and absence of CL (**Figure 5.3A**). Whereas Sdh3p and SdhC were able to form homodimers when translated in the presence of CL-containing LUVs, remarkably, there was no homodimerization detected when these same constructs were translated in the presence of LUVs without CL. The results clearly indicated the need for CL in the homodimerization process of Sdh3p and SdhC; without CL, homodimers were unable to be stabilized by crosslinker and likely unable to form at all.

After establishing that CL is necessary for assembly of the membrane subunits, we wanted to determine whether CL enhances insertion of the proteins into the liposome membrane, facilitates dimerization once the proteins are already inserted into the membrane, or influences both processes. We compared the intensity of translated protein (either Sdh3p or SdhC) found in the top-most floated (incorporated into LUVs, **Figure 5.3B** "F") and bottom-most pelleted (non-

incorporated protein, **Figure 5.3B** "P") fractions of a sucrose cushion when translations were completed in both the presence and absence of CL. We reasoned that if there was an increase in intensity of the protein found in the top (floated) fraction with CL present as compared to when it was absent and/or a decrease in the intensity of the pelleted fraction with CL-containing LUVs, then this would support that CL increases the ability of Sdh3p and SdhC to insert into the liposome membranes. As indicated in **Figure 5.3B**, when comparing the intensity of protein contained within the floated fractions ("F") when CL was present and when it was absent from the LUVs, it was clear that CL was required for insertion of Sdh3p and SdhC.

Also of note was that the translation efficiency in CL-containing and CL-lacking LUVs seemed to be consistent (**Figure 5.3B**, Compare "T" translation lane with and without CL). Therefore, the increase in insertion into the liposome membrane was not solely a reflection of increased translation efficiency in the presence of CL leading to a higher protein concentration so that more protein was inserted, but was instead caused by an increased liposome insertion efficiency.

5.3.4. Heme-dependent homodimerization of Sdh3p and SdhC

In addition to studying the influence of lipid on the homodimerization of Sdh3p and SdhC, we studied the impact of heme on dimerization. Heme is coordinated between the heterodimer of the Complex II membrane subunits (Sdh3p and Sdh4p or SdhC and SdhD), but the function of the heme is up for debate within the Complex II field (See Chapter 1). Based on a homology model of yeast Complex II, the heme coordination site is comprised of a typical His residue on Sdh3p, whereas the proximal His position of Sdh4p is replaced by a Tyr residue [37]. Therefore, it has been postulated that Sdh4p coordinates the heme with a nearby Cys residue,

which has not been observed for any other *b*-type cytochrome, of which Complex II is part [47, 50, 51]. On the other hand, both SdhC and SdhD contain the requisite and traditional His residue to coordinate heme [36]. In our cell-free system, heme appeared to promote the homodimerization of Sdh3p even without crosslinker present, which was remarkable because no other condition seemed to stabilize dimerization in a crosslinker-independent manner (**Figure 5.4A**). On the other hand, the influence of heme was not as apparent with SdhC. Heme did not seem to enhance dimerization when crosslinker was present and it did not sustain a non-covalent interaction (when crosslinker was not present) between SdhC subunits as it did for Sdh3p.

In order to study the effect of heme further, we used site-directed mutagenesis of *SDH3* to alter the native heme axial ligand His106 to an Ala residue [51]. As before, an *in vitro* translation was conducted in the presence of LUVs, the proteoliposomes were purified *via* sucrose floatation, and the samples were treated with both heme and crosslinker. As seen in **Figure 5.4B**, when crosslinker was present we found that heme did not increase the dimerization efficiency of the mutant as it did for the wild type Sdh3p and may have even decreased the ability of the mutant Sdh3p to homodimerize. Even more interesting, heme did not stabilize a dimer of the mutant species without crosslinker, as it did with native Sdh3p, further supporting that heme has a strong influence on the homodimerization and assembly of wild type Sdh3p. Previous studies have shown that when this mutagenesis was conducted in yeast and *Escherichia coli*, the presence of heme did not have a critical role in assembly or activity of Complex II [47, 55]. By contrast, our results indicate that whereas heme may not be an absolute requirement for homodimerization of Sdh3p, it promotes the stability of this interaction.

5.3.5. Sdh4p-, SdhD-, Tim18p-, and YLR164w-dependent destabilization of Sdh3p and SdhC homodimerization

Having investigated the lipid- and heme-dependent dimerization of Sdh3p and SdhC, we next investigated the influence that the native complementary binding partners, Sdh4p and SdhD, have on homodimerization of Sdh3p and SdhC. We co-translated the proteins in the presence of LUVs and floated them on sucrose cushions as above. We found that Sdh4p slightly disrupted the Sdh3p homodimer and SdhD disrupted the SdhC homodimer, which was expected because Sdh3p and Sdh4p are the complementary *S. cerevisiae* constructs and SdhC and SdhD are the partner mammalian porcine constructs (**Figure 5.5**). However, it was remarkable to find that whereas SdhD could also disrupt the Sdh3p homodimerization, Sdh4p was not able to disrupt the SdhC homodimers and could potentially even cause a strengthening of homodimerization.

Further, as mentioned above, Sdh4p contains two homologous proteins in yeast, Tim18p, which is part of the TIM22 import complex of the mitochondrial IM and YLR164w, a protein of unknown function, that is also found in the mitochondria [46]. We wanted to investigate the influence that these proteins may have on Sdh3p and SdhC homodimerization because Tim18p contains a Tyr in the heme-coordination position similar to Sdh4p, but YLR164w contains a His in this position similar to SdhD [47]. As displayed in **Figure 5.5**, both Tim18p and YLR164w disrupted both the Sdh3p and SdhC homodimers. Interestingly, Tim18p seemed to interrupt the homodimers of Sdh3p and SdhC to a slightly greater extent than YLR164w, but both seemed to disrupt the Sdh3p homodimer more strongly than the native complementary protein Sdh4p. However, neither was more effective than mammalian SdhD at disrupting SdhC, and even Sdh3p, homodimers indicating that SdhD is most efficient at interrupting the formation of

homodimers regardless of the species from which its complementary membrane subunit was derived.

These findings are even more intriguing when considering that Tim18p mimics Sdh4p in that both contain Tyr residues in the position expected to coordinate heme, which may assist in explaining why Tim18p seemed to interact with Sdh3p to a greater extent than YLR164w. On the other hand, YLR164w more closely resembles SdhD in that the His is in the putative position to coordinate a heme; however, YLR164w is unable to disrupt Sdh3p or SdhC homodimerization as effectively as SdhD. While these divergent heme coordination residues may influence the interaction between binding partners, they do not seem to definitively determine how strongly two partner proteins are going to interact. Taken together, these novel results implicate yeast-derived homologs of Sdh4p in not only influencing the homodimerization of Sdh3p, but also that of SdhC, the homologous porcine construct. These results provide further support for the hypothesis that the membrane subunits of Complex II are dynamically interacting proteins and may even have a deeper regulatory role in the mitochondria than previously thought.

5.3.6. The Asp 57 Tyr Pathogenic Mutant of SdhD Homodimerizes

After obtaining the surprising and interesting result that Sdh3p and SdhC form homodimers, whereas Sdh4p and SdhD do not form homodimers, we looked further into the implications that homodimerization may have in the molecular etiology of Complex II-associated diseases. We produced a panel of SdhC and SdhD point mutants that have previously been implicated in tumorigenic disease progression and tested them for the ability to alter homodimerization patterns. The majority of mutant constructs behaved in an identical manner to the wild type proteins: SdhC Leu 130 Pro was able to homodimerize similar to wild type SdhC

and seven of the eight SdhD mutants were unable to homodimerize, just as with wild type SdhD (**Figure 5.6A** and **B**). In addition, the homodimers of SdhC Leu 130 Pro were disrupted by SdhD and the SdhD mutants were able to disrupt SdhC homodimerization (data not shown).

However, unlike wild type SdhD, the pathogenic SdhD Asp 57 Tyr mutant showed strong potential for homodimerization (**Figure 5.6B**). This surprising result indicated that this particular mutant of SdhD may contribute to pathogenesis by allowing strong SdhD homodimers to form, perhaps preventing SdhD from interacting with SdhC, breaking up the SdhC homodimers, and forming a stable membrane heterodimer for the assembly of holoenzyme Complex II. In this way, equivalent amounts of membrane protein subunits may be produced in an individual carrying the mutant SdhD, but the inability to disrupt SdhC homodimers and set up native membrane heterodimer interacting sites for Complex II catalytic dimers may contribute to the development of tumorigenesis.

5.4. Brief Conclusions

The membrane subunits of respiratory Complex II, Sdh3p/C and Sdh4p/D, were the focus of the current study and we have used native mitochondrial IM-mimicking (i.e. CL-containing) liposome environments to study the assembly of these proteins. It is a completely novel finding that Sdh3p and SdhC homodimerize when translated in an *in vitro* wheat germ system in the presence of LUVs (**Figure 5.7**). This interaction required a CL-containing lipid environment and was stable enough to be captured through the use of chemical crosslinking agents. In addition, homodimer formation was promoted by heme. On the other hand, when Sdh4p or SdhD (or their homologs) were added to their complementary partner protein of the same species, the homodimerization of Sdh3p and SdhC was disrupted. However, we found no

evidence of a stabilized heterodimer likely due to the lack of proximal side chains with reactivity suitable for the chemical crosslinkers used. These results may also suggest that the heterodimer species may exist in a very dynamic state, constantly sampling the surrounding environment and interacting with other proteins, and may only be stabilized by the presence of the soluble Complex II catalytic dimer. In the future, it will be interesting to investigate the influence that the presence of the soluble catalytic dimer or other TIM22 subunits have on the homodimerization and assembly of the Complex II membrane dimer. In addition, these results shed light on the pathogenicity of certain characterized mutations of Complex II membrane subunits and further consideration is necessary to determine if newly recognized mutations of Complex II may also have implications in the development of disease states by their formation of non-native homodimers.

5.5. Figures and Tables

Protein	Site	Site Significance	Mutagenic Primer (Sense Strand; 5' - 3')
Sdh3	H106A	Heme Coordination	CTTACTTATTTGCAATTGCCTATGGTGGCGCC
SdhC	L130P	Pathogenic	CAGTCTGGAGTGGTTGTCTTGATTCCTACTGTGTTG
SdhD	R35G	Pathogenic	CTGGACTGGTGAGGGGGTTGTCAGTGTTTTG
SdhD	P46L	Pathogenic	GGGCCTACTTTTAGCCGCTTATTTGAATCCTTGCTC
SdhD	D57Y	Pathogenic	CTTATTTGAATCCTTGCTCTGCGATGTACTACTCCCT
SdhD	L60P	Pathogenic	CTTATTTGAATCCTTGCTCTGCGATGGACTACTCCCCGGCCGC
SdhD	H67L	Pathogenic	CTCACTCTCCTTGGTCACTGGGGCATTG
SdhD	Y79C	Pathogenic	CAAGTCGTTACTGACTGCGTGCGAGGGGATGCACTG
SdhD	L104P	Pathogenic	GCTTTCACCTTTGCTGGGCCTTGTTATTTCAAC

Table 5.1. Sdh3, SdhC, and SdhD Mutagenic Primers.

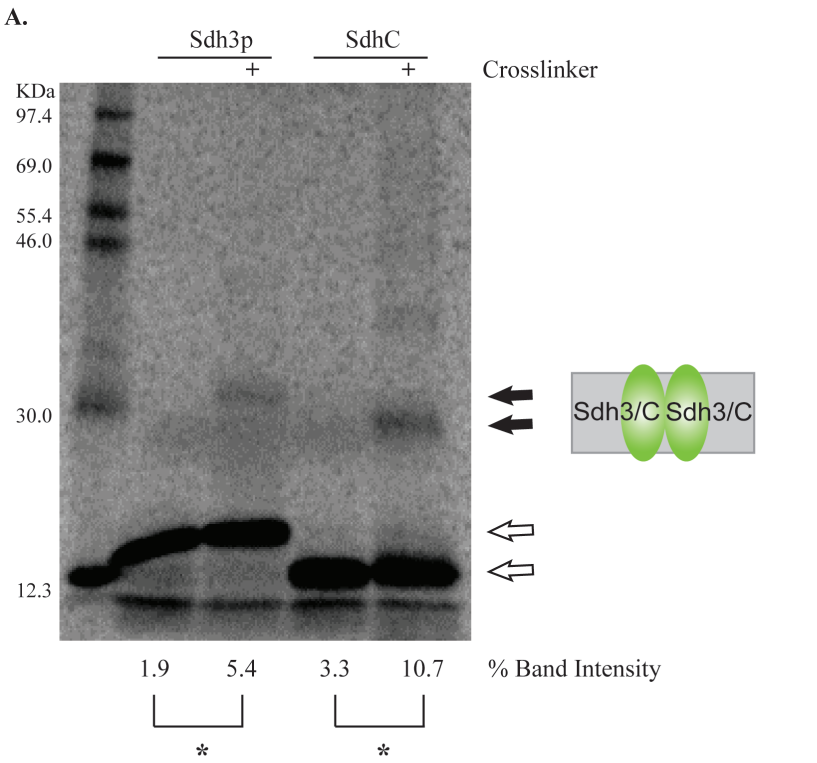
A.
Sdh3p
SdhC
+
+
Crosslinker
KDa
97.4
69.0
55.4
46.0
30.0
12.3
Sdh3/C Sdh3/C
1.9
5.4
3.3
10.7
% Band Intensity
*
*

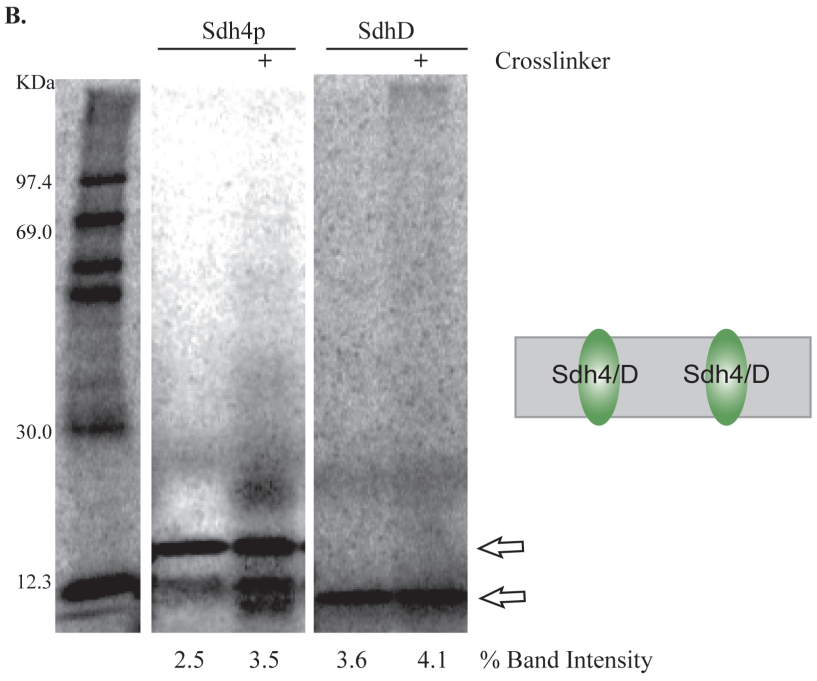
B.
Sdh4p
SdhD
+
+
Crosslinker
KDa
97.4
69.0
30.0
12.3
Sdh4/D
Sdh4/D
2.5
3.5
3.6
4.1
% Band Intensity

Figure 5.1. Complex II Sdh3p/C membrane subunits form homodimers. *In vitro* translations of (**A**) Sdh3p and SdhC or (**B**) Sdh4p and SdhD were conducted separately in the presence of [^{35}S]Methionine and IM-mimicking liposomes, purified *via* a 15% sucrose cushion, and treated with crosslinker (Sdh3p/Sdh4p were treated with DSS and SdhC/SdhD were treated with BMH) or buffer. The dark bands at approximately 15 kDa represent the monomeric species of the proteins (open arrows, with the higher arrow pointing to Sdh3p/Sdh4p and the lower arrow pointing to SdhC/SdhD); the lighter bands running at approximately 30 kDa represent the crosslinked homodimer species (filled arrows). The small molecular weight species present at the bottom of the gel below the monomeric Complex II membrane subunits are most likely protease-digested proteins. Percent Band Intensity was determined as in Section 5.2.5.

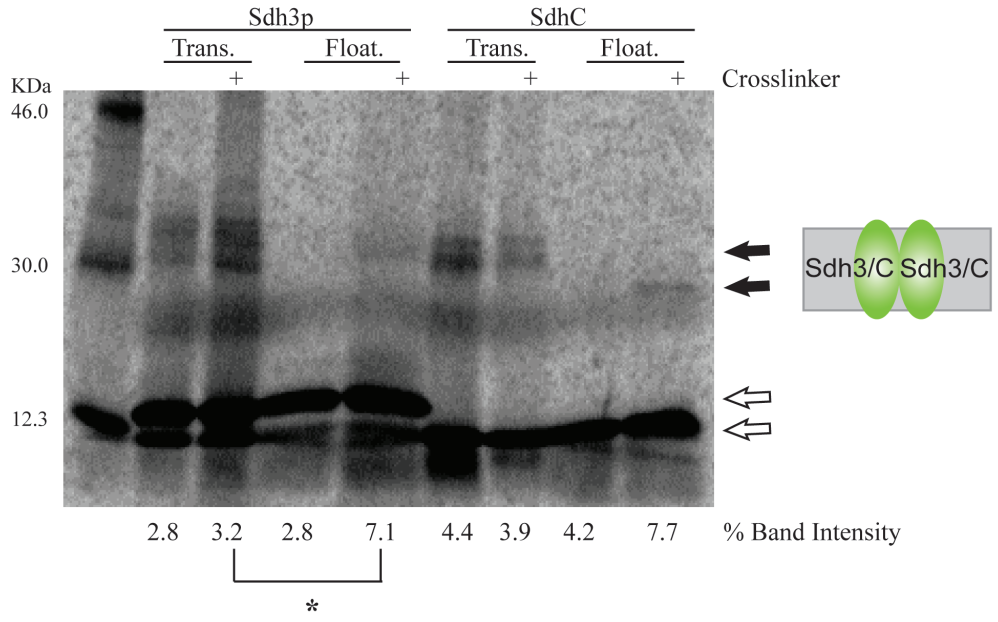

Figure 5.2. Lipid environment is necessary for homodimerization of Sdh3p and SdhC. *In vitro* translations of Sdh3p and SdhC and proteoliposome purifications were conducted as in **Figure 5.1** with and without liposomes. The dark bands at 15 kDa represent the monomeric species of each protein (open arrows). When liposomes are present (labeled "Float." lanes) the species at approximately 30 kDa represents the dimeric species (filled arrows). The bands present at approximately equivalent molecular weights in lanes of the translation without liposomes (labeled "Trans.") represent contaminating accessory wheat germ proteins. Percent Band Intensity was determined as in Section 5.2.5.

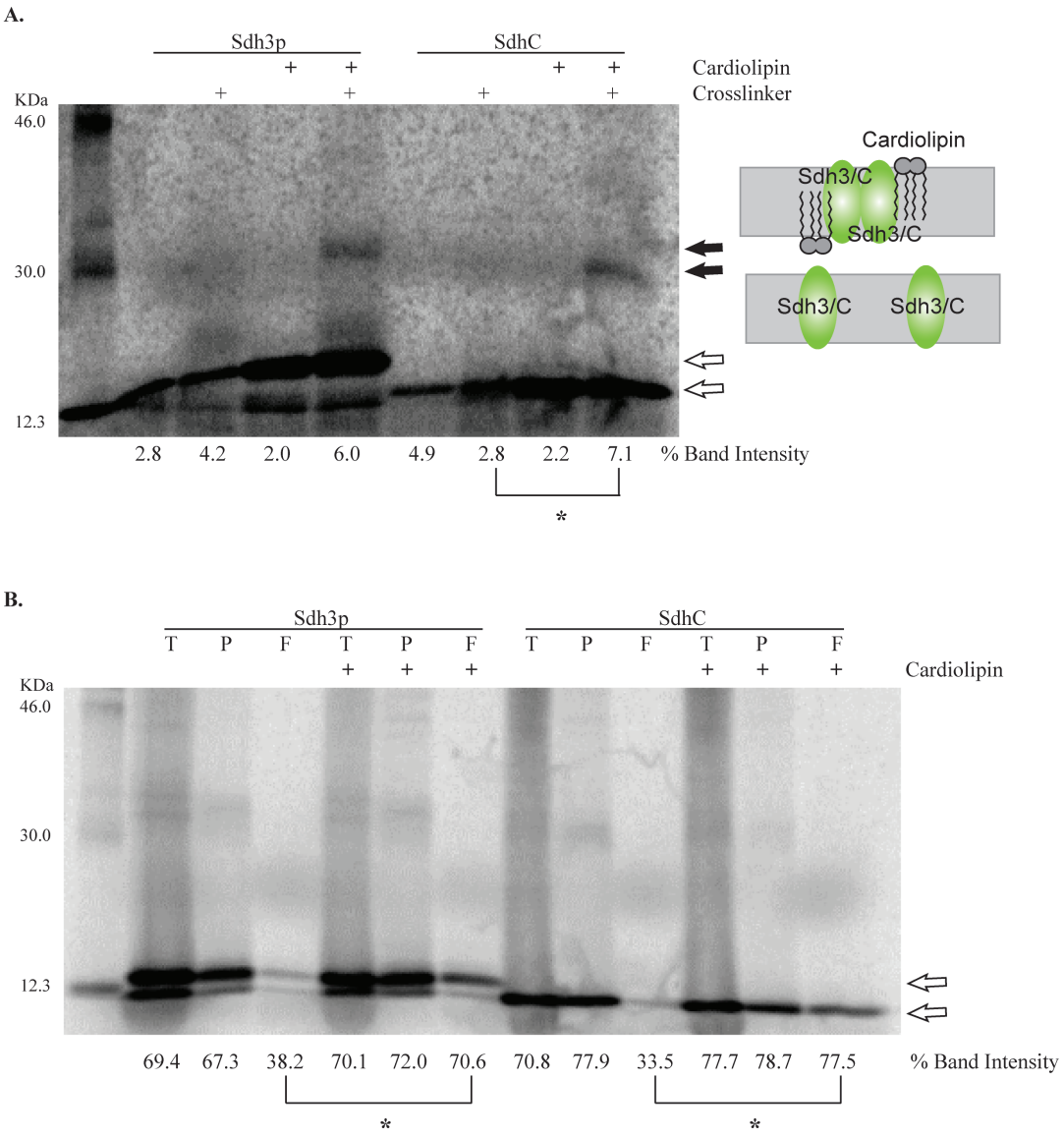

Figure 5.3. CL is necessary for homodimerization of Sdh3p and SdhC. *In vitro* translations of Sdh3p and SdhC were conducted as in **Figure 5.1** in the presence of liposomes with and without cardiolipin. Part of the translation was removed to run immediately on a separate SDS-PAGE gel (**B**) and the remaining translation was purified *via* a 15% sucrose cushion and samples from the floated fraction as well as the pelleted fraction were removed. (**A**) The floated fraction was treated with crosslinker or buffer. Dimers were only present when protein was translated in

the presence of CL-containing liposomes. (**B**) The translation ("T") efficiency, and the pellet ("P") and the floated ("F") fractions incorporation efficiency were compared for the monomeric translated species. Note that the gel was left on the screen for only a couple of hours, compared to the overnight exposure of for the other SDS-PAGE gels. For both (**A**) and (**B**) monomers and dimers are labeled as in **Figure 5.1**. Percent Band Intensity was determined as in Section 5.2.5.

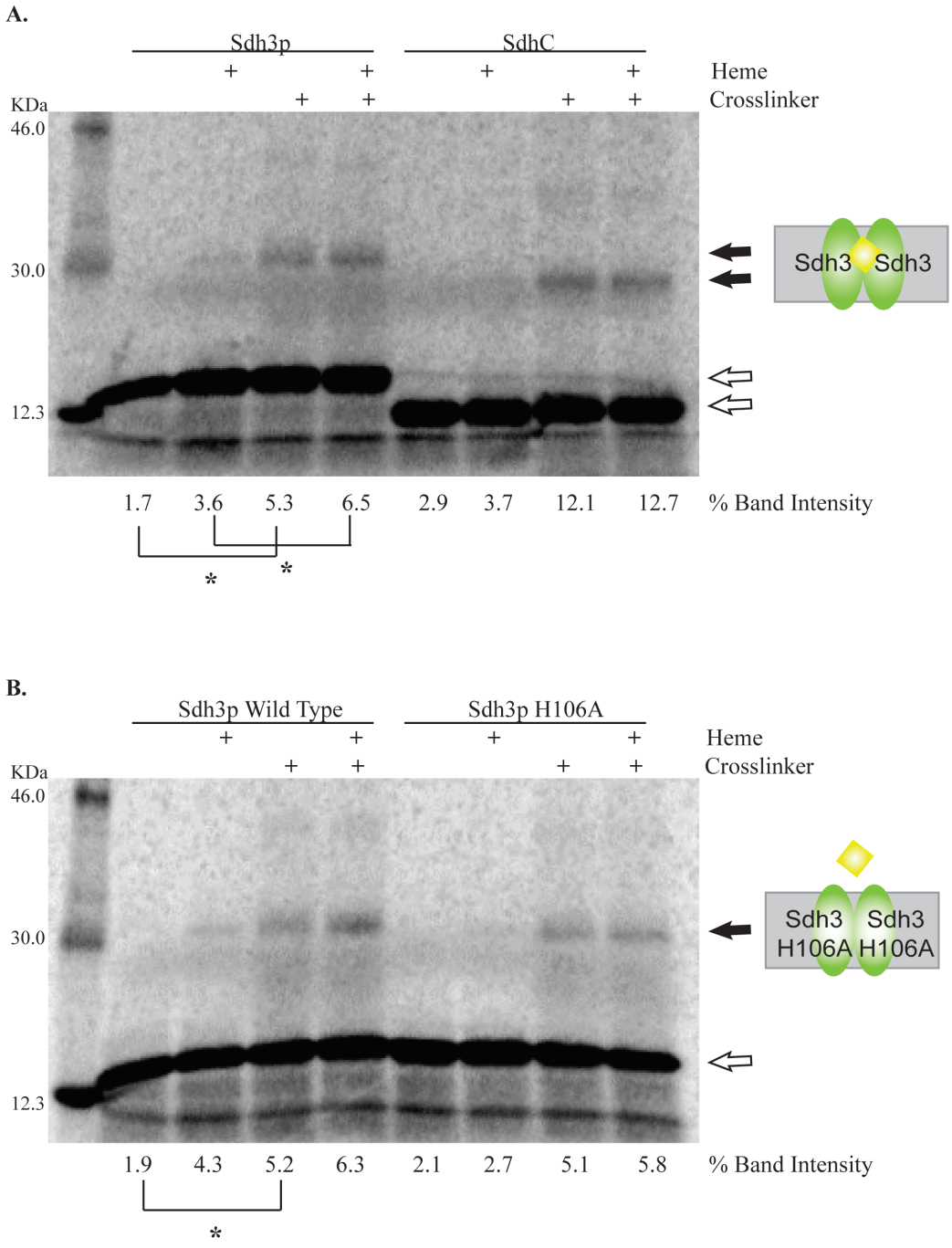

Figure 5.4. Heme enhances the homodimerization of Sdh3p, but not SdhC. Protein was translated and proteoliposomes purified as in **Figure 5.1** and incubated with heme or buffer prior to crosslinker or buffer treatment. Monomer and dimer species are labeled as in **Figure 5.1**. Sdh3p homodimerization was enhanced and stabilized by heme, whereas SdhC

homodimerization was not (**A**). When the heme coordination site was mutagenized (His 106 Ala), the influence of heme was removed and the profile of homodimerization resembled that of SdhC, which was unaffected by heme (**B**). Percent Band Intensity was determined as in Section 5.2.5.

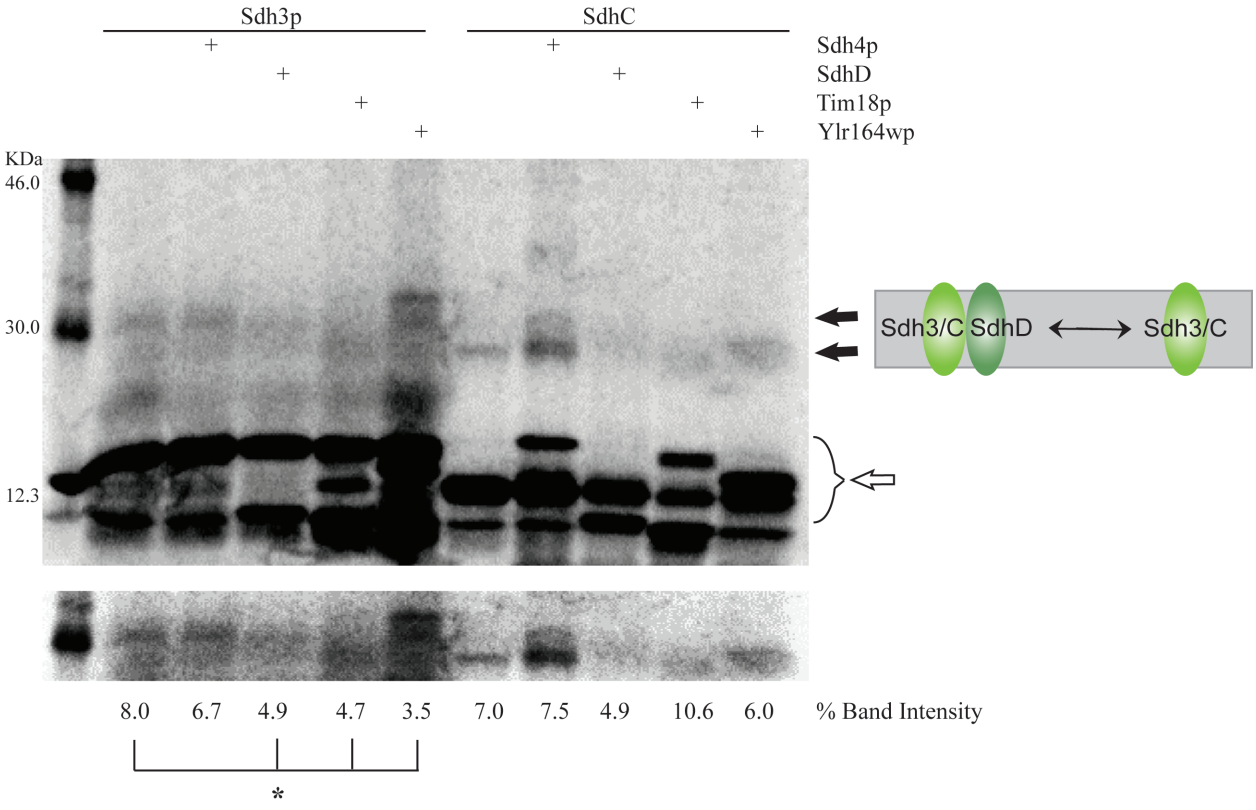

Figure 5.5. Sdh4p, SdhD, and their homologs affect the homodimerization of Sdh3p and SdhC. *In vitro* translations of Sdh3p or SdhC alone or co-translated with Sdh4p, SdhD, Tim18p, and YLR164w were completed, purified, and treated with crosslinker as in **Figure 5.1**. The dark bands between 15-10 kDa represent the monomeric species (indicated by the open arrow; Sdh4p is 16.6 kDa, SdhD is 11 kDa, Tim18p is 18 kDa, and YLR164w is approximately 18 kDa [36, 46, 94]) of the translated proteins and the lighter bands at 30 kDa represent the homodimers (filled arrows) of either Sdh3p or SdhC. If no homodimer band is present, the complementary protein subunit disrupted the homodimerization of Sdh3p or SdhC. Percent Band Intensity was determined as in Section 5.2.5.

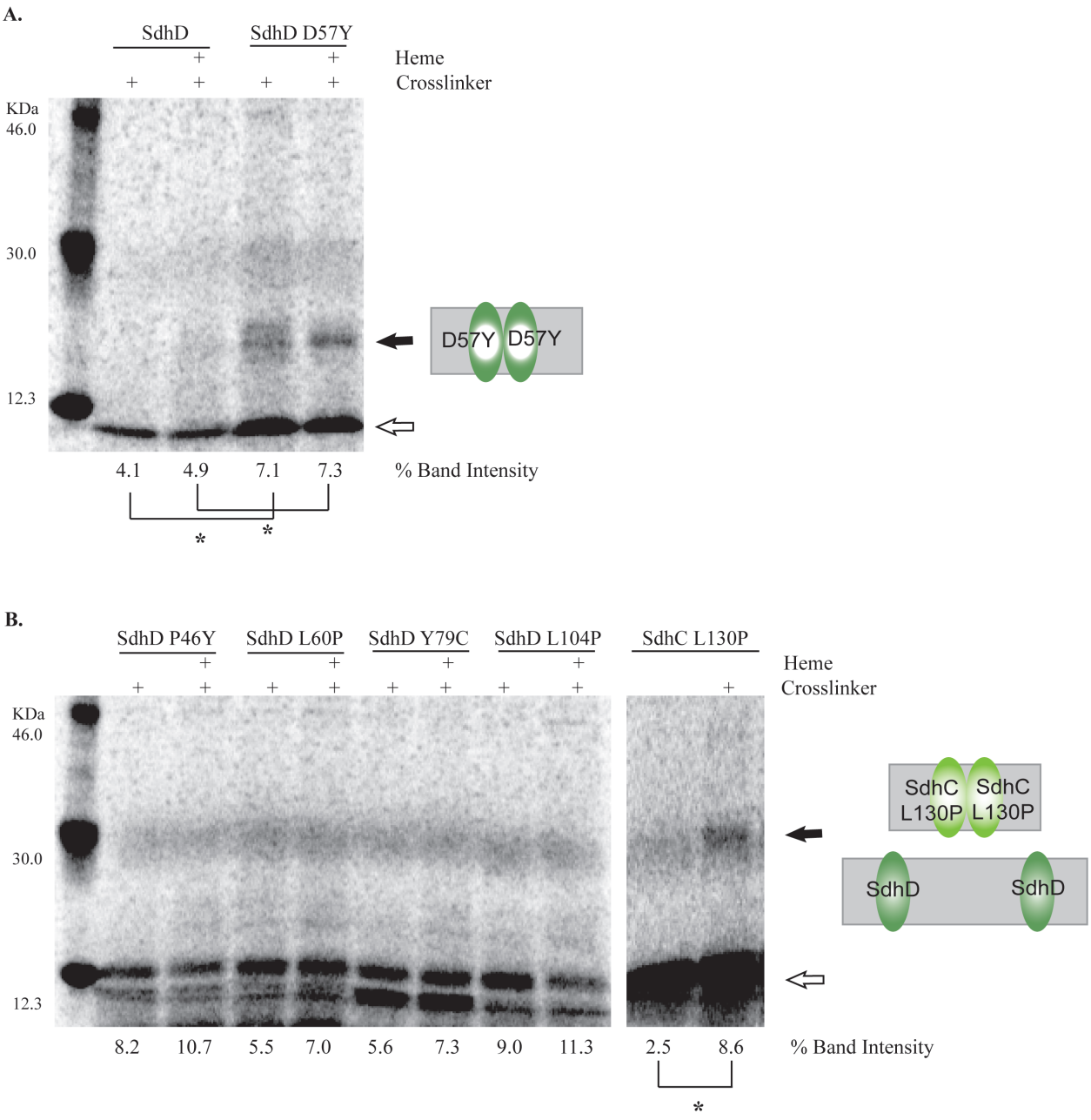

Figure 5.6. SdhD D57Y pathogenic mutant is able to homodimerize, unique among eight SdhC and SdhD pathogenic mutants studied. *In vitro* translations of (**A**) SdhD D57Y or (**B**) SdhC L130P and various SdhD pathogenic mutants were completed and proteoliposomes purified as in **Figure 5.1**. The dark bands between 15-10 kDa represent the monomeric species of the proteins translated (open arrows) and the lighter bands at 30 kDa represent the

homodimers of SdhC and SdhD pathogenic mutants (filled arrows), which only formed in the case of SdhC L158P and SdhD D57Y. Percent Band Intensity was determined as in Section 5.2.5.

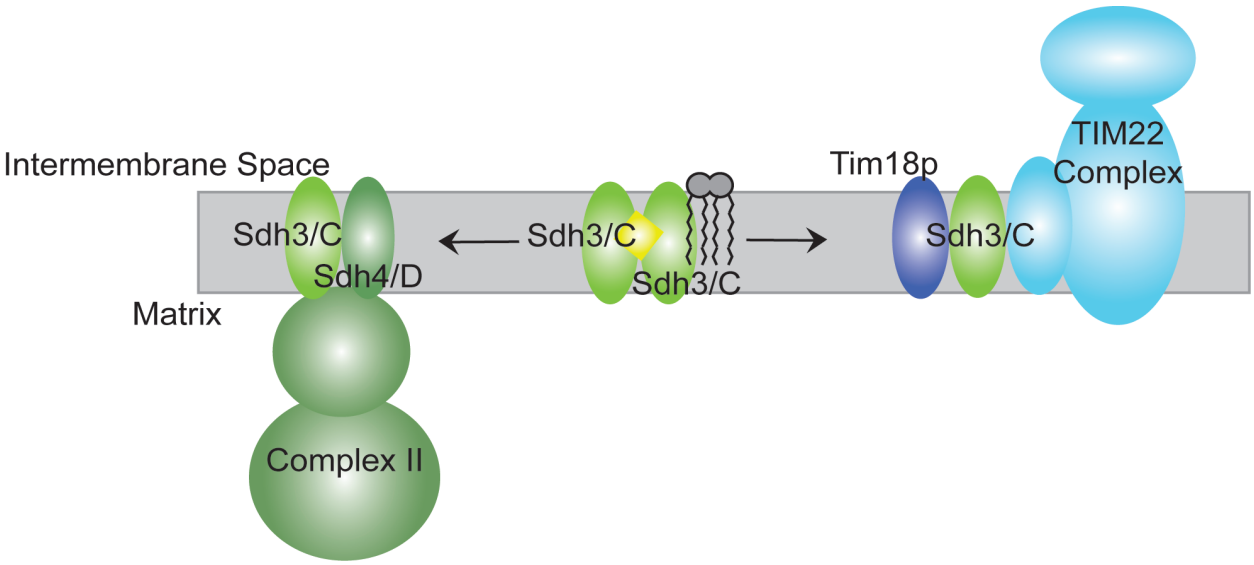

Figure 5.7. Schematic of potential interactions of Sdh3p and SdhC with complementary partner subunits. The growing interactome of Complex II membrane subunits may influence the assembly of holoenzyme Complex II and other mitochondrial IM protein complexes.

Chapter 6

Sdh3 Helix I and its Involvement in Complex II Holoenzyme Assembly

Other colleagues who have contributed to the studies presented in this chapter are Victoria L. Greenwood, Matthew Greenwood, and Nathan N. Alder, all from the University of Connecticut (Storrs, CT 06269, USA).

6.1. Abstract

Despite the fact that respiratory Complex II is the linkage point between the Tricarboxylic Acid (TCA) cycle and the electron transport chain (ETC), marking it as a critical control point central to cellular energy metabolism, little is understood regarding how its four protein subunits and associated cofactors assemble into the holoenzyme. The porcine structure of the complex pointed to particular structural features of SdhC that could interact with SdhB and mediate catalytic and membrane dimer interactions [36]. A soluble helix, termed Helix I, of approximately 15 amino acids at the N-terminus of SdhC (residues 6 to 20) is located in the matrix near the SdhB subunit. This helix accounts for forty percent of the contact area between SdhB and the membrane dimer. Further, Helix I is attached to the main transmembrane segments of SdhC through a flexible linker region and may therefore be important in mediating and recognizing the interaction between the membrane subunits and SdhB depending on local environmental conditions.

Although the crystal structures implicate Helix I as a tremendously important piece in the assembly of holoenzyme Complex II, the helix has not yet been studied in any particular detail. Therefore, the present study utilized nanodisc (ND) reconstitutions of the holoenzyme Complex II to investigate the general assembly of the yeast Complex II and the specific role that Helix I plays in this assembly. The holoenzyme was reconstituted by incubating catalytic dimer resolved directly from solubilized mitochondria with membrane dimer translated in a cell-free system and incorporated into NDs. In order to probe assembly even further, we have engineered mutant constructs of the Complex II Sdh3p membrane subunit in order to use IASD chemical labeling and NBD fluorescence quenching to investigate the dynamics of Helix I. We found preliminary evidence to support that Helix I can sample different conformations depending on

the local environment in order to allow, or inhibit, catalytic dimer attachment and holoenzyme assembly.

6.2. Materials and Methods

For Materials, Lipid Preparation, Mitochondria Solubilization, *In vitro* Translation System, and SDS-PAGE Analysis details, please see Chapter 2.

6.2.1. Catalytic Dimer Isolation

We have previously shown that when NDs lacking cardiolipin (CL) are utilized to isolate Complex II from solubilized membranes, there was a high level of instability between the catalytic and membrane dimers (Chapter 3, [157]). We have exploited these conditions by utilizing DMPC NDs to capture catalytic dimer that has broken free of membrane dimer reconstituted within NDs after metal affinity purification. Membrane Scaffolding Protein (MSP, specifically MSP1E3D1) was synthesized and purified as described [223]. DMPC, MSP1E3D1 (in lipid: MSP1E3D1 ratio of 122:1), DDM-solubilized mitochondria, and MSP buffer ([cholate] = 14.8 mM) were incubated at RT for 30 min. Pre-hydrated Bio-Beads SM Hydrophobic Interaction Adsorbent (Bio-Rad Laboratories, Inc., Hercules, CA) were added and rotated at RT for 2 h to remove detergent and initiate ND self-assembly. After Bio-Bead removal, NDs were incubated with Ni-NTA agarose at RT for 40 min. They were then subject to step gradients of MSP buffer and imidazole (up to 400 mM) to isolate NDs *via* the His-tagged MSP1E3D1. The middle wash fractions (Washes 2A-3B) containing free catalytic dimer were combined, dialyzed into MSP buffer with 100 mM ammonium sulfate to improve catalytic dimer stability, and concentrated in Centricon 3000 MWCO tubes in an Eppendorf Centrifuge 5804R. Ammonium sulfate has previously been shown to enhance reconstitution of Complex II due to

"antichaotropic" activity: the sulfate ion has a structuring effect on water molecules, slowing their diffusion [273]. Catalytic dimer was then prepared for addition to NDs containing Complex II membrane subunits.

6.2.2. Complex II Holoenzyme Reconstitution

Biomimetic lipid mix, MSP1E3D1 (in lipid: MSP1E3D1 ratio of 143:1), *in vitro* translation product, and MSP buffer ([cholate] = 14.8 mM) were incubated at RT for 30 min. Pre-hydrated Bio-Beads SM Hydrophobic Interaction Adsorbent (Bio-Rad Laboratories, Inc., Hercules, CA) were added and rotated at RT for 2 h to remove detergent and initiate ND self-assembly. After Bio-Bead removal, NDs were incubated with isolated catalytic dimer, 3 μM heme, and 0.23 M ammonium sulfate while rotating at RT for 1 h. ND samples were then incubated with Ni-NTA agarose at RT for 40 min and subject to step gradients of MSP buffer and imidazole (up to 400 mM) to isolate NDs *via* the His-tagged MSP1E3D1. The first two elution fractions containing NDs assembled with holoenzyme Complex II were combined, dialyzed into MSP buffer to remove imidazole and concentrated in Centricon 3000 MWCO tubes in an Eppendorf Centrifuge 5804R.

6.2.3. Site-Directed Mutagenesis

Site-directed mutagenesis of Sdh3p Helix I was conducted by PCR of a mature (pre-sequence removed) wild type construct of *SDH3* as previously described [51]. Complimentary mutagenic primers that flanked each of the desired sites (Thr8, Ala13, and Leu18) were designed to change each of the residues at those positions to Cys. The forward primer sequences for Thr8, Ala13, and Leu18 were: 5'- GGCCAGTGAAATGAACTGCAAAGCGGCAATTG-3'; 5'-GAAATGAACACCAAAGCGGCAATTTGTGAAGAACAAATATTAAAC-3'; and 5'-GCGGCAATTGCTGAAGAACAAATATGTAACAAGCAAAGAGC-3', respectively. The

mutagenized constructs were sequenced at the Biotechnology and Bioservices Center in the DNA Biotechnology Facility at the University of Connecticut (Storrs, Connecticut) in order to confirm that mutagenesis occurred.

6.2.4. IASD Labeling

In vitro translations were completed as in Chapter 2 with the addition of ^{35}S-Met and Sdh3p mRNA constructs mutated at various positions along Helix I to contain Cys residues. Translations were halted *via* cycloheximide incubation for 20 min at RT, combined as appropriate (i.e. ^{35}S-Sdh3p and Sdh4p) and added directly to ND reactions. ND assembly reactions were completed as in Section 6.2.2, except after Ni-NTA purification samples were treated with IASD (4-acetamido-4'-((iodoacetyl)amino)stilbene-2-2'-disulfonic acid) for 1, 5, or 10 min at RT. IASD will covalently label only exposed Cys residues and the reaction is quenched upon addition of DTT. Reactions were analyzed *via* SDS-PAGE (Chapter 2): a mobility shift indicates IASD labeling has occurred.

6.2.5. NBD Fluorescence Analysis

In vitro translations (Chapter 2) were completed in the presence of the Sdh3p Helix I Cys mutant construct mRNA and the non-natural NBD-Cys-tRNA^{Cys} analog in order to label Sdh3p at these particular Cys residues with the environmentally-sensitive fluor 7-nitrobenz-2-oxa-1,3-diazolyl (NBD). Translations were halted *via* cycloheximide incubation for 20 min at RT, combined as appropriate (i.e. NBD-Sdh3p with Sdh4p), and added directly to biomimetic ND reactions, assembled as above, without catalytic dimer or heme addition (Section 6.2.2). ND samples were then added to microcell cuvettes and treated with increasing concentrations of either KCl or KI (0 to 0.08 M). NBD emission scans were completed after each addition with the following parameters: λ_{Ex} = 470 nm, λ_{Em} = 510 – 550 nm, 2 sec integration time, 4 nm slit

widths. Samples were corrected as explained below (Section 6.2.6) and Stern Volmer plot analyses were completed to determine extent of quenching at various sites.

6.2.6. Data Representation and Statistical Analysis

SDS-PAGE gels are representative of at least three independent experiments. Band quantification of IASD-labeling of ^{35}S-Sdh3p was completed using Quantity One software and band intensities are represented as the ratio of the Relative Quantity of the labeled band compared to the Relative Quantity of the total (labeled and unlabeled bands combined). K_{sv} values for NBD-labeled Sdh3p were calculated from background subtracted (NDs with unlabeled Sdh3p) and potassium chloride-corrected potassium iodide quenched- NBD emission spectra. The results of IASD labeling band quantification and K_{sv} values resulting from iodide quenching of NBD are shown as means ± standard errors of the means (s.e.m.) of at least three independent experiments. A two-tailed student T-Test (equal variance) was used to determine statistical significance ($p \leq 0.05$) for these measurements (no significance was found).

6.3. Results and Discussion

6.3.1. Cell-free Reconstitution of Complex II within Biomimetic Nanodiscs

In order to begin probing the assembly of Complex II, we used our previously established nanodisc (ND) reconstitution system (Chapter 3, [157]). Briefly, while reconstituting Complex II directly from solubilized mitochondrial membranes, we recognized that the holoenzyme only remained intact when CL was present. When NDs assembled with only DMPC lipids were used to reconstitute the complex, the holoenzyme was not stable and the catalytic dimer broke away from the membrane subunits encapsulated within the NDs. We exploited this event by making DMPC NDs with solubilized mitochondrial membranes, purifying them over a Ni-NTA column, and removing the wash fractions that contained only the catalytic dimer. In parallel, biomimetic

NDs were assembled with membrane dimer that had been translated using a cell-free wheat germ-based system. These NDs were also purified over a Ni-NTA column, but the elution fractions containing NDs with *in vitro* translated membrane dimer were removed. These NDs were then incubated with the purified catalytic dimer, allowing the holoenzyme to assemble. Holoenzyme assembly was qualified by completing a second Ni-NTA purification analysis on the samples: if catalytic dimer appeared in the washes then it was not stably associated into a holoenzyme within NDs, but if it appeared in the ND elution fractions, we had successfully assembled the holoenzyme. **Figure 6.1** shows that when complementary subunits Sdh3p and Sdh4p were assembled within discs, successful holoenzyme Complex II was reconstituted (compare "Sdh3p+Sdh4p" with "Mock"). On the other hand, when only one of the membrane subunits was used for the reconstitution ("Sdh3p" or "Sdh4p"), holoenzyme assembly did not occur and the Ni-NTA elution profiles most closely mimicked that of the "Mock" assembly. With these results, we wondered what is unique about the Sdh3p-Sdh4p dimer, compared to each of the subunits alone, that allowed holoenzyme assembly to occur only in that situation? In order to probe this question more deeply, we decided to take a look at Helix I of Sdh3p, which is hypothesized to be important in modulating attachment of the catalytic dimer to the membrane dimer as it composes forty percent of the contact area between SdhB (Sdh2p in yeast) and the membrane dimer in the porcine crystal structure.

6.3.2. Identification of Helix I in Sdh3p

Our first step was to confirm where α-helical structure was predicted to occur in the amino terminus of the Sdh3p/SdhC subunit of Complex II. The crystal structure of porcine Complex II first indicated that a soluble amino-terminal helix may exist in SdhC and this is

supported by secondary structure prediction sites, JPred3 and PSIPRED [274, 275]. These same prediction sites, as well as the homology model of yeast Complex II, support that a helical segment is also present in the yeast Sdh3p, although this segment may be shorter than that found in SdhC (**Figure 6.2A**). Once we had confirmed the presence of a helical segment in Sdh3p (and SdhC), we designed mutant Sdh3p constructs with single Cys sites at various locations within (or near) Helix I. As the helical wheel plots in **Figure 6.2B** indicate, the three residues chosen occupy different sides of the helix in order to capture the environment surrounding all faces of Helix I. The mutated residues shown here are referred to as Sdh3p Thr8, Ala13, and Leu18 for the remainder of this study. While Sdh3p Thr8 was not predicted to be within the Helix I segment, it is homologous to a residue at the amino-terminal edge of the helix in SdhC, which is why this residue of Sdh3p Helix I was included as well. Note that mutant constructs were also designed for SdhC (Thr7, Met12, Asn17), but these were not utilized in the present studies.

6.3.3. Helix I Potentially Opens Complex II Membrane Dimer to Catalytic Dimer Interaction

In order to begin looking at the role of Helix I in Complex II assembly, we examined the exposure of the helix to Cys-reactive 4-acetamido-4'-((iodoacetyl)amino)stilbene-2-2'-disulfonic acid (IASD). IASD reacts with any solvent-exposed Cys residues, forming a covalent bond. When samples treated with IASD are analyzed using SDS-PAGE, the labeled protein will migrate more slowly through the gel due to the larger molecular weight and this mobility shift in the migration of the protein is monitorable. By comparing the amount of protein that is labeled to the amount that is unlabeled over a certain period of time, the exposure of particular Cys sites can be determined. For the present study, the different Sdh3p mono-Cys mutants were translated in a cell-free wheat germ-based system and assembled into NDs alone or with a wild type partner subunit, Sdh4p. These NDs were subjected to IASD labeling and the results are presented in

Figure 6.3. It is apparent that at position 14, the helix was not very dynamic over time (there was consistent IASD labeling) regardless of whether Sdh3p was alone or in the presence of Sdh4p, but it may have been slightly more shielded overall as compared to the surrounding sites. At position Leu18, there was not a significant change when Sdh3p was alone or with Sdh4p, again supporting that the most C-terminal end of the helix was not very dynamic. At position Thr8, however, there was an increase in site exposure over time when Sdh4p was present as compared to Sdh3p alone. This may indicate that this flexible region before Helix I and/or the amino-terminus of Helix I directed the helix to sample its environment for the presence of the catalytic dimer only when the membrane dimer is appropriately assembled (i.e. Sdh3p interacting with Sdh4p).

In addition, there exist two known homologs of Sdh4p: a membrane protein that is part of the TIM22 protein import complex, Tim18p, and a protein of unknown function, YLR164w. It has previously been shown that Sdh3p is able to interact with Tim18p and is important in the assembly of the TIM22 complex. It is therefore important to understand how Sdh3p differentiates between interactions with Sdh4p and Tim18p and to then determine which holocomplex should be formed [96]. In this way, we wanted to look at the dynamics of Helix I in the presence of Tim18p to determine if the environment sampling, presumably for the catalytic dimer, that occurs in the presence of Sdh4p would also occur in the presence of Tim18p. Interestingly, when Tim18p was added to Sdh3p, there was no change at Thr8 (it behaved similarly to when Sdh3p is alone), but there was a large increase in exposure at Leu18 (**Figure 6.3**). The lack of change at the amino-terminus of Helix I supports that both native Complex II membrane subunits must be present in order for the solvent sampling and catalytic dimer attachment to occur; this will not occur when Tim18p is present. The increase in exposure

at the carboxy-terminal residue Leu18 could support a shift in the conformation of Helix I that may expose residues necessary for interaction with other TIM22 complex proteins to form the holocomplex of TIM22.

In order to investigate the dynamics of Helix I and its conformational changes with a complementary technique, we labeled Sdh3p Helix I with an NBD (fluor 7-nitrobenz-2-oxa-1,3-diazolyl) fluorophore. NBD is a small, environmentally-sensitive probe that when incorporated within a protein allows site-specific environment-sensitive (i.e. conformational) data to be obtained. NDs were formed exactly as with IASD labeling, except Sdh3p was translated in the presence of an amino-acyl tRNA analog that would incorporate Cys residues labeled with NBD at specific mono-cysteine sites within Helix I. We used a soluble iodide molecule to quench fluorescence of NBD, which would only occur if the NBD probe was solvent-exposed, as iodide cannot cross the ND bilayers or enter hydrophobic pockets. It was apparent that when Sdh4p was present, as compared to when Sdh3p was alone or when Tim18p was present, Thr8 was more solvent-exposed, which was indicated by the higher quenching by iodide at this position (**Figure 6.4**). This was consistent with the IASD labeling results that indicated that the amino-terminal Thr8 residue underwent an increase in labeling when Sdh4p was present.

At the carboxy-terminal Leu18, there was a decrease in quenching when Sdh4p was present, as compared to when Sdh3p was alone (**Figure 6.4**). The decrease in exposure supports that in this region of Helix I, there was a shift toward the bilayer or toward the transmembrane segments of Sdh3p, which may be important in setting up the membrane dimer for catalytic dimer attachment. This shift was most likely very slight as the IASD labeling results do not show much change when Sdh4p was introduced into the system. When Thr8 shifted outward to sample the environment, the helix may have twisted so that Leu18 was more likely to be buried

near the membrane. Further, the exposure levels for each of the residues were similar when Sdh3p was alone, supporting the existence of a possible resting state of Helix I along the bilayer. This resting state may be slightly exposed while not actively searching the surrounding environment or may become buried and protected within a region of the bilayer. It appeared that in the presence of Sdh4p, the amino-terminal edge of Helix I (or potential flexible region prior to the helix) flipped to sample the surrounding environment, while the more carboxy-terminal edge seemed to bury itself, possibly anchoring the helix so that it may better sample the environment and bind the catalytic dimer, forming a Complex II holoenzyme.

6.4. Brief Conclusions

Complex II subunit assembly is a very intricate process whose realized complexity is only increasing over time. We study here, for the first time, the dynamics of membrane subunit Sdh3p Helix I through IASD labeling and NBD fluorescence quenching. First, we established that Complex II can be reconstituted in a cell-free system whose membrane environment is recapitulated in ND model membrane systems with an inner membrane (biomimetic)-mimicking lipid composition. Both membrane subunits must be present for catalytic dimer attachment: it appears that Sdh3p alone is not sufficient, but is required for catalytic dimer attachment. Next, we looked in more detail at three separate residues along Sdh3p Helix I that each sample a different helical face, providing information on all sides of the helix. The most amino-terminal Thr8 is most dynamic and may actively sample the local environment for the catalytic dimer (**Figure 6.5**). The middle residue Ala13 and the carboxy-terminal Leu18 seem to be more stable when Sdh4p is present, with Leu18 potentially anchoring itself near the membrane to support catalytic dimer attachment. When Tim18p is present, Leu18 may shift in position allowing the

TIM22 complex to assemble and preventing Complex II catalytic dimer attachment. Overall, while these results shed an initial light on the process of Complex II assembly, much work remains to be done. In particular, more detailed experiments looking at Helix I dynamics when Sdh3p (and SdhC) are paired with each of their binding partners in the presence and absence of the catalytic dimer would further develop our understanding of Complex II holoenzyme assembly.

6.5. Figures

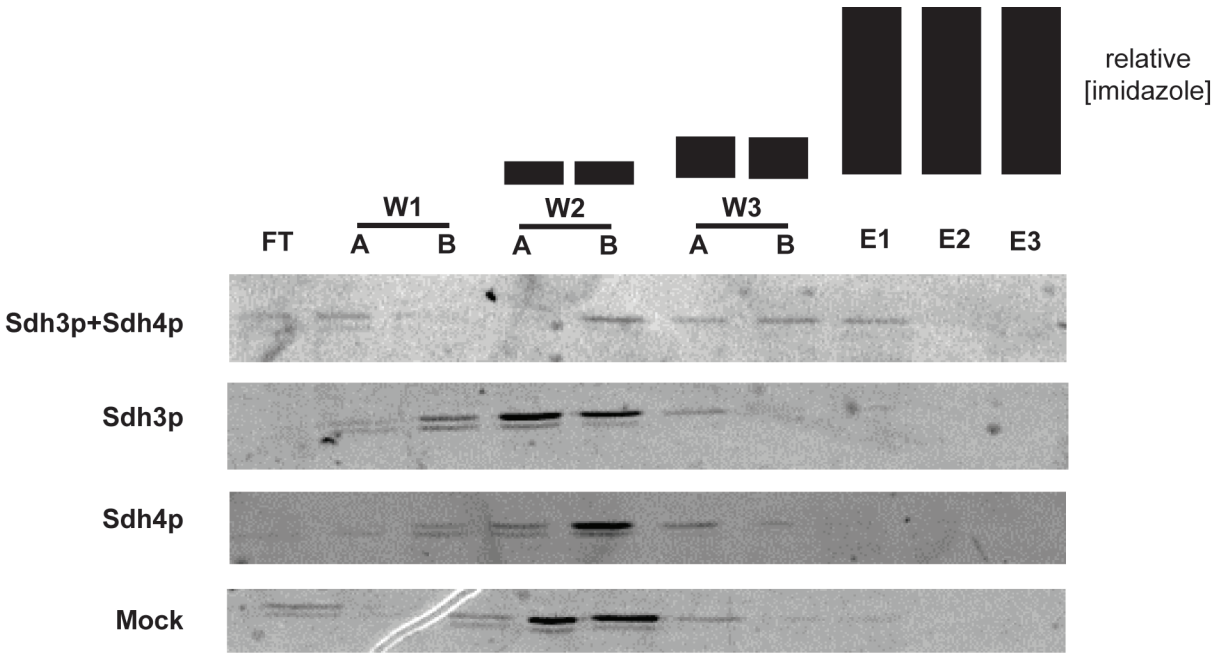

Figure 6.1. The assembly and stability of Complex II holoenzyme is dependent on the presence of both membrane subunits. Complex II reconstitution was attempted by adding purified catalytic dimer to NDs with the indicated membrane subunits. The NDs were then subjected to affinity chromatography for isolation of holoenzyme Complex II encapsulated within NDs. Catalytic dimer co-eluting with MSP1E3D1 (fractions E1 and E2) was considered to be stably associated with the NDs (and therefore the membrane subunits); those eluting at the earlier fractions were not stably associated (free catalytic dimer). The fluorescent FAD signal was used as the marker for the soluble catalytic dimer. Column fractions are FT: flow through; W1A-W3B: column wash steps; E1-E3: column elution steps. Note relative imidazole concentrations depicted above.

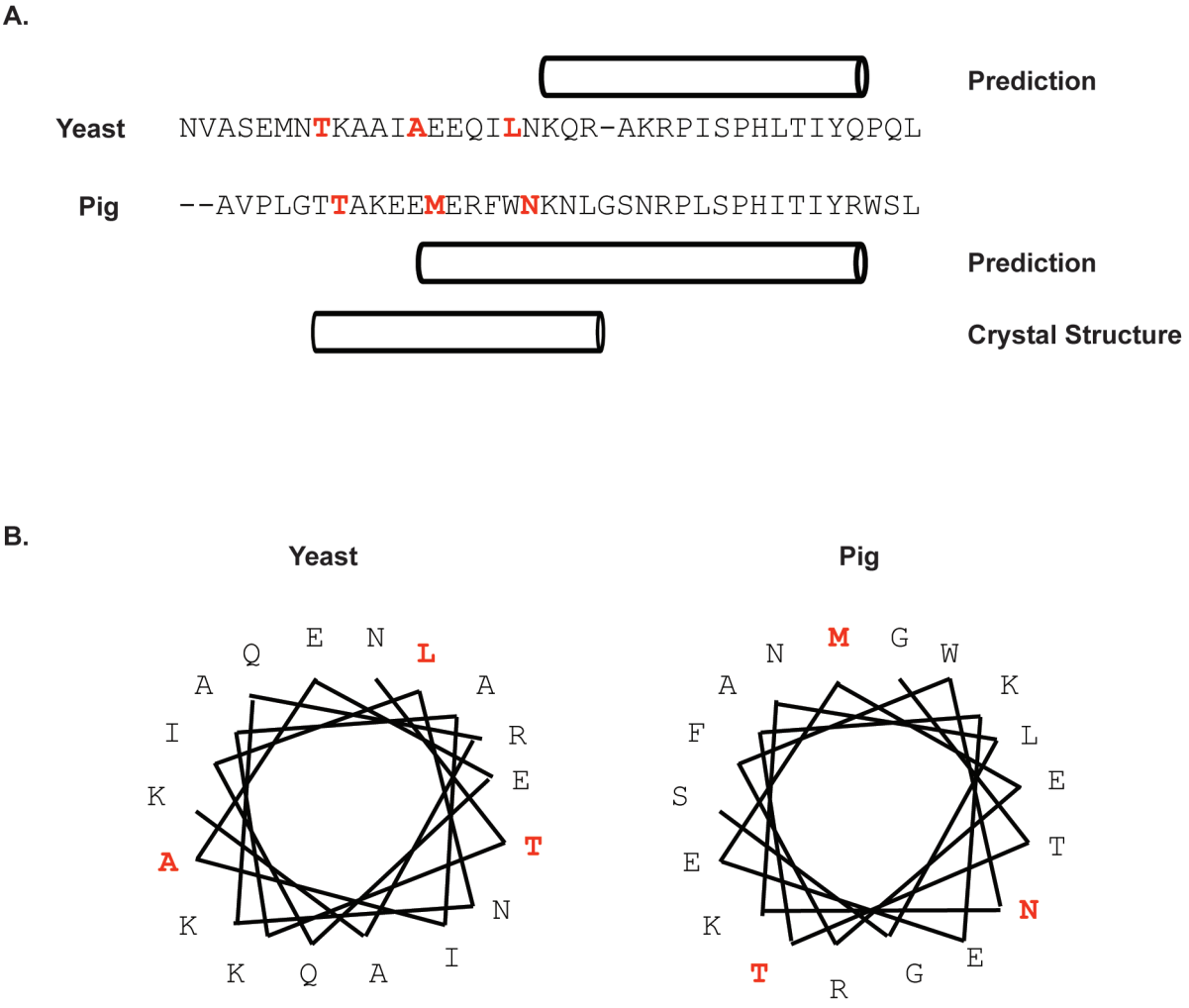

Figure 6.2. Secondary structure prediction of Sdh3p/SdhC amino-terminus. (**A**) Secondary structure prediction programs, Jpred3 [274] and PSIPRED [275], along with the porcine crystal structure [36] and yeast homology model [37], were used to determine the residues comprising Helix I in both yeast and pig. (**B**) Helical wheel plot of the eighteen residues surrounding and comprising Helix I in both yeast and pig. In both (**A**) and (**B**) the residues marked in bold red are those that were mutated to Cys for conformational analyses.

A.

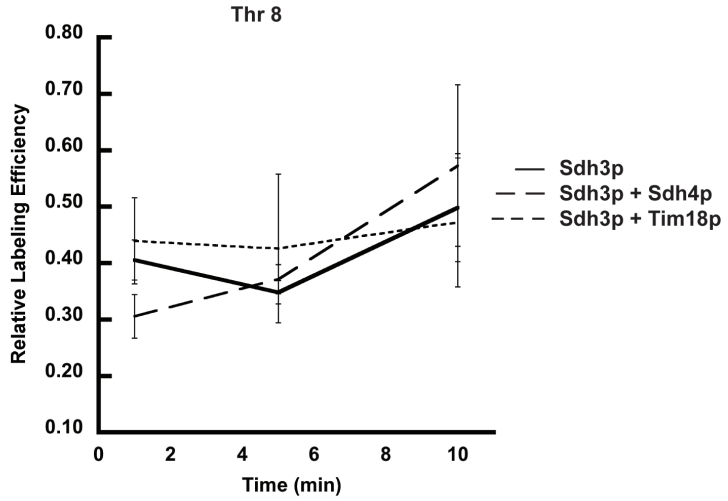
Thr 8
Relative Labeling Efficiency
0.80
0.70
0.60
0.50
0.40
0.30
0.20
0.10
0
2
4
6
8
10
Time (min)
Sdh3p
Sdh3p + Sdh4p
Sdh3p + Tim18p

B.

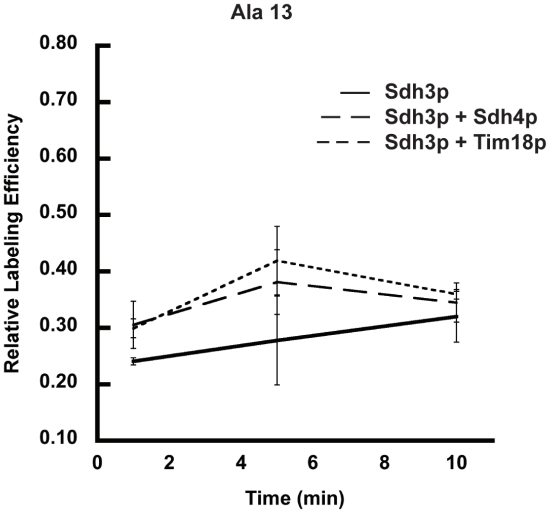
Ala 13
Relative Labeling Efficiency
0.80
0.70
0.60
0.50
0.40
0.30
0.20
0.10
0
2
4
6
8
10
Time (min)
Sdh3p
Sdh3p + Sdh4p
Sdh3p + Tim18p

C.

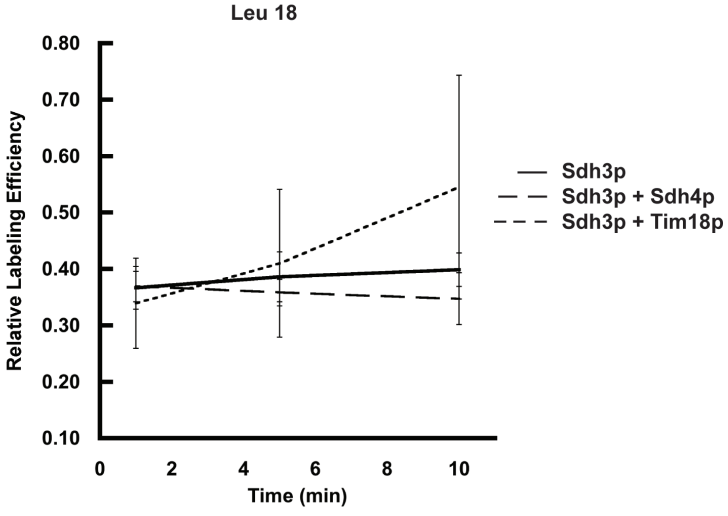
Leu 18
Relative Labeling Efficiency
0.80
0.70
0.60
0.50
0.40
0.30
0.20
0.10
0
2
4
6
8
10
Time (min)
Sdh3p
Sdh3p + Sdh4p
Sdh3p + Tim18p

Figure 6.3. IASD labeling supports sampling of environment by Helix I in the presence of Sdh4p. Each of the residues, Thr8 (**A**), Ala13 (**B**), and Leu18 (**C**), mutated along Helix I samples different faces of the helix, allowing the exposure along different sides and at different points in the helix to be studied. Labeling by Cys-reactive IASD indicated that the amino-terminal Thr8 seemed to increase in exposure upon Sdh3p reconstitution with Sdh4p, while the carboxy-terminal Leu18 increased in exposure in the presence of Tim18p. Data is displayed as the change in the ratio of the intensity of IASD-labeled bands to IASD-labeled and unlabeled bands (total Sdh3p present) over time. Sdh3p was reconstituted alone (solid line), in the presence of Sdh4p (dashed line), or in the presence of Tim18p (short dashed line). Based on a student T-test, no statistical significance was found.

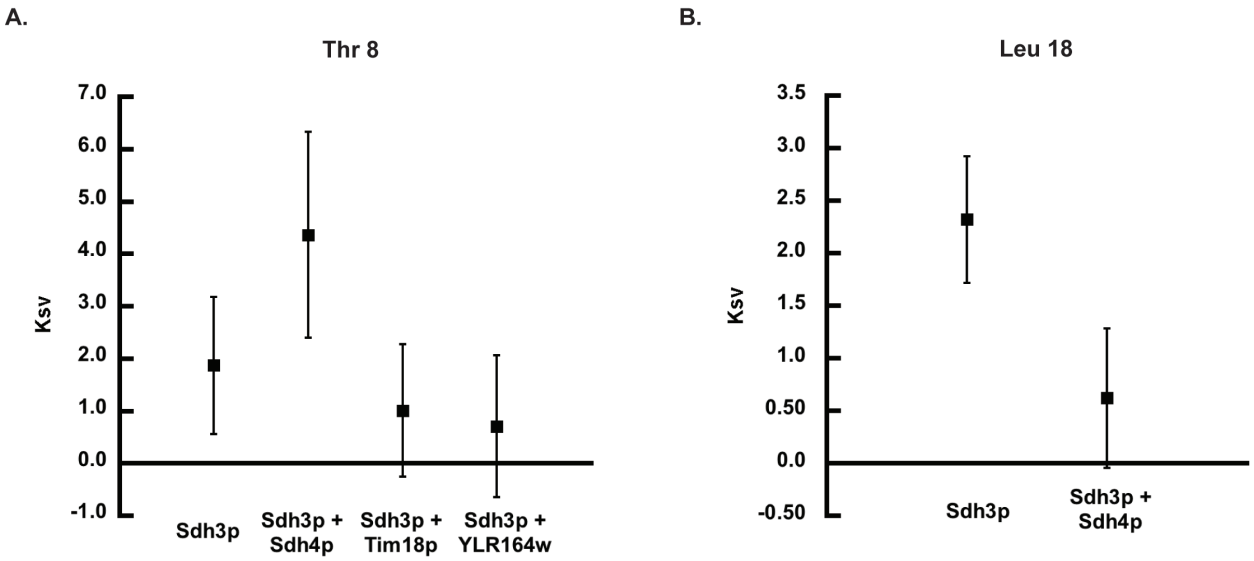

Figure 6.4. NBD fluorescence quenching supports conformational changes of Helix I. The most amino- and carboxy-terminal residues mutated in Helix I (Thr8 (**A**) and Leu18 (**B**), respectively) were labeled with the environmentally-sensitive NBD fluor and treated with increasing concentrations of iodide, which would quench fluorescence if the fluorescent probe was exposed to solvent. In the presence of Sdh4p, fluorescence was quenched at the amino terminal Thr8 of Helix I to a higher degree as compared to when Sdh3p was alone. In contrast, in the presence of Tim18p, the carboxy-terminal Leu18 NBD fluorescence was quenched to a higher degree. Sdh3p was reconstituted alone, in the presence of Sdh4p, or in the presence of Tim18p. Based on a student T-test, no statistically significant differences were found.

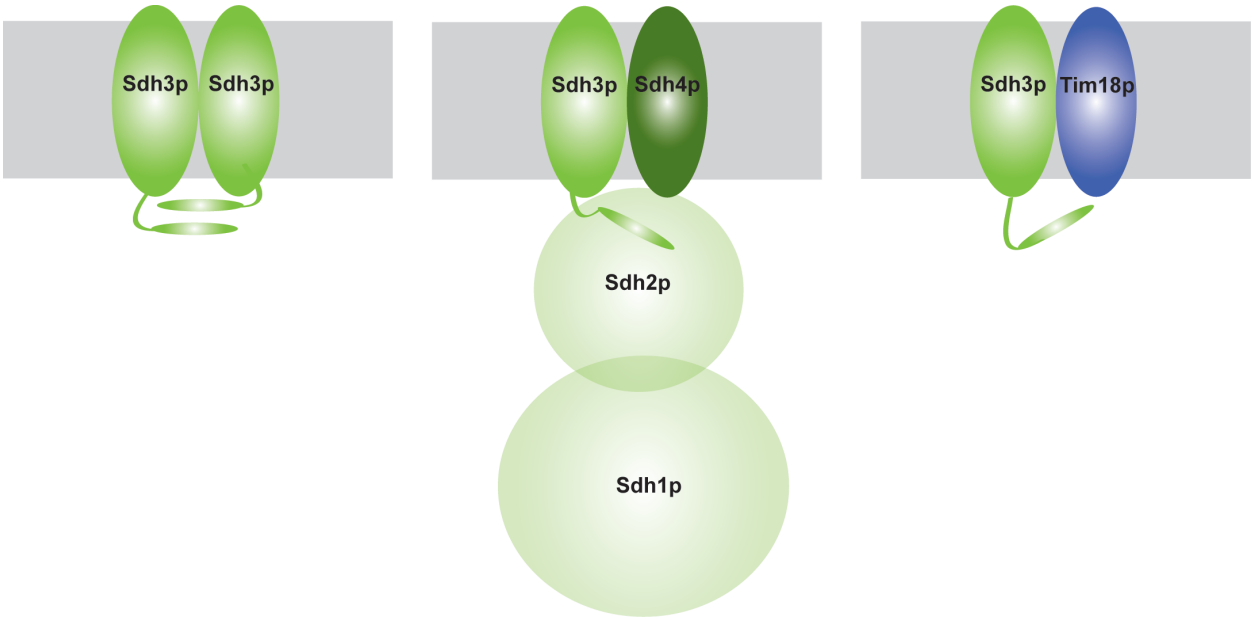

Figure 6.5. Schematic of proposed Helix I conformational dynamics in the presence of Sdh3p binding partners. Sdh3p has the potential to form a homodimer with other Sdh3p proteins, keeping Helix I in a position that leaves all sides relatively similarly exposed. When Sdh4p was present, Helix I tilted so that the more carboxy-terminal Leu18 was partly shielded by the membrane or Sdh3p itself, while the amino-terminal Thr8 was able to sample the environment for the presence of the catalytic dimer to form holoenzyme Complex II. When Tim18p was present, the helix adopted a third conformation in which the more carboxy-terminal Leu18 may become more exposed than the amino-terminal, possibly opening a different binding site and allowing assembly of the TIM22 complex.

Chapter 7

Conclusions

7.1. Overall Conclusions

As the linkage point between the tricarboxylic acid (TCA) cycle and the electron transport chain (ETC), Complex II is critical to mitochondrial, and therefore cellular, energy generation. Mutations in its subunits have been linked to a variety of disease states, including the tumorigenic diseases paraganglioma and pheochromocytoma, as well as early-onset neurodegenerative disorders and the aging process. Complex II is the least studied of the respiratory chain complexes; with its powerful involvement in energy generation and the detrimental implications of its dysfunction, it is imperative to learn more about the mechanisms underlying the assembly and activity of this complex.

My current work has two main novel findings that have extended the overall understanding of Complex II within the field (**Figure 7.1**): 1) Cardiolipin (CL) is necessary for assembly of Complex II membrane subunits as well as in holoenzyme stability and activity, most likely due to its effects on membrane hydration and inter-lipid packing; and 2) Sdh3p/C membrane subunits are able to form homodimers that are stabilized by both heme and CL, but disrupted by partner subunits, Sdh4p/SdhD, and their homologs, Tim18p/YLR164w. In addition to these innovative findings, my work has furthered other recent studies implicating Complex II as a significant contributor to reactive oxygen species (ROS) formed by the respiratory chain. Further, my preliminary work on Helix I of Complex II membrane subunit, Sdh3p/C, supports that this helix may undergo dynamic structural rearrangements depending on the partner proteins that are present within the membrane and may regulate the ability of the Complex II holoenzyme to assemble correctly.

7.2. Complex II and Cardiolipin

While CL has never previously been clearly linked with yeast or mammalian Complex II, I have presented ample evidence that CL is essential for the structure and function of mitochondrial Complex II by: 1) maintaining the interaction between the catalytic dimer and membrane subunits; 2) promoting electron flux from succinate to the ubiquinone reduction site within the bilayer; and 3) reducing ROS production. My results add Complex II to the list of respiratory complexes that require CL for optimal function and assembly. It is of note, however, that during the largely uncharacterized assembly process of Complex II *in vivo* (membrane subunit integration *via* the TIM23 Complex, lateral interaction and heme coordination of Sdh3p/C and Sdh4p/D, and assembly with the catalytic dimer), of which other aspects of my research partly address, the specific roles of CL may differ from its functions in our reconstituted system.

Within the mitochondria, CL is found in regions of high curvature of the IM, such as the cristae invaginations or contact sites between the OM and IM. It has even recently been shown that alterations in the curvature and shape of the cristae affect the stability and efficiency of the overall respiratory chain and that the localization of CL within the membrane has widespread effects in mitochondrial signaling processes [276, 277]. Further, addition of divalent cations to aqueous dispersions of CL induces an inverted micellar phase of the lipid molecules, which allows long hexagonal phase tubules with a high degree of curvature to form. The ability of the divalent cation calcium to alter the curvature and hydration of bilayers that contain CL has implications for how CL is able to affect the stability and activity of Complex II, which is located within the cristae membranes (of the mitochondrial IM).

Using fluorescent probes that intercalate into the bilayer at particular regions (i.e. interfacial vs. acyl chain regions) my work has also supported that when CL is present within a bilayer, that bilayer is more hydrated and the lipid molecules are less closely packed as compared to bilayers lacking CL. When magnesium or calcium are added to the bilayers, those containing CL become increasingly dehydrated and the lipid molecules pack more tightly together as the electrostatic repulsion from anionic CL headgroups is relaxed. My present results, set within the larger field of CL dynamics, suggest that when calcium is present in a bilayer containing Complex II, lipids within the bilayer become more tightly packed and CL may be prevented from directly interacting with the complex, dually inhibiting holoenzyme Complex II stability and activity. Further, as I showed with my crosslinking studies, CL is necessary for assembly of Complex II membrane subunits; therefore, the presence of CL and its hydrating effect on the bilayer in the absence of cations may allow the membrane subunits to move laterally within the bilayer and interact to form heterodimers.

The link between CL and Complex II should be studied further to identify: 1) Which region of CL (i.e. the double headgroup, the quadruple acyl chains, or a combination of both) is most important in supporting holoenzyme stability and activity of Complex II?; 2) Is CL able to bind Complex II directly and/or able to alter bilayer dynamics in a way that may indirectly cause CL to have a supportive effect on the stability and activity of the complex?; and 3) What (if any) is the detailed mechanistic link between rapid increases of calcium within the mitochondria, leading to altered CL structure and function and Complex II dysfunction during apoptotic cell death?

7.3. Assembly of Complex II

Complex II subunit assembly is a very intricate process whose realized complexity is only increasing over time. Little is known regarding how the holoenzyme Complex II assembles and the interaction between the membrane subunits, Sdh3p/C and Sdh4p/D, is especially mysterious. How do they interact once they have been imported into the mitochondria and individually assembled within the IM? What regulates this assembly? Recent work supports that Sdh3p is necessary not only for the interaction with Sdh4p to form Complex II, but that an interaction of Sdh3p with Tim18p is also necessary to assemble the TIM22 protein import complex of the mitochondrial IM [96]. These interactions support that not only are the subunits of Complex II important for energy generation processes within the mitochondria, but also in the regulation and assembly of an IM protein import complex.

My work investigating the factors influencing Complex II membrane subunit assembly and the implications this may have for the surrounding IM environment has led to some surprising results. First, this work has unexpectedly (and for the first time) revealed that Sdh3p/SdhC favor the formation of a homodimer that is able to be captured by chemical crosslinking reagents. Not only this, but CL is required for this homodimerization and heme enhances the homodimer formation of Sdh3p as well. In addition, when Sdh4p/SdhD and their homologs, Tim18p and YLR164w, are present the homodimer is broken, most likely due to the formation of dynamic (i.e. unable to be captured *via* crosslinking agents) heterodimers between partner proteins. These results have far-reaching implications in the Complex II field as this homodimer assembly may expose a novel regulatory process within the IM of mitochondria: when Sdh3p/C does not have a native binding partner with which to interact, it will homodimerize to prevent spurious contacts with other proteins within the protein-rich IM

environment. When an appropriate partner is present, Sdh3p/C will preferentially interact with that protein forming the interactive surface on which a larger complex can assemble.

To take this a step further, while previous crystallographic evidence supports that the soluble Helix I of Sdh3p/C may be involved in Complex II holoenzyme assembly, as it makes up forty percent of the contact area between the membrane subunits and soluble SdhB [36], my preliminary work is the first to provide evidence to support that Helix I is involved in the overall assembly process of the holoenzyme. The position of this helix may be altered depending on which of Sdh3p's partner subunits are present and available within the membrane (e.g. Sdh4p/SdhD or Tim18p). This in turn would alter which holocomplexes would be assembled (e.g. Complex II or TIM22) and could have implications on the energetic state of the membrane and implicate Complex II subunits as key proteins in multiple processes within the mitochondria, not simply energy metabolism.

Multiple questions remain regarding the details of these interactive processes: 1) Does the presence of CL, or other alterations in the lipid environment, influence the dynamics between membrane subunits Sdh3p/C and Sdh4p/D and/or the conformational dynamics of Sdh3p/C Helix I?; 2) Would removal of Helix I from Sdh3p prevent catalytic dimer attachment when Sdh4p is present?; and 3) Which particular residues of Helix I are mediating the attachment of the catalytic and membrane dimers? Further work with site-specifically labeling each residue along the helix and probing the local environment would provide a more significant, detailed picture of the behavior of Helix I.

Overall, the present work supports that CL is an important supporting factor in the stability and assembly not only of the membrane subunits of Complex II, but also of the holoenzyme, as well as in holoenzyme SQR activity. As CL proves to be an influential force in

the overall functionality of Complex II, the link between CL and Complex II should be studied more extensively to determine the mechanistic details governing this interaction. These results could have implications not only for Complex II, but also for other respiratory chain complexes and may even shed light on why Sdh3p is necessary for the assembly of Tim18p into the TIM22 import complex. Finally, from a technical standpoint, many of my studies on the CL-Complex II interaction have required that I develop a novel approach for studying membrane complexes. In the present work, I have solubilized these complexes directly from a native biomembrane and reconstituted them into a model bilayer platform, the nanodisc, whose lipid composition can be precisely defined. This experimental approach can be applied to future studies of Complex II and CL within the laboratory and will also be of particular use in analyzing possible connections between lipid composition, membrane protein assembly, and the molecular basis of diseases (*e.g.*, CL deficiency associated with Barth syndrome).

7.4. Figures

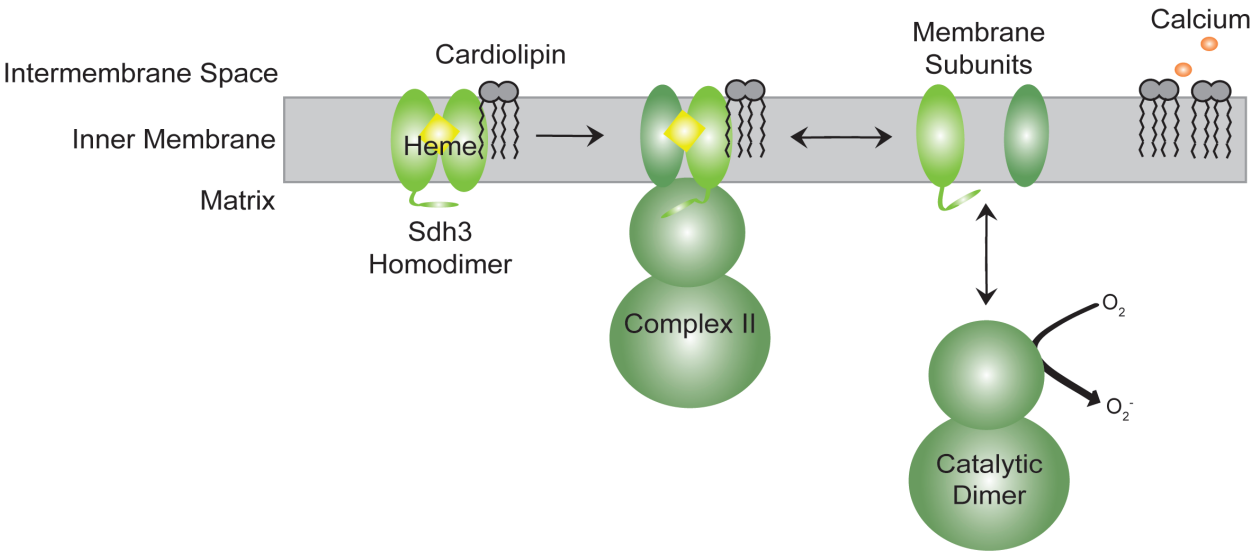

Figure 7.1. Schematic of the overall implications of the present studies on our understanding of respiratory Complex II. Complex II membrane subunit Sdh3p/C is able to form homodimers within the membrane in the presence of heme and CL (left); when Sdh3p/C is alone, Helix I appears to fold into the protein and become more shielded. When an appropriate binding partner is present, such as Sdh4p/SdhD, holoenzyme Complex II assembles and remains stably associated only when CL is present (middle). When CL is not present or prevented from interacting with Complex II due to the presence of divalent cations (right), the following may occur: 1) During assembly, the membrane subunits may not be able to interact appropriately and an interactive face for the attachment of the catalytic dimer is not presented, and/or 2) After Complex II assembly, the catalytic dimer may detach from the membrane dimer and contribute to the formation of ROS if electrons from succinate can no longer be passed to the ubiquinone within the membrane.

Appendices

Appendix A. Complex II Membrane Subunit Mutant Construct Library

Saccharomyces cerevisiae (yeast)		
	Sdh3p	**Sdh4p**
Heme Coordination Sites (green)	H106A	C78A
Amber Suppressor Mutations for Assembly Analysis (red)	S80	S133
Mono-Cysteine Mutations for NBD-Probe Incorporation (yellow)	S80C (131)* N81C (132)* S98C (149)* F137C (188)* T138C (189)*	
Tetra-Cysteine Mutations for FlAsH-Probe Incorporation (black box)	SNWYHQ (80-85) CCPGCC	
Mono-Cysteine Mutations for Helix I Analysis (blue)	T9C A14C L19C	
Homolog Constructs		Tim18 (full-length and mature) YLR164w (full-length and mature)

* Numbers in parentheses are residue number in full-length protein (mRNA tube label)

Sus scrofa (porcine)		
	SdhC	**SdhD**
Amber Suppressor Mutations for Assembly Analysis (red)	S72	M132
Tetra-Cysteine Mutations for FlAsH-Probe Incorporation (black box)	CLGPTL (81-86) CCPGCC	CCPGCC (135) C-Terminal Insertion
Amber Suppressor Mutations for Helix I Analysis (blue)	T4 M9 N14	
Pathogenic Mutations (orange)	L130P	R35G P46L D57Y L60P H67L Y79C L104P

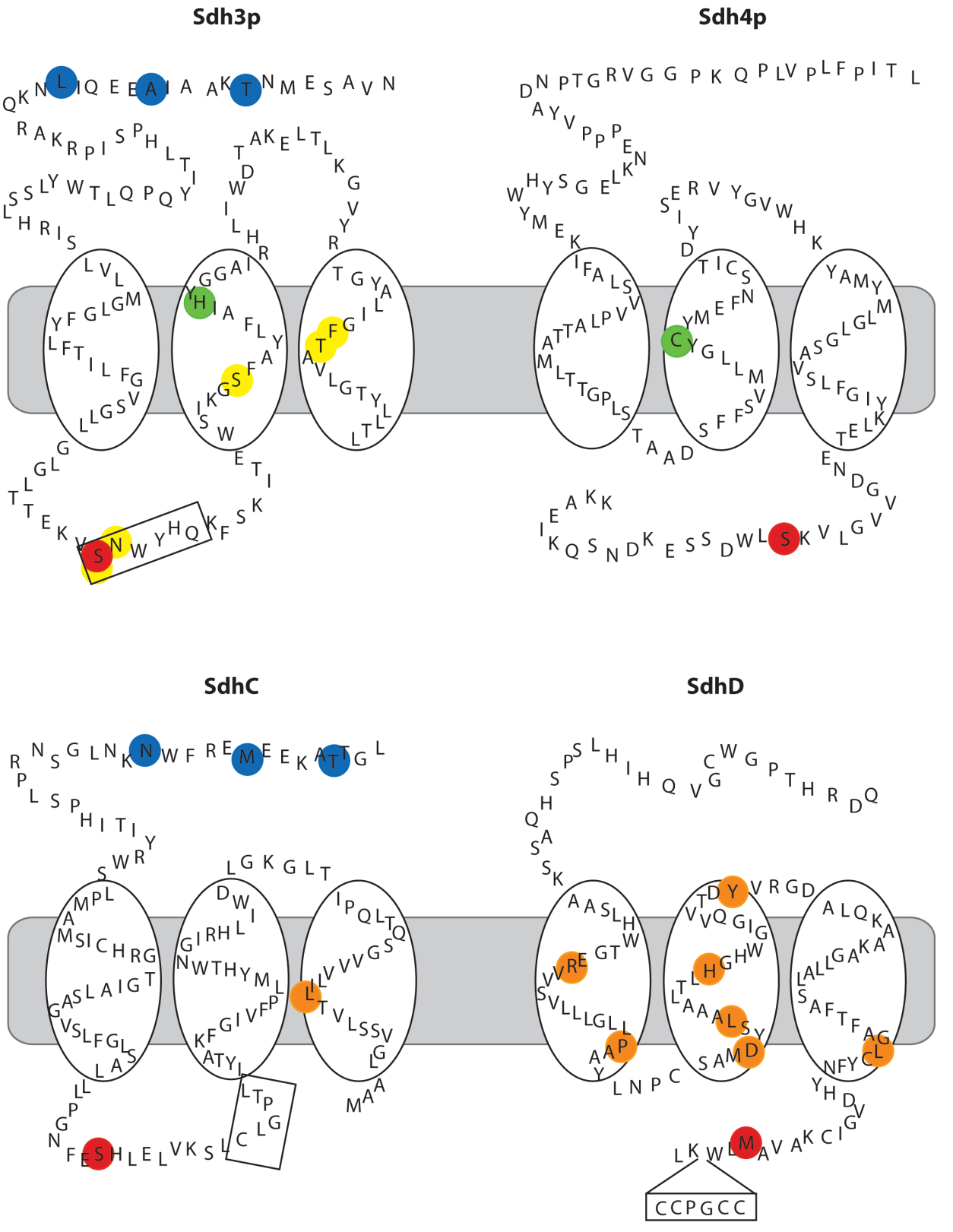
Sdh3p
Sdh4p
SdhC
SdhD
CCPGCC

Appendix B: Complex II Membrane Subunit Purification and Labeling Protocol

B.1. Cell Growth and Autoinduction

B.1.1. Summary

IPTG-based inductions of Sdh3p mature WT and Sdh3p S80C were conducted first (with both denaturing and native purifications), but the resulting protein yield was inconsistent and poor. While the protocol described in this section, which involves an autoinduction procedure, yields small amounts of protein (~ 20 μM), it results in consistent protein yields (protocol is derived from [278]). Note that the autoinduction process is based on the premise that bacteria will consume any glucose in the media first, preventing induction of the protein encoded on a transformed plasmid, but after the limited amount of glucose is consumed, will begin to consume lactose, which will allow induction to occur more naturally and ease the bacteria into the induction process.

B.1.2. Media and Solutions

1. 20X NPS Stock Solution (150 mL)

135 mL	Double Distilled Water		
8.01 g	Ammonium Chloride	NH_4Cl	1 M
10.2 g	Potassium Phosphate Monobasic	KH_2PO_4	0.5 M
10.65 g	Sodium Phosphate Dibasic	Na_2HPO_4	0.5 M

2. 50X 5052 Stock Solution (150 mL)

12.5 g	Glycerol	0.5% (w/v)
36.5 mL	Double Distilled Water	
1.25 g	Glucose	0.05% (w/v)
5.0 g	α-Lactose	0.2% (w/v)

Weigh glycerol directly in glass beaker.
Heat final solution to dissolve lactose.

3. 40% Glucose (w/v)

4 g	Glucose	40% (w/v)
7.4 mL	Double Distilled Water (stirring)	

Heat final solution to dissolve glucose.

4. 200 mM Glucose

0.18 g	Glucose		200 mM
5 mL	Double Distilled Water		

Filter sterilize with 0.22 μm filter.

5. 25 mg/mL Kanamycin

250 mg	Kanamycin		25 mg/mL
10 mL	Double Distilled Water		

6. SOC Media (50 mL)

45 mL	Double Distilled Water		
0.25 g	Yeast Extract		0.5% (w/v)
1.0 g	Tryptone		2% (w/v)
25 mg	Sodium Chloride	NaCl	8.6 mM
9.3 mg	Potassium Chloride	KCl	2.5 mM
102 mg	Magnesium Chloride	$MgCl_2$	10 mM

Autoclave on 30 min Liquid Setting.
Glucose should be added post-autoclave.

5 mL	200 mM Glucose		20 mM

7. MDAG-Agar (500 mL)

465 mL	Double Distilled Water		
5.0 g	Agar		
120 mg	Magnesium Sulfate	$MgSO_4$	2 mM
355 mg	Sodium Sulfate	Na_2SO_4	5 mM
6.25 mL	Glucose		0.5% (w/v)
25 mL	20X NPS Stock Solution		1X

Autoclave on 30 min Liquid Setting.
Allow media to cool while stirring.
Kanamycin should be added when warmer than RT (slightly warm to the touch).

200 μL	25 mg/mL Kanamycin	100 μg/mL

Pour plates immediately after Kanamycin addition.

8. MDAG (50 mL)

46.5 mL	Double Distilled Water		
12.0 mg	Magnesium Sulfate	$MgSO_4$	2 mM
35.5 mg	Sodium Sulfate	Na_2SO_4	5 mM
625 μL	Glucose		0.5% (w/v)
2.5 mL	20X NPS Stock Solution		1X

Autoclave on 30 min Liquid Setting.
Kanamycin should be added post-autoclave step; immediately pre-use.

200 μL	25 mg/mL Kanamycin	100 μg/mL

9. ZYM-5052 (1.6 L)

1.47 L	Double Distilled Water		
16 g	Tryptone		1% (w/v)
8 g	Yeast Extract		0.5% (w/v)
0.385 g	Magnesium Sulfate	$MgSO_4$	2 mM
1.136 g	Sodium Sulfate	Na_2SO_4	5 mM
32 mL	50X 5052 Stock Solution		1X
80 mL	20X NPS Stock Solution		1X

Split into 4 x 400 mL in 2 L flasks.
Autoclave on 30 min Liquid Setting.
Kanamycin should be added to each 400 mL flask post-autoclave; immediately pre-use.

1.6 mL	25 mg/mL Kanamycin	100 μg/mL

B.1.3. Materials

1. SOC, MDAG, ZYM-5052 Media (Above)
2. Plate incubator at 37°C
3. Shaking incubator (at 37°C, 250 RPM)
4. Plastic inoculating spreaders
5. Blue plastic inoculating loops
6. Hallway Centrifuge equipped with GSA Rotor

B.1.4. Methods

1. Transformation of competent cells
    a. Remove BL21(DE3) competent cells from -80°C freezer; thaw on ice ~10 min.
    b. Pre-warm MDAG-Agar (+KAN) plates in 37°C incubator.
    c. Add 1 μL of appropriate DNA to individual pre-chilled 1.5 μL microfuge tubes.
        1- It is advised to also do one Negative Control with 1 μL of Double Distilled Water.
    d. Add 50 μL of thawed competent cells to each tube and mix well.
    e. Incubate on ice for 30 min.
    f. Heat shock the cells by placing them in 42°C water bath for 30 sec.
    g. Return cells to ice for 5 min.
    h. Add 950 μL SOC media to each tube.
    i. Incubate cells on shaking incubator at 37°C (250 RPM) for 1 hr.
    j. Plate cells on MDAG-Agar (+KAN) plates with plastic inoculating spreaders.
        1- Add 25 μL of cells to 175 μL of SOC pool already on the plate.
    k. Incubate plates at 37°C overnight.

2. 1 mL Liquid MDAG (+KAN) Overnight Cultures
    a. Inoculate 1 mL MDAG (+KAN) with a single colony from each plate.
        1- Set up at least 4 cultures plus 1 control (media only) for 5 total.
    b. Incubate at 37°C (250 RPM) overnight.

3. 400 mL Liquid ZYM-5052(+KAN) Overnight Cultures
    a. Inoculate 400 mL ZYM-5052 (+KAN) with 400 μL of 1 mL Overnight Culture.
        1- Use each 1 mL culture for each separate 400 mL culture.
    b. Incubate at 37°C (250 RPM) overnight (for at least 12 hours).
    c. Take Absorbance readings at 600 nm after overnight incubation.
        1- Blank with remaining liquid MDAG (+KAN) from 1 mL Cultures.
        2- Make sure that readings are approximately 2.000 and above.
    d. Split each 400 mL Overnight Culture into 2x 250 mL Plastic Bottles.
    e. Spin in GSA Rotor at 5K RPM for 20 min.
    f. Freeze in Liquid Nitrogen and place in -80°C Freezer until needed.

B.2. Protein Purification

B.2.1. Summary

As mentioned in Section B.1.1., after attempting both denaturing and native purification protocols that are traditionally used in the Alder laboratory, I moved on to an Inclusion Body-based purification as it seemed that no matter how the bacterial cultures were grown and induced, any Complex II subunit protein that was produced aggregated into inclusion bodies. In this protocol, traditional resuspension and probe sonication methods are used to separate inclusion bodies from remaining cellular debris. When the pellets are first collected post-centrifugation they are washed multiple times and finally resuspended in a buffer containing 4 M Urea, which solubilizes the aggregated inclusion body protein pellets. Once any unsolubilized contaminants are removed, the resulting solute is able to be purified and ~ 20 μM of Sdh3 protein is obtained post- dialysis. Note that Buffers 2-5 below should be made day-of (while pellets are thawing) and urea should be added to buffers day-of as well.

B.2.2. Buffers and Solutions

1. Cell Disruption Buffer

295 mL	Double Distilled Water		
0.414 g	Sodium Phosphate Monobasic	NaH_2PO_4	10 mM
60.4 mg	Potassium Chloride	KCl	2.7 mM
2.402 g	Sodium Chloride	NaCl	137 mM

Remove 70 mL for Inclusion Body Buffers (below) before pH.
pH to 7.4 with 3N Sodium Hydroxide.

2. 1 M Magnesium Chloride

0.102 g	Magnesium Chloride	$MgCl_2$	1 M
500 μL	Double Distilled Water		

3. 100 mM Phenylmethanesulfonyl fluoride

17.4 mg	Phenylmethanesulfonyl fluoride	PMSF	100 mM
1 mL	Ethanol	EtOH	

Make 2X 100 mM stocks of PMSF.

4. 20 mg/mL DNase

5 mg	DNase	20 mg/mL
250 μL	Double Distilled Water	

Keep on ice until added to Cell Disruption Buffer.

5. 10 mg/mL Lysozyme

20 mg	Lysozyme	10 mg/mL
2 mL	Double Distilled Water	

Make 2X 10 mg/mL stocks of Lysozyme.

6. Inclusion Body Wash Buffer

45 mL	Cell Disruption Buffer		
18.6 mg	Ethylenediamine Tetraacetic Acid	EDTA	1 mM

pH to 8.0 with 3N Sodium Hydroxide before adding detergent.

5 mL	10% (v/v) Triton X-100	1% (v/v)

7. Inclusion Body Solubilization Buffer

25 mL	Cell Disruption Buffer		
68.1 mg	Imidazole		20 mM
24.02 g	Urea		8 M
77.1 mg	Dithiothreitol	DTT	10 mM

Check pH and make sure ~8.0.
If yes, do not pH with 3 N Sodium Hydroxide as the solution pH is unstable.

8. Column Buffer: Wash 1

100 mL	Double Distilled Water		
0.414 g	Sodium Phosphate Monobasic	NaH_2PO_4	20 mM
4.383 g	Sodium Chloride	NaCl	500 mM
0.204 g	Imidazole		20 mM
36.04 g	Urea		4 M

Remove 27 mL for Column Buffer: Elution (below) before pH.
pH to 7.4 with 3 N Sodium Hydroxide before adding detergent.

12 mL	10% (v/v) Triton X-100	1% (v/v)

9. Column Buffer: Elution

27 mL	Column Buffer: Wash 1	
1.02 g	Imidazole	500 mM

pH to 7.4 with Concentrated Hydrochloric Acid before adding detergent.

3 mL	10% (v/v) Triton X-100	1% (v/v)

10. Column Buffer: Wash 2

13.5 mL	Column Buffer: Wash 1
1.5 mL	Column Buffer: Elution

11. Column Buffer: Wash 3

12 mL	Column Buffer: Wash 1
3 mL	Column Buffer: Elution

12. Column Buffer: Wash 4

7.5 mL	Column Buffer: Wash 1
7.5 mL	Column Buffer: Elution

B.2.3. Materials

1. All Buffers and Solutions (Above)
2. Two ice buckets filled with ice (at least one Tall)
3. Probe Sonicator
4. Hallway Centrifuge equipped with SA-600 rotor
5. Heating Stir Plate
6. Large Blue Metal Rack
7. Albert Lab Ultracentrifuge equipped with 50.2 Ti Rotor
    a. Large ultracentrifuge tubes and Red Titanium Caps (with tightening device)
8. Pliers (to help tighten and remove ultracentrifuge caps)
9. Alder Lab Concentrating Centrifuge
10. BioRad Large PolyPrep Column and Column Rack

B.2.4. Methods

1. Preparation of Inclusion Bodies
    a. Thaw cell pellets on ice for 15 min.
        1- Usually complete this in 2 sets of 4 bottles each.
    b. Weigh cell pellets (also weigh empty bottle for comparison).
        1- Determine weights of cell pellets; average for easier calculations.
    c. For each 1 g of cell pellets add the following:
        1- 5 mL of Cell Disruption Buffer
        2- 5 μL of 1 M Magnesium Chloride
        3- 50 μL of 100 mM PMSF
        4- 5 μL of 20 mg/mL DNase
        5- 80 μL of 10 mg/mL Lysozyme
    d. Resuspend the pellets by swirling the bottles.
    e. Cell Disruption by Sonication.
        1- Prepare an Ice Bath in a 600 mL Beaker.
        2- Parameters: 50% Amp., 30 sec On, 30 sec Off, 5 min Process Time.
        3- Add suspensions to Glass Tubes.
        4- Note that suspensions will NOT become clear.
    f. While first set of 4 bottles Sonicates; Thaw and Resuspend remaining bottles.
    g. Place Sonicated Suspensions in Plastic Tubes.
        1- Should have 4 or 6 tubes depending on total volume.
    h. Centrifuge in Hallway Centrifuge: SA-600 rotor (4°C, 24,000 Xg) for 12 min.
    i. Resuspend the pellets by Sonicating in 10 mL Inclusion Body Wash Buffer.
        1- Resuspend 2 tubes in 10 mL each; Sonicate; Add resuspended solution to next tube; Sonicate; Repeat as necessary until only 2 tubes remaining.
        2- Use the same parameters above except shorten Process Time.
        3- Sonicate only until pellet is in solution.
    j. Centrifuge in SA-600 rotor (4°C, 24,000 Xg) for 15 min.
    k. Repeat steps i and j once more (only 2 tubes at this point).
    l. Weigh pellets (also weigh empty tube for comparison).
        1- Determine weight of pellets; average for easier calculations.

2. Inclusion Body Solubilization
    a. Add ~15 mL Inclusion Body Solubilization Buffer to each tube.
        1- Should have a concentration of ~50-80 mg/mL.
    b. Place small stir bar in each tube and place tubes in Blue Metal Rack.
    c. Place rack on heating stir plate and set to 75°C and ~150 RPM.
    d. Incubate for ~2-3 hrs.
        1- If after ~1.5 hrs it appears that solid is remaining attached to plastic tube, gently scrape off using a spatula and allow to stir.
    e. Centrifuge in Albert Lab Ultracentrifuge: 50.2Ti rotor
        1- Parameters: 4°C, 45,000 Xg, 15 min.
        2- Add all 30 mL to one ultracentrifuge tube.
        3- Fill to right below where Cap inserts with a few mL TX-100.
        4- Note that need to use Red Titanium Caps (Albert Lab).

3. Protein Purification
    a. Prepare Ni-NTA Slurry
        1- Remove 5 mL NEW Ni-NTA (7 mL Recharged) into Falcon Tube.
        2- Centrifuge at 2000 RPM in Alder Lab Concentrating Centrifuge.
        3- Aspirate Ethanol.
    b. Add 30 mL of Protein sample to Ni-NTA; Parafilm; Rotate at 4°C for 35 min.
    c. Add Sample to BioRad Large PolyPrep column.
        1- Collect Flow Through.
        2- Consecutively add 15 mL each of Column Buffer: Washes 1-4 and Column Buffer: Elution.
        3- Collect ALL fractions.

4. Analysis of Yield (Clean Protein usually emerges from column in WASH 4).
    a. Use 2X 15% SDS-PAGE gels: 1X Coomassie Stain and 1X Western Blot.
    b. Concentrate Wash 4 and Dialyze once with excess Column Buffer: Wash 1.
    c. Confirm protein presence and concentration with Pierce A660 Kit.

B.3. Fluorescent Labeling

B.3.1. Summary

The purpose of the above cell growth and purification of Complex II membrane subunits is to prepare protein for fluorescence labeling and liposome incorporation. Below are the basic steps for labeling Sdh3 with the BODIPY-FL fluorophore. The BODIPY probes are ideal for FRET-based analyses due to their high absorbance and quantum yield, absorbance and emission spectral overlap (homoFRET), and their relatively small size (so as not to disrupt protein folding and structure).

B.3.2. Buffers and Solutions

1. BODIPY-FL Iodoacetamide Stock (Molecular Probes D-6003; 417.003 g/mol)

0.1 mg	BODIPY-FL	20 mM
11.76 μL	Dimethylsulfoxide	DMSO

Confirm concentration spectroscopically ($\varepsilon = 79{,}000\ M^{-1}cm^{-1}$):
Dilute 2 μL BODIPY-FL in 2 mL Methanol; Take Absorbance at 504 nm.
Calculate concentration and dilute to 200x concentration of Sdh3 protein.

2. 1 M DTT Stock (in -20°C Freezer)

B.3.3. Materials

1. Purified Protein
2. BODIPY-FL prepared stock
3. Rotisserie
4. Parafilm and Foil
5. BioBeads

B.3.4. Methods: Labeling Reaction

1. Add 250 μL (per proteoliposome formation reaction) of protein to microfuge tube.
    a. Aim for a protein concentration of 10 – 25 μM.
    b. Add 5 μL of BODIPY-FL stock per 250 μL of protein. This should result in a 4X concentration of BODIPY-FL over protein.

2. Parafilm tubes and cover in foil to protect from light.

3. Incubate on rotisserie at RT for 2.5 hrs.

4. Quench reactions with 1 M DTT to result in a final DTT concentration of 10 mM.

5. Purify the FREE dye away from labeled protein with BioBead Pre-incubation
    a. Prehydrate 120 mg BioBeads in 800 μL Column Buffer: Wash 1.
    b. Withdraw buffer and add labeling reaction.
        1- Parafilm tubes and cover in foil.
    c. Incubate on rotisserie at RT for 1 hr.
    d. Remove from BioBeads and place in fresh microfuge tube.
        1- Note that if analyzing labeling efficiency, remove aliquot at this time.

B.4. Proteoliposome Formation

B.4.1. Summary

The proteoliposome formation protocol below is adapted from Nathan Alder's previous protocols for forming proteoliposomes with Tim23 labeled with the NBD fluorescent probe. Note that one of the main changes involves initially placing the sample into the most dense sucrose gradient layer at the bottom so that any unincorporated, aggregated protein and dye will

remain pelleted and the proteoliposomes will float to the top of the gradient (as compared to previous protocols in which the sample is initially placed toward the top of the gradient).

B.4.2. Buffers and Solutions

1. Hydration Buffer

241 mL	Double Distilled Water		
2.5 mL	1 M Tris-HCl, pH 7.4		10 mM
6.3 mL	4 M Sodium Chloride	NaCl	100 mM
500 μL	1 M Magnesium Chloride	$MgCl_2$	2 mM

2. Biomimetic Liposome Formation (LUVs)

170 μL	18:1; 16:0-phosphatidylcholine	POPC	40 mol%
162 μL	18:1; 16:0-phosphatidylethanolamine	POPE	40 mol%
168 μL	Tetraoleoylcardiolipin	CL	20 mol%

Dry lipids under nitrogen stream for ~15 min.
Dry lipids under a vacuum in the RT desiccator (D-AL setting) overnight.
Hydrate lipids in 500 μL Hydration Buffer and let sit at RT with intermittent vortexing until all lipids are in solution.
Extrude 17X through 0.1 μm pore membrane (two filters on each side).
Store at RT until use.

3. 5% (w/v) Dodecyl-β-D-maltoside

10 mg	Dodecyl-β-D-maltoside	DDM	5% (w/v)
200 μL	Double Distilled Water		

Note that this stock is 98 mM, which is much greater than the CMC of 0.16 mM.

4. 10% (w/w) Sucrose Solution

1.0 g	Sucrose	10% (w/w)
9.0 g	Hydration Buffer	

Prepare scale with weigh boat and small beaker holding open 15 mL Falcon tube.
Weigh out 1.0 g sucrose into weigh boat.
Pipette Hydration Buffer into Falcon tube until total weight is 10.0 g.

5. 20% (w/w) Sucrose Solution

2.0 g	Sucrose	20% (w/w)
8.0 g	Hydration Buffer	

Prepare scale with weigh boat and small beaker holding open 15 mL Falcon tube.
Weigh out 2.0 g sucrose into weigh boat.
Pipette Hydration Buffer into Falcon tube until total weight is 10.0 g.

6. 50% (w/w) Sucrose Solution

5.0 g	Sucrose	50% (w/w)
5.0 g	Hydration Buffer	

Prepare scale with weigh boat and small beaker holding open 15 mL Falcon tube.
Weigh out 5.0 g sucrose into weigh boat.
Pipette Hydration Buffer into Falcon tube until total weight is 10.0 g.
Intermittently vortex and run sample under hot tap water to dissolve sucrose.

B.4.3. Materials

1. Liposomes
2. Labeled Protein
3. Buffers and Stock Solutions (Above)
4. Rotisserie
5. Foil and Parafilm
6. Alder Lab Ultracentrifuge equipped with Swinging Bucket Rotor (TLS-55)
    a. Buckets and appropriate centrifuge tubes

B.4.4. Methods

1. Incubate LUVs and BODIPY-Sdh3 separately with DDM.
    a. Add 5 μL of 5% (w/v) DDM stock to 70 μL of liposomes.
        1- Note that this is for EACH proteoliposome reaction that is planned.
    b. Add 16.4 μL of 5% (w/v) DDM stock to 250 μL BODIPY-Sdh3 samples.
    c. Incubate all on rotisserie at RT for 20 min.

2. Combine solubilized protein and liposome samples for a total volume of ~325 μL.
    a. Incubate on rotisserie at RT for 1 hr.

3. Proteoliposome formation with BioBeads.
    a. Prehydrate 120 mg BioBeads in 800 μL Hydration Buffer
        1- Make sure to prepare 2x each of the BioBead samples above for EACH proteoliposomes formation reaction.
        2- Incubate at RT for at least 2 hrs.
        3- Withdraw excess Hydration Buffer from one tube for each sample.
    b. Add samples to BioBeads.
        1- Parafilm tubes and wrap in foil.
        2- Incubate on rotisserie at RT for 2.5 hrs.
        3- Withdraw excess Hydration Buffer from remaining BioBead tubes.
    c. Remove sample from rotisserie and add to second set of BioBeads.
        1- Parafilm tubes and wrap in foil.
        2- Incubate on rotisserie at RT overnight.
        3- Remove sample from BioBeads and place in fresh microfuge tube.

4. Sucrose Gradient Density Centrifugation Purification.
    a. Add equal volume (as sample) of 50% sucrose to each proteoliposome sample.
        1- Layer into bottom of Ultracentrifuge tube.
    b. Layer 650 μL of 20% sucrose on top, followed by 650 μL of 10% sucrose.
    c. Centrifuge in Swinging Bucket Rotor (TLS-55) in Alder Lab Ultracentrifuge.
        1- Parameters: 55,000 RPM, 1 hr, 15°C, Accel/Decel = 2.
    d. Split into 9 x 200 μL Fractions.
        1- Pool fractions 2-4 and Dilute to 750 μL total with Hydration Buffer.

5. Samples are ready for Fluorescence-based analysis.
    a. Analyze 250 μL samples in quartz microcuvettes.
    b. Programs: BFL Em Scan; BOD Anisotropy

Appendix C: Investigation into the Influence of Amount and Type of Cardiolipin on Complex II Activity: Additional Tests

Other colleagues who have contributed to the studies presented in this appendix are Matthew Greenwood and Nathan N. Alder. Both are from the University of Connecticut (Storrs, CT 06269, USA).

Figures C.8 and **C.9** derived from: Hwang M.-S., Schwall C.T., Pazarentzos E., Datler C., Alder N.N., and Grimm S., Mitochondrial Ca2+ influx targets cardiolipin to disintegrate respiratory chain complex II for cell death induction, *Cell Death and Differentiation* (2014).

C.1. Abstract

Chapter 3 introduced how cardiolipin (CL) has a great effect on the activity, as well as stability, of Complex II within the nanodisc (ND) model membrane system. The studies presented here further explored these findings by investigating whether the acyl chain composition or the anionic headgroup of CL was stabilizing the holoenzyme. First, by titrating the amount of tetraoleoyl-CL (TOCL; four 18:1 Δ^9 acyl chains) present in the NDs we found that when TOCL neared levels present in the native IM, maximal activity and stability of Complex II was reached. Second, the headgroup and alkyl chains of CL were also investigated and did not seem to have a large effect on either the stability or activity of Complex II within NDs, under unstressed conditions. Finally, the effect of each of the CL types in the presence of the divalent cations magnesium and calcium was examined and it was found that the presence of these cations can greatly inhibit Complex II activity, most likely through interactions with CL, as these effects were dependent on the type of CL present.

C.2. Methods

C.2.1. Nanodisc (ND) Compositions

All materials and methods used are identical to those described in Chapters 2 and 3. However, the lipid compositions used to assemble the NDs differ and for this reason, they are outlined here. For experiments varying the amount of TOCL, lipid stocks were mixed to form: 0 mol% TOCL (50:50 mol% POPC:POPE); 5 mol% TOCL (47.5:47.5:5 mol% POPC:POPE:TOCL); 10 mol% TOCL (45:45:10 mol% POPC:POPE:TOCL); 20 mol% (40:40:20 mol% POPC:POPE:TOCL); 30 mol% TOCL (40:30:30 mol% POPC:POPE:TOCL). For experiments varying the type of CL or studying the effects of divalent cations, the overall lipid ratio was 40:40:20 mol% of POPC:POPE:Anionic Lipid, respectively. The types of CL that were substituted include: TOCL (18:1 Δ^9 acyl chains), TMCL (14:0 acyl chains), dTOCL (a deoxy version of TOCL lacking the hydroxyl group in the central glycerol of the headgroup), and POPG (the negatively charged precursor of CL). As stated, the lipid preparation and ND assembly were otherwise identical to that described in Chapters 2 and 3.

C.2.2. Cation Incubations and Titrations

For high concentrations of cations, NDs were formed and metal-affinity purification Elutions 1 and 2 were combined and dialyzed into MSP buffer containing 100 mM of the appropriate cation. For the low concentration titrations of cations, Elutions 1 and 2 were combined and concentrated. Samples were split and incubated with the appropriate concentration of cation (0 mM to 20 mM) prior to activity assay measurements. Both succinate dehydrogenase (SDH) and succinate: ubiquinone oxidoreductase (SQR) activity assays were performed as described in Chapter 3.

C.2.3. Complex II Affinity Assay

NDs were formed and metal-affinity purification Elutions 1 and 2 were combined and dialyzed into MSP buffer lacking NaCl, split into separate samples and subject to low calcium concentration titrations, between 0 mM and 20 mM. Samples were rotated for 15 min at RT and then added to Ni-NTA agarose and further rotated for 40 min at RT. After nanodiscs were subjected to a second metal-affinity chromatography purification, samples were taken from each fraction that emerged from the column and analyzed *via* 12% SDS-PAGE for the presence of FAD as in Chapter 2.

C.3. Results

C.3.1. Amount of TOCL

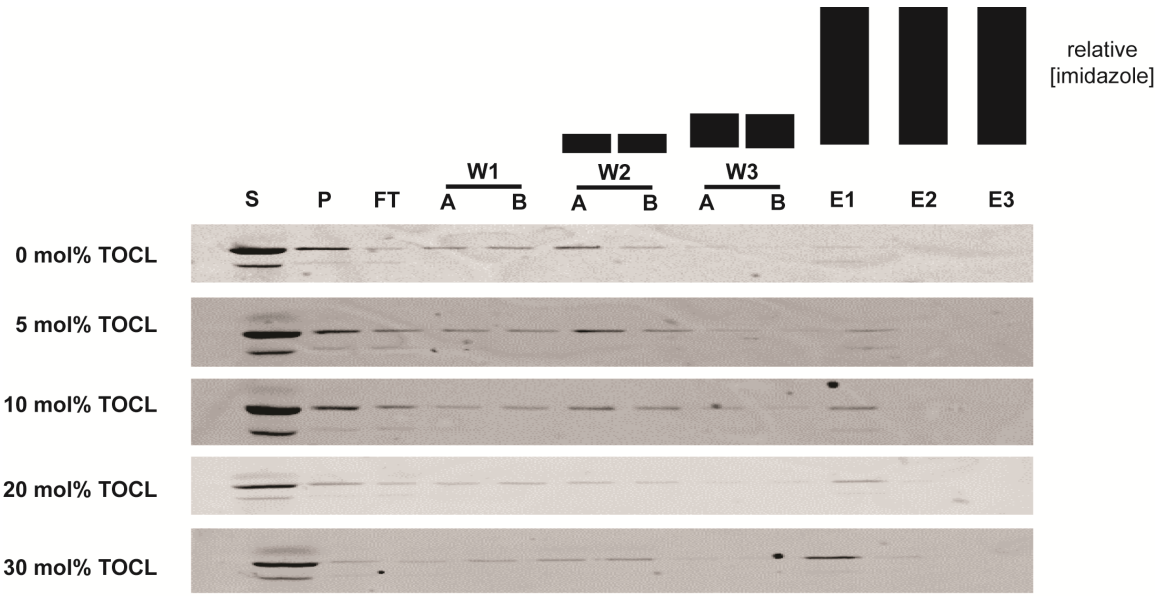

Figure C.1. The affinity of Complex II catalytic and membrane dimers is dependent on amount of TOCL present in NDs. Membrane proteins from dodecyl-β-D-maltoside (DDM)-solubilized mitochondria were reconstituted into NDs with the indicated mol% TOCL and subjected to affinity chromatography to isolate the NDs. Subunits co-eluting with MSP1E3D1 (fractions E1 and E2) were considered to be stably associated with the NDs; those eluting at the earlier fractions were not stably associated. Monitoring the fluorescence of FAD was used as the marker for the soluble catalytic dimer. Abbreviations are S: supernatant and P: pellet from mitochondrial solubilization; FT: column flow through; W1A-W3B: column wash steps; E1-E3: column elution steps. Note relative imidazole concentrations depicted above lane labels.

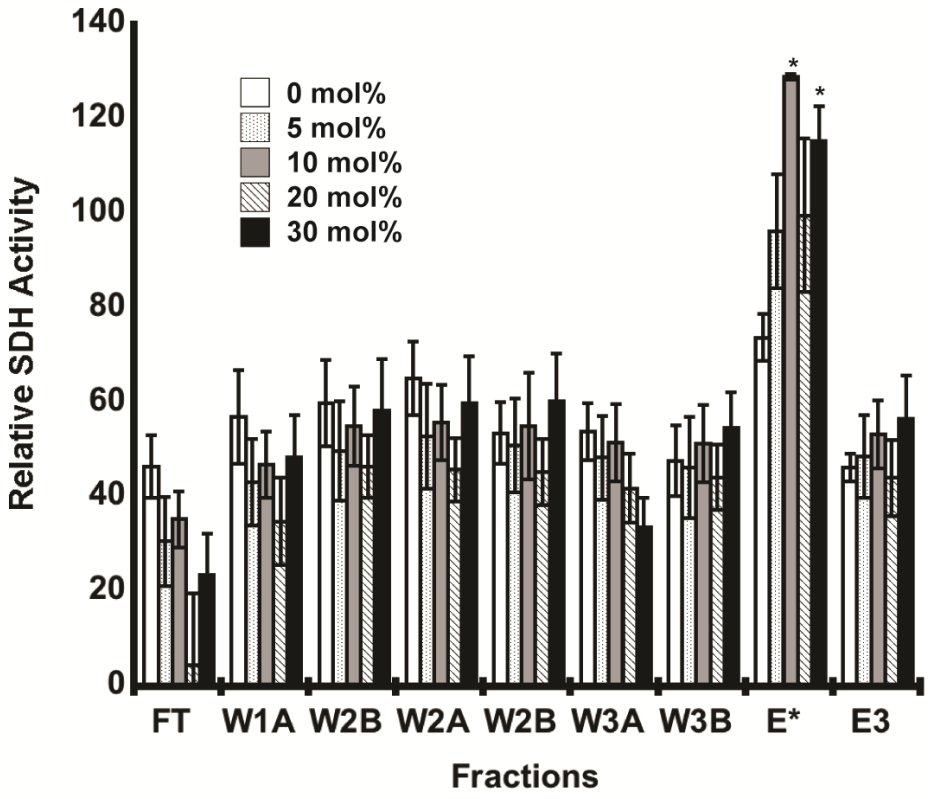

Figure C.2. The amount of TOCL present in NDs affects Complex II catalytic dimer activity. Relative succinate dehydrogenase (SDH) activity of column fractions for ND samples with the indicated mol% TOCL: 0 mol% (white), 5 mol% (dotted), 10 mol% (gray), 20 mol% (diagonal lines), and 30 mol% (black). E* represents fractions E1 and E2, which were pooled, and statistical differences are represented in relation to 20 mol% TOCL NDs (* = $p < 0.001$).

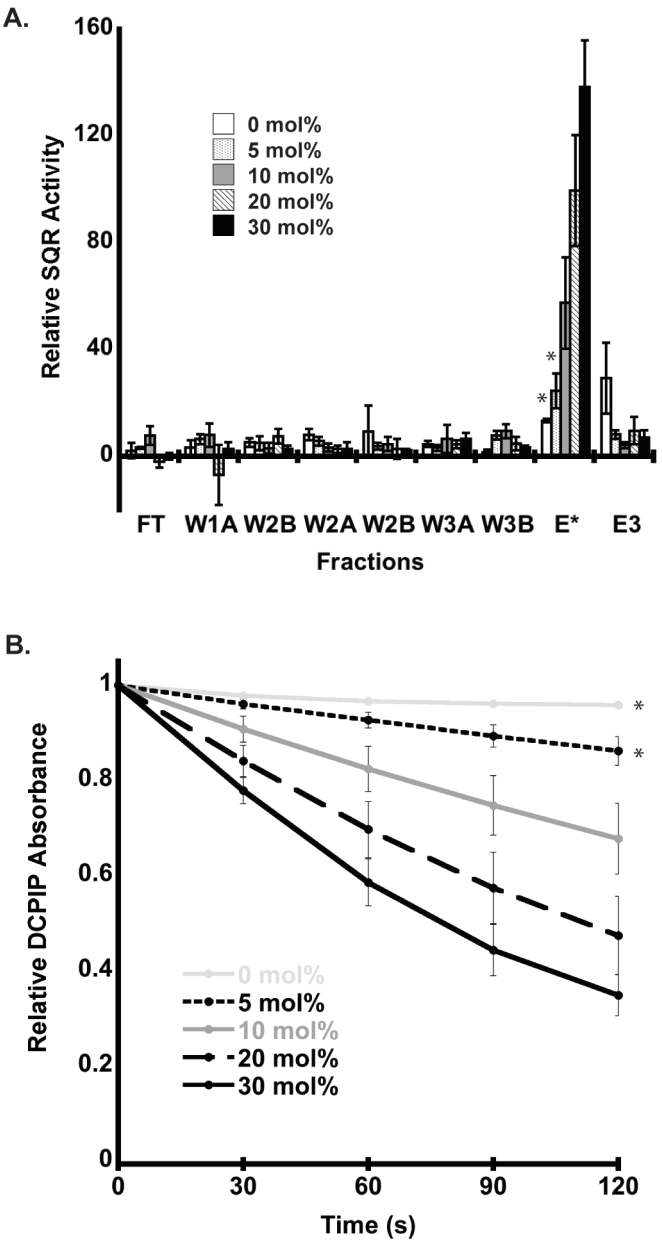

Figure C.3. The amount of TOCL present in NDs affects Complex II holoenzyme activity. (**A**) Relative succinate: quinone oxidoreductase (SQR) activity of column fractions for ND samples with the indicated mol% TOCL, determined from the initial reaction velocity (30 s following succinate addition). ND samples are labeled as in **Figure C.2** and E* represents fractions E1 and E2, which were pooled. Statistical differences are represented in relation to 20

mol% TOCL NDs (* = $p < 0.05$). (**B**) Signal-averaged time course traces of SQR activity for Complex II reconstituted in NDs with varying mol% TOCL, including 0 mol% (light gray line), 5 mol% (broken line), 10 mol% (dark gray line), 20 mol% (dashed line), and 30 mol% (black line). Statistical differences are represented in relation to 20 mol% TOCL NDs (* = $p < 0.01$).

C.3.2. Type of CL

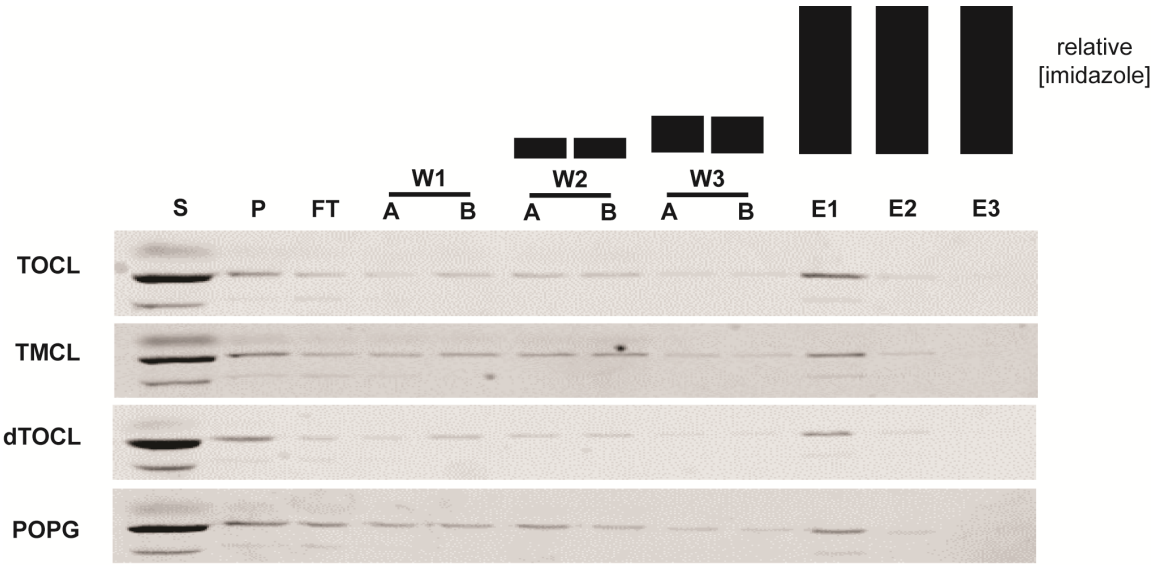

Figure C.4. The type of CL present in NDs does not affect Complex II catalytic dimer and membrane dimer affinities. Elution profiles of NDs assembled with indicated CL compositions. Preparation of samples and column fraction designations are identical to those in **Figure C.1**.

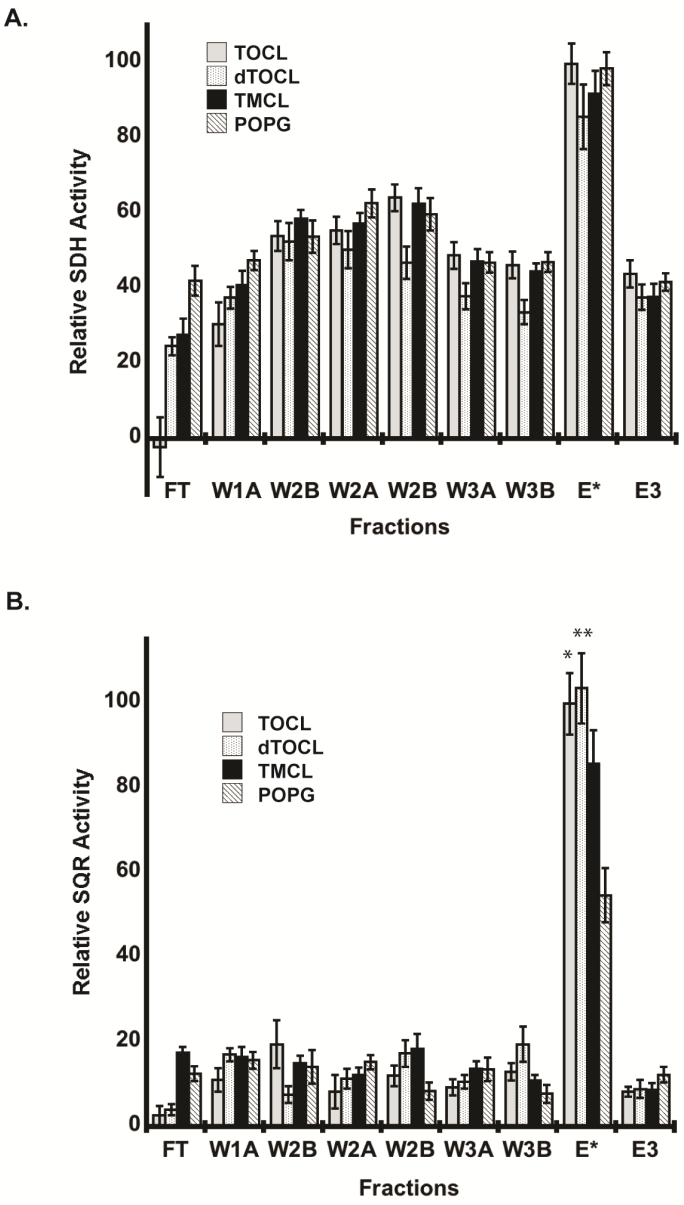

Figure C.5. The type of CL present in NDs does not affect Complex II catalytic or holoenzyme activities. (**A**) Relative SDH activity of column fractions for ND samples with the indicated CL type, including TOCL (light gray), dTOCL (dotted), TMCL (black) and POPG (diagonal lines). (**B**) Relative SQR activity of column fractions for ND samples with the indicated CL type, determined from the initial reaction velocity (30 s following succinate addition) and labeled as in (**A**). For both (**A**) and (**B**), E* represents fractions E1 and E2, which

were pooled, and statistical differences are represented in relation to POPG-containing NDs (* = $p < 0.01$).

C.3.3. Addition of Divalent Cations

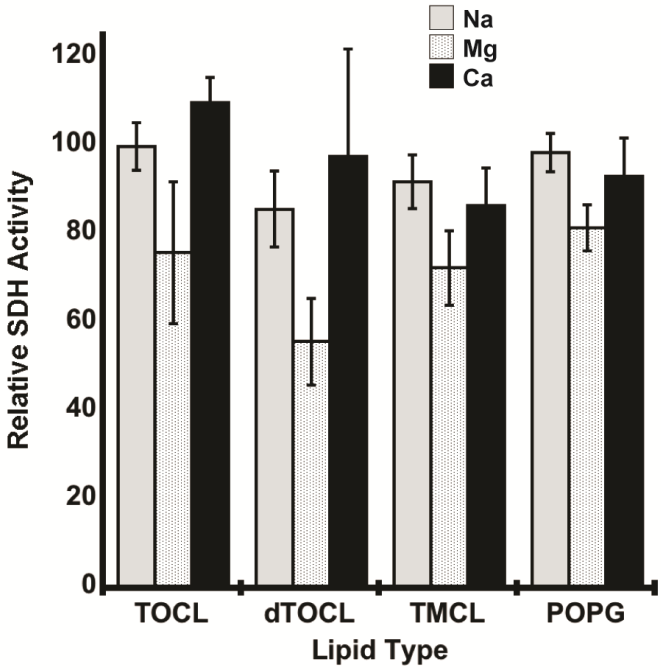

Figure C.6. Divalent cations display little ability to affect Complex II catalytic dimer activity, even at high concentrations. Relative SDH activity of column fractions for ND samples with the indicated CL type and treated with the indicated cations, including sodium (Na, light gray), magnesium (Mg, dotted), and calcium (Ca, black). Each cation is present at extremely high (100 mM) concentration in order to initially determine if there was a monitorable effect. Statistical differences were determined in relation to sodium-treated NDs within each CL type, but none were found to be significant.

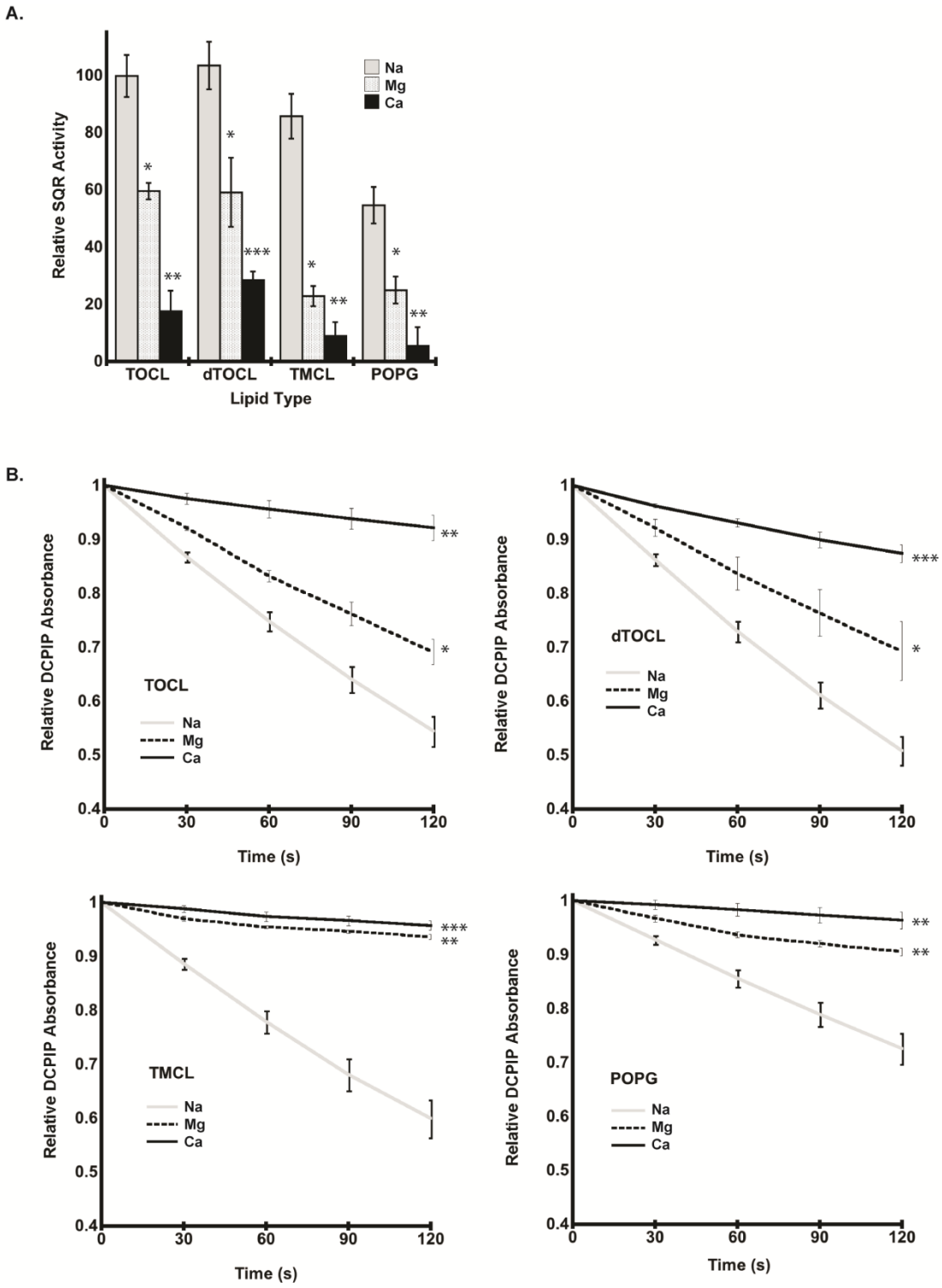

Figure C.7. High concentrations of divalent cations are able to decrease the holoenzyme activity of Complex II. (**A**) Relative SQR activity of column fractions for ND samples with the

indicated CL type and cation treatments, determined from the initial reaction velocity (30 s following succinate addition). Note that E* represents fractions E1 and E2, which were pooled. (**B**) Signal-averaged time course traces of SQR activity for Complex II reconstituted in NDs with varying CL types. For both (**A**) and (**B**), cation concentrations are identical to and treatments are labeled as in **Figure C.6** (gray line, Na^{+}; dashed black line, Mg^{2+}; solid black line, Ca^{2+}) and statistical differences are represented in relation to sodium-treated NDs within each CL type (* = $p < 0.05$, ** = $p < 0.01$, and *** = $p < 0.001$).

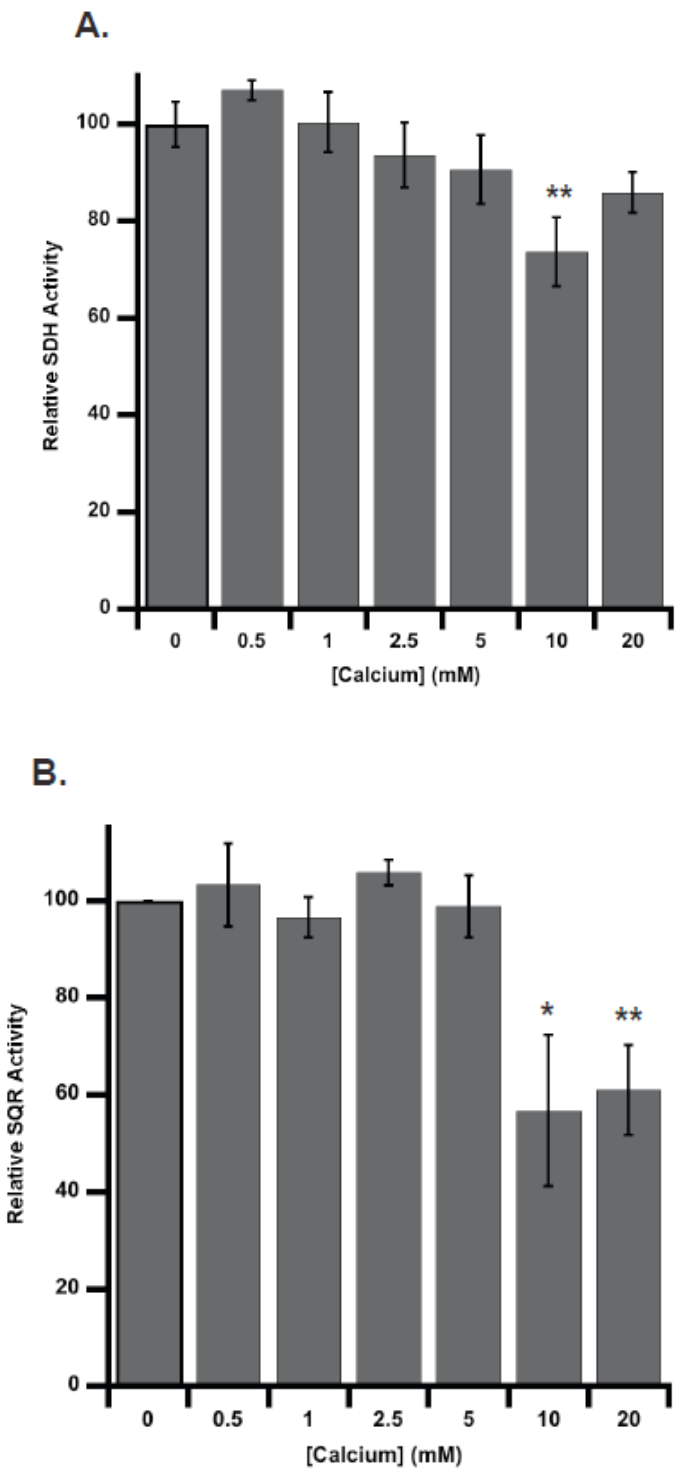

Figure C.8. The activities of Complex II are selectively Ca^{2+}-dependent and low concentrations of cation can decrease holoenzyme activity. (**A**) Succinate dehydrogenase

(SDH, PMS-mediated) activity monitoring the presence of the catalytic dimer is overall not Ca^{2+}-dependent. (**B**) Succinate: quinone oxidoreductase (SQR, DB-mediated) activity monitoring the presence of the holoenzyme is Ca^{2+}-dependent reflecting the decreased affinity between the catalytic and membrane dimers. Error bars are representative of s.e.m. for at least four separate experiments and statistical differences are represented in relation to addition of 0 mM Ca^{2+} (* = $p \leq 0.05$; ** = $p \leq 0.01$).

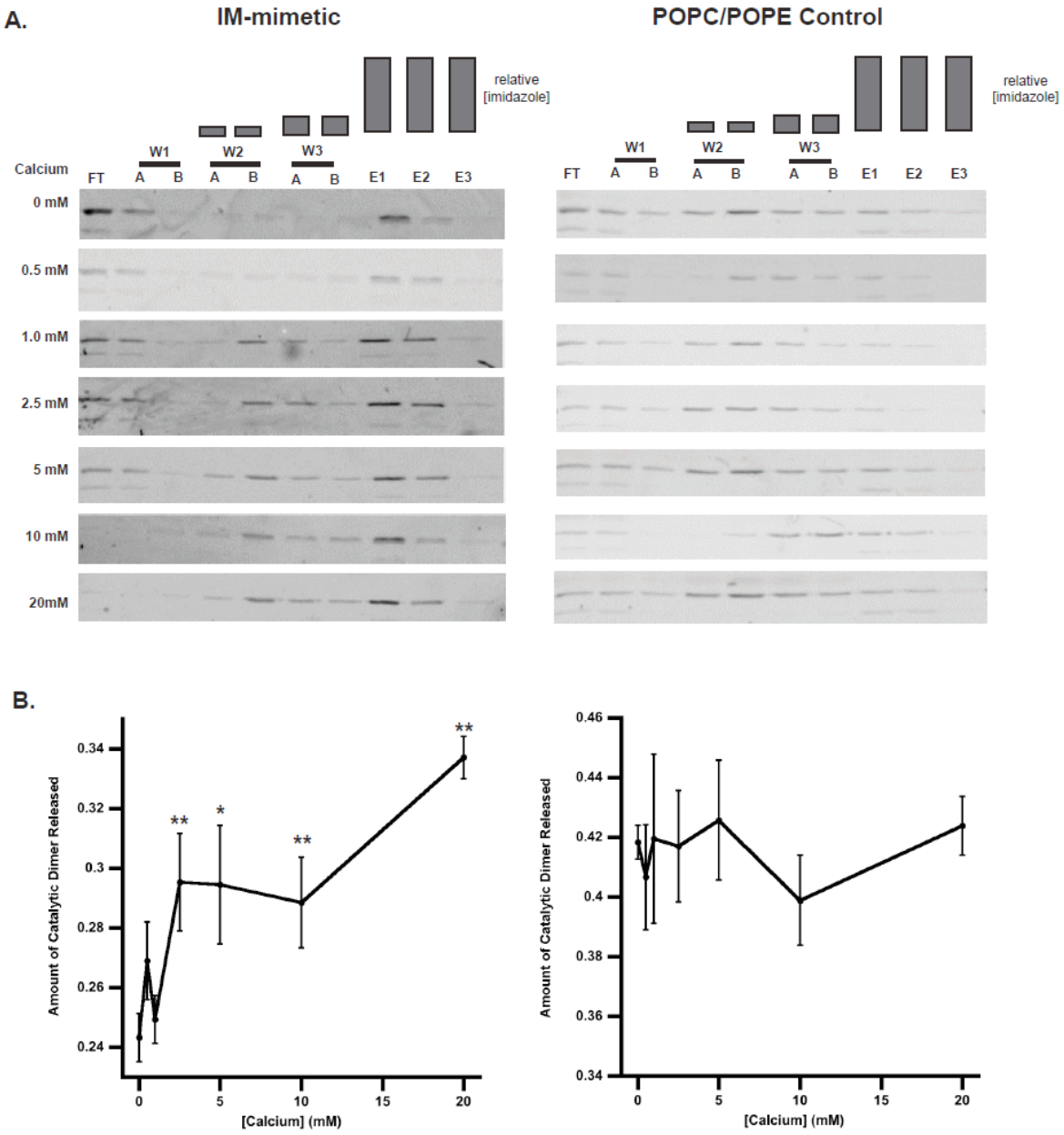

Figure C.9. The stability of Complex II is Ca^{2+}-dependent (even at low concentrations) and mediated by CL. Supernatant resulting from DDM-solubilized mitochondria were reconstituted into nanodiscs with (IM-mimetic) and without (POPC/POPE control) cardiolipin. Nanodiscs were subjected to Ni-NTA affinity chromatography and then treated with the indicated concentration of Ca^{2+}. Subunits co-eluting the MSP1E3D1 (E1 and E2) were considered to be stably assembled within the nanodiscs; subunits emerging from the column at earlier fractions,

such as in the middle wash fractions, were not. (**A**) SDS-PAGE analysis of the column fractions. The fluorescent FAD signal was used as a marker for the soluble catalytic dimer as FAD is covalently bound to Sdh1p. Abbreviations indicate the following column fractions: FT: flow through; W1A-W3B: wash steps; E1-E3 elution steps. (**B**) Quantification of FAD band intensity comparing the predominant middle Wash fraction (W2B in most cases or W3A under some conditions) and combined selected Wash with E1 and E2 (which represents the total of the catalytic dimer in the predominant wash and all that remains connected to the membrane dimer within nanodiscs). A larger ratio indicates a less stable complex (i.e. more catalytic dimer is not stably associated with nanodiscs and washes off the column prior to E1 and E2). Error bars are representative of s.e.m. for at least three separate experiments and statistical differences are represented in relation to addition of 0 mM Ca^{2+} (* = $p \leq 0.05$; ** = $p \leq 0.01$).

References

[1] J. Nunnari, A. Suomalainen, Mitochondria: In Sickness and in Health, Cell, 148 (2012) 1145-1159.

[2] N. Alder, Biogenesis of Lipids and Proteins within Mitochondrial Membranes, in: P. Yeagle (Ed.) The Structure of Biological Membranes, CRC Press, Boca Raton, 2011, pp. 315-377.

[3] A.M. Distler, J. Kerner, C.L. Hoppel, Proteomics of mitochondrial inner and outer membranes, PROTEOMICS, 8 (2008) 4066-4082.

[4] G. Daum, Lipids of mitochondria, Biochimica et biophysica acta, 822 (1985) 1-42.

[5] A.M. Brusque, R. Borba Rosa, P.F. Schuck, K.B. Dalcin, C.A. Ribeiro, C.G. Silva, C.M. Wannmacher, C.S. Dutra-Filho, A.T. Wyse, P. Briones, M. Wajner, Inhibition of the mitochondrial respiratory chain complex activities in rat cerebral cortex by methylmalonic acid, Neurochem Int, 40 (2002) 593-601.

[6] A. Magalon, R. Arias-Cartin, A. Walburger, Chapter Six - Supramolecular Organization in Prokaryotic Respiratory Systems, in: K.P. Robert (Ed.) Advances in Microbial Physiology, vol. Volume 61, Academic Press, 2012, pp. 217-266.

[7] R.A. Stuart, Supercomplex Organization of the Yeast Respiratory Chain Complexes and the ADP/ATP Carrier Proteins, Methods in enzymology, 456 (2009) 191-208.

[8] J.A. Enriquez, G. Lenaz, Coenzyme Q and the Respiratory Chain: Coenzyme Q Pool and Mitochondrial Supercomplexes, Molecular Syndromology, 5 (2014) 119-140.

[9] E. Mileykovskaya, P.A. Penczek, J. Fang, V.K.P.S. Mallampalli, G.C. Sparagna, W. Dowhan, Arrangement of the Respiratory Chain Complexes in Saccharomyces cerevisiae Supercomplex III2IV2 Revealed by Single Particle Cryo-Electron Microscopy, Journal of Biological Chemistry, 287 (2012) 23095-23103.

[10] S. Bazan, E. Mileykovskaya, V.K. Mallampalli, P. Heacock, G.C. Sparagna, W. Dowhan, Cardiolipin-dependent reconstitution of respiratory supercomplexes from purified Saccharomyces cerevisiae complexes III and IV, The Journal of biological chemistry, 288 (2013) 401-411.

[11] M. van der Laan, N. Wiedemann, D.U. Mick, B. Guiard, P. Rehling, N. Pfanner, A role for Tim21 in membrane-potential-dependent preprotein sorting in mitochondria, Current biology : CB, 16 (2006) 2271-2276.

[12] M. van der Laan, D.P. Hutu, P. Rehling, On the mechanism of preprotein import by the mitochondrial presequence translocase, Biochimica et Biophysica Acta (BBA) - Molecular Cell Research, 1803 (2010) 732-739.

[13] R. Acín-Pérez, P. Fernández-Silva, M.L. Peleato, A. Pérez-Martos, J.A. Enriquez, Respiratory Active Mitochondrial Supercomplexes, Molecular Cell, 32 (2008) 529-539.

[14] N. Kovářová, T. Mráček, H. Nůsková, E. Holzerová, M. Vrbacký, P. Pecina, K. Hejzlarová, K. Kľučková, J. Rohlena, J. Neuzil, J. Houštěk, High Molecular Weight Forms of Mammalian Respiratory Chain Complex II, PLoS ONE, 8 (2013) e71869.

[15] G. Lenaz, M.L. Genova, Structure and organization of mitochondrial respiratory complexes: a new understanding of an old subject, Antioxidants & redox signaling, 12 (2010) 961-1008.

[16] G. Lenaz, R. Fato, G. Formiggini, M.L. Genova, The role of Coenzyme Q in mitochondrial electron transport, Mitochondrion, 7 Suppl (2007) S8-33.

[17] M.L. Genova, G. Lenaz, Functional role of mitochondrial respiratory supercomplexes, Biochimica et biophysica acta, 1837 (2014) 427-443.

[18] G. Lenaz, M.L. Genova, Structural and functional organization of the mitochondrial respiratory chain: A dynamic super-assembly, The International Journal of Biochemistry & Cell Biology, 41 (2009) 1750-1772.

[19] S. Marchi, C. Giorgi, J.M. Suski, C. Agnoletto, A. Bononi, M. Bonora, E. De Marchi, S. Missiroli, S. Patergnani, F. Poletti, A. Rimessi, J. Duszynski, M.R. Wieckowski, P. Pinton, Mitochondria-ros crosstalk in the control of cell death and aging, J Signal Transduct, 2012 (2012) 329635.

[20] I.M. Ahmad, M.Y. Abdalla, Mitochondria-Mediated Oxidative Stress and Cancer Therapy Oxidative Stress in Cancer Biology and Therapy, in: D.R. Spitz, K.J. Dornfeld, K. Krishnan, D. Gius (Eds.), Springer New York, 2012, pp. 3-19.

[21] C. Cortés-Rojo, E. Calderón-Cortés, M. Clemente-Guerrero, M. Estrada-Villagómez, S. Manzo-Avalos, R. Mejía-Zepeda, I. Boldogh, A. Saavedra-Molina, Elucidation of the effects of

lipoperoxidation on the mitochondrial electron transport chain using yeast mitochondria with manipulated fatty acid content, Journal of Bioenergetics and Biomembranes, 41 (2009) 15-28.

[22] F. Diaz, J.A. Enríquez, C.T. Moraes, Cells Lacking Rieske Iron-Sulfur Protein Have a Reactive Oxygen Species-Associated Decrease in Respiratory Complexes I and IV, Molecular and cellular biology, 32 (2012) 415-429.

[23] C.R.D. Lancaster, Succinate:quinone oxidoreductases: an overview, Biochimica et Biophysica Acta (BBA) - Bioenergetics, 1553 (2002) 1-6.

[24] R.S. Lemos, A.S. Fernandes, M.M. Pereira, C.M. Gomes, M. Teixeira, Quinol:fumarate oxidoreductases and succinate:quinone oxidoreductases: phylogenetic relationships, metal centres and membrane attachment, Biochimica et Biophysica Acta (BBA) - Bioenergetics, 1553 (2002) 158-170.

[25] C. Hägerhäll, Succinate: quinone oxidoreductases: Variations on a conserved theme, Biochimica et Biophysica Acta (BBA) - Bioenergetics, 1320 (1997) 107-141.

[26] C.R.D. Lancaster, Respiratory Chain Complex II and Succinate: Quinone Oxidoreductases, in: J.L. Editors-in-Chief: William, M.D. Lane (Eds.) Encyclopedia of Biological Chemistry, Elsevier, New York, 2004, pp. 681-687.

[27] T.M. Iverson, Structure of the Escherichia coli Fumarate Reductase Respiratory Complex, Science, 284 (1999) 1961-1966.

[28] C.R.D. Lancaster, A. Kroger, M. Auer, H. Michel, Structure of fumarate reductase from Wolinella succinogenes at 2.2A resolution, Nature, 402 (1999) 377-385.

[29] T.M. Iverson, C. Luna-Chavez, L.R. Croal, G. Cecchini, D.C. Rees, Crystallographic studies of the Escherichia coli quinol-fumarate reductase with inhibitors bound to the quinol-binding site, The Journal of biological chemistry, 277 (2002) 16124-16130.

[30] V. Yankovskaya, R. Horsefield, S. Tornroth, C. Luna-Chavez, H. Miyoshi, C. Leger, B. Byrne, G. Cecchini, S. Iwata, Architecture of succinate dehydrogenase and reactive oxygen species generation, Science, 299 (2003) 700-704.

[31] R. Horsefield, S. Iwata, B. Byrne, Complex II from a structural perspective, Current protein & peptide science, 5 (2004) 107-118.

[32] H. Shimizu, A. Osanai, K. Sakamoto, D.K. Inaoka, T. Shiba, S. Harada, K. Kita, Crystal structure of mitochondrial quinol-fumarate reductase from the parasitic nematode Ascaris suum, Journal of biochemistry, 151 (2012) 589-592.

[33] L.S. Huang, T.M. Borders, J.T. Shen, C.J. Wang, E.A. Berry, Crystallization of mitochondrial respiratory complex II from chicken heart: a membrane-protein complex diffracting to 2.0 A, Acta crystallographica. Section D, Biological crystallography, 61 (2005) 380-387.

[34] L.S. Huang, G. Sun, D. Cobessi, A.C. Wang, J.T. Shen, E.Y. Tung, V.E. Anderson, E.A. Berry, 3-nitropropionic acid is a suicide inhibitor of mitochondrial respiration that, upon oxidation by complex II, forms a covalent adduct with a catalytic base arginine in the active site of the enzyme, The Journal of biological chemistry, 281 (2006) 5965-5972.

[35] L.S. Huang, J.T. Shen, A.C. Wang, E.A. Berry, Crystallographic studies of the binding of ligands to the dicarboxylate site of Complex II, and the identity of the ligand in the "oxaloacetate-inhibited" state, Biochimica et biophysica acta, 1757 (2006) 1073-1083.

[36] F. Sun, X. Huo, Y. Zhai, A. Wang, J. Xu, D. Su, M. Bartlam, Z. Rao, Crystal structure of mitochondrial respiratory membrane protein complex II, Cell, 121 (2005) 1043-1057.

[37] K.S. Oyedotun, B.D. Lemire, The quaternary structure of the Saccharomyces cerevisiae succinate dehydrogenase. Homology modeling, cofactor docking, and molecular dynamics simulation studies, The Journal of biological chemistry, 279 (2004) 9424-9431.

[38] E. Maklashina, G. Cecchini, The quinone-binding and catalytic site of complex II, Biochimica et biophysica acta, 1797 (2010) 1877-1882.

[39] T.M. Iverson, Catalytic mechanisms of complex II enzymes: A structural perspective, Biochimica et Biophysica Acta (BBA) - Bioenergetics, 1827 (2013) 648-657.

[40] S.S. Hasan, E. Yamashita, C.M. Ryan, J.P. Whitelegge, W.A. Cramer, Conservation of lipid functions in cytochrome bc complexes, Journal of molecular biology, 414 (2011) 145-162.

[41] C. Arnarez, S.J. Marrink, X. Periole, Identification of cardiolipin binding sites on cytochrome c oxidase at the entrance of proton channels, Sci. Rep., 3 (2013).

[42] G. Cecchini, Function and structure of complex II of the respiratory chain, Annual review of biochemistry, 72 (2003) 77-109.

[43] K.M. Robinson, R.A. Rothery, J.H. Weiner, B.D. Lemire, The covalent attachment of FAD to the flavoprotein of Saccharomyces cerevisiae succinate dehydrogenase is not necessary for import and assembly into mitochondria, European Journal of Biochemistry, 222 (1994) 983-990.

[44] L. Yu, C.A. Yu, Interaction between Succinate-Dehydrogenase and Ubiquinone-Binding Protein from Succinate-Ubiquinone Reductase, Biochimica et biophysica acta, 593 (1980) 24-38.

[45] S.S. Szeto, S.N. Reinke, B.D. Sykes, B.D. Lemire, Ubiquinone-binding site mutations in the Saccharomyces cerevisiae succinate dehydrogenase generate superoxide and lead to the accumulation of succinate, The Journal of biological chemistry, 282 (2007) 27518-27526.

[46] B.D. Lemire, K.S. Oyedotun, The Saccharomyces cerevisiae mitochondrial succinate:ubiquinone oxidoreductase, Biochimica et biophysica acta, 1553 (2002) 102-116.

[47] E. Maklashina, S. Rajagukguk, W.S. McIntire, G. Cecchini, Mutation of the heme axial ligand of Escherichia coli succinate-quinone reductase: implications for heme ligation in mitochondrial complex II from yeast, Biochimica et biophysica acta, 1797 (2010) 747-754.

[48] B. Daignan-Fournier, M. Valens, B.D. Lemire, M. Bolotin-Fukuhara, Structure and regulation of SDH3, the yeast gene encoding the cytochrome b560 subunit of respiratory complex II, The Journal of biological chemistry, 2690 (1994) 15469-15472.

[49] B.L. Bullis, B.D. Lemire, Isolation and characterization of the Saccharomyces cerevisiae SDH4 gene encoding a membrane anchor subunit of succinate dehydrogenase, The Journal of biological chemistry, 269 (1994) 6543-6549.

[50] K.S. Oyedotun, B.D. Lemire, The Saccharomyces cerevisiae succinate-ubiquinone reductase contains a stoichiometric amount of cytochrome b562, FEBS letters, 442 (1999) 203-207.

[51] K.S. Oyedotun, P.F. Yau, B.D. Lemire, Identification of the heme axial ligands in the cytochrome b562 of the Saccharomyces cerevisiae succinate dehydrogenase, The Journal of biological chemistry, 279 (2004) 9432-9439.

[52] L. Yu, J. Xu, P.E. Haley, C. Yu, Properties of bovive heart mitochondrial cytochrome b560, Journal of Biological Chemistry, 262 (1987) 1137-1143.

[53] S.K. Shenoy, L. Yu, C. Yu, Identification of quinone-binding and heme-ligating residues of the smallest membrane-anchoring subunit (QPs3) of bovine heart mitochondrial succinate:ubiquinone reductase, The Journal of biological chemistry, 274 (1999) 8717-8722.

[54] S.K. Shenoy, L. Yu, C.A. Yu, The smallest membrane anchoring subunit (QPs3) of bovine heart mitochondrial succinate-ubiquinone reductase. Cloning, sequencing, topology, and Q-binding domain, The Journal of biological chemistry, 272 (1997) 17867-17872.

[55] K.S. Oyedotun, C.S. Sit, B.D. Lemire, The Saccharomyces cerevisiae succinate dehydrogenase does not require heme for ubiquinone reduction, Biochimica et biophysica acta, 1767 (2007) 1436-1445.

[56] K.S. Oyedotun, B.D. Lemire, The Saccharomyces cerevisiae succinate-ubiquinone oxidoreductase. Identification of Sdh3p amino acid residues involved in ubiquinone binding, The Journal of biological chemistry, 274 (1999) 23956-23962.

[57] K.S. Oyedotun, B.D. Lemire, The Quinone-binding sites of the Saccharomyces cerevisiae succinate-ubiquinone oxidoreductase, The Journal of biological chemistry, 276 (2001) 16936-16943.

[58] J. Ruprecht, S. Iwata, R.A. Rothery, J.H. Weiner, E. Maklashina, G. Cecchini, Perturbation of the quinone-binding site of complex II alters the electronic properties of the proximal [3Fe-4S] iron-sulfur cluster, The Journal of biological chemistry, 286 (2011) 12756-12765.

[59] C.C. Page, C.C. Moser, X. Chen, P.L. Dutton, Natural engineering principles of electron tunnelling in biological oxidation-reduction, Nature, 402 (1999) 47-52.

[60] E. Maklashina, R.A. Rothery, J.H. Weiner, G. Cecchini, Retention of Heme in Axial Ligand Mutants of Succinate-Ubiquinone Oxidoreductase (Complex II) from Escherichia coli, Journal of Biological Chemistry, 276 (2001) 18968-18976.

[61] A. Lemarie, S. Grimm, Mutations in the heme b-binding residue of SDHC inhibit assembly of respiratory chain complex II in mammalian cells, Mitochondrion, 9 (2009) 254-260.

[62] Q.M. Tran, R.A. Rothery, E. Maklashina, G. Cecchini, J.H. Weiner, The Quinone Binding Site in Escherichia coli Succinate Dehydrogenase Is Required for Electron Transfer to the Heme b, Journal of Biological Chemistry, 281 (2006) 32310-32317.

[63] Q.M. Tran, R.A. Rothery, E. Maklashina, G. Cecchini, J.H. Weiner, Escherichia coli succinate dehydrogenase variant lacking the heme b, Proceedings of the National Academy of Sciences, 104 (2007) 18007-18012.

[64] Q.M. Tran, C. Fong, R.A. Rothery, E. Maklashina, G. Cecchini, J.H. Weiner, Out of plane distortions of the heme b of Escherichia coli succinate dehydrogenase, PLoS ONE, 7 (2012) e32641.

[65] F. Sun, Q. Zhou, X. Pang, Y. Xu, Z. Rao, Revealing various coupling of electron transfer and proton pumping in mitochondrial respiratory chain, Curr Opin Struct Biol, 23 (2013) 526-538.

[66] C. Lemaire, G. Dujardin, Preparation of respiratory chain complexes from Saccharomyces cerevisiae wild-type and mutant mitocondria, Methods in Molecular Biology, 432 (2008) 65-81.

[67] J. Rutter, D.R. Winge, J.D. Schiffman, Succinate dehydrogenase - Assembly, regulation and role in human disease, Mitochondrion, 10 (2010) 393-401.

[68] S. Drose, L. Bleier, U. Brandt, A common mechanism links differently acting complex II inhibitors to cardioprotection: modulation of mitochondrial reactive oxygen species production, Molecular pharmacology, 79 (2011) 814-822.

[69] I. Siebels, S. Drose, Q-site inhibitor induced ROS production of mitochondrial complex II is attenuated by TCA cycle dicarboxylates, Bba-Bioenergetics, 1827 (2013) 1156-1164.

[70] B.L. Trumpower, Z. Simmons, Diminished inhibition of mitochondrial electron transfer from succinate to cytochrome c by thenoyltrifluoroacetone induced by antimycin, Journal of Biological Chemistry, 254 (1979) 4608-4616.

[71] H. Miyadera, K. Shiomi, H. Ui, Y. Yamaguchi, R. Masuma, H. Tomoda, H. Miyoshi, A. Osanai, K. Kita, S. Ōmura, Atpenins, potent and specific inhibitors of mitochondrial complex II (succinate-ubiquinone oxidoreductase), Proceedings of the National Academy of Sciences, 100 (2003) 473-477.

[72] S. Ralph, R. Moreno-Sánchez, J. Neuzil, S. Rodríguez-Enríquez, Inhibitors of Succinate: Quinone Reductase/Complex II Regulate Production of Mitochondrial Reactive Oxygen Species and Protect Normal Cells from Ischemic Damage but Induce Specific Cancer Cell Death, Pharmaceutical Research, 28 (2011) 2695-2730.

[73] L.F. Dong, V.J. Jameson, D. Tilly, J. Cerny, E. Mahdavian, A. Marin-Hernandez, L. Hernandez-Esquivel, S. Rodriguez-Enriquez, J. Stursa, P.K. Witting, B. Stantic, J. Rohlena, J. Truksa, K. Kluckova, J.C. Dyason, M. Ledvina, B.A. Salvatore, R. Moreno-Sanchez, M.J. Coster, S.J. Ralph, R.A. Smith, J. Neuzil, Mitochondrial targeting of vitamin E succinate enhances its pro-apoptotic and anti-cancer activity via mitochondrial complex II, The Journal of biological chemistry, 286 (2011) 3717-3728.

[74] K.K. Lee, K. Fujimoto, C. Zhang, C.T. Schwall, N.N. Alder, C.A. Pinkert, W. Krueger, T. Rasmussen, U.A. Boelsterli, Isoniazid-induced cell death is precipitated by underlying mitochondrial complex I dysfunction in mouse hepatocytes, Free Radic Biol Med, 65C (2013) 584-594.

[75] W. Neupert, J.M. Herrmann, Translocation of Proteins into Mitochondria, Annual review of biochemistry, 76 (2007) 723-749.

[76] M.B. McNeil, P.C. Fineran, Prokaryotic assembly factors for the attachment of flavin to complex II, Biochimica et biophysica acta, 1827 (2013) 637-647.

[77] M.B. McNeil, P.C. Fineran, The conserved RGxxE motif of the bacterial FAD assembly factor SdhE is required for succinate dehydrogenase flavinylation and activity, Biochemistry, 52 (2013) 7628-7640.

[78] H.J. Kim, D.R. Winge, Emerging concepts in the flavinylation of succinate dehydrogenase, Biochimica et biophysica acta, 1827 (2013) 627-636.

[79] M.B. McNeil, J.S. Clulow, N.M. Wilf, G.P. Salmond, P.C. Fineran, SdhE is a conserved protein required for flavinylation of succinate dehydrogenase in bacteria, The Journal of biological chemistry, 287 (2012) 18418-18428.

[80] D. Kregiel, Succinate Dehydrogenase of Saccharomyces cerevisiae- The unique enzyme of TCA cycle- Current knowledge and new perspectives, in: R.A. Canuto (Ed.) Dehydrogenases, InTech, 2012.

[81] R. Lill, U. Mühlenhoff, Iron–sulfur-protein biogenesis in eukaryotes, Trends in Biochemical Sciences, 30 (2005) 133-141.

[82] D.C. Johnson, D.R. Dean, A.D. Smith, M.K. Johnson, Structure, function, and formation of biological iron-sulfur clusters, Annual review of biochemistry, 74 (2005) 247-281.

[83] T.A. Rouault, Biogenesis of iron-sulfur clusters in mammalian cells: new insights and relevance to human disease, Disease Models & Mechanisms, 5 (2012) 155-164.

[84] N. Maio, A. Singh, H. Uhrigshardt, N. Saxena, W.-H. Tong, Tracey A. Rouault, Cochaperone Binding to LYR Motifs Confers Specificity of Iron Sulfur Cluster Delivery, Cell Metabolism, 19 (2014) 445-457.

[85] U. Na, W. Yu, J. Cox, D.K. Bricker, K. Brockmann, J. Rutter, C.S. Thummel, D.R. Winge, The LYR Factors SDHAF1 and SDHAF3 Mediate Maturation of the Iron-Sulfur Subunit of Succinate Dehydrogenase, Cell Metab, (2014).

[86] J.G. Van Vranken, D.K. Bricker, N. Dephoure, S.P. Gygi, J.E. Cox, C.S. Thummel, J. Rutter, SDHAF4 Promotes Mitochondrial Succinate Dehydrogenase Activity and Prevents Neurodegeneration, Cell Metab, (2014).

[87] G. Cecchini, I. Schroder, R.P. Gunsalus, E. Maklashina, Succinate dehydrogenase and fumarate reductase from Escherichia coli, Biochimica et biophysica acta, 1553 (2002) 140-157.

[88] K. Nakamura, M. Yamaki, M. Sarada, S. Nakayama, C.R.T. Vibat, R.B. Gennis, T. Nakayashiki, H. Inokuchi, S. Kojima, K. Kita, Two Hydrophobic Subunits Are Essential for the Heme b Ligation and Functional Assembly of Complex II (Succinate-Ubiquinone Oxidoreductase) from Escherichia coli, Journal of Biological Chemistry, 271 (1996) 521-527.

[89] K.A. Davis, Y. Hatefi, Succinate dehydrogenase. I. Purification, molecular properties, and substructure, Biochemistry, 10 (1971) 2509-2516.

[90] W.G. Hanstein, K.A. Davis, M.A. Ghalambor, Y. Hatefi, Succinate dehydrogenase. II. Enzymatic properties, Biochemistry, 10 (1971) 2517-2524.

[91] T.M. Iverson, E. Maklashina, G. Cecchini, Structural Basis for Malfunction in Complex II, Journal of Biological Chemistry, 287 (2012) 35430-35438.

[92] P.R. Rich, A. Marechal, The mitochondrial respiratory chain, Essays in biochemistry, 47 (2010) 1-23.

[93] E. Dibrov, S. Fu, B.D. Lemire, The Saccharomyces cerevisiae TCM62 gene encodes a chaperone necessary for the assembly of the mitochondrial succinate dehydrogenase (complex II), The Journal of biological chemistry, 273 (1998) 32042-32048.

[94] O. Kerscher, N.B. Sepuri, R.E. Jensen, Tim18p Is a New Component of the Tim54p-Tim22p Translocon in the Mitochondrial Inner Membrane, Molecular Biology of the Cell, 11 (2000) 103-116.

[95] C.M. Koehler, M.P. Murphy, N.A. Bally, D. Leuenberger, W. Oppliger, L. Dolfini, T. Junne, G. Schatz, E. Or, Tim18p, a New Subunit of the TIM22 Complex That Mediates Insertion of Imported Proteins into the Yeast Mitochondrial Inner Membrane, Molecular and cellular biology, 20 (2000) 1187-1193.

[96] N. Gebert, M. Gebert, S. Oeljeklaus, K. von der Malsburg, David A. Stroud, B. Kulawiak, C. Wirth, René P. Zahedi, P. Dolezal, S. Wiese, O. Simon, A. Schulze-Specking, Kaye N. Truscott, A. Sickmann, P. Rehling, B. Guiard, C. Hunte, B. Warscheid, M. van der Laan, N. Pfanner, N. Wiedemann, Dual Function of Sdh3 in the Respiratory Chain and TIM22 Protein Translocase of the Mitochondrial Inner Membrane, Molecular Cell, 44 (2011) 811-818.

[97] S.S. Szeto, S.N. Reinke, K.S. Oyedotun, B.D. Sykes, B.D. Lemire, Expression of Saccharomyces cerevisiae Sdh3p and Sdh4p paralogs results in catalytically active succinate dehydrogenase isoenzymes, The Journal of biological chemistry, 287 (2012) 22509-22520.

[98] M. Eisenbach, G.N. Cohen-Ben-Lulu, N.R. Francis, E. Shimoni, D. Noy, Y. Davidov, K. Prasad, Y. Sagi, G. Cecchini, R.M. Johnstone, The bacterial flagellar switch complex is getting more complex, Embo J, 27 (2008) 1134-1144.

[99] H. Ardehali, Z. Chen, Y. Ko, R. Mejia-Alvarez, E. Marban, Multiprotein complex containing succinate dehydrogenase confers mitochondrial ATP-sensitive K+ channel activity, Proceedings of the National Academy of Sciences of the United States of America, 101 (2004) 11880-11885.

[100] A.S. Hoekstra, J.P. Bayley, The role of complex II in disease, Biochimica et biophysica acta, 1827 (2013) 543-551.

[101] P. Rustin, A. Rotig, Inborn errors of complex II--unusual human mitochondrial diseases, Biochimica et biophysica acta, 1553 (2002) 117-122.

[102] C. Bardella, P.J. Pollard, I. Tomlinson, SDH mutations in cancer, Biochimica et biophysica acta, 1807 (2011) 1432-1443.

[103] B.A. Ackrell, Cytopathies involving mitochondrial complex II, Mol Aspects Med, 23 (2002) 369-384.

[104] H.X. Hao, O. Khalimonchuk, M. Schraders, N. Dephoure, J.P. Bayley, H. Kunst, P. Devilee, C.W. Cremers, J.D. Schiffman, B.G. Bentz, S.P. Gygi, D.R. Winge, H. Kremer, J. Rutter, SDH5, a gene required for flavination of succinate dehydrogenase, is mutated in paraganglioma, Science, 325 (2009) 1139-1142.

[105] B.E. Baysal, Clinical and molecular progress in hereditary paraganglioma, Journal of medical genetics, 45 (2008) 689-694.

[106] E. Gottlieb, I.P.M. Tomlinson, Mitochondrial tumour suppressors: a genetic and biochemical update, Nat Rev Cancer, 5 (2005) 857-866.

[107] E. Mbaya, B. Oules, C. Caspersen, R. Tacine, H. Massinet, M. Pennuto, D. Chretien, A. Munnich, A. Rotig, R. Rizzuto, G.A. Rutter, P. Paterlini-Brechot, M. Chami, Calcium signalling-dependent mitochondrial dysfunction and bioenergetics regulation in respiratory chain Complex II deficiency, Cell death and differentiation, 17 (2010) 1855-1866.

[108] C.L. Quinlan, A.L. Orr, I.V. Perevoshchikova, J.R. Treberg, B.A. Ackrell, M.D. Brand, Mitochondrial complex II can generate reactive oxygen species at high rates in both the forward and reverse reactions, The Journal of biological chemistry, 287 (2012) 27255-27264.

[109] A. Solans, A. Zambrano, M. Rodríguez, A. Barrientos, Cytotoxicity of a mutant huntingtin fragment in yeast involves early alterations in mitochondrial OXPHOS complexes II and III, Human molecular genetics, 15 (2006) 3063-3081.

[110] G. Liot, B. Bossy, S. Lubitz, Y. Kushnareva, N. Sejbuk, E. Bossy-Wetzel, Complex II inhibition by 3-NP causes mitochondrial fragmentation and neuronal cell death via an NMDA- and ROS-dependent pathway, Cell death and differentiation, 16 (2009) 899-909.

[111] W. Habano, T. Sugai, S. Nakamura, N. Uesugi, T. Higuchi, M. Terashima, S. Horiuchi, Reduced expression and loss of heterozygosity of the SDHD gene in colorectal and gastric cancer, Oncology reports, 10 (2003) 1375-1380.

[112] B.E. Baysal, R.E. Ferrell, J.E. Willett-Brozick, E.C. Lawrence, D. Myssiorek, A. Bosch, A. van der Mey, P.E. Taschner, W.S. Rubinstein, E.N. Myers, C.W. Richard, 3rd, C.J. Cornelisse, P. Devilee, B. Devlin, Mutations in SDHD, a mitochondrial complex II gene, in hereditary paraganglioma, Science, 287 (2000) 848-851.

[113] S. Niemann, U. Muller, Mutations in SDHC cause autosomal dominant paraganglioma, type 3, Nat Genet, 26 (2000) 268-270.

[114] R.F. Badenhop, J.C. Jansen, P.A. Fagan, R.S. Lord, Z.G. Wang, W.J. Foster, P.R. Schofield, The prevalence of SDHB, SDHC, and SDHD mutations in patients with head and neck paraganglioma and association of mutations with clinical features, Journal of medical genetics, 41 (2004) e99.

[115] B.E. Baysal, J.E. Willett-Brozick, E.C. Lawrence, C.M. Drovdlic, S.A. Savul, D.R. McLeod, H.A. Yee, D.E. Brackmann, W.H. Slattery, 3rd, E.N. Myers, R.E. Ferrell, W.S. Rubinstein, Prevalence of SDHB, SDHC, and SDHD germline mutations in clinic patients with head and neck paragangliomas, Journal of medical genetics, 39 (2002) 178-183.

[116] T.D. Poeppel, A. Yuece, C. Boy, K.A. Metz, E. Kaminsky, H.P. Neumann, S.J. Rosenbaum, K. Mann, L.C. Moeller, Novel SDHD Gene Mutation (H102R) in a Patient With Metastatic Cervical Paraganglioma Effectively Treated by Peptide Receptor Radionuclide Therapy, Journal of Clinical Oncology, 29 (2011) e812-e815.

[117] F. Schiavi, T. Savvoukidis, F. Trabalzini, F. Grego, M. Piazza, P. AmistÀ, S. DemattÈ, A.D. Piano, M.E. Cecchini, Z. Erlic, P. De Lazzari, F. Mantero, G. Opocher, Paraganglioma Syndrome, Annals of the New York Academy of Sciences, 1073 (2006) 190-197.

[118] J.W.M. Lenders, G. Eisenhofer, M. Mannelli, K. Pacak, Phaeochromocytoma, The Lancet, 366 (2005) 665-675.

[119] N. Burnichon, J.-J. Brière, R. Libé, L. Vescovo, J. Rivière, F. Tissier, E. Jouanno, X. Jeunemaitre, P. Bénit, A. Tzagoloff, P. Rustin, J. Bertherat, J. Favier, A.-P. Gimenez-Roqueplo, SDHA is a tumor suppressor gene causing paraganglioma, Human molecular genetics, 19 (2010) 3011-3020.

[120] D. Astuti, F. Latif, A. Dallol, P.L. Dahia, F. Douglas, E. George, F. Skoldberg, E.S. Husebye, C. Eng, E.R. Maher, Gene mutations in the succinate dehydrogenase subunit SDHB cause susceptibility to familial pheochromocytoma and to familial paraganglioma, American journal of human genetics, 69 (2001) 49-54.

[121] L. Fishbein, K.L. Nathanson, Pheochromocytoma and paraganglioma: understanding the complexities of the genetic background, Cancer Genetics, 205 (2012) 1-11.

[122] C.J. Ricketts, J.R. Forman, E. Rattenberry, N. Bradshaw, F. Lalloo, L. Izatt, T.R. Cole, R. Armstrong, V.K.A. Kumar, P.J. Morrison, A.B. Atkinson, F. Douglas, S.G. Ball, J. Cook, U. Srirangalingam, P. Killick, G. Kirby, S. Aylwin, E.R. Woodward, D.G.R. Evans, S.V. Hodgson, V. Murday, S.L. Chew, J.M. Connell, T.L. Blundell, F. MacDonald, E.R. Maher, Tumor risks and genotype–phenotype–proteotype analysis in 358 patients with germline mutations in SDHB and SDHD, Human Mutation, 31 (2010) 41-51.

[123] S.R. McWhinney, B. Pasini, C.A. Stratakis, Familial Gastrointestinal Stromal Tumors and Germ-Line Mutations, New England Journal of Medicine, 357 (2007) 1054-1056.

[124] Y. Ni, X. He, J. Chen, J. Moline, J. Mester, M.S. Orloff, M.D. Ringel, C. Eng, Germline SDHx variants modify breast and thyroid cancer risks in Cowden and Cowden-like syndrome via FAD/NAD-dependant destabilization of p53, Human molecular genetics, 21 (2012) 300-310.

[125] B.E. Baysal, A recurrent stop-codon mutation in succinate dehydrogenase subunit B gene in normal peripheral blood and childhood T-cell acute leukemia, PLoS ONE, 2 (2007) e436.

[126] T. Albayrak, V. Scherhammer, N. Schoenfeld, E. Braziulis, T. Mund, M.K. Bauer, I.E. Scheffler, S. Grimm, The tumor suppressor cybL, a component of the respiratory chain, mediates apoptosis induction, Mol Biol Cell, 14 (2003) 3082-3096.

[127] T. Ishii, K. Yasuda, A. Akatsuka, O. Hino, P.S. Hartman, N. Ishii, A mutation in the SDHC gene of complex II increases oxidative stress, resulting in apoptosis and tumorigenesis, Cancer research, 65 (2005) 203-209.

[128] A.-P. Gimenez-Roqueplo, J. Favier, P. Rustin, J.-J. Mourad, P.-F. Plouin, P. Corvol, A. Rötig, X. Jeunemaitre, The R22X Mutation of the SDHD Gene in Hereditary Paraganglioma Abolishes the Enzymatic Activity of Complex II in the Mitochondrial Respiratory Chain and Activates the Hypoxia Pathway, The American Journal of Human Genetics, 69 (2001) 1186-1197.

[129] A.-P. Gimenez-Roqueplo, J. Favier, P. Rustin, C. Rieubland, V. Kerlan, P.-F. Plouin, A. Rötig, X. Jeunemaitre, Functional Consequences of a SDHB Gene Mutation in an Apparently Sporadic Pheochromocytoma, Journal of Clinical Endocrinology & Metabolism, 87 (2002) 4771-4774.

[130] M.P. Paranagama, K. Sakamoto, H. Amino, M. Awano, H. Miyoshi, K. Kita, Contribution of the FAD and quinone binding sites to the production of reactive oxygen species from Ascaris suum mitochondrial complex II, Mitochondrion, 10 (2010) 158-165.

[131] A. Lemarie, L. Huc, E. Pazarentzos, A.L. Mahul-Mellier, S. Grimm, Specific disintegration of complex II succinate:ubiquinone oxidoreductase links pH changes to oxidative stress for apoptosis induction, Cell death and differentiation, 18 (2011) 338-349.

[132] J. Huang, B.D. Lemire, Mutations in the C. elegans succinate dehydrogenase iron-sulfur subunit promote superoxide generation and premature aging, Journal of molecular biology, 387 (2009) 559-569.

[133] N. Ishii, M. Fujii, P.S. Hartman, M. Tsuda, K. Yasuda, N. Senoo-Matsuda, S. Yanase, D. Ayusawa, K. Suzuki, A mutation in succinate dehydrogenase cytochrome b causes oxidative stress and ageing in nematodes, Nature, 394 (1998) 694-697.

[134] J. Guo, B.D. Lemire, The Ubiquinone-binding Site of the Saccharomyces cerevisiae Succinate-Ubiquinone Oxidoreductase Is a Source of Superoxide, J. Biol. Chem., 278 (2003) 47629-47635.

[135] M.A. Selak, S.M. Armour, E.D. MacKenzie, H. Boulahbel, D.G. Watson, K.D. Mansfield, Y. Pan, M.C. Simon, C.B. Thompson, E. Gottlieb, Succinate links TCA cycle dysfunction to oncogenesis by inhibiting HIF-α prolyl hydroxylase, Cancer Cell, 7 (2005) 77-85.

[136] E. Hensen, J.-P. Bayley, Recent advances in the genetics of SDH-related paraganglioma and pheochromocytoma, Familial Cancer, 10 (2011) 355-363.

[137] A. Lemarie, S. Grimm, Mitochondrial respiratory chain complexes: apoptosis sensors mutated in cancer[quest], Oncogene, 30 (2011) 3985-4003.

[138] S. Grimm, Respiratory chain complex II as general sensor for apoptosis, Biochimica et biophysica acta, 1827 (2013) 565-572.

[139] H. Palsdottir, C. Hunte, Lipids in membrane protein structures, Biochimica et Biophysica Acta (BBA) - Biomembranes, 1666 (2004) 2-18.

[140] M. Bogdanov, J. Sun, H.R. Kaback, W. Dowhan, A Phospholipid Acts as a Chaperone in Assembly of a Membrane Transport Protein, Journal of Biological Chemistry, 271 (1996) 11615-11618.

[141] M. Bogdanov, W. Dowhan, Phospholipid-assisted protein folding: phosphatidylethanolamine is required at a late step of the conformational maturation of the polytopic membrane protein lactose permease, Embo J, 17 (1998) 5255-5264.

[142] T. Becker, S.E. Horvath, L. Bottinger, N. Gebert, G. Daum, N. Pfanner, Role of phosphatidylethanolamine in the biogenesis of mitochondrial outer membrane proteins, The Journal of biological chemistry, 288 (2013) 16451-16459.

[143] W. Dowhan, Molecular basis for membrane phospholipid diversity: why are there so many lipids?, Annual review of biochemistry, 66 (1997) 199-232.

[144] S.M. Claypool, C.M. Koehler, The complexity of cardiolipin in health and disease, Trends in Biochemical Sciences, 37 (2012) 32-41.

[145] R. Arias-Cartin, S. Grimaldi, J. Pommier, P. Lanciano, C. Schaefer, P. Arnoux, G. Giordano, B. Guigliarelli, A. Magalon, Cardiolipin-based respiratory complex activation in bacteria, Proceedings of the National Academy of Sciences of the United States of America, 108 (2011) 7781-7786.

[146] T.H. Haines, N.A. Dencher, Cardiolipin: a proton trap for oxidative phosphorylation, FEBS letters, 528 (2002) 35-39.

[147] W. Hübner, H.H. Mantsch, M. Kates, Intramolecular hydrogen bonding in cardiolipin, Biochimica et Biophysica Acta (BBA) - Biomembranes, 1066 (1991) 166-174.

[148] M. Kates, J.-Y. Syz, D. Gosser, T. Haines, pH-dissociation characteristics of cardiolipin and its 2′-deoxy analogue, Lipids, 28 (1993) 877-882.

[149] C. Hunte, H. Palsdottir, B.L. Trumpower, Protonmotive pathways and mechanisms in the cytochrome bc1 complex, FEBS letters, 545 (2003) 39-46.

[150] T.H. Haines, A new look at Cardiolipin, Biochimica et Biophysica Acta (BBA) - Biomembranes, 1788 (2009) 1997-2002.

[151] G. Olofsson, E. Sparr, Ionization Constants pKa of Cardiolipin, PLoS ONE, 8 (2013) e73040.

[152] M.G. Baile, K. Whited, S.M. Claypool, Deacylation on the matrix side of the mitochondrial inner membrane regulates cardiolipin remodeling, Mol Biol Cell, 24 (2013) 2008-2020.

[153] G. Paradies, V. Paradies, F.M. Ruggiero, G. Petrosillo, Cardiolipin and mitochondrial function in health and disease, Antioxidants & redox signaling, 20 (2014) 1925-1953.

[154] C. Arnarez, J.P. Mazat, J. Elezgaray, S.J. Marrink, X. Periole, Evidence for cardiolipin binding sites on the membrane-exposed surface of the cytochrome bc1, Journal of the American Chemical Society, 135 (2013) 3112-3120.

[155] K. Shinzawa-Itoh, H. Aoyama, K. Muramoto, H. Terada, T. Kurauchi, Y. Tadehara, A. Yamasaki, T. Sugimura, S. Kurono, K. Tsujimoto, T. Mizushima, E. Yamashita, T. Tsukihara, S. Yoshikawa, Structures and physiological roles of 13 integral lipids of bovine heart cytochrome c oxidase, The EMBO Journal, 26 (2007) 1713-1725.

[156] M. Schlame, Thematic Review Series: Glycerolipids. Cardiolipin synthesis for the assembly of bacterial and mitochondrial membranes, Journal of lipid research, 49 (2008) 1607-1620.

[157] C.T. Schwall, V.L. Greenwood, N.N. Alder, The stability and activity of respiratory Complex II is cardiolipin-dependent, Biochimica et Biophysica Acta (BBA) - Bioenergetics, 1817 (2012) 1588-1596.

[158] K. Pfeiffer, V. Gohil, R.A. Stuart, C. Hunte, U. Brandt, M.L. Greenberg, H. Schagger, Cardiolipin stabilizes respiratory chain supercomplexes, The Journal of biological chemistry, 278 (2003) 52873-52880.

[159] M. Zhang, E. Mileykovskaya, W. Dowhan, Gluing the respiratory chain together. Cardiolipin is required for supercomplex formation in the inner mitochondrial membrane, The Journal of biological chemistry, 277 (2002) 43553-43556.

[160] C. Lange, J.H. Nett, B.L. Trumpower, C. Hunte, Specific roles of protein-phospholipid interactions in the yeast cytochrome bc1 complex structure, Embo J, 20 (2001) 6591-6600.

[161] H. Schagger, K. Pfeiffer, Supercomplexes in the respiratory chains of yeast and mammalian mitochondria, Embo J, 19 (2000) 1777-1783.

[162] H. Schagger, Respiratory chain supercomplexes of mitochondria and bacteria, Biochimica et biophysica acta, 1555 (2002) 154-159.

[163] S.M. Claypool, Y. Oktay, P. Boontheung, J.A. Loo, C.M. Koehler, Cardiolipin defines the interactome of the major ADP/ATP carrier protein of the mitochondrial inner membrane, The Journal of cell biology, 182 (2008) 937-950.

[164] S.M. Claypool, Cardiolipin, a critical determinant of mitochondrial carrier protein assembly and function, Biochimica et Biophysica Acta (BBA) - Biomembranes, 1788 (2009) 2059-2068.

[165] B. Hoffmann, A. Stockl, M. Schlame, K. Beyer, M. Klingenberg, The Reconstituted Adp Atp Carrier Activity Has an Absolute Requirement for Cardiolipin as Shown in Cysteine Mutants, Journal of Biological Chemistry, 269 (1994) 1940-1944.

[166] R.N.A.H. Lewis, R.N. McElhaney, The physicochemical properties of cardiolipin bilayers and cardiolipin-containing lipid membranes, Biochimica et Biophysica Acta (BBA) - Biomembranes, 1788 (2009) 2069-2079.

[167] E. van den Brink-van der Laan, J. Antoinette Killian, B. de Kruijff, Nonbilayer lipids affect peripheral and integral membrane proteins via changes in the lateral pressure profile, Biochimica et Biophysica Acta (BBA) - Biomembranes, 1666 (2004) 275-288.

[168] A.E. Gad, R. Broza, G.D. Eytan, Calcium-induced fusion of proteoliposomes and protein-free liposomes. Effect of their phosphatidylethanolamine content on the structure of fused vesicles, Biochimica et biophysica acta, 556 (1979) 181-195.

[169] N. Khalifat, J.-B. Fournier, M.I. Angelova, N. Puff, Lipid packing variations induced by pH in cardiolipin-containing bilayers: The driving force for the cristae-like shape instability, Biochimica et Biophysica Acta (BBA) - Biomembranes, 1808 (2011) 2724-2733.

[170] M.B. Sankaram, G.L. Powell, D. Marsh, Effect of acyl chain composition on salt-induced lamellar to inverted hexagonal phase transitions in cardiolipin, Biochimica et Biophysica Acta (BBA) - Biomembranes, 980 (1989) 389-392.

[171] M. Dahlberg, Polymorphic Phase Behavior of Cardiolipin Derivatives Studied by Coarse-Grained Molecular Dynamics, The Journal of Physical Chemistry B, 111 (2007) 7194-7200.

[172] A. Ortiz, J.A. Killian, A.J. Verkleij, J. Wilschut, Membrane Fusion and the Lamellar-to-Inverted-Hexagonal Phase Transition in Cardiolipin Vesicle Systems Induced by Divalent Cations, Biophysical journal, 77 (1999) 2003-2014.

[173] S. Pöyry, T. Róg, M. Karttunen, I. Vattulainen, Mitochondrial Membranes with Mono- and Divalent Salt: Changes Induced by Salt Ions on Structure and Dynamics, The Journal of Physical Chemistry B, 113 (2009) 15513-15521.

[174] R.P. Rand, S. Sengupta, Cardiolipin forms hexagonal structures with divalent cations, Biochimica et Biophysica Acta (BBA) - Biomembranes, 255 (1972) 484-492.

[175] M. Ren, C.K. Phoon, M. Schlame, Metabolism and function of mitochondrial cardiolipin, Prog Lipid Res, 55C (2014) 1-16.

[176] M. Schlame, Cardiolipin remodeling and the function of tafazzin, Biochimica et Biophysica Acta (BBA) - Molecular and Cell Biology of Lipids, 1831 (2013) 582-588.

[177] A.S. Joshi, J. Zhou, V.M. Gohil, S. Chen, M.L. Greenberg, Cellular functions of cardiolipin in yeast, Biochimica et Biophysica Acta (BBA) - Molecular Cell Research, 1793 (2009) 212-218.

[178] F. Jiang, H.S. Rizavi, M.L. Greenberg, Cardiolipin is not essential for the growth of Saccharomyces cerevisiae on fermentable or non-fermentable carbon sources, Molecular Microbiology, 26 (1997) 481-491.

[179] V. Koshkin, M.L. Greenberg, Oxidative phosphorylation in cardiolipin-lacking yeast mitochondria, The Biochemical journal, 347 (2000) 687-691.

[180] Q. Zhong, V.M. Gohil, L. Ma, M.L. Greenberg, Absence of Cardiolipin Results in Temperature Sensitivity, Respiratory Defects, and Mitochondrial DNA Instability Independent of pet56, J. Biol. Chem., 279 (2004) 32294-32300.

[181] V. Koshkin, M.L. Greenberg, Cardiolipin prevents rate-dependent uncoupling and provides osmotic stability in yeast mitochondria, The Biochemical journal, 364 (2002) 317-322.

[182] M. Schlame, D. Rua, M.L. Greenberg, The biosynthesis and functional role of cardiolipin, Prog Lipid Res, 39 (2000) 257-288.

[183] F. Jiang, M.T. Ryan, M. Schlame, M. Zhao, Z. Gu, M. Klingenberg, N. Pfanner, M.L. Greenberg, Absence of Cardiolipin in the crd1 Null Mutant Results in Decreased Mitochondrial Membrane Potential and Reduced Mitochondrial Function, Journal of Biological Chemistry, 275 (2000) 22387-22394.

[184] V.M. Gohil, M.N. Thompson, M.L. Greenberg, Synthetic Lethal Interaction of the Mitochondrial Phosphatidylethanolamine and Cardiolipin Biosynthetic Pathways in Saccharomyces cerevisiae, Journal of Biological Chemistry, 280 (2005) 35410-35416.

[185] S.-C. Chang, P.N. Heacock, C.J. Clancey, W. Dowhan, The PEL1 Gene (Renamed PGS1) Encodes the Phosphatidylglycero-phosphate Synthase ofSaccharomyces cerevisiae, Journal of Biological Chemistry, 273 (1998) 9829-9836.

[186] S.-C. Chang, P.N. Heacock, E. Mileykovskaya, D.R. Voelker, W. Dowhan, Isolation and Characterization of the Gene (CLS1) Encoding Cardiolipin Synthase in Saccharomyces cerevisiae, Journal of Biological Chemistry, 273 (1998) 14933-14941.

[187] L. Böttinger, S.E. Horvath, T. Kleinschroth, C. Hunte, G. Daum, N. Pfanner, T. Becker, Phosphatidylethanolamine and Cardiolipin Differentially Affect the Stability of Mitochondrial Respiratory Chain Supercomplexes, Journal of molecular biology, 423 (2012) 677-686.

[188] S.M. Claypool, K. Whited, S. Srijumnong, X. Han, C.M. Koehler, Barth syndrome mutations that cause tafazzin complex lability, The Journal of cell biology, 192 (2011) 447-462.

[189] A.J. Chicco, G.C. Sparagna, Role of cardiolipin alterations in mitochondrial dysfunction and disease, American journal of physiology. Cell physiology, 292 (2007) C33-44.

[190] A. Nath, W.M. Atkins, S.G. Sligar, Applications of phospholipid bilayer nanodiscs in the study of membranes and membrane proteins, Biochemistry, 46 (2007) 2059-2069.

[191] C.D. Blanchette, J.A. Cappuccio, E.A. Kuhn, B.W. Segelke, W.H. Benner, B.A. Chromy, M.A. Coleman, G. Bench, P.D. Hoeprich, T.A. Sulchek, Atomic force microscopy differentiates discrete size distributions between membrane protein containing and empty nanolipoprotein particles, Biochimica et biophysica acta, 1788 (2009) 724-731.

[192] A. Helenius, K. Simons, Solubilization of membranes by detergents, Biochimica et Biophysica Acta (BBA) - Reviews on Biomembranes, 415 (1975) 29-79.

[193] V. Reisinger, L.A. Eichacker, Solubilization of membrane protein complexes for blue native PAGE, Journal of proteomics, 71 (2008) 277-283.

[194] C. Klammt, D. Schwarz, K. Fendler, W. Haase, V. Dötsch, F. Bernhard, Evaluation of detergents for the soluble expression of α-helical and β-barrel-type integral membrane proteins by a preparative scale individual cell-free expression system, FEBS Journal, 272 (2005) 6024-6038.

[195] J.A. Whiles, R. Deems, R.R. Vold, E.A. Dennis, Bicelles in structure–function studies of membrane-associated proteins, Bioorganic Chemistry, 30 (2002) 431-442.

[196] C.R. Sanders, R.S. Prosser, Bicelles: a model membrane system for all seasons?, Structure, 6 (1998) 1227-1234.

[197] J.L. Popot, Amphipols, nanodiscs, and fluorinated surfactants: three nonconventional approaches to studying membrane proteins in aqueous solutions, Annual review of biochemistry, 79 (2010) 737-775.

[198] T.J. Knowles, R. Finka, C. Smith, Y.-P. Lin, T. Dafforn, M. Overduin, Membrane Proteins Solubilized Intact in Lipid Containing Nanoparticles Bounded by Styrene Maleic Acid Copolymer, Journal of the American Chemical Society, 131 (2009) 7484-7485.

[199] M.C. Orwick, P.J. Judge, J. Procek, L. Lindholm, A. Graziadei, A. Engel, G. Gröbner, A. Watts, Detergent-Free Formation and Physicochemical Characterization of Nanosized Lipid–Polymer Complexes: Lipodisq, Angewandte Chemie, 124 (2012) 4731-4735.

[200] M. Orwick-Rydmark, J.E. Lovett, A. Graziadei, L. Lindholm, M.R. Hicks, A. Watts, Detergent-Free Incorporation of a Seven-Transmembrane Receptor Protein into Nanosized Bilayer Lipodisq Particles for Functional and Biophysical Studies, Nano Letters, 12 (2012) 4687-4692.

[201] S. Rajesh, T. Knowles, M. Overduin, Production of membrane proteins without cells or detergents, New Biotechnology, 28 (2011) 250-254.

[202] A. Long, C. OBrien, K. Malhotra, C. Schwall, A. Albert, A. Watts, N. Alder, A detergent-free strategy for the reconstitution of active enzyme complexes from native biological membranes into nanoscale discs, BMC Biotechnology, 13 (2013) 41.

[203] Y. Moritani, S.M. Nomura, I. Morita, K. Akiyoshi, Direct integration of cell-free-synthesized connexin-43 into liposomes and hemichannel formation, The FEBS journal, 277 (2010) 3343-3352.

[204] M. van der Laan, M. Meinecke, J. Dudek, D.P. Hutu, M. Lind, I. Perschil, B. Guiard, R. Wagner, N. Pfanner, P. Rehling, Motor-free mitochondrial presequence translocase drives membrane integration of preproteins, Nature cell biology, 9 (2007) 1152-1159.

[205] J.L. Rigaud, B. Pitard, D. Levy, Reconstitution of Membrane-Proteins into Liposomes - Application to Energy-Transducing Membrane-Proteins, Bba-Bioenergetics, 1231 (1995) 223-246.

[206] D.D. Lasic, Novel applications of liposomes, Trends in biotechnology, 16 (1998) 307-321.

[207] I.L. Nantes, K.C. Mugnol, Incorporation of respiratory cytochromes in liposomes: an efficient strategy to study the respiratory chain, Journal of liposome research, 18 (2008) 175-194.

[208] J.J. Wuu, J.R. Swartz, High yield cell-free production of integral membrane proteins without refolding or detergents, Biochimica et Biophysica Acta (BBA) - Biomembranes, 1778 (2008) 1237-1250.

[209] M.A. Goren, B.G. Fox, Wheat germ cell-free translation, purification, and assembly of a functional human stearoyl-CoA desaturase complex, Protein expression and purification, 62 (2008) 171-178.

[210] M.A. Goren, A. Nozawa, S. Makino, R.L. Wrobel, B.G. Fox, Cell-Free Translation of Integral Membrane Proteins into Unilamelar Liposomes, Method Enzymol, 463 (2009) 647-673.

[211] E.S. Sevova, M.A. Goren, K.J. Schwartz, F.F. Hsu, J. Turk, B.G. Fox, J.D. Bangs, Cell-free synthesis and functional characterization of sphingolipid synthases from parasitic trypanosomatid protozoa, The Journal of biological chemistry, 285 (2010) 20580-20587.

[212] C. Roos, L. Kai, D. Proverbio, U. Ghoshdastider, S. Filipek, V. Dotsch, F. Bernhard, Co-translational association of cell-free expressed membrane proteins with supplied lipid bilayers, Mol Membr Biol, 30 (2013) 75-89.

[213] A.R. Long, C.C. O'Brien, N.N. Alder, The Cell-Free Integration of a Polytopic Mitochondrial Membrane Protein into Liposomes Occurs Cotranslationally and in a Lipid-Dependent Manner, PLoS ONE, 7 (2012) e46332.

[214] A. Jesorka, O. Orwar, Liposomes: technologies and analytical applications, Annu Rev Anal Chem (Palo Alto Calif), 1 (2008) 801-832.

[215] J. Borch, T. Hamann, The nanodisc: a novel tool for membrane protein studies, Biological chemistry, 390 (2009) 805-814.

[216] T.H. Bayburt, Y.V. Grinkova, S.G. Sligar, Self-assembly of discoidal phospholipid bilayer nanoparticles with membrane scaffold proteins, Nano Letters, 2 (2002) 853-856.

[217] I.G. Denisov, Y.V. Grinkova, A.A. Lazarides, S.G. Sligar, Directed self-assembly of monodisperse phospholipid bilayer Nanodiscs with controlled size, Journal of the American Chemical Society, 126 (2004) 3477-3487.

[218] T.H. Bayburt, S.G. Sligar, Membrane protein assembly into Nanodiscs, FEBS letters, 584 (2010) 1721-1727.

[219] F. Katzen, T.C. Peterson, W. Kudlicki, Membrane protein expression: no cells required, Trends in biotechnology, 27 (2009) 455-460.

[220] S.G. Sligar, T.H. Bayburt, M.A. Schuler, N.R. Civjan, Y.V. Grinkova, I.G. Denisov, Membrane Scaffold Proteins, in: U. States (Ed.), vol. 7,083,958 B2, The Board of Trustees of the University of Illinois, United States, 2006.

[221] G. Cavigiolio, B. Shao, E.G. Geier, G. Ren, J.W. Heinecke, M.N. Oda, The Interplay between Size, Morphology, Stability, and Functionality of High-Density Lipoprotein Subclasses†, Biochemistry, 47 (2008) 4770-4779.

[222] C.D. Blanchette, R. Law, W.H. Benner, J.B. Pesavento, J.A. Cappuccio, V. Walsworth, E.A. Kuhn, M. Corzett, B.A. Chromy, B.W. Segelke, M.A. Coleman, G. Bench, P.D. Hoeprich, T.A. Sulchek, Quantifying size distributions of nanolipoprotein particles with single-particle analysis and molecular dynamic simulations, Journal of lipid research, 49 (2008) 1420-1430.

[223] T.K. Ritchie, Y.V. Grinkova, T.H. Bayburt, I.G. Denisov, J.K. Zolnerciks, W.M. Atkins, S.G. Sligar, Reconstitution of Membrane Proteins in Phospholipid Bilayer Nanodiscs, Methods in enzymology, 464 (2009) 211-231.

[224] C.R. Morgan, C.M. Hebling, K.D. Rand, D.W. Stafford, J.W. Jorgenson, J.R. Engen, Conformational transitions in the membrane scaffold protein of phospholipid bilayer nanodiscs, Molecular & cellular proteomics : MCP, 10 (2011) M111 010876.

[225] M. Alami, K. Dalal, B. Lelj-Garolla, S.G. Sligar, F. Duong, Nanodiscs unravel the interaction between the SecYEG channel and its cytosolic partner SecA, Embo J, 26 (2007) 1995-2004.

[226] M. Nakano, M. Fukuda, T. Kudo, M. Miyazaki, Y. Wada, N. Matsuzaki, H. Endo, T. Handa, Static and dynamic properties of phospholipid bilayer nanodiscs, Journal of the American Chemical Society, 131 (2009) 8308-8312.

[227] T. Raschle, S. Hiller, T.Y. Yu, A.J. Rice, T. Walz, G. Wagner, Structural and functional characterization of the integral membrane protein VDAC-1 in lipid bilayer nanodiscs, Journal of the American Chemical Society, 131 (2009) 17777-17779.

[228] H. Tsukamoto, I. Szundi, J.W. Lewis, D.L. Farrens, D.S. Kliger, Rhodopsin in Nanodiscs Has Native Membrane-like Photointermediates, Biochemistry, 50 (2011) 5086-5091.

[229] T.H. Bayburt, Y.V. Grinkova, S.G. Sligar, Assembly of single bacteriorhodopsin trimers in bilayer nanodiscs, Archives of biochemistry and biophysics, 450 (2006) 215-222.

[230] M.J. Ranaghan, C.T. Schwall, N.N. Alder, R.R. Birge, Green Proteorhodopsin Reconstituted into Nanoscale Phospholipid Bilayers (Nanodiscs) as Photoactive Monomers, Journal of the American Chemical Society, 133 (2011) 18318-18327.

[231] M. Alami, K. Dalal, B. Lelj-Garolla, S.G. Sligar, F. Duong, Nanodiscs unravel the interaction between the SecYEG channel and its cytosolic partner SecA, Embo J, 26 (2007) 1995-2004.

[232] K. Dalal, C.S. Chan, S.G. Sligar, F. Duong, Two copies of the SecY channel and acidic lipids are necessary to activate the SecA translocation ATPase, Proceedings of the National Academy of Sciences, 109 (2012) 4104-4109.

[233] J.L. Baylon, I.L. Lenov, S.G. Sligar, E. Tajkhorshid, Characterizing the membrane-bound state of cytochrome P450 3A4: structure, depth of insertion, and orientation, Journal of the American Chemical Society, 135 (2013) 8542-8551.

[234] K. Malhotra, N.N. Alder, Advances in the use of nanoscale bilayers to study membrane protein structure and function, Biotechnology and Genetic Engineering Reviews, 30 (2014) 79-93.

[235] L. Nasvik Ojemyr, C. von Ballmoos, R.B. Gennis, S.G. Sligar, P. Brzezinski, Reconstitution of respiratory oxidases in membrane nanodiscs for investigation of proton-coupled electron transfer, FEBS letters, 586 (2012) 640-645.

[236] Y. Kobashigawa, K. Harada, N. Yoshida, K. Ogura, F. Inagaki, Phosphoinositide-incorporated lipid-protein nanodiscs: A tool for studying protein-lipid interactions, Analytical biochemistry, 410 (2011) 77-83.

[237] D.N. Amin, G.L. Hazelbauer, Influence of membrane lipid composition on a transmembrane bacterial chemoreceptor, The Journal of biological chemistry, 287 (2012) 41697-41705.

[238] C.D. Sloan, M.T. Marty, S.G. Sligar, R.C. Bailey, Interfacing lipid bilayer nanodiscs and silicon photonic sensor arrays for multiplexed protein-lipid and protein-membrane protein interaction screening, Analytical chemistry, 85 (2013) 2970-2976.

[239] M. Numata, Y.V. Grinkova, J.R. Mitchell, H.W. Chu, S.G. Sligar, D.R. Voelker, Nanodiscs as a therapeutic delivery agent: inhibition of respiratory syncytial virus infection in the lung, International Journal of Nanomedicine, 8 (2013) 1417-1427.

[240] P. Bhattacharya, S. Grimme, B. Ganesh, A. Gopisetty, J.R. Sheng, O. Martinez, S. Jayarama, M. Artinger, M. Meriggioli, B.S. Prabhakar, Nanodisc-incorporated hemagglutinin provides protective immunity against influenza virus infection, Journal of virology, 84 (2010) 361-371.

[241] G. Daum, S.M. Gasser, G. Schatz, Import of proteins into mitochondria: energy-dependent, two-step processing of the intermembrane space enzyme cytochrome b2 isolated yeast mitochondria, The Journal of biological chemistry, 257 (1982) 13075-13080.

[242] C. Schwall, N. Alder, Site-Specific Fluorescent Probe Labeling of Mitochondrial Membrane Proteins, in: D. Rapaport, J.M. Herrmann (Eds.) Membrane Biogenesis, vol. 1033, Humana Press, 2013, pp. 103-120.

[243] S.J. Kolb, A. Hudmon, T.R. Ginsberg, M.N. Waxham, Identification of Domains Essential for the Assembly of Calcium/Calmodulin-dependent Protein Kinase II Holoenzymes, Journal of Biological Chemistry, 273 (1998) 31555-31564.

[244] P. Gonzalez-Cabo, S. Ros, F. Palau, Flavin Adenine Dinucleotide Rescues the Phenotype of Frataxin Deficiency, PLoS ONE, 5 (2010) e8872.

[245] M. Schlame, M. Ren, The role of cardiolipin in the structural organization of mitochondrial membranes, Biochimica et biophysica acta, 1788 (2009) 2080-2083.

[246] D.B. Ostrander, M. Zhang, E. Mileykovskaya, M. Rho, W. Dowhan, Lack of Mitochondrial Anionic Phospholipids Causes an Inhibition of Translation of Protein Components of the Electron Transport Chain, Journal of Biological Chemistry, 276 (2001) 25262-25272.

[247] R. Horsefield, V. Yankovskaya, G. Sexton, W. Whittingham, K. Shiomi, S. Ōmura, B. Byrne, G. Cecchini, S. Iwata, Structural and Computational Analysis of the Quinone-binding Site of Complex II (Succinate-Ubiquinone Oxidoreductase), Journal of Biological Chemistry, 281 (2006) 7309-7316.

[248] N. Dave, J. Liu, Programmable Assembly of DNA-Functionalized Liposomes by DNA, ACS nano, 5 (2011) 1304-1312.

[249] U. Jakobsen, A.C. Simonsen, S. Vogel, DNA-Controlled Assembly of Soft Nanoparticles, Journal of the American Chemical Society, 130 (2008) 10462-10463.

[250] A.P. Demchenko, Y. Mély, G. Duportail, A.S. Klymchenko, Monitoring Biophysical Properties of Lipid Membranes by Environment-Sensitive Fluorescent Probes, Biophysical journal, 96 (2009) 3461-3470.

[251] Y.-L. Zhang, J.A. Frangos, M. Chachisvilis, Laurdan fluorescence senses mechanical strain in the lipid bilayer membrane, Biochemical and Biophysical Research Communications, 347 (2006) 838-841.

[252] H. Bouvrais, T. Pott, L.A. Bagatolli, J.H. Ipsen, P. Méléard, Impact of membrane-anchored fluorescent probes on the mechanical properties of lipid bilayers, Biochimica et Biophysica Acta (BBA) - Biomembranes, 1798 (2010) 1333-1337.

[253] T. Parasassi, M. Di Stefano, M. Loiero, G. Ravagnan, E. Gratton, Cholesterol modifies water concentration and dynamics in phospholipid bilayers: a fluorescence study using Laurdan probe, Biophysical journal, 66 (1994) 763-768.

[254] I.G. Denisov, M.A. McLean, A.W. Shaw, Y.V. Grinkova, S.G. Sligar, Thermotropic Phase Transition in Soluble Nanoscale Lipid Bilayers, The Journal of Physical Chemistry B, 109 (2005) 15580-15588.

[255] P.L. Chong, B. Venegas, M. Olsher, Fluorescence detection of signs of sterol superlattice formation in lipid membranes, Methods Mol Biol, 400 (2007) 159-170.

[256] O. Maniti, M. Cheniour, M.-F. Lecompte, O. Marcillat, R. Buchet, C. Vial, T. Granjon, Acyl chain composition determines cardiolipin clustering induced by mitochondrial creatine kinase binding to monolayers, Biochimica et Biophysica Acta (BBA) - Biomembranes, 1808 (2011) 1129-1139.

[257] P. Fuchs, A. Parola, P.W. Robbins, E.R. Blout, Fluorescence polarization and viscosities of membrane lipids of 3T3 cells, Proceedings of the National Academy of Sciences of the United States of America, 72 (1975) 3351-3354.

[258] B.R. Lentz, Membrane "fluidity" as detected by diphenylhexatriene probes, Chemistry and Physics of Lipids, 50 (1989) 171-190.

[259] C. Ho, S.J. Slater, C.D. Stubbs, Hydration and Order in Lipid Bilayers, Biochemistry, 34 (1995) 6188-6195.

[260] P.B. Santhosh, S. Penič, J. Genova, A. Iglič, V. Kralj-Iglič, N.P. Ulrih, A study on the interaction of nanoparticles with lipid membranes and their influence on membrane fluidity, Journal of Physics: Conference Series, 398 (2012) 012034.

[261] C.G. Sinn, M. Antonietti, R. Dimova, Binding of calcium to phosphatidylcholine–phosphatidylserine membranes, Colloids and Surfaces A: Physicochemical and Engineering Aspects, 282–283 (2006) 410-419.

[262] M. Dahlberg, A. Maliniak, Molecular Dynamics Simulations of Cardiolipin Bilayers, The Journal of Physical Chemistry B, 112 (2008) 11655-11663.

[263] H. Yang, Y. Xu, Z. Gao, Y. Mao, Y. Du, H. Jiang, Effects of Na+, K+, and Ca2+ on the Structures of Anionic Lipid Bilayers and Biological Implication, The Journal of Physical Chemistry B, 114 (2010) 16978-16988.

[264] D. Jiao, C. King, A. Grossfield, T.A. Darden, P. Ren, Simulation of Ca2+ and Mg2+ Solvation Using Polarizable Atomic Multipole Potential, The Journal of Physical Chemistry B, 110 (2006) 18553-18559.

[265] U.R. Pedersen, C. Leidy, P. Westh, G.H. Peters, The effect of calcium on the properties of charged phospholipid bilayers, Biochimica et Biophysica Acta (BBA) - Biomembranes, 1758 (2006) 573-582.

[266] M.G. Baile, M. Sathappa, Y.W. Lu, E. Pryce, K. Whited, J.M. McCaffery, X. Han, N.N. Alder, S.M. Claypool, Unremodeled and remodeled cardiolipin are functionally indistinguishable in yeast, The Journal of biological chemistry, 289 (2014) 1768-1778.

[267] K.S. Oyedotun, B.D. Lemire, The Saccharomyces cerevisiae succinate dehydrogenase anchor subunit, Sdh4p: mutations at the C-terminal Lys-132 perturb the hydrophobic domain, Bba-Bioenergetics, 1411 (1999) 170-179.

[268] T. Volkmer, C. Becker, A. Prodohl, C. Finger, D. Schneider, Assembly of a transmembrane b-type cytochrome is mainly driven by transmembrane helix interactions, Biochimica et biophysica acta, 1758 (2006) 1815-1822.

[269] A. Prodohl, C. Dreher, R. Hielscher, P. Hellwig, D. Schneider, Heterologous expression and in vitro assembly of the transmembrane cytochrome b6, Protein expression and purification, 56 (2007) 279-285.

[270] M. Weber, A. Prodohl, C. Dreher, C. Becker, J. Underhaug, A.S. Svane, A. Malmendal, N.C. Nielsen, D. Otzen, D. Schneider, SDS-facilitated in vitro formation of a transmembrane B-type cytochrome is mediated by changes in local pH, Journal of molecular biology, 407 (2011) 594-606.

[271] H.K. Saini-Chohan, S. Dakshinamurti, W.A. Taylor, G.X. Shen, R. Murphy, G.C. Sparagna, G.M. Hatch, Persistent pulmonary hypertension results in reduced tetralinoleoyl-cardiolipin and mitochondrial complex II + III during the development of right ventricular hypertrophy in the neonatal pig heart, American journal of physiology. Heart and circulatory physiology, 301 (2011) H1415-1424.

[272] W.A. Taylor, G.M. Hatch, Identification of the human mitochondrial linoleoyl-coenzyme A monolysocardiolipin acyltransferase (MLCL AT-1), The Journal of biological chemistry, 284 (2009) 30360-30371.

[273] K.A. Davis, Y. Hatefi, Resolution and reconstitution of complex II (succinate-ubiquinone reductase) by salts, Archives of biochemistry and biophysics, 149 (1972) 505-512.

[274] C. Cole, J.D. Barber, G.J. Barton, The Jpred 3 secondary structure prediction server, Nucleic acids research, 36 (2008) W197-W201.

[275] D.W.A. Buchan, S.M. Ward, A.E. Lobley, T.C.O. Nugent, K. Bryson, D.T. Jones, Protein annotation and modelling servers at University College London, Nucleic acids research, 38 (2010) W563-W568.

[276] S. Cogliati, C. Frezza, Maria E. Soriano, T. Varanita, R. Quintana-Cabrera, M. Corrado, S. Cipolat, V. Costa, A. Casarin, Ligia C. Gomes, E. Perales-Clemente, L. Salviati, P. Fernandez-Silva, Jose A. Enriquez, L. Scorrano, Mitochondrial Cristae Shape Determines Respiratory Chain Supercomplexes Assembly and Respiratory Efficiency, Cell, 155 (2013) 160-171.

[277] V.E. Kagan, C.T. Chu, Y.Y. Tyurina, A. Cheikhi, H. Bayir, Cardiolipin asymmetry, oxidation and signaling, Chem Phys Lipids, 179 (2014) 64-69.

[278] F.W. Studier, Protein production by auto-induction in high-density shaking cultures, Protein expression and purification, 41 (2005) 207-234.